Lappeenranta
University of Technology

Jari Heinonen

CHROMATOGRAPHIC RECOVERY OF CHEMICALS FROM ACIDIC BIOMASS HYDROLYSATES

Thesis for the degree of Doctor of Science (Technology) to be presented with due permission for public examination and criticism in Auditorium 1383 at Lappeenranta University of Technology, Lappeenranta, Finland on the 13th of December 2013, at noon.

Acta Universitatis
Lappeenrantaensis 555

Supervisor	Prof. Tuomo Sainio Laboratory of Separation Technology Department of Chemical Technology Faculty of Technology Lappeenranta University of Technology
Reviewers	Prof. Dr.-Ing. Malte Kaspereit Lehrstuhl für Thermische Verfahrenstechnik Friedrich-Alexander-Universität Erlangen-Nürnberg Erlangen, Germany
	Associate Prof. Yoshiaki Kawajiri School of Chemical and Biomolecular Engineering Georgia Institute of Technology Atlanta, USA
Opponent	Prof. Dr.-Ing. Malte Kaspereit Lehrstuhl für Thermische Verfahrenstechnik Friedrich-Alexander-Universität Erlangen-Nürnberg Erlangen, Germany

ISBN 978-952-265-526-4
ISBN 978-952-265-527-1 (PDF)
ISSN-L 1456-4491
ISSN 1456-4491

Lappeenrannan teknillinen yliopisto
Yliopistopaino 2013

ABSTRACT

Jari Heinonen
Chromatographic recovery of chemicals from acidic biomass hydrolysates

Lappeenranta, 2013
97 p.

Acta Universitatis Lappeenrantaensis 555
Diss. Lappeenranta University of Technology

ISBN 978-952-265-526-4, ISBN 978-952-265-527-1 (PDF), ISSN-L 1456-4491, ISSN 1456-4491

Lignocellulosic biomasses (e.g., wood and straws) are a potential renewable source for the production of a wide variety of chemicals that could be used to replace those currently produced by petrochemical industry. This would lead to lower greenhouse gas emissions and waste amounts, and to economical savings.

There are many possible pathways available for the manufacturing of chemicals from lignocellulosic biomasses. One option is to hydrolyze the cellulose and hemicelluloses of these biomasses into monosaccharides using concentrated sulfuric acid as catalyst. This process is an efficient method for producing monosaccharides which are valuable platform chemicals. Also other valuable products are formed in the hydrolysis. Unfortunately, the concentrated acid hydrolysis has been deemed unfeasible mainly due to high chemical consumption resulting from the need to remove sulfuric acid from the obtained hydrolysates prior to the downstream processing of the monosaccharides. Traditionally, this has been done by neutralization with lime. This, however, results in high chemical consumption. In addition, the by-products formed in the hydrolysis are not removed and may, thus, hinder the monosaccharide processing. In order to improve the feasibility of the concentrated acid hydrolysis, the chemical consumption should be decreased by recycling of sulfuric acid without neutralization. Furthermore, the monosaccharides and the other products formed in the hydrolysis should be recovered selectively for efficient downstream processing. The selective recovery of the hydrolysis by-products would have additional economical benefits on the process due to their high value.

In this work, the use of chromatographic fractionation for the recycling of sulfuric acid and the selective recovery of the main components from the hydrolysates formed in the concentrated acid hydrolysis was investigated. Chromatographic fractionation based on the electrolyte exclusion with gel type strong acid cation exchange resins in acid (H^+) form as a stationary phase was studied.

A systematic experimental and model-based study regarding the separation task at hand was conducted. The phenomena affecting the separation were determined and their effects elucidated. Mathematical models that take accurately into account these phenomena were derived and used in the simulation of the fractionation process. The main components of the concentrated acid hydrolysates (sulfuric acid, monosaccharides, and acetic acid) were included into this model. Performance of the fractionation process was investigated experimentally and by simulations. Use of different process options was also studied.

Sulfuric acid was found to have a significant co-operative effect on the sorption of the other components. This brings about interesting and beneficial effects in the column operations. It is especially beneficial for the separation of sulfuric acid and the monosaccharides.

Two different approaches for the modelling of the sorption equilibria were investigated in this work: a simple empirical approach and a thermodynamically consistent approach (the Adsorbed Solution theory). Accurate modelling of the phenomena observed in this work was found to be possible using the simple empirical models. The use of the Adsorbed Solution theory is complicated by the nature of the theory and the complexity of the studied system. In addition to the sorption models, a dynamic column model that takes into account the volume changes of the gel type resins as changing resin bed porosity was also derived.

Using the chromatography, all the main components of the hydrolysates can be recovered selectively, and the sulfuric acid consumption of the hydrolysis process can be lowered considerably. Investigation of the performance of the chromatographic fractionation showed that the highest separation efficiency in this separation task is obtained with a gel type resin with a high crosslinking degree (8 wt. %); especially when the hydrolysates contain high amounts of acetic acid. In addition, the concentrated acid hydrolysis should be done with as low sulfuric acid concentration as possible to obtain good separation performance. The column loading and flow rate also have large effects on the performance.

In this work, it was demonstrated that when recycling of the fractions obtained in the chromatographic fractionation are recycled to preceding unit operations these unit operations should included in the performance evaluation of the fractionation. When this was done, the separation performance and the feasibility of the concentrated acid hydrolysis process were found to improve considerably.

Use of multi-column chromatographic fractionation processes, the Japan Organo process and the Multi-Column Recycling Chromatography process, was also investigated. In the studied case, neither of these processes could compete with the single-column batch process in the productivity. However, due to internal recycling steps, the Multi-Column Recycling Chromatography was found to be superior to the batch process when the product yield and the eluent consumption were taken into account.

Keywords: chromatography, electrolyte exclusion, ion exchange resin, lignocellulose, monosaccharides, acetic acid, hydroxymethylfurfural, furfural, hydrolysate, multi-column process, salting out, focusing effect, Adsorbed Solution theory

UDC: 66.081.3:661.728:665.944:66.094.1

FOREWORD

This thesis is based on studies that have been carried out in the Chemical Separation Methods research group of the Laboratory of Separation Technology at Lappeenranta University of Technology over the period of 2008-2013. I wish to express my graditude to my supervisor, Professor Tuomo Sainio, for all his help and support during this thesis work, and for the opportunity to be a part of the Chemical Separation Methods group. I would also like to thank the reviewers of this manuscript, Professor Malte Kaspereit from the Friedrich-Alexander-Universität and Associate Professor Yoshiaki Kawajiri from the Georgia Institute of Technology for their valuable comments and suggestions.

A substantial part of this work is based on a research project Chromatographic separation for 2nd generation bioethanol manufacture, funded by the Academy of Finland during 2008-2010 (Grant SA/121280). I am grateful for Ms. Anu Tamminen and Ms. Jaana Uusitalo from VTT Biotechnology for their co-operation during that project.

Co-operation of Professor Andreas Seidel-Morgenstern and M.Sc. Hector Rubiera Landa from Max Planck Institute for Dynamics of Complex Technical Systems is also highly appreciated.

The financial support from the Graduate School in Chemical Engineering during 2008-2012 is gratefully acknowledged. I would also like to thank the following foundations and trusts for their generous financial support: Lappeenrannan teknillisen yliopiston tukisäätiö, Suomen Kulttuurirahaston Etelä-Karjalan rahasto, Emil Aaltosen säätiö, and Walter Ahlströmin säätiö.

The current and former staff of our research group also deserves my warmest thanks – I have enjoyed every day that I have worked with you. I am especially grateful for M.Sc. Ilkka Suppula and Ms. Anne Hyrkkänen for their skillful assistance in the experimental work.

Finally, I owe my deepest gratitude to my family, relatives, and friends for their support throughout this work and whole life.

Lappeenranta, 28th of November, 2013

Jari Heinonen

LIST OF PUBLICATIONS

This thesis is mainly based on the following five publications, which are referred to by Roman numerals in the text.

I Heinonen, J., Sainio, T., Chromatographic recovery of monosaccharides for the production of bioethanol from wood, *Industrial & Engineering Chemistry Research* 49 (2010), 2907-2915.

II Heinonen, J., Tamminen, A., Uusitalo, J., Sainio, T., Ethanol production from wood via concentrated acid hydrolysis, chromatographic separation, and fermentation, *Journal of Chemical Technology and Biotechnology* 87 (2012), 689-696.

III Heinonen, J., Sainio, T., Modelling and performance evaluation of chromatographic monosaccharide recovery from concentrated acid lignocellulosic hydrolysates, *Journal of Chemical Technology and Biotechnology* 87 (2012), 1676-1686.

IV Heinonen, J., Rubiera Landa, H.O., Sainio, T., Seidel-Morgenstern, A., Use of adsorbed solution theory to model competitive and co-operative sorption on elastic ion exchange resins, *Separation and Purification Technology* 95 (2012), 235-247.

V Heinonen, J., Sainio, T., Electrolyte exclusion chromatography using a multi-column recycling process: Fractionation of concentrated acid lignocellulosic hydrolysates, submitted to *Separation and Purification Technology* in 2013.

The original journal articles have been reproduced with permission of the copyright holders. Some of the figures shown in this thesis are identical with those in the original papers. This is in agreement with the policy of the publishers (Elsevier, SCI, and ACS).

In addition to the scientific journal articles listed above, this thesis is based on research published in the following peer-reviewed scientific conference paper and book chapter.

Heinonen, J., Laatikainen, M., Sainio, T., Separation of electrolytes and organic solutes on elastic ion exchange resins: Modelling approaches, in *IEX 2012 – The International Ion Exchange Conference*, Cox, M. (ed.), Cambridge, UK, September 19-21, 2012.

Heinonen, J., Sainio, T., Chromatographic fractionation of lignocellulosic hydrolysates, in *Advances in Chemical Engineering Vol. 42 – Chemical engineering for renewables conversion*, Murzin, D.Y. (ed.), Academic Press, San Diego, USA, 2013, pp. 261-350.

The author of this thesis is the principal author both publications, which are not included here.

Author's contribution in the appended publications

I The author planned and carried out all experiments and analyzed the data. Interpretation of the results was done together with the co-author. The paper was written together with the co-author.

II The author planned and participated in the experimental work related to the concentrated acid hydrolysis and chromatographic separation. Interpretation of the results and writing of the paper was done together with the co-authors.

III The author planned and carried out all experiments and simulations, and analyzed the data. Interpretation and correlation of the results was done by the author. Development of the model and writing of the paper was done together with the co-author.

IV The author planned and carried out all experiments and simulations, and analyzed the data. Interpretation and correlation of the results was done together with the co-authors. Development of the model and writing of the paper was done together with the co-authors.

V The author planned and participated in the experimental work. Interpretation and correlation of the results was done by the author. The paper was written together with the co-author.

Author's other journal publications

Sainio, T., Turku, I., Heinonen, J., Adsorptive Removal of Fermentation Inhibitors from Concentrated Acid Hydrolysates of Lignocellulosic Biomass, *Bioresource Technology* 102 (2011), 6048-6057.

Laatikainen, M., Heinonen, J., Sainio, T., Modeling of Chromatographic Separation of Concentrated-Acid Hydrolysates, *Separation and Purification Technology* 80 (2011), 610-619.

Virolainen, S., Heinonen, J., Paatero, E., Selective recovery of germanium with N-methylglucamine –functional resin, *Separation and Purification Technology* 104 (2013) 193-199.

Hellstén, S., Heinonen, J., Sainio, T., Size-exclusion chromatographic separation of hydroxy acids and sodium hydroxide in spent pulping liquor, *Separation and Purification Technology* 118 (2013), 234-241.

Hellstén, S., Lahti, J., Heinonen, J., Kallioinen, M., Mänttäri, M., Sainio, T., Purification process for recovering hydroxy acids from soda black liquor, *Chemical Engineering Research and Data*, 2013, DOI: 10.1016/j.cherd.2013.06.001.

TABLE OF CONTENTS

NOMENCLATURE

Symbols

a	activity, mol/L
$a_{\pm}$	mean activity of an electrolyte, mol/L
A_{col}	column cross-sectional area, m^2
C	liquid phase concentration, mol/L
C^{feed}	concentration in feed solution, mol/L
C^{in}	concentration at column inlet, mol/L
$C_X^{step\ k}$	average concentration in outlet stream X in step k of the Japan Organo process, mol/L
d_{bed}	resin bed diameter, cm and m
d_p	particle diameter, m
D_{ax}	axial dispersion coefficient, m^2/s
D^P	diffusion coefficient, m^2/s
E_{Don}	Donnan potential, V
EC	eluent consumption needed to obtain one mole of monosaccharides, L/mol
F	Faraday constant, 96485.31 As/mol
h_{bed}	column (resin bed) height, cm and m
I	ionic strength on molar scale, mol/L
k_m	intraparticle mass transfer coefficient, 1/s
k_S	salting out (Setchenov) coefficient, L/mol
m	molality, mol/(kg solvent)
L	flow path length, m
n	total mole amount in liquid and solid phases within volume element, mol
n_{col}	number of columns, -
n^{out}	mole amount in outlet stream/fraction, mol
$n_{sub,2}$	number of port switches in step 2 of the Japan Organo process, -
Δp	pressure drop, bar and Pa
Pr_{sugar}	productivity of the chromatographic fractionation process with respect to the monosaccharides, mol/(m^3 h) and kg/(m^3 h)
Pu	product purity, %
q	solid phase concentration, mol/L
q^*	solid phase concentration at equilibrium with C, mol/L
$\bar{q}$	average solid phase concentration, mol/L
q_{sat}	saturation capacity, mol/L
R	universal gas constant, 8.3145 J/(mol K)
t	temporal coordinate, s
t_{cycle}	cycle time, h
t_{step}	duration of step, min
T	temperature, °C and K
v	superficial velocity, m/s
V_{bed}	resin bed volume, mL and m^3
V^{feed}	feed (injection) volume, L
$\dot{V}$	volumetric flow rate, mL/min and m^3/h
V_m	molar volume, L/mol

x	ionic valence (charge number), -
Y	product yield, %
z	spatial coordinate, m
Δz	length of volume element, m

Greek letters

α	isotherm parameter
β	isotherm parameter
γ	liquid phase activity coefficient, -
$\gamma_{\pm}$	molal mean activity coefficient of an electrolyte, -
δ_1	resin shrinking model parameter, -
δ_2	resin shrinking model parameter, mol/L
ε	local bed porosity, -
θ	extent of resin shrinking, -
κ	isotherm parameter
μ	dynamic fluid viscosity, Pas (= kg/(m s))
ν	stoichiometric number, -
Π	swelling pressure, Pa
ρ	density of the fluid, kg/m^3
τ	isotherm parameter
υ	ratio of extract and raffinate outlet streams in the Japan Organo process, -
φ	electric potential, V
Φ_S	sphericity factor of solid particle, -
ψ_p	volume fraction of polymer, -
ω	isotherm parameter

Subscripts and superscripts

acid	in sulfuric acid
AcOH	acetic acid
eluent	eluent
E	extract outlet stream in the Japan Organo process
feed	feed solution
group	functional group in ion exchange resin
H2SO4	sulfuric acid
i	component i
I	intermediate outlet stream in the Japan Organo process
k	glucose and xylose
ref	reference state
R	raffinate outlet stream in the Japan Organo process
s	step number in the MCRC process
sugar	all monosaccharides
t	stream number in the MCRC process
w	solvent (water)
water	in water
X	outlet stream in the Japan Organo process

Acronyms

AcOH	acetic acid
AS	adsorbed solution
DVB	divinylbenzene
EEC	electrolyte exclusion chromatography
H^+	proton
H_2SO_4	sulfuric acid
HMF	hydroxymethylfurfural
JO	Japan Organo
MCRC	Multi-Column Recycling Chromatography
PS	polystyrene
PVP	poly-4-vinyl-pyridine
SMB	simulated moving bed
SSR	steady state recycling chromatography
TMB	true moving bed

1 INTRODUCTION

New renewable sources for fuels and chemicals are being investigated widely as the known crude oil reserves are running out and global climate is warming up due to increasing air pollution. One potential renewable source are the lignocellulosic biomasses which are the most abundant biomass type on Earth [1,2,3]. The range of different kinds of lignocellulosic biomasses is wide and includes for example, wood, forestry and agricultural residues, bamboo, energy crops, processing waste materials, construction waste, and beet pulp [4-10]. Utilization of these biomasses for chemical production does not create direct competition between food and chemical processing, as these biomasses are non-edible by humans.

It has been estimated that worldwide total sustainable biomass energy potential is approximately 100 EJ/a [3]; which in 2010 corresponded to 18 % of world's total energy consumption [11]. It is clear, that fuels derived from lignocellulosic biomasses are not sufficient to satisfy the need for transportation fuels. Therefore, it would be better to use these biomasses for the production of industrial and fine chemicals. Petrochemical industry requires annually approximately three million barrel-of-oil-equivalents of fossil fuels for the production of 80 million tons of chemicals. The large amount of oil-derived chemicals could be reduced considerably by replacing these products with lignocellulose derived alternatives [12,13]. This would lead to lower greenhouse gas emissions, lower waste amounts (due to higher level of utilization of the raw materials), and to economical savings [12,14,15].

There are many possible process options available for upgrading lignocellulosic biomasses to chemicals (see for example Refs. [2,6,10,16-20]). One option is to hydrolyze the polysaccharides (cellulose and hemicelluloses) in these biomasses into monosaccharides (simple sugars; e.g., glucose) which are valuable platform chemicals [10,15,20-22].

Hydrolysis of lignocellulosic biomasses can be conducted either as a mineral acid catalyzed or as an enzymatically catalyzed process [5,6,10,23-25]. Enzymatic hydrolysis is a highly selective process in which no by-products are formed. However, it is a very slow method [4,5,8,26-29]. Acid hydrolysis, on the other hand, is a fast method and either dilute or concentrated acid catalysts can be used. Usually sulfuric acid is used as the catalyst. The negative aspects of the acid catalyzed hydrolysis are high acid consumption and corrosion problems in the concentrated acid hydrolysis, and formation of hydrolysis by-products especially in the dilute acid hydrolysis [4,6,9,10, 23-25,30].

In two-step concentrated sulfuric acid hydrolysis, a high total monosaccharide yield is obtained: 80 % or higher [4,6,7,23-25,30]. In addition, only small amounts of by-products (mainly acetic acid, furfural, and hydroxymethylfurfural (HMF)) are formed [6,7,23,24,30-32]. The disadvantages of the concentrated acid hydrolysis process are the aforementioned high hydrolysis acid consumption and corrosion problems. The high acid consumption results

from the need to remove the hydrolysis acid from the hydrolysates obtained in the process prior to the downstream processing of the monosaccharides. Traditionally the acid removal has been done by neutralization with slaked lime, $Ca(OH)_2$. This, however, results in high chemical costs of the hydrolysis as large amounts of fresh sulfuric acid and lime are needed in every hydrolysis. As a by-product of the neutralization process, gypsum, $CaSO_4$, is generated in large quantities [6,23,24,30].

In addition to the removal of sulfuric acid, there is also a need for the recovery of the hydrolysis by-products from the hydrolysates as these are valuable chemicals, but often hinder the downstream processing of the monosaccharides. The removal and recovery of these by-products cannot be done efficiently with the lime neutralization [33,34]. The negative aspects listed here have made the concentrated acid hydrolysis process unpopular.

Scope of the thesis

As mentioned, the concentrated acid hydrolysis is an efficient method for production of monosaccharides, and also other valuable chemicals, from lignocellulosic biomasses. However, due to the issues related to the hydrolysis acid consumption and selective recovery of the hydrolysis products, it has been deemed as an uneconomical and unfeasible method. In order to improve the economics and feasibility of the concentrated acid hydrolysis process, the hydrolysis acid should be recovered without neutralization and recycled back to the hydrolysis. In addition, selective recovery of the monosaccharides and hydrolysis by-products would enhance the downstream processing of the monosaccharides. This would also improve the feasibility of the process as the by-products are valuable chemicals.

One process option that could be used for reaching the aforementioned goals is the chromatographic fractionation [35,36]. Use of the electrolyte exclusion chromatography [37-39] for the fractionation of lignocellulosic hydrolysates has been investigated prior to and outside this work by a number of authors [7,40-50]. However, most of these publications deal with the fractionation of dilute acid hydrolysates [42,46] or the binary separation of sulfuric acid and glucose [40,41,43,44,45,47,48,50]. In academia, Sun *et al*. [7] have investigated the fractionation of actual concentrated acid lignocellulosic hydrolysates. However, merely the continuous chromatographic fractionation was investigated in Ref. [7], and no details regarding the basic phenomena related to the separation task at hand were given. In addition, Laatikainen *et al*. [49] have studied the modelling of the chromatographic fractionation of concentrated acid hydrolysates using a rigorous thermodynamic model. Few pilot scale investigations have also been conducted [45,47,48] and few patents have been made [23,24,51]. However, despite the number of papers dealing with the chromatographic fractionation of acidic lignocellulosic hydrolysates or solutions presenting these, the in-depth knowledge of this separation is scarce. No systematic studies regarding the phenomena occurring in the separation or the separation performance could be found prior to this work.

The purpose of this thesis is to provide *a systematic experimental and model-based study of the use of chromatography for the fractionation of concentrated acid lignocellulosic hydrolysates into sulfuric acid, monosaccharide, and by-product (acetic acid) fractions.* This thesis tries to give answers to the following questions:

- Is chromatography an efficient method for the fractionation of concentrated acid hydrolysates?
- Can the chemical consumption of the concentrated acid hydrolysis process be reduced with chromatographic fractionation?
- What phenomena affect the separation?
- Can the observed phenomena be modeled accurately with simple models?
- How does the hydrolysate composition affect the fractionation?
- What kind of chromatographic process option should be used?

The chromatographic separation step studied here is one part of a multi-step pathway for the production of monosaccharides and other valuable products from lignocellulosic biomasses via concentrated acid hydrolysis. The main unit operations of this process are shown in Fig. 1. The purification of the concentrated acid hydrolysates in this work is assumed to be carried out in two steps. First, adsorption is used to remove some of the by-products formed in the hydrolysis, i.e., furans and possible phenolic compounds (Fig. 1). This step is not studied here as investigations of this step has been conducted by several authors [33,52-56].

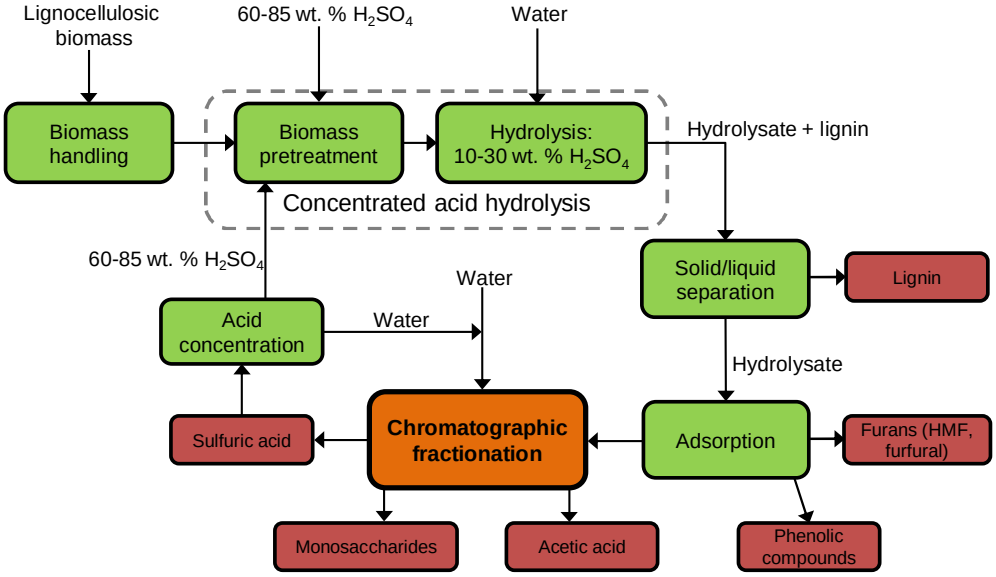

Figure 1. Production of chemicals from lignocellulosic biomasses via two-step concentrated sulfuric acid hydrolysis process.

In the second part of the hydrolysate purification, chromatography is used (Fig. 1). This thesis focuses on this separation step. The chromatographic separation method investigated here is

the electrolyte exclusion chromatography (*EEC*). In this method, separation of strong electrolytes (sulfuric acid) from organic nonelectrolytes (monosaccharides) and weak electrolytes (acetic acid) is based on electrostatic interactions [37-39]. *Sulfonated gel type strong acid polystyrene–divinylbenzene (PS–DVB) cation exchange resins in acid (H^+) form* are used as stationary phase in this work.

The main emphasis in this thesis is to *determine the phenomena related to the separation task at hand*, and to *develop a simple model that takes these phenomena accurately into account*. This includes modelling of the sorption equilibria as well as the resin volume changes of the gel type resins. *Two different approaches for the modelling of the sorption equilibria* are investigated here: a simple empirical approach and the Adsorbed Solution theory [57-59].

For gel type resins, like those used in here, resin volume changes due to changes in liquid phase composition can be significant, and have to be taken into account in the modelling. In this work, a simple *equilibrium model for the resin volume changes* as well as *a dynamic column model* that takes into account the resin volume changes is presented.

The *performance of the chromatographic separation process is investigated experimentally* and by *numerical simulations*. The effect of *the resin crosslinking degree* on the separation is investigated as well as the effects of *hydrolysate composition* and *operating parameters*. In addition, *different process options available for the chromatographic fractionation* of concentrated acid lignocellulosic hydrolysates are investigated. These are *single-column batch process*, the *Japan Organo (JO) process* [60], and the Sequential Simulated Moving Bed process [61]. In this work, the last mentioned process is termed as *the Multi-Column Recycling Chromatography* (abbreviated as MCRC).

Limitations

Not all aspects related to the separation task at hand are investigated in this work. As was mentioned above, the purification of the concentrated acid hydrolysates is assumed to be done in two steps (Fig. 1). In the first step, adsorption [33,52-56] is used to remove the small amounts of hydroxymethylfurfural, furfural, and possible phenolic compounds formed in the hydrolysis [10,34,62,63]. This thesis focuses on the second step of the hydrolysate purification in which chromatography is used to fractionate the furan- and phenol-free hydrolysates into sulfuric acid, monosaccharides, and acetic acid fractions. Therefore, only these components were taken into account in most of the studies done in this work.

Investigation of the chromatographic fractionation of dilute acid lignocellulosic hydrolysates is omitted from this work. Comprehensive information about the fractionation of these hydrolysates can be found from literature [33,42,46,52-56]. The main concern with the dilute acid hydrolysates is not in the recovery of hydrolysis acid, but the recovery of the hydrolysis by-products which can be done using chromatography or adsorption [33,42,46,52-56].

However, the models derived here for the fractionation of the concentrated acid hydrolysates are also applicable for the fractionation of the dilute acid hydrolysates.

The effect of temperature on the separation performance is also not investigated here. Neuman *et al*. [40] found out that a temperature of 50 – 60 °C is optimal for the separation task at hand. Therefore, all experiments in this work were carried out at a temperature of 50 °C which was the highest temperature permitted by the experimental equipment.

Only the use of gel type strong acid PS–DVB resins in acid form as stationary phase is investigated here. The choice of the resin type and the ionic form (H^+) was done on the basis of literature information regarding the electrolyte exclusion [38,39], and on the basis of earlier studies dealing with the chromatographic fractionation of lignocellulosic hydrolysates [40-42]. The modelling is done only in case of one resin.

The investigation of suitable process options for the separation task at hand is by far not complete as only three processes (single-column batch process, the JO process, and the MCRC process) are studied. Full comparison of these process options was not done during this work. The JO process was chosen to be studied here as it is an industrially proven simulated moving bed (SMB) process used in the sweeteners industry [60,64,65]. Likewise, the MCRC process is an industrially proven process. It is an interesting process option for the separation task at hand as it is used in chromatographic fractionation of sugar molasses which is also based on the electrolyte exclusion [61]. Steady state recycling (SSR) chromatography was omitted from here as it has been investigated elsewhere [50].

Structure of the thesis

This thesis consists of a literature review regarding the subject of this work and presentation of the most important experimental methods and results obtained in this work. Introductions to the concentrated acid hydrolysis of lignocellulosic biomasses, concept of chromatographic fractionation of the obtained hydrolysates, and products recovered from these hydrolysates will be given in Chapter 2. Basics of liquid chromatography will be discussed in Chapter 3 and phenomena affecting the sorption of solutes specifically in the electrolyte exclusion chromatography and in the separation task at hand will be reviewed in Chapter 4. The advanced chromatographic separation processes studied in this work will be introduced in Chapter 5.

The models derived in this work for the separation task at hand will be presented in Chapter 6 and the experimental methods used here will be reviewed in Chapter 7. In Chapter 8, the most important results obtained in this work will be presented and discussed. Conclusions drawn from this work will be presented in Chapter 9.

Journal publications that are related to this thesis are given as appendices.

2 CONVERSION OF LIGNOCELLULOSIC BIOMASSES FOR CHEMICAL PRODUCTION

In this Chapter, the method of producing monosaccharides, and also other valuable products, from lignocellulosic biomasses via concentrated acid hydrolysis will be presented. Also the chromatographic fractionation of the concentrated acid hydrolysates will be introduced. First, a short introduction to the composition of the lignocellulosic biomasses will be given.

2.1 Composition of lignocellulosic biomasses

Lignocellulosic biomasses include, for example, wood, forestry and agricultural residues, bamboo, energy crops, processing waste materials, construction waste, and beet pulp [4-10]. These materials consist mainly of cellulose, hemicelluloses, and lignin (Table 1). In addition, small amounts of ash, acids, and extractives are found from lignocellulosic biomasses [4,6].

Table 1. Cellulose, hemicellulose, and lignin contents of lignocellulosic biomasses [6,8,10].

	Cellulose, %	Hemicelluloses, %	Lignin, %
Hardwood	40-75	10-40	15-25
Softwood	30-50	25-40	25-35
Wheat straw	30	50	15
Rice straw	32-47	19-27	5-24
Sugarcane bagasse	40	24	25
Switch grass	32-45	25-32	12-18
Grasses	25-40	25-50	10-30

Cellulose is the main component of lignocellulosic biomasses (Table 1). It is a linear homopolymer consisting of 2 000-27 000 cellobiose (a dimer of two glucose monomers) units. The cellobiose units are linked together with β-(1,4)-glycosidic bonds [4,9,10,66-68]. Cellulose chains form numerous intra- and intermolecular hydrogen bonds via the hydroxyl groups in the sugar molecules. This results in a highly ordered crystalline structure interspersed with less-ordered amorphous regions [4,10,23,24].

Hemicelluloses surround the cellulose chains. These are amorphous linear heteropolymers with monomeric side chains. Structural units of hemicellulose chains depend on the type of the lignocellulosic biomass. The chains consist of hexose (e.g., glucose, mannose, galactose, and rhamnose) and pentose (e.g., xylose and arabinose) sugars, acetic acid, and sugar acids [4,6,9,10,66]. The monosaccharides in hemicelluloses are also linked together by β-(1,4)-glycosidic bonds [4,10,67-69].

The third major constituent of lignocellulosic raw materials is lignin which is an aromatic three dimensional polymer consisting different kinds of phenylpropane units [4,9,10]. The

role of lignin is to strengthen and shield the polysaccharide network [4]. Usually, softwoods contain more lignin than hardwoods (Table 1).

2.2 Products obtained from lignocellulosic hydrolysates

Petrochemical industry requires annually approximately three million barrel-of-oil-equivalents of non-renewable fossil fuels for the production of 80 million tons of chemicals. The large amount of the oil-derived chemicals could be reduced considerably by replacing part of these chemicals with alternatives derived from lignocellulosic biomasses [12,13]. This would lead to decreased greenhouse gas emissions, chemical pollution, wastes, and energy consumption, and to economical savings [12,14].

Monosaccharides are the main products formed in the concentrated acid hydrolysis of lignocellulosic biomasses. They are valuable platform chemicals that can be converted into a wide variety of products either by bio- or thermochemical means [12,14,21,22,70].

In addition to the monosaccharides, also other valuable products are formed during the concentrated acid hydrolysis either through degradation of the monosaccharides or directly from the polysaccharides, extractives and lignin. The most important of these are acetic acid, hydroxymethylfurfural, and furfural [10] which are also valuable platform chemicals [71-74].

In this Chapter, potential products obtainable from monosaccharides, acetic acid, HMF, and furfural recovered from lignocellulosic hydrolysates will be introduced.

2.2.1 Products obtained from monosaccharides

The spectrum of chemical products manufactured from monosaccharides is vast and novel end-products emerge continuously. Only a short list of the possible end products will be given in this Chapter.

Monosaccharides are highly reactive compounds due to the high amount of functional groups in their molecules [15,21,22]. Monosaccharide molecules usually have hydroxyl groups attached to all carbon atoms except one. In addition, monosaccharide molecules can change conformation (mutarotation) between different ring and open-chain conformations; of these the first mentioned are the dominant conformations. In the open-chain conformation, monosaccharides contain also one aldehyde or ketone group. Thus, monosaccharides can undergo a variety of reactions that are typical for alcohols and aldehydes or ketones [21]. These facts make monosaccharides highly valuable platform chemicals [12,14,21,22,70]. In addition, some monosaccharides are valuable even without any modifications. For example, galactose is a crucial component in many biological processes [75].

The reactions required to upgrade monosaccharides to other chemicals always involve reduction of the oxygen content, i.e., the reactivity, of the molecules [15,21,22]. In

petrochemical processes, on the contrary, oxygen is added to alkanes and other hydrocarbons [22]. This is more energy intensive than the removal of oxygen [76], making chemical production from monosaccharides an intriguing option.

Chemicals can be produced from monosaccharides by bio- and thermochemical means. Biochemical processes are usually selective and do not require extreme operating conditions. However, these processes are usually slow [77,78]. Fermentative production of alcohols from monosaccharides is one widely studied area [1,31,70,79-85]. Ethanol is the most investigated alcohol and it can be produced, for example, using yeasts such as *Saccharomyces cerevisiae* and *Pichia stipitis* [1,31,70,79-83]. Also production of higher alcohols (e.g., isobutanol and 1-butanol) has been studied. 1-butanol can be manufactured in the so-called ABE (acetone–butanol–ethanol) process using e.g., *Clostridia acetobutylicum*. Like the name of the ABE process suggests, also acetone and ethanol are produced in this process [81-85].

Carboxylic acids, amino acids, aldehydes, ketones, esters, ethers, polymers, alcohols, alkanes and alkenes can also be manufactured from monosaccharides via biochemical routes [13,14,21,77,78,86]. One of the most interesting products is succinic acid produced from glucose and xylose with, for example, *Escherichia coli* [78], *Anaerobiospirillum succiniciproducens* [14], *Actinobacillus succinogenes* [87]. Succinic acid is a precursor for many important industrial chemicals and consumer products including food additives, pharmaceutical products, and organic solvents (1,4-butanediol, tetrahydrofuran, γ-butyrolactone, N-methyl pyrrolidinone, 2-pyrrolidinone) [14,78,87,88].

Another important precursor manufactured biochemically from monosaccharides is isobutene which is a valuable intermediate in the production of for example fuel additives (ETBE, isooctane, MTBE), polymers (butyl rubber), methacrolein, and antioxidants. Currently 10 million tons of isobutene is produced yearly by petrochemical industry [13]. Lactic acid produced biochemically from glucose is also an important precursor chemical: in the USA the volume of lactic acid derived products is expected to rise to 1.4-1.8 million tons per year [89].

On the contrary to the biochemical manufacturing processes, thermochemical manufacturing processes are fast, but often require high temperatures [15,22]. In addition, heterogeneous catalysts are usually needed [1,15,22,86,90]. Monosaccharides can be converted efficiently to monofunctional hydrocarbons and alkanes and alkenes in the presence of Pt-Re/C catalyst (800 °C temperature, 18-27 bar pressure). More than 90 % of the energy content of monosaccharides is retained in the products while more than 80 % of the oxygen is removed [15].

Monosaccharides can also be converted into furans thermochemically in the presence of heterogeneous catalysts [76]. Glucose can be converted to large variety of components (e.g., 1,4-diacids, glucaric acid, glutamic acid, 3-hydroxybutyrolactone, and sorbitol) using photo-oxidation [90]. Glucose can also be converted to sorbitol in the presence of Ru/Ti catalyst

(T = 90-120 °C, H_2 overpressure). Sorbitol can be used as an intermediate in production of polymers, plastizisers, solvents, and pharmaceutical products [22].

2.2.2 Other valuable products

Acetic acid is used in many applications. Over 65 % of acetic acid is used in polymers derived from vinyl acetate, or cellulose. Of these, poly(vinylacetate) is used in paints and coatings or in the production of poly(vinyl alcohol) and plastics. Cellulose acetate is used to produce acetate fibers. Acetic acid, like its esters, are also used as solvents. [71]

Approximately 200 000 tons of furfural is annually produced from lignocellulosic biomasses. It is a flexible platform chemical that can be used for example in the production of furan derivatives like 2-methyltetrahydrofuran and 2-methylfuran which are fuel additives [73,74]. In addition, it can be used with acetone to produce liquid alkanes through aldol condensation and hydrogenation [73]. Furfural can also be converted to levulinic acid to be used in the production of many chemicals, including butene and chemicals and fuels derived from it [20].

HMF is also a versatile platform chemical that can be used for the production of a wide variety of fine chemicals, polymeric materials, pharmaceuticals, and biofuels. HMF can, for example, be selectively oxidized to 2,5-di-furandicarboxylic acid which can be used to replace terephthalic acid in the synthesis of polyesters [72]. In addition, it can be used to produce numerous furan derivatives, succinate, esters, and levulinic acid [20,74].

2.3 Concentrated acid hydrolysis

Cellulose and hemicelluloses in lignocellulosic biomasses can be utilized in producing monosaccharides and also other valuable chemicals. For this purpose, the biomass must be hydrolyzed, i.e., the polysaccharide chains must be cleaved to monosaccharides. Dilute or concentrated mineral acids can be used to catalyze the hydrolysis of the polysaccharides [5-7,9,10,25,31,91].

Sulfuric acid is most often used as a catalyst in acid hydrolysis although the use of hydrochloric, sulphurous, acetic, and phosphoric acids has also been studied [6,7,9,10,23-25,69,92-95]. In this work, only the concentrated sulfuric acid hydrolysis will be introduced as the purpose of this thesis is to investigate the chromatographic fractionation of the hydrolysates obtained from this hydrolysis process.

Acid catalyzed hydrolysis is a complex heterogeneous reaction scheme depending not only on the hydrolysis conditions (temperature, hydrolysis acid concentration) but also on the physical factors (crystallinity of cellulose, swelling of the lignocellulosic material, shearing forces in the hydrolysis reactor) [67,68]. Details of the hydrolysis mechanisms can be found from Refs. [2], [67], and [68].

In the hydrolysis, cellulose chains break down into glucose monomers. These in turn may degrade to hydroxymethyl furfural (HMF) [9,10,34,63,94]. Eventually HMF breaks down into formic and levulinic acids [10,63,96]. Amorphous regions of cellulose chains are more easily hydrolyzed than the crystalline regions [10].

Hemicelluloses are amorphous and are, therefore, more easily hydrolyzed to monosaccharides than cellulose [5,6,9,10,27,94,97]. As a consequence, in acid hydrolysis, monosaccharides derived from hemicelluloses are more easily degraded to furans due to longer availability for degradation reactions. The degradation products of hemicellulosic pentose and hexose sugars are furfural and HMF, respectively [5,6,9,10,27,34,63,94,98-100]. These can in turn degrade to formic and levulinic acids [10,101]. The degradation reactions of the monosaccharides are considerably slower than the release rate of the monosaccharides during the concentrated acid hydrolysis, and their concentrations are usually low in the concentrated acid hydrolysates [10,25-27,31,93].

Hydrolysis of hemicelluloses leads also to the formation of acetic acid. It is formed when acetyl groups of hemicellulosic sugars are cleaved off. This cleavage occurs already at mild conditions and, therefore, the formation of acetic acid does not depend significantly on the hydrolysis conditions. [10]

Lignin is highly resistant for chemical and enzymatic modifications and therefore breaks down only partially during acid hydrolysis yielding phenolic compounds [10,62-63,102]. Phenolic compounds may also be formed during the hydrolysis from the extractives in the lignocellulosic biomasses [9,10,34,63,102]. The concentrations of the phenolic compounds in acidic hydrolysates are usually very low due to the resistant nature of lignin and due to low solubility in acidic medium [9,10,62,94].

Concentrated acid hydrolysis is done in two steps at temperatures below 100 °C (see Fig.1) [7,10,23,24,30-32,92]. In the first step, the lignocellulosic biomass is mixed with 65-85 wt. % sulfuric acid at a temperature of 30-55 °C to break down the crystalline cellulose and solubilize the biomass [7,23-25,30,32,67,68,92,103]. The duration of the decrystallization step is less than two hours. The actual hydrolysis is commenced after the pretreatment step by diluting the hydrolysis acid to 20-30 wt. % and increasing the temperature to 80-100 °C. The reaction is continued for 40-480 min [7,23,24,32,92].

Concentrated acid hydrolysis gives a high total monosaccharide yield: even 80 % or higher [4, 6,7,23-25,30]. Only small amounts of by-products (mainly acetic acid, furfural, and hydroxymethyl furfural (HMF)) are formed [6,7,23,24,30-32]. Acetic acid is the most abundant by-product found in the concentrated acid hydrolysates [31,46,42]. Furfural and HMF are the only furans found in significant quantities in the hydrolysates [10,63,94,96]. Most of the unreacted lignin precipitates (90 % at pH 2.6 [104]) during the hydrolysis due to

low solubility in acidic conditions [25,104-106] and can be separated from the hydrolysate by filtration (see Fig. 1).

The disadvantages of the concentrated acid hydrolysis process are corrosion problems related to the high acid concentration and high hydrolysis acid consumption. The hydrolysis acid must be removed from the hydrolysate prior to downstream processing of the monosaccharides. Traditionally the acid removal has been done by neutralization with $Ca(OH)_2$. This, however, results in high chemical costs of the hydrolysis. In addition, high amounts of $CaSO_4$ are generated [6,23,24,30], and the ethanol yield in fermentation is relatively low [63].

In addition to the removal of sulfuric acid, there is also a need for the recovery of the hydrolysis by-products from the hydrolysates as these are valuable chemicals, but often hinder the downstream processing of the monosaccharides. The removal and recovery of these by-products cannot be done efficiently with the lime neutralization [33,34].

2.4 Chromatographic fractionation of lignocellulosic hydrolysates

The disadvantages regarding the economics of the concentrated acid hydrolysis have made it unpopular. However, the economics of the process can be increased considerably if the hydrolysis acid could be recycled and reused instead of neutralizing. In addition, the by-products formed during the acid catalyzed hydrolysis should be recovered selectively due to their high value. This would also improve the processability of the monosaccharides. One separation technique that can be used to achieve the aforementioned goals is the electrolyte (or ion) exclusion chromatography [23,24,31,37,40-51,91,107].

In the electrolyte exclusion chromatography, strong electrolytes (e.g., sulfuric acid) are excluded from the resin phase completely or partially due to electrical repulsion caused by the fixed ionic groups in the resin [37-39]. Therefore, the strong electrolytes propagate fast through the column [37,108]. Associated weak electrolytes (e.g., acetic acid) and nonelectrolytes (e.g., monosaccharides, furfural, HMF) are not affected by the electrolyte exclusion and are sorbed to the resin. As a consequence, the strong electrolytes are separated from the weak electrolytes and the nonelectrolytes [37-39]. Details of the electrolyte exclusion chromatography can be found from Chapter 4.2.1.

Using the electrolyte exclusion chromatography, the concentrated acid hydrolysates can be fractionated into sulfuric acid fraction, monosaccharide fraction, and various by-product fractions (acetic acid, HMF, furfural, and possibly phenols). The fractionation can be done in a single step using solely the electrolyte exclusion chromatography (see for example Chapter 8.2.3), however, it has been observed that it would be more economical to do the fractionation in two steps [7,31,46,56,91]. First, the monosaccharide degradation products (and possible phenolic compounds) are removed from the hydrolysates using adsorption [33,52-56].

Afterwards, sulfuric acid and acetic acid are separated from the monosaccharides using the electrolyte exclusion chromatography [7,23,24,40-51,91,107]. The monosaccharide fraction and the acetic acid fraction are then led to downstream processing (see Chapter 2.2) whereas the sulfuric acid fraction is recycled back to the hydrolysis through a concentration step. In this step, sulfuric acid is concentrated to 70 wt. % [23,24] for example by using multiple effect evaporator [92,109] or vapor compression distillation [23,24,109].

Prior to and outside this work, a number of investigations regarding the chromatographic fractionation of lignocellulosic hydrolysates or synthetic solutions presenting these hydrolysates have been done [7,23,24,40-51]. However, none of these studies presents a systematic investigation of the subject. In the following, these investigations and the most important results obtained in them are summarized.

Neuman *et al*. [40] studied experimentally the effects of the column loading and temperature on the separation of glucose (1.0 wt. %) and sulfuric acid (7.7 wt. %) with a gel type strong acid PS–DVB cation exchange resin in acid (H^+) form (Amberlite IR-118, 4.5 wt. % DVB) in a batch column. The separation efficiency was found to increase with decreasing column loading. The highest efficiency was obtained at temperatures of 55 °C and 68 °C. Neuman *et al*. [40] also noted that the sulfuric acid profile had a diffuse front and a shock layer at the back of the profile. Also elongated front of the glucose profile was observed: a phenomenon resulting from the co-operative effect of sulfuric acid on the monosaccharide sorption [40].

Nanguneri and Hester [41] studied the chromatographic fractionation of sulfuric acid (8.0 wt. %) and glucose (17.35 wt. %) with a gel type strong acid cation exchange resin in acid form (Amberlite IR-122, sulfonated PS–DVB resin, 10 wt. % DVB content). The unsymmetrical shape of the sulfuric acid profile was clearly seen also in these experiments. Elongated front of the glucose profile due to sulfuric acid was also observed [41].

Xie *et al*. [46] compared two resins for the chromatographic fractionation of dilute acid (1 wt. % sulfuric acid) corn stover hydrolysate at a temperature of 60 °C. The resins used in this study were Dowex 99 (a gel type strong acid resin) in H^+ form and a weakly basic poly-4-vinyl-pyridine resin (PVP). Fractionation of the hydrolysate into sulfuric acid, monosaccharide, and various by-product fractions was achieved with both resins. With Dowex 99, no additional regeneration of the resin was needed. PVP resin, on the other hand, exchanged the sulfate ions of sulfuric acid to hydroxide ions, and therefore an additional regeneration step with a base was required to elute sulfate ions from the resin [46].

Continuous chromatographic fractionation of hydrolysates or synthetic sulfuric acid–monosaccharide mixture has also been investigated [7,42-44]. Springfield and Hester [43,44] investigated continuous separation of sulfuric acid (10 wt. %) and glucose (10 wt. %) using a four-zone simulated moving bed chromatography (SMB) (see Chapter 5.1) with Dowex Monosphere 99 resin. 98 % of sulfuric acid was collected to the raffinate stream and 96 % of

the glucose to the extract stream. Weak focusing was also noted for glucose in the experiments [43].

Use of a nine zone SMB system for chromatographic fractionation of an authentic dilute acid yellow poplar hydrolysate has been investigated by Wooley *et al*. [42]. Dowex 99 (sulfonated PS–DVB resin, 6 wt. % DVB content) in acid form was used as a stationary phase and water as an eluent. Good separation efficiency was achieved: recoveries of glucose and xylose in the raffinate stream were 0.88 and 0.83, respectively. The purity of sugar stream was 100 % [42].

Sun *et al*. [7] investigated the SMB fractionation of authentic concentrated sulfuric acid (27 wt. %) hydrolysates of bamboo. In this study, the fractionation of the hydrolysates was done in two steps. First, the removal of color compounds was done carried out using adsorption on activated carbon. In the second step, binary fractionation of the remaining hydrolysate containing mainly sulfuric acid and monosaccharides was conducted using the Intermittent SMB [7,110]. An anion exchange resin (DIAION MA03SS) in sulfate form was used as a stationary phase and water as an eluent. 90.5 % pure sulfuric acid and 98.4 % pure monosaccharide streams were obtained [7].

Use of steady state recycling (SSR) chromatography [111,112] for fractionation of concentrated sulfuric acid and glucose has also been investigated. Considerably better separation efficiency could be obtained with the SSR when compared to batchwise chromatography [50].

Some patents regarding the electrolyte exclusion fractionation of concentrated acid lignocellulosic hydrolysates with strong acid cation exchange resins as stationary phases have also been made [23,24,51]. Farone and Cuzens [23,24] patented a method for obtaining 90% pure sulfuric acid and 94% pure monosaccharide streams from concentrated acid hydrolysate (33.6 wt. % sulfuric acid, 23.0 wt. % monosaccharides) using a gel type cation exchange resin in acid form as a stationary phase (CS16GC, Finex Oy, Finland) [23,24]. This separation process is part of a larger process concept known as the Arkenol process [45,47,48,113] which consists of a two-step concentrated acid hydrolysis of lignocellulosic biomasses and chromatographic fractionation of the obtained hydrolysates [23,24]. In the Arkenol process the hydrolysates are fractionated into sulfuric acid and monosaccharide streams using a four-zone SMB process.

The feasibility of the Arkenol process has also been investigated on pilot scale [45,47,48]. At the Izumi biorefinery (Izumi, Japan), production of monosaccharides and ethanol from wood wastes using the Arkenol process was studied during a five-year campaign (2002-2007) [48].

Amalgamated Research Inc. (USA) [45,47] made a pilot scale investigation of intensification of the chromatographic fractionation in the Arkenol process [23,24] by using fractal-based fluid distributors in the inlets and outlets of the columns of the SMB process. A 75 %

reduction in the size of the chromatographic equipment and less diluted product streams were obtained while maintaining the required product purities and yields [45,47].

In the near future, the Arkenol process will also reach production scale in the USA [113]: BlueFire Renewables is building two biorefineries that will produce ethanol from cellulosic waste materials. The plants are expected to produce approximately 15 000 m^3 (Lancaster, California) and 72 000 m^3 (Fulton, Mississippi) of fuel-grade ethanol per year [113].

As could be seen from above, the fractionation of actual concentrated acid hydrolysates has not been investigated extensively and the in-depth knowledge regarding this separation step is scarce. According to the author's knowledge only few academic studies [7,47,49,50] deal with this issue and none of them presents a systematic and detailed investigation of this topic. It is the goal of this thesis to correct this by presenting a systematic study of the use of the electrolyte exclusion chromatography for the fractionation of concentrated acid lignocellulosic hydrolysates into sulfuric acid, monosaccharide, and by-product fractions.

3 BASIC CONCEPTS OF LIQUID CHROMATOGRAPHY

The basic concepts related to the liquid chromatography will be introduced in this Chapter. First, a short introduction to the liquid chromatography will be given. Following this, the sorption isotherms are introduced. The last part of this Chapter will deal with ion exchange resins which are stationary phases used in the electrolyte exclusion chromatography.

3.1 Liquid chromatography

Chromatography is a powerful chemical separation method in which separation of components (adsorbates) in a carrier liquid (eluent) is based on different interactions between these components and a stationary phase (adsorbent). The stationary phase is packed to a column through which the eluent percolates [35,36,114]. The sample that is to be fractionated is injected into the eluent stream. The choice of the stationary phase depends on the separation task at hand. In liquid chromatography in fixed beds, for example, activated carbon, zeolites, polymeric adsorbents, or ion exchange resins can be used as stationary phases [36-39,91,114,115]. The stationary phase materials are usually highly porous and, therefore, have large surface areas for sorption [114]. The pore size distribution of these materials affects the mass transfer in the separation processes [39].

Chromatography is utilized on both analytical and preparative scale. On analytical scale, the goal is to separate complex mixtures in order to identify and quantitize the components of these mixtures [35,36,114]. The separation of sample components is complete due to small column loadings used: the concentrations are small and no interactions between the components occur in the column. The feed volume does not affect the retention times and shapes of the component bands [35,36,114].

Preparative chromatography aims at isolating a certain amount of a purified component for further processing. On preparative scale, the column loadings are large, and there are often interactions between the components [35,36,114]. The separation is often incomplete and the component bands overlap each other. The shape and retention times of the component bands, and peak maximas depend on the composition and size of the feed injection [35,36,114].

In the basic implementation mode of chromatography, the single-column batch chromatography (Fig. 2), an eluent (e.g., water, organic solvent, or a mixture of these) is continuously pumped through a column packed with the stationary phase and, at certain time intervals, the mixture that is to be fractionated is injected to the eluent stream at the column inlet. The components in the feed mixture are pushed by the eluent and travel through the packed bed with different velocities due to different interactions between these components and the stationary phase. Components that are strongly sorbed to the stationary phase propagate slower through the column than components that are weakly sorbed. As a

consequence, the components are separated from each other and exit the column at different times by the eluent.

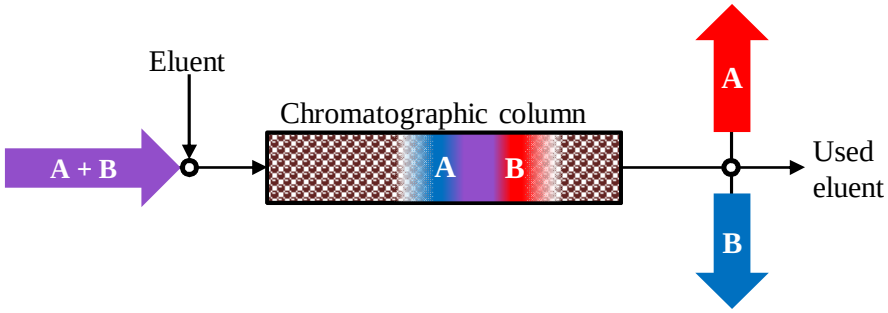

Figure 2. Operating principle of single-column batch chromatography. Separation of A (red) and B (blue) in a column filled with a stationary phase (brown spheres).

3.2 Sorption isotherms

Distribution of components between liquid and solid phases at equilibrium is described by sorption isotherms. These isotherms give the sorbed amount as a function of liquid phase concentration:

$$q = f(C), \tag{1}$$

where q is the concentration in the solid phase in equilibrium with the liquid phase and C is the liquid phase concentration in equilibrium. The concentration of the sorbing component in the solution phase affects the sorption: the higher the concentration, the higher the sorbed amount. At very low concentrations there is lots of space available on the stationary phase surface for sorption and the sorption isotherms are linear (Fig. 3), i.e., the sorbed amount of a component is proportional to the liquid phase concentration of this component. With increasing concentration, the isotherms become nonlinear as a limited amount of substance can be sorbed to a certain volume/mass of a stationary phase. The nonlinearity of the isotherms depends on the concentration range of interest, sorbing component, retention mechanisms, and phase system used [36]. On preparative scale, the sorption isotherms are usually nonlinear.

Three types of nonlinear isotherms can be distinguished (Fig. 3). First type is the concave downward shaped (favorable) isotherm, i.e., the slope of the isotherm decreases with increasing concentration. Decreasing isotherm slope means that the distribution coefficients become smaller with increasing concentration. The most well-known model used to describe this kind of sorption behavior is the Langmuir sorption isotherm model [36]:

$$q = \frac{q_{sat}\omega C}{1+\omega C}, \tag{2}$$

where q_{sat} is the saturation capacity and ω is an isotherm parameter.

Second type of sorption isotherm is the concave upward shaped (unfavorable) isotherm (Fig. 3), i.e, the slope of the isotherm increases with increasing concentration; at least in the concentration range that is normally used [36-39]. Sorption isotherms that are concave upward shaped can be modeled, for example, by using simple empirical anti-Langmuir sorption isotherm model written as

$$q = \frac{\omega_1 C}{1 - \omega_2 C}. \tag{3}$$

Third isotherm type is the so called S-shaped isotherm containing both concave downward and concave upward regions (Fig. 3) [36]. On a sufficiently large concentration range the concave upward shaped isotherms (e.g., Eq. (3)) become S-shaped. This is because the curvature of the isotherm changes to concave downward at certain concentration due to limited amount of the stationary phase surface available for sorption. S-shaped sorption behavior can be described with the so-called quadratic sorption isotherm model

$$q = \frac{q_{sat}\left(\omega_1 C + 2\omega_2 C^2\right)}{1 + \omega_1 C + \omega_2 C^2}, \tag{4}$$

which is also applicable for concave upward shaped isotherms.

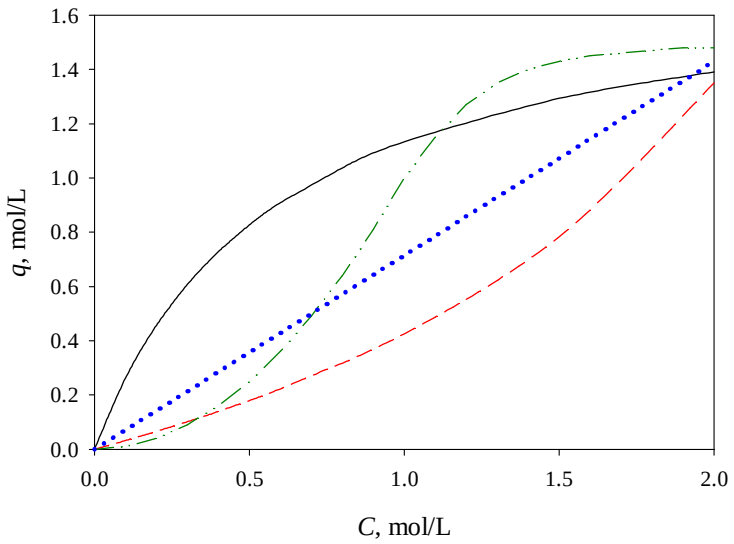

Figure 3. Different types of sorption isotherms: linear (dot), concave downward shaped (solid), concave upward shaped (dash), and S-shaped (dash-dot-dot).

Usually the sorbed amount of component depends on the concentration of this component but also on the concentrations of the other components present in the system [36]. This results from the fact that there is often competition between the components for interaction with the stationary phase, i.e., increase in one component's concentration leads to decreased sorption of the other(s). Competition for sorption between the components depends on the sorption mechanisms. If these mechanisms are different there may be no competition between the components. Or, in some cases, there is even co-operation between the components for sorption, i.e., increase in one component's concentration leads to increased sorption of the other(s) [36,114]. The interactions between components complicate the modelling of the sorption behavior as the competing components must be included in the sorption model of a certain component [36].

3.3 Ion exchange resins

Ion exchangers are insoluble solid materials which carry fixed charges (positive or negative) and exchangeable cations (cation exchanger) or anions (anion exchanger). The most important class of ion exchangers are the ion exchange resins which consist of a polymeric matrix into which functional ionic groups are attached, i.e., they are solid polyelectrolytes. The resin matrix is irregular, macromolecular, three-dimensional network of hydrocarbon chains. Ion exchange resins are made insoluble by crosslinking the polymer chains in the resin matrix. Due to the polymeric nature of the resins, the ion exchange resins can swell and shrink depending on the liquid phase composition [39].

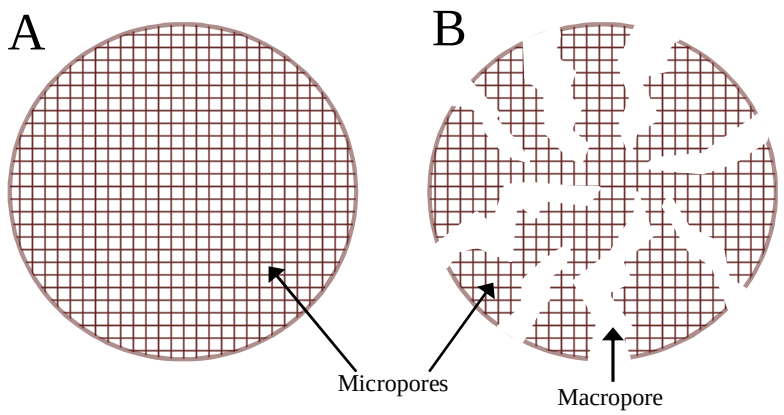

Figure 4. Pore structures of a swollen gel type ion exchange resin (A) and macroporous ion exchange resin (B)

Most common ion exchange resins are made by copolymerization of styrene and divinylbenzene which acts as a crosslinking agent. As a result, a polystyrene–divinylbenzene (PS–DVB) resin is formed. The amount of the crosslinking agent determines the type of the ion exchange resin (Fig. 4). Resins with low degree of DVB (less than 12 %) are gel type

resins into which micropores are formed when the resin swells (Fig. 4). Macroporous resins which contain high amount of DVB, on the other hand, have permanent macropores in addition to the micropores (Fig. 4) [39,116]. The structure of these resins is so rigid that resin swelling is significantly lower than in the case of gel type resins. The large permanent pores of the macroporous resins (Fig. 4) allow the sorption of larger molecules which are unable to enter the pores of gel type resins due to size exclusion effects (see Chapter 4.2.3) [116].

Functional ionic groups are typically added to the resins after the polymerization although they can also be added already to the monomers. These groups have opposite charge than the exchangeable counter-ions which they carry. Depending on the type of the ionic group ion exchange resins are divided into strong and weak resins. The ionic groups in strong ion exchange resins are ionized in the whole pH range, while the ionization of the weak ionic groups depends on the pH. Many different types of ionic groups can be added to the resin matrices. Most common ionic groups in cation exchange resins are sulfonic acid $–SO_3^-H^+$ (strong) and carboxylic acid $–COO^-H^+$ (weak) groups. [39]

In this work, gel type sulfonated ($–SO_3^-$) strong cation exchange resins with PS–DVB matrix in acid (H^+) form are used as a stationary phase. Here, the ion exchange resins act merely as sorbents and charge carriers, and no ion exchange occurs.

4 FUNDAMENTAL PHENOMENA IN CHROMATOGRAPHIC FRACTIONATION OF CONCENTRATED ACID HYDROLYSATES

Chromatographic fractionation of concentrated acid lignocellulosic hydrolysates is based on the electrolyte exclusion chromatography. Although the electrolyte exclusion is the main sorption mechanism in this method, there are also other mechanisms that affect the sorption of the components of the hydrolysates. In the following Chapters, the sorption mechanisms appearing in the separation task at hand will be elucidated. But prior to this, the principles of resin volume changes will be discussed as the stationary phases used in this work are gel type ion exchange resins for which volume changes can be significant.

4.1 Resin volume changes

Ion exchange resins sorb solvents in which they are placed and swell due to this. The swelling results from osmotic pressure difference between the external solution and the resin phase (solution inside the resin pores): the solute concentration is considerably higher in the resin than in the external solution. In order to decrease the osmotic pressure difference, solvent is taken up by the resin to solvate the solutes in the resin pores. This results in swelling of the resin. [38,39]

When ion exchange resins swell, the solvent molecules form solvation shells with the ionic groups and counter-ions of the resin. The swelling continues only until equilibrium is attained. In this equilibrium, the solvation of the ions which causes swelling of the resin is balanced by the elastic forces of the resin matrix (matrix's resistance for stretching). [38,39]

The solution inside the pores of a resin is under higher pressure than the external solution due to the contradictive forces of the resin matrix. This pressure difference is known as the swelling pressure Π [39]:

$$\Pi V_{\mathrm{m,w}} = -RT \ln \bar{a}_{\mathrm{w}} , \tag{5}$$

where $V_{\mathrm{m,w}}$ is partial molar volume of solvent, R is universal gas constant (8.3145 J/(mol K), T is temperature, a_{w} is activity of solvent, and over-bar refers to resin phase. The swelling pressure affects the solvent uptake and, thus, the solvent activity in the resin. Swelling pressure increases when the resin swells due to an increase in the elastic forces opposing the swelling, and also when the degree of resin crosslinking increases due to stronger forces opposing the swelling. Swelling pressure also affects the sorption of solutes; especially larger solutes (see Chapter 4.2.3). [39]

Many forces contribute to resin swelling. The formation of solvation shells for the counter-ions and ionic groups is an important factor contributing to swelling. The electrostatic

repulsion between the ionic groups in the resin also contributes to resin swelling as well as the interactions between the solvent and the resin matrix. [38,39]

Increase in the solute concentration decreases the resin swelling due to decrease in the osmotic pressure difference: solvent is drawn from the resin to solvate the solutes in the bulk solution. This is particularly clear with strong electrolytes which cause considerable decrease in the swelling (i.e., shrinking) at high electrolyte concentrations [38,39].

Polar solvents are better swelling agents than nonpolar solvents due to stronger interactions between the solvent and the ions, and the ionic and the polar groups of the resin. Complete ionization of the ionic groups also increases swelling because of greater solvation. On the other hand, ion pair formation and association of the counter-ions and the ionic groups decreases the solvation tendency and the swelling. Strong affinity of the fixed ionic groups towards the solvent increases the swelling. Ion exchange resins with high ion exchange capacity swell more than resin with small capacity due to the higher ion concentration in the resin which results in higher osmotic pressure difference [38,39].

With gel type resins (weakly crosslinked), the resin swelling depends strongly on the valence of the counter-ion. These resins contain large amounts of “free water”, i.e., solvent not bound to the solvation shells of the ionic species in the resin. The amount of “free water” depends on the number of the counter-ions in the resin which in turn depends on the valence of the ions. When univalent counter-ions are replaced with bivalent ions, the number of counter-ions and the tendency to take up “free water” is cut to half, and the resin swelling decreases [38,39]. For example, swelling of gel type sulfonated PS–DVB resins decreases according to the sequence $Na^{+}>Ca^{2+}>Al^{3+}$ [38]. The “free water” content does not necessarily parallel the resin swelling. For example if a counter-ion is replaced with a counter-ion with larger solvated volume, the resin swells, but at the same time the increased swelling pressure decreases the “free water” content by squeezing it out of the resin [39].

With moderately and highly crosslinked resins the swelling is strongly affected by the solvation tendency and the size of the counter-ion: ions with large solvated volume result in greater swelling. With alkali-ions, the swelling increases according to the sequence $Cs^{+}<Rb^{+}<K^{+}<Na^{+}<Li^{+}$. In very highly crosslinked resins, the ionic solvation may be incomplete due to steric obstructions. In this case, resin swelling depends on the size of the actual ion [39].

The effect of temperature on the swelling of common ion exchange resins is not very significant. Usually the resin swelling increases with increasing temperature due to increase in the elasticity of the resin matrix. [38]

Resin volume changes affect the diffusion of solutes and dispersion of solute bands in column operations. When resin swells the pore size of the resin increases and therefore also the

diffusion rates increase. The opposite is true when resin shrinks. Resin shrinking increases also dispersion and favors channeling especially at the column walls [39].

4.2 Sorption mechanisms

In the chromatographic fractionation of concentrated acid lignocellulosic hydrolysates using stong acid cation exchange resins in acid form as a stationary phase, the electrolyte exclusion is the main sorption mechanism. However, it only affects the sorption of sulfuric acid. The sorption of the other components is affected by van der Waals forces, size exclusion, and salting out. All these mechanisms will be elucidated in this Chapter.

4.2.1 Electrolyte exclusion

Chromatographic separation of strong electrolytes from weak electrolytes and nonelectrolytes is based on the electrolyte exclusion. Strong electrolytes are excluded from the resin phase (i.e., the solution phase inside the resin pores) due to electrostatic interactions (Fig. 5). Associated weak electrolytes and nonelectrolytes are not affected by the electrolyte exclusion and are sorbed to the resin. As a consequence, the strong electrolytes propagate through the column faster than the associated weak electrolytes and nonelectrolytes and separation occurs. No ion exchange occurs in the electrolyte exclusion unless the liquid phase contains ions that are different to the exchangeable counter-ions in the resin [37-39].

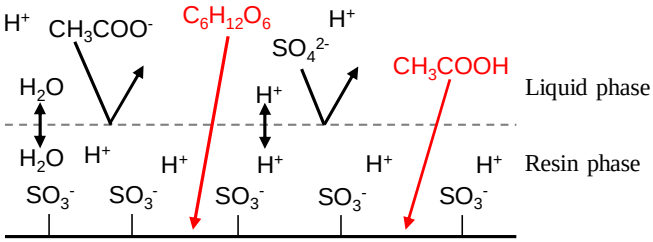

Figure 5. Effect of the electrolyte exclusion on the sorption of a strong electrolyte (sulfuric acid, H_2SO_4), weak electrolyte (acetic acid, CH_3COOH), and nonelectrolyte (glucose, $C_6H_{12}O_6$).

The electrolyte exclusion can be explained in terms of the Donnan potential as follows. When a strong acid cation exchange resin is put into a dilute solution of a strong electrolyte, there exists a large concentration difference between the phases. Cation concentration is higher in the resin phase whereas the mobile anion concentration is higher in the bulk solution phase. Diffusion of the cations from the resin phase to the bulk solution phase and the opposite movement of the anions from the bulk solution phase to the resin phase would erode these concentration differences. However, with ionic species this diffusion would interfere with electroneutrality. The first few ions that try to diffuse create an electrical potential difference between the phases known as the Donnan potential which draws the cations back to the resin

phase and the anions back to the bulk solution phase [37-39]. As the anions of a strong electrolyte cannot diffuse into the resin phase, neither can the cations of the electrolyte as electroneutrality condition must hold in the bulk solution phase. As a consequence, the strong electrolyte is excluded from the resin phase.

The ions' tendency to level out the concentration differences between the phases is counterbalanced by the effects of the electrical field and equilibrium, called the Donnan equilibrium, is formed. The Donnan equilibrium states that the electrical potential of each ion is equal in the bulk solution and resin phases [38,39]. As a consequence, the co-ions (ion with same sign of charge as the fixed ionic groups in the resin) are repelled from the resin phase and, therefore, the counter-ion concentration remains higher and co-ion concentration lower in the resin phase than in the bulk solution phase. The situation is analogous for both cation and anion exchangers; only the sign of the Donnan potential is different. For cation exchangers the Donnan potential is negative, and for anion exchangers it is positive [38].

The Donnan potential, and thus the electrolyte exclusion, depends on many factors [37-39]. The absolute value of the Donnan potential increases with decreasing bulk solution concentration and with increasing resin phase (inside resin pores) counter-ion concentration. Ion exchange resins have high internal counter-ion concentration when the ion exchange capacity is high and the degree of resin crosslinking is high. Resins with high degree of crosslinking swell less than resins with low degree of crosslinking which means that these resins have higher charge density and, thus, cause stronger electrolyte exclusion effect [39].

Complete electrolyte exclusion can be achieved only at infinite dilution. With increasing electrolyte concentration in the bulk solution, the exclusion effect diminishes and eventually vanishes completely [37-39]. Due to this, the sorption isotherms of strong electrolytes are unfavorable (concave upward; see Fig. 3) when the electrolyte exclusion is the main sorption mechanism. In addition, the slopes of the sorption isotherms are zero at infinite dilution due to complete exclusion [37,39,49,107].

Although all kinds of ion exchangers (weak and strong, and anionic and cationic) can be used in the electrolyte exclusion chromatography, the separation efficiency is favored by high ionization level of the functional groups [37,39]. Ion association and ionic pair formation between the counter-ions and the ionic groups localizes counter-ions and weakens the exclusion. For example, when weak cation exchange resins are only partially ionized they sorb acids like nonelectrolytes [39]. Strong ion exchangers perform better in the electrolyte exclusion as their functional groups are totally ionized in the whole pH range [37,39].

The electrolyte exclusion is stronger for counter-ions with low valence due to the fact that the electrostatic force that affects the ion is proportional to the charge of the ion. The Donnan potential required to balance the tendency of the counter-ions to diffuse into the bulk solution is smaller with counter-ions with high valence. However, high co-ion valence leads to

stronger exclusion of electrolytes. Size of the ions also affects the electrolyte exclusion: large ions may be excluded from highly crosslinked resin due to steric effects. [39]

Complex formation between the ions in bulk solution and counter-ions in the resin can also weaken the electrolyte exclusion. For example, sulfuric acid is sorbed on strong base anion exchange resin in sulfate form because the sulfate counter-ions can form HSO_4^--complexes with the protons of sulfuric acid. As a result, one sulfate counter-ion (valence of -2) is replaced by two HSO_4^- counter-ions (valence of -1) and sulfuric acid is sorbed. Sorption of strong electrolytes is also enhanced by increasing temperature and by different interactions between electrolyte and ion exchange resin [38,39].

In some cases, multivalent counter-ions can associate strongly with the functional groups in the resin. This leads to deviations from typical sorption behavior associated with the electrolyte exclusion. Even the sign of the Donnan potential may be reversed, i.e., cation exchanger behaves like an anion exchange resin. This kind of behavior is more pronounced with cation exchangers with tri- or quadrivalent counter-ions. [39]

The effect of the electrolyte exclusion on the sorption of weak electrolytes is small. This is because of the low level of dissociation of the weak electrolytes in the presence of the counter-ions in the resin [37-39]. In addition, for example, with acidic lignocellulosic hydrolysates the high sulfuric acid concentration prevents dissociation of acetic acid [49,107]. Associated weak electrolytes are sorbed to the resin like nonelectrolytes (Fig. 5) [39].

Associated weak electrolytes and nonelectrolytes do not have a direct effect on the electrolyte exclusion [37-39]. However, they can have an indirect effect on the exclusion if they affect the resin swelling. For example, if the swelling increases, the charge density decreases and, therefore, the exclusion effect weakens. The resin shrinking, naturally, has an opposite effect.

In the quantitative treatment of the electrolyte exclusion [39], the system can be assumed to consist of three component types: the resin matrix with the functional groups, the various mobile ionic species, and the solvent. In the electrolyte exclusion, the equilibrium distribution of ionic species between two phases, i.e., bulk solution phase and resin phase (solution inside resin pores), is affected by the electric potential difference between the phase. In equilibrium, the Donnan potential E_{Don}, i.e., the electrical potential difference between the ion exchanger and the bulk solution can be quantitized with [39]

$$E_{\mathrm{Don}} \equiv \overline{\varphi} - \varphi = \frac{1}{x_{\mathrm{i}} F}\left(RT \ln \frac{a_{\mathrm{i}}}{\overline{a}_{\mathrm{i}}} - \Pi V_{\mathrm{m,i}} \right), \tag{6}$$

where φ is electric potential, x_{i} is ionic valence (charge number), F is Faraday constant (96485.31 As/mol), a_{i} is activity of ionic species i, and $V_{\mathrm{m,i}}$ is partial molar volume of i. Eq. (6) holds for any mobile ionic species present in the system when $V_{\mathrm{m,i}}$ is assumed to be

constant. When Eq. (6) is applied to counter-ion, it is seen that the Donnan potential depends on the concentration (or activity) difference between the phases and counter-ion valence. In the case of co-ion, Eq. (6) shows the dependence of the exclusion on E_{Don} and co-ion valence.

Two additional relationships are needed when Eq. (6) is applied to the sorption of a strong electrolyte AY by an ion exchanger in A form. When electrolyte AY is dissociated, the following equality holds

$$x_{\mathrm{A}}\nu_{\mathrm{A}} = -x_{\mathrm{Y}}\nu_{\mathrm{Y}}\,, \tag{7}$$

where ν is the stoichiometric number. Partial molar volume of the electrolyte is

$$V_{\mathrm{m,AY}} = \nu_{\mathrm{A}}V_{\mathrm{m,A}} + \nu_{\mathrm{Y}}V_{\mathrm{m,Y}}\,. \tag{8}$$

To obtain equation for the sorbed amount of the electrolyte, Eqs. (6) for both mobile ionic species, A and Y, are first combined with Eqs. (7) and (8) [39]:

$$RT\ln\left[\left(\frac{a_{\mathrm{A}}}{\overline{a}_{\mathrm{A}}}\right)^{\nu_{\mathrm{A}}}\left(\frac{a_{\mathrm{Y}}}{\overline{a}_{\mathrm{Y}}}\right)^{\nu_{\mathrm{Y}}}\right] = \Pi V_{\mathrm{m,AY}}\,. \tag{9}$$

By replacing the product of the cation and anion activities in Eq. (9) with mean activity $a_{\pm}$

$$\left(a_{\pm}\right)^{\nu} = \left(a_{\mathrm{A}}\right)^{\nu_{\mathrm{A}}}\left(a_{\mathrm{Y}}\right)^{\nu_{\mathrm{Y}}}, \tag{10}$$

where $\nu = \nu_{\mathrm{A}} + \nu_{\mathrm{Y}}$, and by substituting Eq. (5) into Eq. (9), one obtains the general thermodynamic formulation of the Donnan equilibrium [39]

$$\left(\frac{\overline{a}_{\pm}}{a_{\pm}}\right)^{\nu} = \left(\frac{\overline{a}_{\mathrm{w}}}{a_{\mathrm{w}}}\right)^{V_{\mathrm{m,AY}}/V_{\mathrm{m,w}}}\,. \tag{11}$$

Mean activities and ionic molalities m_{i} are interrelated in the solution and the resin phases by

$$\left(a_{\pm}\right)^{\nu} = \left(m_{\mathrm{A}}\right)^{\nu_{\mathrm{A}}}\left(m_{\mathrm{Y}}\right)^{\nu_{\mathrm{Y}}}\left(\gamma_{\pm}\right)^{\nu}, \tag{12A}$$

$$\left(\overline{a}_{\pm}\right)^{\nu} = \left(\overline{m}_{\mathrm{A}}\right)^{\nu_{\mathrm{A}}}\left(\overline{m}_{\mathrm{Y}}\right)^{\nu_{\mathrm{Y}}}\left(\overline{\gamma}_{\pm}\right)^{\nu}, \tag{12B}$$

where $\gamma_{\pm}$ is the molal mean activity coefficient of an electrolyte. Electroneutrality conditions in the bulk solution phase and the resin phase are

$$\left|x_{\mathrm{A}}\right| m_{\mathrm{A}} = \left|x_{\mathrm{Y}}\right| m_{\mathrm{Y}}\,, \tag{13A}$$

$$\left|x_{\mathrm{A}}\right| \overline{m}_{\mathrm{A}} = \overline{m}_{\mathrm{group}} + \left|x_{\mathrm{Y}}\right| \overline{m}_{\mathrm{Y}}\,, \tag{13B}$$

where $\overline{m}_{\mathrm{group}}$ is the molality of the functional groups in the resin.

By substituting Eqs. (12) and (13) into Eq. (11) one obtains [39]

$$\left(\frac{\overline{m}_{\mathrm{Y}}}{m_{\mathrm{Y}}}\right)^{\nu_{\mathrm{Y}}} = \left(\frac{|x_{\mathrm{Y}}|m_{\mathrm{Y}}}{|x_{\mathrm{Y}}|\overline{m}_{\mathrm{Y}} + \overline{m}_{\mathrm{group}}}\right)^{\nu_{\mathrm{A}}} \left(\frac{\gamma_{\pm}}{\overline{\gamma}_{\pm}}\right)^{\nu} \left(\frac{\overline{a}_{\mathrm{w}}}{a_{\mathrm{w}}}\right)^{V_{\mathrm{m,AY}}/V_{\mathrm{m,w}}} . \tag{14}$$

The last factor on the right hand side of Eq. (14) accounts for the effects of swelling pressure and ionic size on the electrolyte sorption. These effects are usually small [39].

For electrolytes with $\nu = 2$ (e.g., 1,1-valent; 2,2-valent; etc.), Eq. (14) can be solved for the molality of the co-ion in the resin phase [39]

$$\overline{m}_{\mathrm{Y}} = \frac{1}{|x_{\mathrm{Y}}|}\left[\frac{\left(\overline{m}_{\mathrm{group}}\right)^2}{4} + \left(x_{\mathrm{Y}} m_{\mathrm{Y}}\right)^2 \left(\frac{\gamma_{\pm}}{\overline{\gamma}_{\pm}}\right)^2 \left(\frac{\overline{a}_{\mathrm{w}}}{a_{\mathrm{w}}}\right)^{V_{\mathrm{m,AY}}/V_{\mathrm{m,w}}}\right]^{1/2} - \frac{\overline{m}_{\mathrm{group}}}{2|x_{\mathrm{Y}}|} . \tag{15}$$

The sorbed amount of electrolyte can be obtained from the molality of the co-ion in the resin.

For very dilute solutions ($m_{\mathrm{Y}} << \overline{m}_{\mathrm{group}}$) Eq. (15) reduces to [39]

$$\overline{m}_{\mathrm{Y}} = \left(m_{\mathrm{Y}}\right)^2 \frac{|x_{\mathrm{Y}}|}{\overline{m}_{\mathrm{group}}} \left(\frac{\gamma_{\pm}}{\overline{\gamma}_{\pm}}\right)^2 \left(\frac{\overline{a}_{\mathrm{w}}}{a_{\mathrm{w}}}\right)^{V_{\mathrm{m,AY}}/V_{\mathrm{m,w}}} \tag{16}$$

The unfavorable shape of the sorption isotherm of strong electrolyte can be clearly seen from Eqs. (15) and (16) as $\overline{m}_{\mathrm{Y}}$ is directly proportional to the square of the molality of the co-ion m_{Y} in the bulk solution.

4.2.2 van der Waals forces

Sorption of nonelectrolytes (and associated weak electrolytes) on an ion exchange resin with a hydrocarbon matrix is affected by van der Waals forces (London interactions and dipole–dipole interactions). These interactions favor local sorption of hydrocarbon groups of solutes to the resin matrix and, thus, enhance the sorption of nonelectrolytes and associated weak electrolytes. London interactions between the solute molecules and the resin matrix are weak interactions and depend on the molecular structure of the hydrocarbon chains of the solutes and of the matrix: if these are of similar type, stronger sorption occurs. [38,39]

Dipole–dipole interactions between polar solvent molecules, and between solvent and solute molecules are strong interactions [38,39]. As a result from these interactions organic solutes tend to coagulate or to be squeezed out of the polar solution onto a phase boundary. [39]

With ion exchange resins, interactions between polar solute groups and fixed ionic groups or counter-ions may be the strongest factor enhancing or reducing sorption. The ionic groups render the resins into strongly polar sorbents which tend to sorb polar substances more strongly than nonpolar [38,117]. Repulsive forces may also exist between the polar fixed ionic groups and nonelectrolytes [117]. In addition, solvation of fixed ionic groups with the solute molecules can be one sorption mechanism with ion exchange resins. [38,39]

Usually the sorption isotherms of nonelectrolytes are favorable (concave downward; see Fig. 3) at least to some extent [38,39]. However, exceptions to this kind of sorption behavior can also be found [107,118-121]. For example the sorption isotherms of monosaccharides on strong acid cation exchange resins are slightly unfavorable (see Fig. 3). This is due to non-idealities in the solution phase resulting from small distribution coefficients [118-121].

4.2.3 Size exclusion

Molecular size of the sorbing components may also affect the sorption. Large molecules might not be sorbed because their size prevents their diffusion into the pores of the stationary phase (Fig. 6) [39,114].

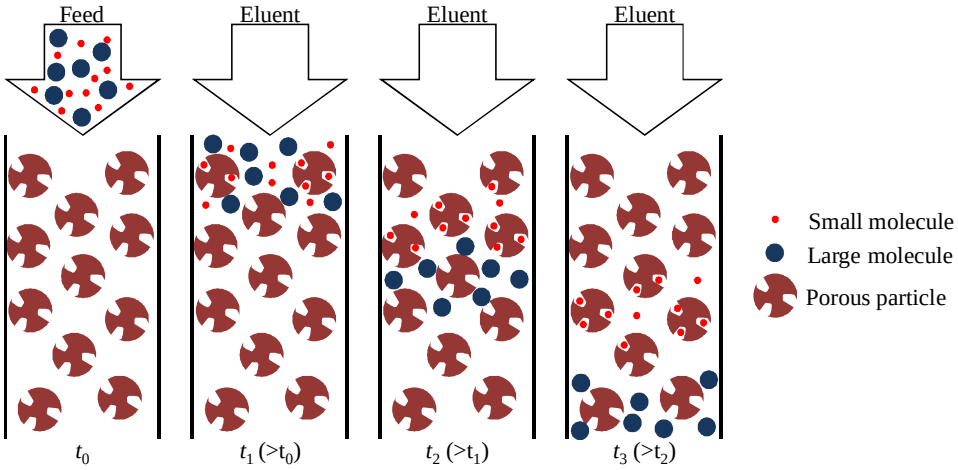

Figure 6. Effect of size exclusion on the elution of solutes: large molecules are excluded from the sorbent and propagate fast through the column.

With resins that swell and shrink considerably due to changes in the bulk solution phase composition, the pore size, and, therefore, also the effect of size exclusion on the sorption, depends on resin swelling. Those components that cause strong swelling (increase in pore size) are more easily sorbed [38]. If the size exclusion is the main mechanism affecting the sorption of a component, the sorption isotherm is of form

$$q = \omega C\,,\ 0 \le \omega \le 1. \tag{17}$$

In Eq. (17), the value of ω is less than unity due to the exclusion.

The degree of resin crosslinking also affects the sorption of solute molecules of different sizes through swelling pressure (see Chapter 4.1) which tends to squeeze solvent and solute molecules out of the resin phase. Large molecules are more strongly affected than small ones. The importance of the swelling pressure effect increases as the degree of resin crosslinking and solute molecule size increase. [39]

4.2.4 Salting out

Salting out is a special case of partition chromatography in which the separation is based mainly on the differences between the solubilities of the solutes in the liquid and stationary phases (solution in the resin pores) [122]. In the salting out chromatography, addition of a salt to a bulk solution decreases the solubility of organic nonelectrolytes and associated weak electrolytes to the bulk solution. These components are salted out from the bulk solution phase to the solution phase inside the resin pores (co-operative effect on sorption) [117,123].

The salting out tendency of ions follows the so-called Hofmeister series [124-129]. The effectiveness of the salting out capability in decreasing order for the cations is [126,129]

$$N(CH_3)_4^+ > NH_4^+ > Cs^+ > Rb^+ > K^+ > Na^+ > Li^+ Mg^{2+} > Ca^{2+}, \quad (18)$$

and for the anions is

$$CO_3^{2-} > SO_4^{2-} > OH^-, F^- > Cl^- > Br^- > NO_3^- > I^- > ClO_4^- < SCN^-. \quad (19)$$

The mechanism how the electrolyte ions affect the solubility of the solutes (e.g., proteins) is not entirely clear [124-129]. However, at the moment it is believed that the ions have both direct and indirect specific effects on the solute molecules [125-128]. The indirect effect means that the ions affect the water structure around solutes which in turn affects the physical properties of these solutes [39,127]. The ions can be classified into two classes: kosmotropes and chaotropes. Of these, the first mentioned interact strongly with the water molecules increasing the ordering of the water molecules around the salt ions (solvation) and, thus, causing salting out of neutral solutes, i.e., decrease the solubility. Chaotropes, on the other hand, interact only weakly with the water molecules making the nearby water less ordered and, therefore, causing salting in of solutes, i.e., increase the solubility [125-128].

The indirect salting out effect (Fig. 7) with ion exchange resins can be explained as follows. Only “free water”, i.e., the water that is not bound to ionic solvation shells, is available for dissolving nonelectrolytes and associated weak electrolytes. Inside the pores of an ion exchange resin, the “free water” content is low due to solvation of the fixed ionic groups and the counter-ions. Due to this, nonelectrolytes are salted out from the resin phase to the bulk solution phase where the “free water” content is higher [39]. However, with ion exchange resins the salting out works in two ways. If a strong electrolyte is added to the bulk solution, nonelectrolytes are salted out from the solution to the resin phase and their sorption increases.

At least in the case of proteins and other macromolecules, the direct effect of salt ions is thought to be more important than the indirect effect [124-129]. The electrolyte ions interact directly with the surface of the solute changing the surface charge of the molecules by sorbing to the molecule surface. For example, large halide anions (I^-, Br^-) are less effective salting out agents than small halide anions (F^-, Cl^-) in the case of neutral solutes. Larger halides sorb on the protein surface and give the surface a negative charge which leads to surface–surface

repulsion and therefore stabilization of neutral solutes, i.e., salting out does not occur [129]. For proteins, the direction of the anionic Hofmeister series (Eq. (19)) depends on the sign of the surface charge and on the polarity of peptide side chains: the solubility of the neutral and negatively charged proteins follows the order given in Eq. (19) while for positively charged proteins the order is reversed [129].

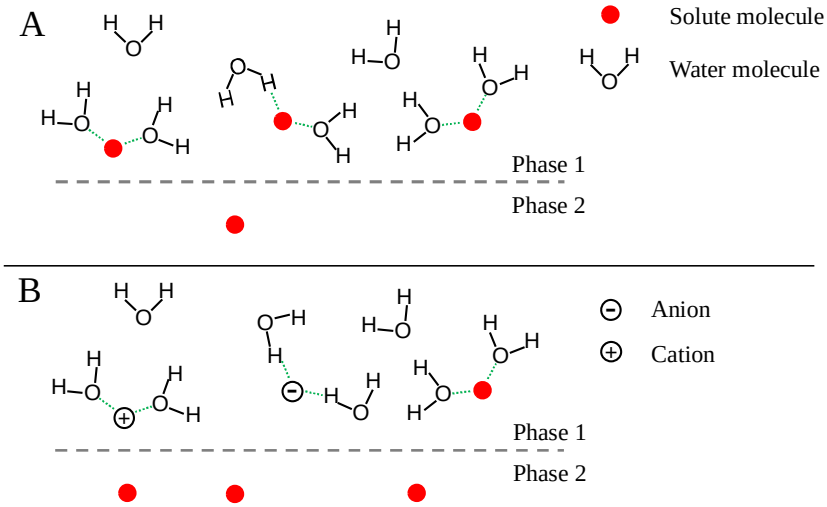

Figure 7. Illustration of the indirect effect of salt ions on the distribution of a solute between phases in a two-phase system. A = phase 1 contains pure water; B = phase 1 contains added salt.

Regardless the mechanism of salting out effect, the quantitative treatment can be done as follows. If sorption of a solute N in the presence of a strong electrolyte is enhanced by salting out the sorption isotherm of N can be formulated as

$$q_{\mathrm{N}} = \omega a_{\mathrm{N}} = \omega \gamma_{\mathrm{N}} C_{\mathrm{N}}\,, \tag{20}$$

where a_{N} is the activity of N and γ_{N} is the activity coefficient of N. In salting out, the strong electrolyte affects the activity of N. In the simplest case, γ_{N} can be obtained from the empirical Setchenov equation [49]

$$\gamma_{\mathrm{N}} = \frac{k_S}{\ln 10} I\,, \tag{21}$$

where k_{S} is the conventional salting out (Setchenov) coefficient and I is ionic strength. On molar scale I is given by

$$I = \frac{1}{2}\sum_{\mathrm{i}=1}^{\mathrm{n}} C_{\mathrm{i}} \left(x_{\mathrm{i}}\right)^2 . \tag{22}$$

Summation in Eq. (22) goes through all ions present in the system.

5 MULTI-COLUMN CHROMATOGRAPHIC PROCESSES

In addition to the single-column batchwise chromatographic separation process, there are also a number of multi-column processes available for chromatographic separations. Most of these are continuous or semi-continuous, but also batchwise multi-column processes are known (see below). When properly optimized, these schemes can yield lower eluent consumption, higher productivity, higher product concentrations, higher product purities, and enhanced utilization of the stationary phase [36,130]. In addition, they are easy to scale up or down [36].

Naturally, the optimal process scheme depends on the separation task. Some of the multi-column processes available are only capable for binary separations in one step while others are applicable to ternary or even more complex separations.

In this work, concentrated acid lignocellulosic hydrolysates are fractionated into three fractions using the electrolyte exclusion chromatography: sulfuric acid fraction, monosaccharide fraction, and acetic acid fraction. Other by-products than acetic acid formed in the hydrolysis are assumed to be removed by adsorption [33,52-56] prior to the acid–monosaccharide separation (see Fig. 1). Chromatographic processes for binary fractionations are not applicable in this case as the goal is to do the fractionation in a single step.

In this Chapter, three multi-column process options available for chromatographic separations are introduced: the basic four-zone simulated moving bed (SMB), the Japan Organo (JO) process, and the Multi-Column Recycling Chromatography (MCRC). Of these, the first mentioned can only be applied for binary separation in one step. Therefore, it is not applicable for the separation task at hand. However, it is introduced as it is crucial for understanding the operating principle of more advanced SMB schemes, like the JO process.

5.1 Four-zone simulated moving bed process

Continuous processes are most efficiently carried out in a counter-current manner. In chromatography, this means that the solid and liquid phases should move counter-currently. However, this kind of truly continuous chromatographic counter-current processes (true moving bed, TMB) do not exist as the counter-current movement of the solid and liquid phases is challenging to implement [36,114,130]. Nevertheless, the TMB process remains as an important concept in theoretical studies.

Due to the impracticality of the TMB process, continuous chromatographic separation processes are implemented as multi-column simulated moving bed (SMB) processes (Fig. 8). In SMB, continuous counter-current movement of solid and liquid phases is simulated by periodically shifting the column inlet and outlet ports in the direction of the liquid flow [36]. If the time between the port switching and the columns are infinitely short, SMB and TMB processes are equal [36].

The SMB was originally developed for separations in petrochemical industry [131]. Today variations of this process can be found from petrochemical industry [64,65,131], sweeteners industry [60,61,132,133], fine chemicals industry, and pharmaceutical industry [134-141].

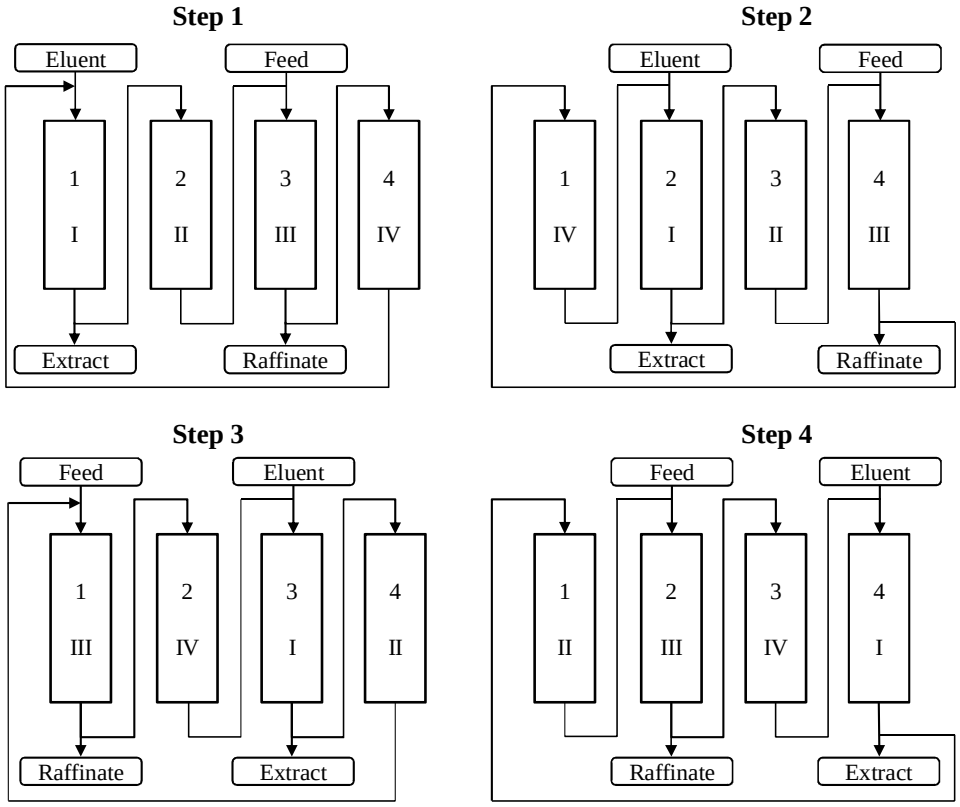

Figure 8. Four-zone simulated moving bed chromatographic process with four columns for binary separations. Eluent = eluent inlet stream, Feed = feed inlet stream, Extract = outlet stream of the most retained component, Raffinate = outlet stream of the least retained component. Arabic numerals stand for column number and Roman numerals stand for SMB zone number.

A conventional SMB process for binary fractionations consists of four zones which all have different functions (Fig. 8). The basic four-zone SMB process is divided into zones by two inlets (feed and eluent) and two outlets (extract and raffinate). Each zone contain one or more columns. Desorption of the more retained component occurs in zone I which is located between the eluent inlet and extract outlet ports (Fig. 8). Regeneration of the solid phase occurs in this zone. Zone I also prevents the movement of the more retained component from zone I to zone IV (through the recycling stream) and is therefore called buffer zone. [36]

The actual separation occurs in Zones II and III (Fig. 8). Zone II is located between the extract outlet and feed inlet ports (Fig. 8). Desorption of the less retained component occurs in zone

II. The columns between the feed inlet and raffinate outlet ports belong to zone III (Fig. 8). Sorption of the more retained component occurs in this zone. Components of a binary mixture have overlapping profiles in zones II and III. [36]

The last zone in the SMB train, zone IV, is for the sorption of the less retained component. It contains the columns between the raffinate outlet and eluent inlet ports (Fig. 8). It functions also as a buffer zone: the movement of the less retained component from zone IV to zone I is prevented with zone IV. [36]

Eluent and feed solution are continuously introduced to the first columns of zones I and III, respectively. The less retained component is continuously taken out from the system as raffinate stream at the outlet of the last column of zone III. Likewise, the more retained component is taken out as extract stream at the outlet of the last column of zone I. [36]

When the ports in an SMB system are shifted towards the liquid flow (Fig. 8) the solid phase moves to the opposite direction. In the example process shown in Fig. 8, this means that the position of column 3 is shifted from zone III to zone II, and the position of column 2 is shifted from zone II to zone I, etc. If the SMB zones would contain more than one column, then each column would be shifted one position to opposite direction of the liquid flow. For example, if zone III would contain three columns, the first column of zone III would become the last column of zone II, the middle column of zone III would become the first column of zone III, the last column would become the middle column of zone III, and the first column of zone IV would become the last column of zone III.

The separation of components of a binary mixture in an SMB process is achieved by adjusting the flow rates and the port switching time. The more retained component should move with the solid phase toward the extract outlet and the less retained component with the liquid phase towards the raffinate outlet. In other words, the less retained component should be made to propagate faster than the port switching and the more retained component slower than the port switching. [36]

5.2 Japan Organo process

The Japan Organo (JO) process (also known as the Pseudo SMB) is an SMB process that can be used to accomplish ternary (or more complex) fractionations. The origins of this process are in the sweeteners industry [60,64,65,142,143].

One cycle of the JO process consists of two steps (Fig. 9). In step 1, the feed stream is introduced to the system through the inlet of the first column of zone III, and the intermediately retained component is taken out from the system at the outlet of the last column of zone II. Eluent is fed through the inlet of the first column of zone I (Fig. 9). Feeding of the eluent in step 1 is not necessary but may improve the separation performance

[60]. The column train is disconnected between the zones II and III. Flow rates in zones I and II are equal as well as the flow rates in zones III and IV. More than one component can be withdrawn consecutively from the end of zone II in step 1 due to the batchwise operation mode. Raffinate and extract ports can also be open in step 1 allowing the withdrawal of the least and most retained components, respectively [60].

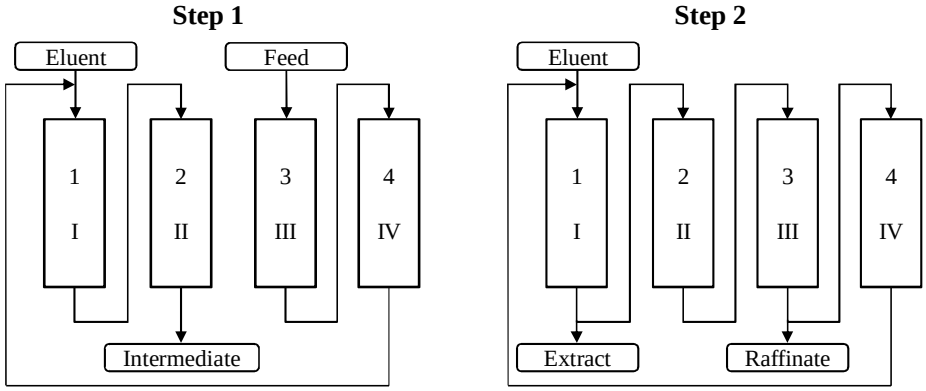

Figure 9. Japan Organo process for ternary fractionations. Intermediate = outlet stream of the intermediately retained component; for the designations of the other streams, see caption of Fig. 8.

In step 2, only eluent is introduced to the system (Fig. 9). The system is operated like a standard four-zone SMB without the feed stream: flow rates in zones II and III are equal [60,142]. The least and most retained components are taken out from the system in raffinate and extract streams, respectively [60,64,65,142]. Step 2 is continued for several SMB switches before step 1 is conducted again. In the end of step 2, the intermediately retained component should be located upstream from the feed point (in zone II) so that it can be collected during the next cycle (first step) [60,64,65].

The number of switches in step 2 can be equal or different to the number of columns. If they are equal, the feed is always introduced to the same column [64,65]. The amount of feed can be increased as the number of port switches in step 2 increases. This is because the effective column length increases with increasing number of port switches, and larger amounts of the least and most retained components can be separated from the intermediate component. If the amount of feed is larger than the loading capacity of zone III, the raffinate and extract streams may become contaminated with the intermediate component [64].

Duration of step 1 depends on the elution of the intermediate component. Too short duration leads to the contamination of the extract stream with the intermediate component as too low amount of it is removed in step 1. On the other hand, too long duration leads to contamination of the intermediate component's outlet stream with the most retained component. For the duration of step 2, the effects are opposite [65].

5.3 Multi-Column Recycling Chromatography

In addition to the continuous or semicontinuos SMB processes also multi-column batchwise chromatographic processes have been introduced. Finnish Sugar Co. (now part of DuPont) has developed a multi-column separation process, known as the Sequential SMB, for the fractionation of sugar beet molasses into salt, sucrose, and betaine fractions using the electrolyte exclusion chromatography [61,144-148]. Despite its name, there is no counter-current movement of the liquid and solid phases as in conventional SMB processes: the ports are not switched synchronously in the direction of the fluid flow during a cycle [36,61,144-148]. In addition, in the Sequential SMB, column outlet streams are not split at product collection nodes (extract and raffinate) as in SMBs. Instead the whole stream is taken out of the system or led to the next column. One thing common for both processes is the cyclic operation mode [36,61,144-148]. The Sequential SMB can be operated already with two columns, while typically three to eight columns are used [61,144-148]. Here, the Sequential SMB is termed as the *Multi-Column Recycling Chromatography* (abbreviated as MCRC).

One cycle in the MCRC process consists of three operations: feeding, elution, and closed loop recycling (Fig. 10). Each operation is conducted at least once in a full cycle. They can be conducted in series or they can overlap. For example, recycling can be carried out in a closed loop of two columns while simultaneously eluent is fed to and products are collected from one other column [61,144].

In the feeding operation (Fig. 10A), the feed mixture is introduced to at least one column. Simultaneously, eluent can be fed to at least one other column, and at least one product fraction is collected. If products are withdrawn from the same column where the feed is introduced into (Fig. 10A), the eluent consumption is typically reduced because the feed is used to elute the solutes in this column [61,144-148].

During the elution operation there is no feeding (Fig. 10B). The eluent is fed to at least one column and simultaneously product fractions are collected from at least one column [61,144]. The duration of this step depends on the set purity constraints.

In the closed loop recycling operation, liquid inside the columns is circulated in at least one closed loop (Fig. 10C). No eluent or feed is introduced into the process and no products are withdrawn. Besides further separating the components, the purpose of such closed loop recycling is to adjust their positions relative to the outlets for product collection in the next step [61,144]. The eluent consumption can often be lowered considerably by the closed loop recycling.

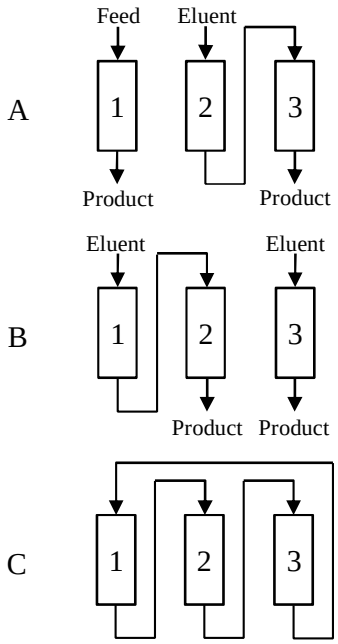

Figure 10. Illustration of operations carried out in a cycle of a Multi-Column Recycling Chromatography process. A = feeding; B = elution; C = closed loop recycling.

If the separation of components is not sufficient at the outlet of the last column, the stream from the last column can be recycled to the first column to be processed during the following cycle. Such recycle fractions are termed as *prefeed fraction* (recycled before the next feeding) or *postfeed fraction* (recycled immediately after the next feeding). In ternary fractionation, the prefeed fraction typically contains the mixture of the first and the intermediate eluting components, whereas the postfeed fraction contains the mixture of the intermediate and the last eluting component.

The eluent consumption in the MCRC process can be lowered also by reintroducing parts of the collected product fractions back to the process as eluent substitute. Position and time of such reintroduction must be so that the components in these fractions do not end up as impurities to wrong product fractions. This method is also beneficial for the product yield and purity. [148]

6 MODELLING

6.1 Phase equilibrium

Accurate phase equilibrium models are essential for the rigorous modelling of chromatographic separation processes. The phase equilibria models include the sorption isotherm models and the possible model for resin volume changes.

Outside this work, Laatikainen *et al*. [49] have presented a rigorous phase equilibrium model that is suitable for modelling the phase equilibria in the system studied here. Although the model of Laatikainen *et al*. [49] is thermodynamically rigorous, it contains a large number of adjustable parameters and needs to be solved iteratively; which is time consuming. Thus, it is poorly suited for process design and optimization purposes.

In this work, the goal is to present a model that is accurate but also suitable for process design and optimization purposes of the chromatographic fractionation of concentrated acid hydrolysates. Two different approaches to the modelling of the sorption equilibria were used here: a simple nonlinear empirical isotherm models that take into account solute interactions, and the Adsorbed Solution theory [57-59]. Sorption equilibria were modeled only in the case of one stationary phase used in this work: sulfonated gel type strong acid cation exchange resin in acid form with PS-DVB matrix (8 wt. % DVB content, CS16GC, Finex Oy, Finland).

As gel type resins were used as a stationary phase in this work, the resin volume changes resulting from changes in the solution composition had to be taken into account in the modelling. In here, a simple empirical equilibrium model was used to model these changes.

6.1.1 Empirical approach for the sorption equilibrium

A sorption model which is suitable for process design purposes was developed in this work for the chromatographic fractionation of concentrated acid lignocellulosic hydrolysates on a strong acid cation exchange resin in acid form. Simple empirical isotherm models that take into account the solute interactions were used to describe the sorption of the main components (sulfuric acid, monosaccharides, and acetic acid) of these hydrolysates. As for the monosaccharides, only glucose and xylose sorption was modeled due to the fact that other monosaccharides present in the studied system behave similarly as these two (see Ref. [46]).

Sorption of sulfuric acid on a strong acid cation exchange resin in acid form is affected by the electrolyte exclusion. At infinite dilution, the electrolyte exclusion is complete and sulfuric acid sorption is zero. Due to this, the slope of the isotherm must be zero at infinite dilution. A simple power law type model was used to describe the sulfuric acid sorption:

$$q_{\mathrm{H2SO4}} = \alpha_{\mathrm{H2SO4}} (C_{\mathrm{H2SO4}})^{\beta_{\mathrm{H2SO4}}}, \tag{23}$$

where α and β are positive parameters.

Monosaccharide sorption isotherms on a strong acid cation exchange resin in acid form were found to be slightly unfavorable. Similar behavior of monosaccharides has also been observed earlier with strong acid cation exchange resin in calcium form [118-121] and in acid form [41]. This isotherm shape originates from non-idealities in the liquid phase resulting from small distribution coefficients [118-121].

In this work, it was noticed that sulfuric acid has a strong co-operative effect on the sorption of the other components present in the studied system. This effect was first observed by Neuman *et al*. [40] for sorption of glucose in the presence of sulfuric acid, and verified later for glucose, xylose, acetic acid, furfural, and HMF by Laatikainen *et al*. [49] The co-operative effect is due to salting out phenomenon (see Chapter 4.2.4).

The sorption of glucose and xylose on a strong acid cation exchange resin in acid form can be described with a simple anti-Langmuir type isotherm model

$$q_{\mathrm{k}} = \frac{(\alpha_{\mathrm{k}} + \beta_{\mathrm{k}} C_{\mathrm{H2SO4}}) C_{\mathrm{k}}}{1 - \sum_{\mathrm{j}=1}^{\mathrm{n}} \kappa_{\mathrm{j}} C_{\mathrm{j}}}, \tag{24}$$

in which the co-operative effect of sulfuric acid on the sorption is taken into account as a linear dependency of the Henry constant on the liquid phase concentration of sulfuric acid. In Eq. (24) κ is a positive parameter, subscript k stands for glucose and xylose, and the sum in the nominator stands for the total monosaccharide concentration.

Acetic acid is a weak electrolyte ($K_{\mathrm{a}} \approx 1.6 \cdot 10^{-5}$ mol/L at 50 °C [149]). In concentrated acid hydrolysate and in presence of a strong acid cation exchange resin in acid form, acetic acid can be assumed to be completely associated. Therefore it can be treated as a nonelectrolyte. In the concentration range in which acetic acid is found in the lignocellulosic hydrolysates, the sorption of acetic acid on a strong acid cation exchange resin in acid form can be described with a linear isotherm model

$$q_{\mathrm{AcOH}} = (\alpha_{\mathrm{AcOH}} + \beta_{\mathrm{AcOH}} C_{\mathrm{H2SO4}}) C_{\mathrm{AcOH}}. \tag{25}$$

Also in Eq. (25) the co-operative effect of sulfuric acid on the sorption is taken into account as a linear dependency of the Henry constant on C_{H2SO4}.

6.1.2 Prediction of the sorption equilibrium with Adsorbed Solution theory

In addition to the use of the simple empirical sorption isotherm models, a thermodynamically more consistent approach to the multi-component sorption equilibrium was also taken. This approach is based on the well-known Ideal Adsorbed Solution (IAS) theory [57-59] developed by Myers and Prausnitz [58], and Radke and Prausnitz [59].

In the IAS theory both the fluid and adsorbed phase (on a solid stationary phase) are assumed to be ideal. When this assumption is not valid, a more general model, the Real Adsorbed Solution (RAS) theory can be used. In this model the adsorbed phase activity coefficients are taken into account [57,150-155]. A further hardly applied approach to reality can be made by assuming that both adsorbed and liquid phases are nonideal: the Adsorbed Solution theory. This approach had to be used in this work due to the complexity of the studied system.

Conventionally, the implicit algebraic equations of the IAS theory, and also those of the extended models, are solved iteratively [57,150-155]. However, recently Rubiera Landa *et al*. [156] presented a non-iterative solution method for the IAS theory equations. This method is is easy to implement and fast to compute [156]. In this work, the novel method of Rubiera Landa *et al*. [156] was used to solve the equations of the Adsorbed Solution (AS) theory.

Pure component sorption equilibrium. In order to take nonideal behavior of the liquid phase into account, liquid phase concentration C was substituted by the liquid phase activity a_i by introducing liquid phase activity coefficients γ_i:

$$a_\mathrm{i} = \gamma_\mathrm{i} C_\mathrm{i} . \tag{26}$$

These activities were used in the single component sorption isotherm models directly by just exchanging C_i by a_i. No detailed discussion regarding the physical relevance of the original and the modified single component isotherm models is attempted here. For the purpose of this work, the single component isotherm models given below are seen as a tool to quantify the single component behavior sufficiently accurately as required in the mixture theories.

Sorption of acetic acid can be described with a model analogous to the single component Langmuir isotherm [36]

$$q_\mathrm{AcOH} = \frac{q_\mathrm{sat,AcOH}\omega_\mathrm{1,AcOH}a_\mathrm{AcOH}}{1+\omega_\mathrm{1,AcOH}a_\mathrm{AcOH}} . \tag{27}$$

Sorption of glucose and xylose can be modeled using a model analogous to the quadratic isotherm [36] which can reproduce the unfavourable shape of the monosaccharide isotherms

$$q_\mathrm{i} = \frac{q_\mathrm{sat,i}(\omega_\mathrm{1,i}a_\mathrm{i} + 2\omega_\mathrm{2,i}a_\mathrm{i}^2)}{1+\omega_\mathrm{1,i}a_\mathrm{i} + \omega_\mathrm{2,i}a_\mathrm{i}^2}, \ \mathrm{i = glucose, xylose} . \tag{28}$$

For sulfuric acid, a sorption model analogous to the Redlich-Peterson model [36] can be used

$$q_\mathrm{H2SO4} = \frac{\omega_\mathrm{1,H2SO4}a_\mathrm{H2SO4}}{1+\omega_\mathrm{2,H2SO4}\left(a_\mathrm{H2SO4}\right)^{\tau_\mathrm{H2SO4}}} \tag{29}$$

where τ is a parameter.

Multi-component sorption equilibrium. The fundamental equations of the Adsorbed Solution theory are analogous to those of the IAS theory with the addition of certain adsorbed phase activity coefficients [57,150-155]. The solution method of Rubiera Landa *et al*. [156] used in this work is presented in Paper IV. It should be emphasized that the use of liquid or adsorbed phase activities does not change the essential features of this method.

Calculation of the activity coefficient for both liquid and adsorbed phase presented in Paper IV. The activity coefficients in the liquid phase were calculated using the well-known generalized Pitzer model [157,158] which was modified by Fernández-Mérida *et al*. [159] to be better suited for polar nonelectrolytes (e.g., monosaccharides). Due to the complexity of the studied system, the simple empirical Setchenov equation (Eq. (21)) was not applicable for the calculation of activity coefficients of the monosaccharides and acetic acid in the presence of sulfuric acid. Adsorbed phase activity coefficients of sulfuric acid were calculated with an empirical activity coefficient model derived in this work. For other components, adsorbed phase activity coefficients were taken as unity.

6.1.3 Resin volume changes

Modelling of the chromatographic fractionation of concentrated acid lignocellulosic hydrolysates using a gel type strong acid cation exchange resin in acid form as a stationary phase is complicated due to changes in the resin volume. These changes occur when the solution phase composition changes during the separation. Accurate modelling of the resin volume changes is crucial in order to precisely model the separation task at hand.

Many approaches to model resin volume changes in sorption processes have been applied [160-164]. In aqueous solutions, the activity of water is the main solution property of interest (see Eq. (5)) [39]. In this work, it is demonstrated that the volume changes of the strong acid cation exchange resin particles can be directly related to the sorbed amount of sulfuric acid. A simple empirical correlation for the extent of resin volume changes was applied

$$\theta = \frac{V_{\text{bed,acid}}}{V_{\text{bed,water}}} = 1 - \frac{\delta_1 q_{\text{H2SO4}}}{\delta_2 + q_{\text{H2SO4}}}, \tag{30}$$

where θ is the extent of resin shrinking i.e., the ratio of resin bed volume (V_{bed}) in sulfuric acid to resin bed volume in water, q_{H2SO4} is the sorbed amount of sulfuric acid, and δ_1 and δ_2 are positive parameters. Eq. (30) is scaled so that θ is unity in pure water.

6.2 Dynamic column model

Prior to this work, several dynamic column models have been used for the modelling of chromatographic fractionation of acidic lignocellulosic hydrolysates [40,41,42,46]. The first dynamic column models used were an equilibrium-dispersive model used by Neuman *et al*. [40] and a plate model used by Nanguneri and Hester [41]. A more accurate column model,

the VERSE (VErsatile Reaction and SEparation) model including column mass balances for both bulk solution and resin pore solution, and the possibility for chemical reaction was used by Wooley *et al*. [42] and Xie *et al*. [46]. Unfortunately, these models are not adequate for the modelling of the fractionation of concentrated acid hydrolysates with gel type cation exchange resins. This is because these models do not take into account volume changes of the gel type resin caused by sulfuric acid in the hydrolysates.

Outside this work, Laatikainen *et al*. [49] have also presented a dynamic model that is suitable for the modelling of the chromatographic fractionation of concentrated acid hydrolysates with gel type cation exchange resins. The model given in Ref. [49] takes into account the resin volume changes due to changes in component concentrations as changing resin bed porosity.

In this work, a slightly simpler approach, than the one used by Laatikainen *et al*. [49], for the modelling of the column dynamics was taken. The model derived in this work differs from the one given in Ref. [49] mainly due to the fact that the resin volume changes in this model are assumed to depend only on the changes in the concentration of sulfuric acid.

In the approach in which the resin volume changes are taken into account as changing resin bed porosity, the resin particles are assumed to be attached to a fixed two-dimensional grid [162]. This means that when the liquid phase concentration of sulfuric acid changes, the particle diameter and, therefore, also the void volume (bed porosity) changes.

Mass balance for component i over a small volume element of length Δz in a chromatographic column can be written as

$$\frac{\partial}{\partial t}\left(C_{\mathrm{i}}\varepsilon\right)A_{\mathrm{col}}\Delta z+\frac{\partial}{\partial t}\left(q_{\mathrm{i}}(1-\varepsilon)\right)A_{\mathrm{col}}\Delta z=-\frac{\partial}{\partial z}\left(\dot{V}C_{\mathrm{i}}\right)\Delta z+D_{\mathrm{ax,i}}A_{\mathrm{col}}\frac{\partial}{\partial z}\left(\varepsilon\frac{\partial C_{\mathrm{i}}}{\partial z}\right)\Delta z\,, \tag{31}$$

where ε is local bed porosity, $\dot{V}$ is volumetric flow rate, A_{col} is column cross-sectional area, D_{ax} is axial dispersion coefficient, t and z are temporal and spatial coordinates, respectively.

In principle, the volumetric flow rate is also a locally varying property according to

$$\frac{\partial\dot{V}}{\partial z}\Delta z=\sum_{j=1}^{N+1}V_{\mathrm{m},j}\frac{\partial n_j}{\partial t}, \tag{32}$$

where n is the total amount of component j in the liquid and solid phases within the volume element. Note that the summation in Eq. (32) includes also the eluent (component N+1). Use of Eq. (32) thus requires modelling also the sorption of the eluent. For the sake of simplicity, the sorption of the eluent was not taken into account here, and the volumetric flow rate was assumed constant. With this assumption, application of the chain rule to Eq. (31) yields the final form of the column mass balance equation:

$$\frac{\partial C_{\mathrm{i}}}{\partial t} = -\frac{\dot{V}}{\varepsilon A_{\mathrm{col}}}\frac{\partial C_{\mathrm{i}}}{\partial z} + \frac{(q_{\mathrm{i}} - C_{\mathrm{i}})}{\varepsilon}\frac{\partial \varepsilon}{\partial t} - \frac{1-\varepsilon}{\varepsilon}\frac{\partial q_{\mathrm{i}}}{\partial t} + \frac{D_{\mathrm{ax,i}}}{\varepsilon}\frac{\partial}{\partial z}\left(\varepsilon\frac{\partial C_{\mathrm{i}}}{\partial z}\right). \tag{33}$$

The second term on the right hand side of Eq. (33) takes into account the influence of changing phase ratio on the liquid phase concentration of i.

Danckwert's boundary conditions were used:

$$\frac{\partial C_{\mathrm{i}}}{\partial z} = \frac{\dot{V}}{A_{\mathrm{col}}\varepsilon}\frac{\left(C_{\mathrm{i}} - C_{\mathrm{i}}^{\mathrm{in}}\right)}{D_{\mathrm{ax,i}}},\ z = 0, \tag{34A}$$

$$\frac{\partial C_{\mathrm{i}}}{\partial z} = 0\,,\ z = h_{\mathrm{bed}} \tag{34B}$$

where $C_{\mathrm{i}}^{\mathrm{in}}$ is concentration of i at the column inlet (z = 0) and h_{bed} is the column height. Local bed porosity was calculated from

$$\varepsilon = 1 - \theta(1 - \varepsilon_{\mathrm{ref}})\,, \tag{35}$$

where $\varepsilon_{\mathrm{ref}}$ is bed porosity in reference state, which was in this case a column equilibrated with pure water. The rate of bed porosity change is obtained through derivation of Eq. (35):

$$\frac{\partial \varepsilon}{\partial t} = -\frac{\partial \theta}{\partial t}(1 - \varepsilon_{\mathrm{ref}})\,. \tag{36}$$

An equation for the rate of bed porosity change depending on the rate of sulfuric acid sorption is obtained by using chain rule and and Eq. (30):

$$\frac{\partial \varepsilon}{\partial t} = \frac{\alpha_\theta \beta_\theta}{(\beta_\theta + q_{\mathrm{H2SO4}})^2}\frac{\partial q_{\mathrm{H2SO4}}}{\partial t}(1 - \varepsilon_{\mathrm{ref}})\,. \tag{37}$$

By relating the extent of resin shrinking to the sorbed amount of sulfuric acid, the effect of sorption kinetics on the resin volume changes is taken into account.

Solid film linear driving force model was used to describe mass transfer kinetics:

$$\frac{\partial \bar{q}_{\mathrm{i}}}{\partial t} = k_{\mathrm{m,i}}(q_{\mathrm{i}}^{*} - \bar{q}_{\mathrm{i}}) + \frac{\bar{q}_{\mathrm{i}}}{1-\varepsilon}\frac{\partial \varepsilon}{\partial t}, \tag{38}$$

where $k_{\mathrm{m,i}}$ is intraparticle mass transfer coefficient, q_{i}^{*} is solid phase concentration of i at equilibrium with liquid phase concentration C_{i}, and $\bar{q}_{\mathrm{i}}$ is average solid phase concentration of i. The last term on the right hand side of Eq. (38) originates from changes in the phase ratio.

The intraparticle mass transfer coefficient is calculated from

$$k_{\mathrm{m,i}} = \frac{60 D_{\mathrm{i}}^{\mathrm{p}}}{d_{\mathrm{p}}^2}, \tag{39}$$

where D_i^P is diffusion coefficient which depends on resin volume. The correlation of Mackie and Meares [49,165] can be used to calculate D_i^P:

$$D_i^P = D_{i,ref}^P \left[\frac{(1-\psi_p)(1+\psi_{p,ref})}{(1+\psi_p)(1-\psi_{p,ref})} \right]^2 = D_{i,ref}^P \left[\frac{(1-\psi_{p,ref}/\theta)(1+\psi_{p,ref})}{(1+\psi_{p,ref}/\theta)(1-\psi_{p,ref})} \right]^2, \quad (40)$$

where ψ_p is volume fraction of polymer, and subscript ref refers to reference state. Here, water swollen CS16GC was taken as a reference state and $\psi_{p,ref} = 0.391$ [49].

Particle diameter d_p in Eq. (39) can be calculated from

$$d_p = d_{p,ref} \left(\frac{1-\varepsilon}{1-\varepsilon_{ref}} \right)^{1/3}, \quad (41)$$

where $d_{p,ref}$ is particle diameter in the reference state.

Method of lines [166] was used to solve the partial differential equations in Eq. (33). Same column model was used in the modelling of the single-column batch process and the multi-column processes. The diffusion coefficients in reference state in Eq. (40) and the axial dispersion coefficients (same value for all components) in Eq. (33) were estimated by fitting the simulated elution profiles to those obtained experimentally using batch chromatography.

6.3 Pressure drop

Pressure drop limits the flow rates in chromatographic separation processes and has to be taken into account in the designing of these processes. In this work, maximum feasible flow rates were calculated using Ergun equation [167]

$$\frac{\Delta p}{L} = \frac{150\mu v}{\Phi_S{}^2 d_p{}^2} \frac{(1-\varepsilon_{bed})^2}{\varepsilon_{bed}{}^3} + \frac{1.75\rho v^2}{\Phi_S d_p} \frac{1-\varepsilon_{bed}}{\varepsilon_{bed}{}^3}, \quad (42)$$

where Δp is pressure drop, L is flow path length, μ is dynamic viscosity of the fluid, Φ_S is sphericity factor of solid particles (unity for spherical resin beads), ρ is density of the fluid, and v is superficial velocity. Eq. (42) is applicable to all flow rate regions [167].

6.4 Evaluation of separation process performance

The performance of the chromatographic separation processes studied in this work was evaluated using various performance parameters: the productivity of the separation process with respect to the monosaccharides Pr_{sugar}, the product yield Y_i, the product purity Pu_i, and the eluent consumption needed for obtaining one mole of monosaccharides EC. Equations used for the calculation of these parameters are given in Table 2.

Table 2. Performance parameters used in the evaluation of the chromatographic separation processes studied in this work.

	Batch process*	Japan Organo process**	MCRC process***
Yield	$Y_i = \frac{n_i^{out}}{C_i^{feed} V^{feed}}$	$Y_{sugar,I} = \frac{C_{sugar,I}^{step\ 1} \dot{V}_{eluent,1}}{C_{sugar}^{feed} \dot{V}_{feed,1}}$ $Y_{H2SO4,R} = \frac{C_{H2SO4,R}^{step\ 1} \dot{V}_{feed,1} t_{step,1} + C_{H2SO4,R}^{step\ 2} (1-\varphi) \dot{V}_{eluent,2} n_{sub,2} t_{step,2}}{C_{H2SO4}^{feed} \dot{V}_{feed,1} t_{step,1}}$ $Y_{AcOH,E} = \frac{C_{AcOH,E}^{step\ 2} \dot{V}_{eluent,2} \varphi n_{sub,2} t_{step,2}}{C_{AcOH}^{feed} \dot{V}_{feed,1} t_{step,1}}$	$Y_i = \frac{n_i^{out}}{C_i^{feed} \dot{V}_{feed,1} t_{step,1}}$
Productivity with respect to monosaccharides	$Pr_{sugar} = \frac{Y_{sugar} C_{sugar}^{feed} V^{feed}}{(1-\varepsilon_{bed}) V_{bed} t_{cycle}}$	$Pr_{sugar} = \frac{n_{glucose}^{out,I} + n_{xylose}^{out,I}}{n_{col} V_{bed} (1-\varepsilon_{bed}) (t_{step,1} + n_{sub,2} t_{step,2})}$	$Pr_{sugar} = \frac{n_{glucose}^{out} + n_{xylose}^{out}}{n_{col} V_{bed} (1-\varepsilon_{bed}) t_{cycle}}$
Eluent consumption	$EC = \frac{t_{cycle} \dot{V} - V^{feed}}{Y_{sugar} C_{sugar}^{feed} V^{feed}}$		$EC = \frac{\sum_{s=1}^{4} \sum_{t=1}^{n} \dot{V}_{s,t} t_{step,s}}{n_{glucose}^{out} + n_{xylose}^{out}}$
Purity	$Pu_i = \frac{n_i^{out}}{\sum_j n_j^{out}}$	$Pu_{i,X} = \frac{C_{i,X}}{\sum_{j=1}^{n} C_{j,X}}$	$Pu_i = \frac{n_i^{out}}{\sum_j n_j^{out}}$

* Batch process: see Paper III for symbols.

** JO process: $n_i^{out,I}$ = mole amount of i (= glucose, xylose) in the intermediate outlet stream; n_{col} = number of columns; $n_{sub,2}$ = number of port switches in step 2; subscript X = outlet stream X (= raffinate, extract, intermediate); $C_{i,X}^{step\ k}$ = average concentration of component i in the outlet stream X in step k; C_i^{feed} = feed concentration of component I; $\dot{V}_{feed,1}$ = feed flow rate in step 1; and $\dot{V}_{eluent,2}$ = eluent flow rate in step 2.

*** MCRC process: see Paper V for symbols.

7 EXPERIMENTAL

All experiments in this work were done on a laboratory scale. Isotherm measurements were done using batch and column methods. Batchwise chromatographic fractionation in single-column and in multi-column systems were conducted. All chromatographic fractionation experiments were done using approximately 100 mL resin bed (h_{bed} 20 cm) and using top–down flow. Both authentic concentrated acid hydrolysates and synthetic solutions were used as feed in the separation experiments. Hydrolysate preparations were done in glass reactors (1 L and 3 L) using softwood (spruce and pine) and hardwood (birch) chips as raw materials.

7.1 Materials

Analytical grade chemicals (sulfuric acid, hydrochloric acid, glucose, xylose, acetic acid, HMF, furfural, sodium hydroxide, ammonium sulfate, sodium sulfate, and sodium chloride) were used in preparation of synthetic solutions used in this work. Purified water was used as an eluent in the chromatographic separations and in preparation of all synthetic solutions.

Three gel type sulfonated poly(styrene-co-divinylbenzene) (PS–DVB) strong acid cation exchange resins with varying crosslinking degrees were used (Table 3). The resins are commercially available from Finex Oy (Finland). Prior to usage, all resins were converted to acid (H^+) form with 1 M hydrochloric acid using standard methods [39]. Volumetric capacities (Table 3) of the resins were measured using standard methods [39].

Table 3. Properties of the gel type strong acid cation exchange resins used in this work. Resins were supplied by Finex Oy (Finland).

	CS09GC	CS12GC	CS16GC
Resin matrix	PS-DVB	PS-DVB	PS-DVB
Functional group	Sulfonic acid	Sulfonic acid	Sulfonic acid
Degree of crosslinking, -	4.5	6.0	8.0
Mean particle size, µm	211.0	217.0	217.5 / 246.0[a]
Vol. capacity (H+), mequiv/mL[b]	1.07	1.51	1.93

[a] Two batches of CS16GC with different mean particle sizes were used.
[b] Volumetric capacities were measured using standard methods [39].

7.2 Concentrated acid hydrolysis

Two-step concentrated acid hydrolysis experiments were conducted in order to prepare authentic hydrolysates for the fractionation experiments. Spruce and birch chips (ground using hammer mill to a particle size of one to five millimeters), and mixed spruce and pine cutter saw dust were used as raw materials. Details about the hydrolysis method can be found from Papers II and V.

7.3 Equilibrium measurements

7.3.1 Sorption isotherms

The sorption isotherms of the main component of lignocellulosic hydrolysates (sulfuric acid, glucose, xylose, acetic acid, HMF, and furfural) were measured only in the case of one stationary phase: CS16GC (d_p 246 µm, for details see Table 3). The isotherms were measured at a temperature of 50 °C.

The sulfuric acid sorption isotherm was measured using the perturbation method [36,168,169] (a.k.a. the pulse on a plateau method). In this method, the column is first equilibrated with a given acid concentration of 0.05 – 4.0 mol/L (plateau concentration). Then a small pulse with slightly higher (or lower) concentration is injected to the eluent stream which has the same acid concentration as the plateau. The retention time of the small pulse is measured. This value corresponds to the slope of the isotherm at the plateau concentration. Sulfuric acid isotherm was measured only in pure water.

The acetic acid isotherm was measured using the frontal analysis method [36] in pure water and in various sulfuric acid solutions (C_{H2SO4} up to 4.0 mol/L). Feed concentration of acetic acid ranged from 0.03 to 0.33 mol/L (2 – 20 g/L).

The batch method was used to measure the glucose and xylose isotherms in pure water and in sulfuric acid solutions with initial concentrations of 1, 2, and 4 mol/L. Initial glucose and xylose concentrations ranged from 0.005 to 0.7 mol/L. Each batch contained 5 g of water-swollen resin and 7 mL of solution. The batches were equilibrated for seven hours. The effect of liquid phase dilution due to resin shrinking was corrected by means of the swelling data measured at the same acid concentrations.

The Henry constants of the glucose and xylose isotherms were measured by injecting small dilute monosaccharide pulses into a column. Measurements were done in pure water and in sulfuric acid solutions with concentrations corresponding to the equilibrium concentrations of sulfuric acid in the batch experiments.

7.3.2 Resin volume changes

The stationary phases used in this work were gel type resins. It is a well-known fact that resin volume changes due to changes in liquid phase composition can be significant with gel type resins [39,170]. Therefore, the extent of volume changes of the resins was determined experimentally. Resin volume changes were measured only with sulfuric acid as it was the only solute in the studied system causing notable volume changes in the concentration range used. Both batch method and equilibrium method in a column were used to measure the resin volume changes. Details about the measurements are given in Papers I and III.

7.4 Salting out

The co-operative effect of strong electrolytes on the sorption of neutral components due to salting out (see Chapter 4.2.4) was investigated by batchwise pulse elution experiments. The effect of sulfuric acid, H_2SO_4, sodium sulfate, Na_2SO_4, ammonium sulfate, $(NH_4)_2SO_4$, and sodium chloride, NaCl, on the sorption of glucose was studied. The ionic strength and glucose concentration of the solutions were kept constant at 4.5 mol/L and 0.4 mol/L, respectively. CS16GC resin (see Table 3) was used as a stationary phase and purified water as an eluent. Prior to the experiments, the resin was converted to the same cationic form as the electrolyte (e.g., NH_4^+ form when $(NH_4)_2SO_4$ was used as the electrolyte) using standard methods [39]. Same column and experimental conditions were used as in the single-column batchwise fractionation of concentrated acid hydrolysates (see Paper III for details).

7.5 Fractionation of concentrated acid lignocellulosic hydrolysates

7.5.1 Single-column batchwise fractionation

Single-column batchwise chromatographic fractionation experiments were done to obtain data for the validation of the models derived in this work, and to investigate the effect of the resin crosslinking on the separation performance. Fractionation experiments were done with both authentic concentrated acid hydrolysates and synthetic solutions presenting concentrated acid hydrolysates. Top–down flow was used in all experiments. For details about the experiments and the experimental setup, see Papers I, II, III, and IV.

7.5.2 Fractionation using Multi-Column Recycling Chromatography

Usability of the MCRC process scheme designed in this work for the separation task at hand was validated experimentally using both synthetic and authentic concentrated acid (20 wt. %) lignocellulosic hydrolysates. Details regarding the experiments and the experimental setup are given in Paper V.

7.6 Chemical analyses

Concentrations of monosaccharides, acetic acid, hydroxymethyl furfural (HMF), and furfural were measured with an off-line HPLC system (HP 1100 Hewlett-Packard/Agilent) equipped with refractive index and variable wavelength UV detectors. Sulfuric acid concentrations were determined from online conductivity measurements and by potentiometric titrations. Details are given in Papers I and II.

8 RESULTS AND DISCUSSION

The aim of this work was to investigate systematically the use of the electrolyte exclusion chromatography for the fractionation of concentrated acid lignocellulosic hydrolysates. The most important results obtained in this work will be presented and discussed in this Chapter.

8.1 Phase Equilibrium

Three gel type strong acid cation exchange resins in acid form with varying degrees of crosslinking (see Table 3) were used in this work as stationary phases. However, extensive investigation of the phase equilibria was done only in the case of one resins: CS16GC with 8 wt. % DVB content. This resin was chosen on the basis of results obtained from the investigation of the effect of resin cross-linking on the fractionation of concentrated acid hydrolysates (see Chapter 8.2.3 and 8.2.4). Detailed discussion of the phase equilibria is given in Papers III and IV.

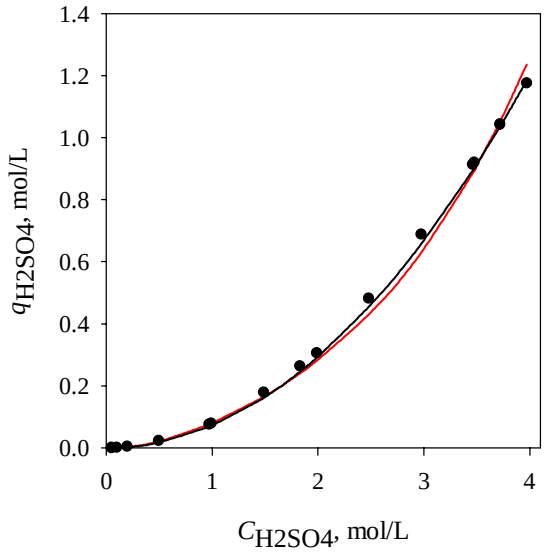

Figure 11. Sorption of sulfuric acid from water on a gel type strong acid cation exchange resin (CS16GC) in acid form at a temperature of 50 °C. Lines: black = fit of Eq. (23) (the empirical approach; Chapter 6.1.1); red = fit of (Eq. (29) (the AS theory, Chapter 6.1.2). For model parameters, see Papers III and IV.

Sorption isotherm of sulfuric acid on CS16GC resin in H^+ form is shown in Fig. 11. As a result from the electrolyte exclusion which affects the sulfuric acid sorption, the isotherm is clearly concave upward shaped. At infinite dilution, the Henry constant of the isotherm is zero: the electrolyte exclusion is strong enough to prevent all HSO_4^- and SO_4^{2-} ions from

entering the pores of the resin. Therefore, sulfuric acid is completely excluded from the resin as the electroneutrality condition must be valid. The effect of the electrolyte exclusion on the sulfuric acid sorption diminishes with increasing sulfuric acid concentration and, thus, the sulfuric acid sorption increases (Fig. 11). Eventually, the exclusion effect disappears completely and the isotherm becomes linear.

A good correlation between the experimental and calculated results for the sulfuric acid sorption was obtained with both of the sorption models studied in this work (Fig. 11). With the Redlich–Peterson model (Eq. (29)) the fit of the calculated results is slightly inaccurate due to the activity coefficient data used in this work. For details, see Paper IV.

In this work, it was found out that sulfuric acid has a very strong co-operative effect on the sorption of the other components in the studied system (glucose, xylose, and acetic acid) due to the salting out effect. This is illustrated in Figs. 12 and 13 for glucose and acetic acid. For details about this effect, see Chapter 4.2.4 and Paper III. For glucose, this kind of behavior has also been observed earlier by Neuman *et al.* [40]. The salting out effect has a strong impact on the separation of sulfuric acid and monosaccharides (see below).

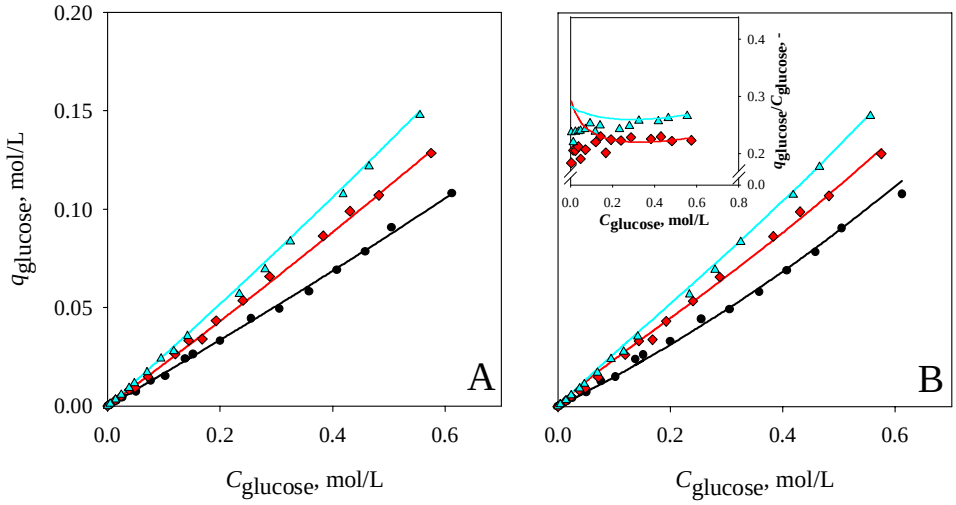

Figure 12. Sorption of glucose from water and from sulfuric acid solutions on a gel type strong acid cation exchange resin (CS16GC) in acid form at a temperature of 50 °C. Model: A = the empirical approach; B = the AS theory. Inset of B: slopes of the isotherms, calculated with the AS theory, in the presence of H_2SO_4. Symbols: (●) water, (◆) 0.97 mol/L H_2SO_4, and (▲) 1.84 mol/L H_2SO_4. Lines are the model fits. For model parameters, see Papers III and IV.

A good correlation between the experimental and calculated sorption isotherms of glucose, xylose, and acetic acid was obtained with the empirical approach (Eqs. (24) and (25)).

Example of this is shown in Fig. 12A for glucose. The co-operative effect of sulfuric acid on the sorption is well described with linear dependency of the Henry constant on the liquid phase sulfuric acid concentration. For details, see Paper III.

In the case of the AS theory, the fit of the pure component isotherm model (Eq. (28)) to the experimental sorption data of glucose, xylose, and acetic acid was found to be good (for glucose, see Fig. 12B). Also in the presence of sulfuric acid, a satisfactory correlation between the results was obtained (Fig. 12B). However, with the monosaccharides, inflection points not seen in the experimental isotherms were noted in the calculated ones: the slopes of the isotherms first decrease then pass through a minimum and finally begin to increase in the presence of sulfuric acid (Fig. 12B inset). This property originated from the fact that the AS theory tends to predict concave downward shaped isotherms for the monosaccharides in the presence of sulfuric acid. The shapes of the calculated monosaccharide isotherms could be corrected partially by using the liquid phase activities (see Paper IV). Unfortunately, this resulted in the inflection points in the calculated isotherms. Eradication of the inflection points would require the use of a more complicated model with a greater number of adjustable parameters and was, therefore, omitted from this work.

With the AS theory, no inflection points were observed in the sorption isotherms of acetic acid in the presence of sulfuric acid (Fig. 13). This is because the acetic acid sorption isotherm on CS16GC is slightly concave downward also in the presence of sulfuric acid.

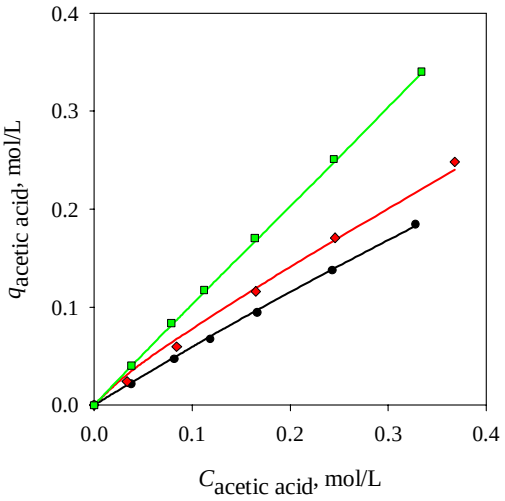

Figure 13. Sorption of acetic acid from water and from sulfuric acid solutions on a gel type strong acid cation exchange resin (CS16GC) in acid form at a temperature of 50 °C. Lines: isotherms calculated with the AS theory. Symbols: (●) water, (◆) 0.96 mol/L H_2SO_4, and (■) 3.92 mol/L H_2SO_4. For model parameters, see Paper IV.

As gel type ion exchange resins were used in this work as stationary phases, significant volume changes due to changes in the liquid phase composition were expected. However, in the studied concentration ranges, significant resin volume changes were observed only in the case of sulfuric acid (Fig. 14). These volume changes must be taken into account in the modelling of the separation process. Here, only the volume changes of CS16GC resin were modeled but the same model (Eq. (30)) is applicable to the other resins as well. The resin volume changes were found to be well described by the simple equilibrium model derived in this work (Eq. (30)).

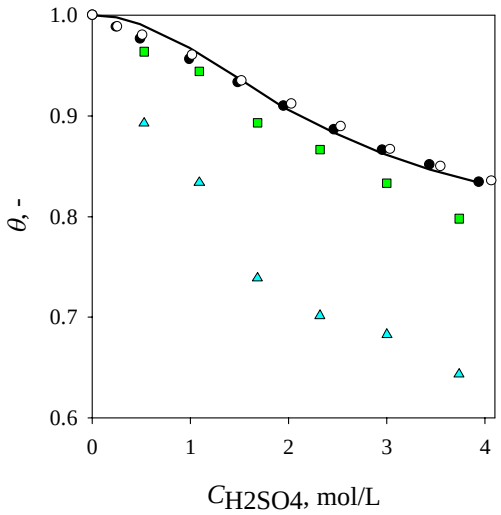

Figure 14. Effect of sulfuric acid on the volume of gel type strong acid cation exchange resins CS09GC (▲), CS12GC (■), and CS16GC (●) in acid form at a temperature of 50 °C. For CS16GC, results from two independent experiments are shown (filled and open symbols). Line: fit of Eq. (30). For model parameters, see Paper III.

8.2 Fractionation using single-column batch chromatography

In papers I – IV, the single-column batchwise chromatographic fractionation of concentrated acid lignocellulosic hydrolysates was investigated. Both authentic concentrated acid hydrolysates and synthetic solutions presenting these hydrolysates were used as feed solutions.

Typical column outlet profiles obtained in the single-column batchwise chromatographic fractionation of concentrated acid lignocellulosic hydrolysates using CS16GC resin (8 wt. % DVB) in acid (H^+) form are shown in Fig. 15.

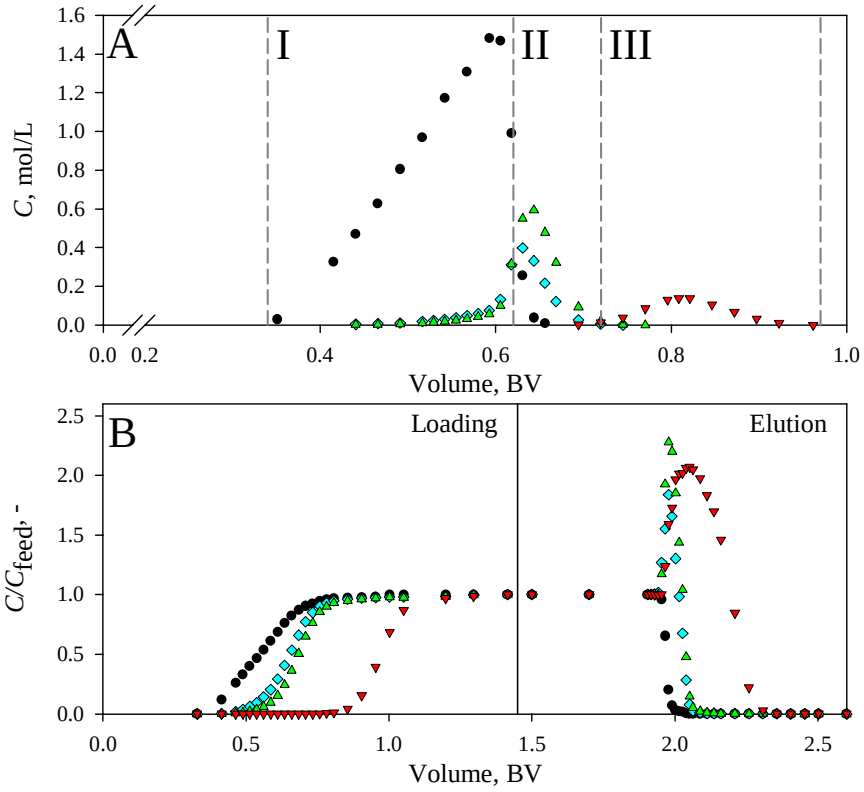

Figure 15. Typical outlet profiles obtained in single-column chromatographic fractionation of concentrated acid lignocellulosic hydrolysates with CS16GC resin in acid form at a temperature of 50 °C. A = pulse experiment; B = loading and elution curve experiment. Experimental conditions: see Papers III and IV. Feed composition in A: see caption of Fig. 5 in Paper III; feed composition in B: see caption of Fig. 6 in Paper IV. Symbols: black ● = sulfuric acid; cyan ◆ = glucose; green ▲ = xylose; red ▼ = acetic acid. Dashed vertical lines in A: illustration of fractionation cut points. Roman numerals in A: I = sulfuric acid fraction; II = monosaccharide fraction; III = acetic acid fraction.

Sulfuric acid is the first eluting component in the fractionation of lignocellulosic hydrolysates on strong acid cation exchange resin in acid form (Fig. 15). As a strong electrolyte, its sorption is affected by the electrolyte exclusion. Due to the complete exclusion at infinite dilution the breakthrough of sulfuric acid occurs at the void volume of the resin bed (Fig. 15). As the sulfuric acid concentration increases, the strength of the electrolyte exclusion decreases and, thus, the sulfuric acid sorption increases (see Fig. 11). As a result, the propagation velocity associated with a certain sulfuric acid concentration decreases with increasing sulfuric acid sorption and a diffuse front of the sulfuric acid profile is formed (Fig. 15). At the

rear of the sulfuric acid profile, a shock layer exists: the low sulfuric acid concentrations propagate faster than the high ones because of the isotherm shape, but due to physical reasons the low concentrations cannot pass the high ones. This results in a shock layer (Fig. 15).

The monosaccharides elute under and after sulfuric acid (Fig. 15). The co-operative effect of sulfuric acid on the sorption of the monosaccharides due to the salting out (see Chapter 4.2.4) observed in this work is seen as interesting phenomena in the column operations. The outlet profiles of the monosaccharides have elongated fronts under the sulfuric acid profile. This is clearly seen in the pulse elution case (Fig. 15A). Sulfuric acid increases the sorption of the monosaccharides which in column operations means that the propagation of the monosaccharides is slowed down by sulfuric acid. This effect becomes stronger as sulfuric acid concentration increases. The phenomenon is opposite to the tag-along effect [36] often seen in chromatographic separations. The co-operative effect is beneficial for the separation efficiency as it improves the separation between the monosaccharides and sulfuric acid. Without the existence of this effect the monosaccharides would elute completely under the sulfuric acid profile and no separation between these two components would be obtained.

Another interesting phenomenon arising from the co-operative effect of sulfuric acid on the monosaccharide sorption is the focusing of the monosaccharides at the rear of the sulfuric acid profile (Fig. 15). The monosaccharide concentrations were found to increase above the feed values at the rear of the sulphuric acid profile. For detailed discussion of the focusing, see Paper III. Focusing of later eluting components is rarely seen in chromatography, but, like in this case, it can be beneficial for the separation performance.

The co-operative effect of sulfuric acid on the sorption of acetic acid is not clearly seen in the pulse elution case (Fig. 15A) due to the largely different sorption strengths of these components (see Chapter 8.1). However, in the case of loading and elution (Fig. 15B), the focusing of acetic acid at the rear of the sulfuric acid profile is clear. However, the elongation of the acetic acid front is not evident from the loading profile either (Fig. 15B).

The possible fractionation cut points are illustrated in the case of the pulse elution in Fig. 15A. At least three fractions can be obtained when gel type strong acid cation exchange resin in acid form is used as a stationary phase: sulfuric acid, monosaccharide, and acetic acid fractions. Additional fractions for hydroxymethylfurfural and furfural would be obtained if the same separation method would be used for their recovery (see Fig. 21).

The first cut point in Fig. 15A determines the starting points of the cycle and the sulfuric acid fraction. The position of the second cut point, which determines the starting point of the monosaccharide fraction, is important for the purity and yield of the sulfuric acid and monosaccharide fractions. If this cut point is shifted to the right, purity of the monosaccharides increases drastically as the portion of the sulfuric acid shock layer ending to this fraction becomes considerably smaller (Fig. 15A). Also, the sulfuric acid yield increases.

However, as a result the monosaccharide yield and sulfuric acid purity decreases. Shift in the position of the second cut point to the left increases the productivity of the monosaccharides as well as the sulfuric acid purity, but decreases the monosaccharide purity and the sulfuric acid yield.

The third cut point determines the starting point of the acetic acid fraction (Fig. 15A). Position of this cut point affects the yield and purity of the monosaccharide and acetic acid fractions. However, shift in the position of this point does not have such a dramatic effect on the monosaccharide purity as the shift in the second cut point due to the shape of the monosaccharide profile rear and acetic acid profile (Fig. 15A). The fourth cut point determines the ending point of the acetic acid fraction and the cycle.

8.2.1 Salting out

In order to find out whether other strong electrolytes than sulfuric acid have a strong co-operative effect on the sorption of nonelectrolytes, pulse elution experiments were done with electrolyte–glucose mixtures. CS16GC resin was used as a stationary phase. In each case, the ionic form of the resin corresponded to the cation of the strong electrolyte. In addition to sulfuric acid, Na_2SO_4, $(NH_4)_2SO_4$, and NaCl were used in this investigation.

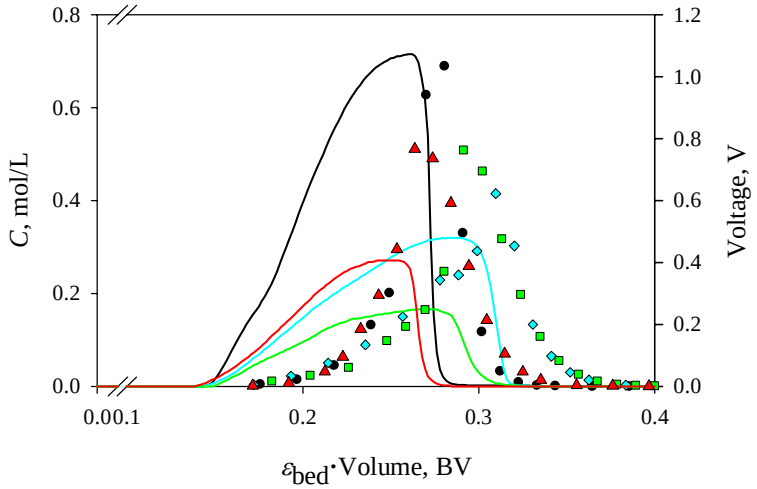

Figure 16. Effect of strong electrolytes (lines) on the elution of glucose (symbols) on CS16GC resin. Colors: H_2SO_4 (black), Na_2SO_4 (green), $(NH_4)_2SO_4$ (red), and NaCl (cyan). Resin in the same ionic form as the cation of the electrolyte. Feed composition: 4.5 mol/L ionic strength, 0.4 mol/L glucose. Experimental conditions: same as in the model validation; see Paper III for details. Electrolyte concentrations shown as a voltage obtained from the conductivity detector.

It was found out that ammonium sulfate (NH_4^+ form resin) is most strongly excluded from the resin due to the electrolyte exclusion (Fig. 16). However, exclusion of sulfuric acid (H+ form resin) is only slightly weaker. Of the sulfates, Na_2SO_4 (Na^+ form resin) has the strongest sorption on the resin. The effect of the cation (H^+, Na^+, NH_4^+) on the elution behavior of the strong electrolytes can be explained by the different degrees of resin swelling depending on the ionic form [39]. Differences in the elution behavior of Na_2SO_4 and NaCl (Fig. 16) clearly demonstrates the effect of the co-ion size on the electrolyte exclusion: co-ions with higher valence lead to stronger exclusion (see Chapter 4.2.1) [39].

The elution behavior of glucose in the presence of $(NH_4)_2SO_4$, Na_2SO_4, and NaCl was found to be similar as with sulfuric acid as a strong electrolyte (Fig. 16). This clearly indicates that each of these strong electrolytes have a strong co-operative effect on the sorption of glucose. In the presence of each electrolyte, the elongated front of glucose under the electrolyte profile and the focusing of glucose are clearly seen (Fig. 16).

Although the exclusion of $(NH_4)_2SO_4$ from NH_4^+ resin is slightly stronger than that of sulfuric acid from H^+ form resin, the focusing of glucose is stronger on H^+ form resin (Fig. 16). This is due to weaker retention of glucose on H^+ form resin. Weaker retention leads to faster propagation of the rear of the glucose profile after some separation between the electrolyte and glucose has been achieved. As a result, the glucose profile “squeezes” more in this case assuming that the elution behavior of the strong electrolyte remains the same with both ionic forms. Therefore, stronger focusing is obtained when the retention of glucose is weaker.

In order to verify the effect of the glucose sorption strength on the focusing, the elution of sulfuric acid and a monosaccharide was simulated with different values of the Henry constant of the monosaccharide isotherm (Fig. 17). Similar differences in the focusing were observed in the simulations as in the experimental outlet profiles of glucose on H^+ form resin and on NH_4^+ form resin (Fig. 17). This confirms that the weaker focusing of glucose on NH_4^+ form resin is caused by the stronger retention of glucose.

With the Na^+ form resin and Na_2SO_4 as the strong electrolyte, the focusing of glucose was approximately as strong as with the NH_4^+ form resin although the exclusion of Na_2SO_4 was weaker on Na^+ form resin than that of $(NH_4)_2SO_4$ on the NH_4^+ form resin (Fig. 16). Also this results from the different sorption strength of glucose on Na^+ and NH_4^+ form resins: retention of glucose on Na^+ form resin is weaker and results in stronger focusing.

Weakest focusing for glucose was obtained with the Na^+ form resin and NaCl as strong electrolyte (Fig. 16). This is due to the weak exclusion of NaCl on Na^+ form resin: the electrolyte profile is wide and a large part of the glucose elutes under its profile. Due to long elongated front of glucose under the NaCl profile, there is not enough glucose for strong focusing at the rear of the electrolyte profile.

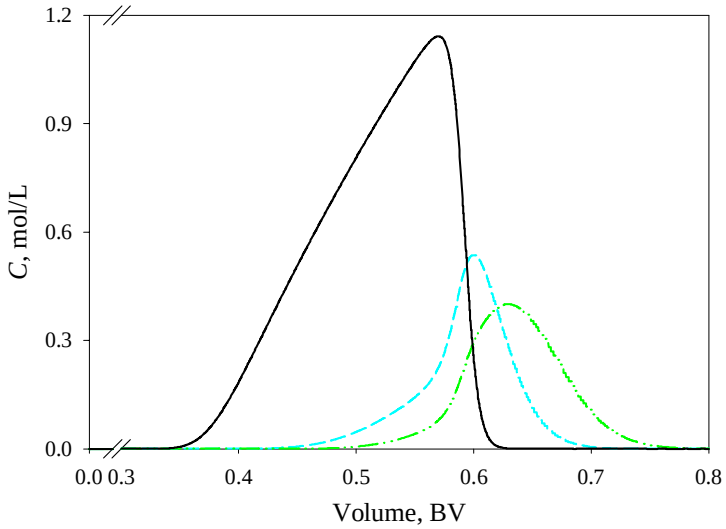

Figure 17. Effect of the Henry constant of the monosaccharide isotherm (α in Eq. (24)) on the elution behavior of a monosaccharide in the presence of a strong electrolyte. Feed composition: 1.5 mol/L electrolyte, 0.4 mol/L monosaccharide. Calculated results. Lines: black solid = electrolyte; cyan dash = monosaccharide, α = 0.164; green dash-dot-dot = monosaccharide, α = 0.25. Operating conditions and other parameters: see Paper III.

8.2.2 Modelling of the chromatographic fractionation

A model suitable for the investigation of the chromatographic fractionation of lignocellulosic hydrolysates was developed in this work. Although the model was derived for the fractionation of concentrated acid hydrolysates, it is also well applicable for the fractionation of dilute acid hydrolysates. The main differences between these hydrolysates are in the concentrations of sulfuric acid and hydrolysis by-products. Detailed description of the modelling is given in Papers III (the empirical approach) and IV (the AS theory).

Prediction of the elution behavior in the studied system was investigated with the two approaches used for the modelling of the sorption equilibria (see Chapter 8.1): the empirical approach (Chapter 6.1.1) and the Adsorbed Solution theory (Chapter 6.1.2). Same dynamic column model (Chapter 6.2) and resin shrinking model (Chapter 6.1.3) were used.

Both sorption models could reproduce the characteristic features of the studied system satisfactorily (Figs. 18 and 19). The empirical approach gave a slightly more accurate prediction than the Adsorbed Solution theory. The effect of sulfuric acid on the profiles of the other components was well taken into account with both models. However, the AS theory was found to predict that a slightly larger amount of glucose elutes under the sulfuric acid profile

than was observed in the experiments (Fig. 18B). Due to this, the focusing of glucose according to the AS theory is not as strong as it should be according to the experimental results. The inaccuracies in the profiles calculated with the AS theory result from the inflection points in the calculated monosaccharide isotherms (see Chapter 8.1).

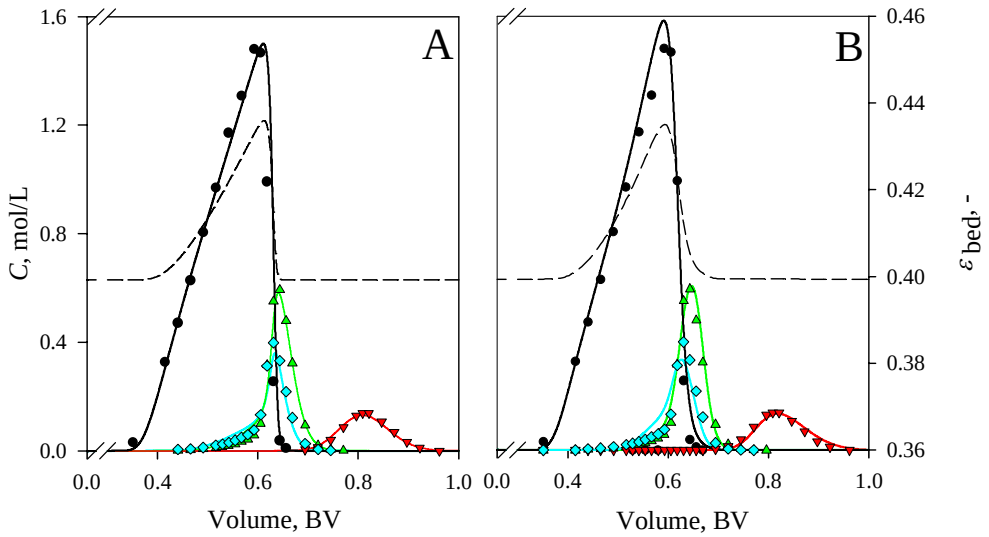

Figure 18. Effect of sorption model on the prediction of the elution of a 10 vol. % pulse of synthetic hydrolysate solution with CS16GC resin in acid form at a temperature of 50 °C. A = the empirical approach; B = the AS theory. Feed composition: see caption of Fig. 5 in Paper III. Experimental conditions: see Paper III. Symbols: see caption of Fig. 15. Solid lines: calculated results; line colors correspond to the symbol colors, see caption of Fig. 15. Dashed line: calculated bed porosity. Model parameters are given in Papers III and IV.

Although a good correlation between the empirical approach and experimental results was achieved in the case of pulse elution, some inaccuracies were observed in the predicted loading and elution curves (Fig. 19A) [171]. The calculated sulfuric acid loading curve was found to be less steep than observed in the experiments. In addition, according to the model, acetic acid breakthrough occurs too early. This affects also the calculated elution profile of acetic acid (Fig. 19A). The aforementioned inaccuracies are probably due to the simple resin shrinking model (Eq. (30)). Correlation between the calculated and experimental monosaccharide profiles was good.

With the AS theory, the steepness of the sulfuric acid loading curve was found to change at the breakthrough point of the monosaccharides (Fig. 19B). This stems from the influence of monosaccharides on the adsorbed phase activity coefficient of sulfuric acid (see Paper IV). In addition, the calculated monosaccharide profiles were found to be too steep at low

concentrations and exhibit slight overshoots before reaching the feed concentration level (Fig. 19B). The overshoots were caused by the AS theory which tends to predict competitive sorption between the monosaccharides and acetic acid. This is seen as the displacement of the monosaccharides from the solid phase by acetic acid. In the experimental results these overshoots were not seen as sorption on an elastic ion exchange resin can occur without competition.

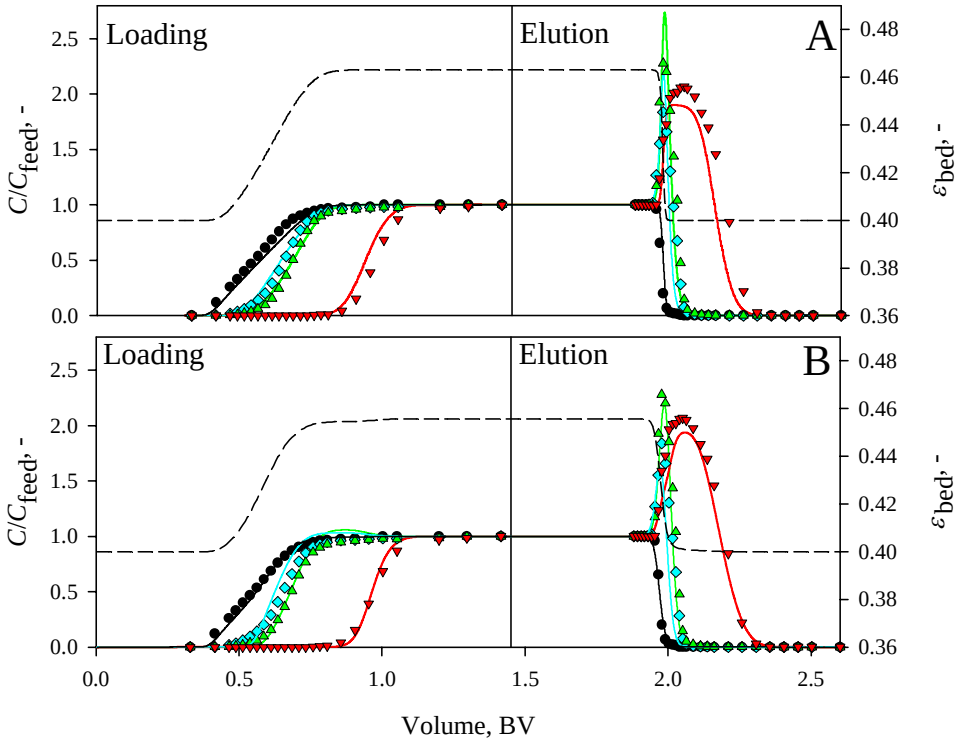

Figure 19. Effect of sorption model on the prediction of the loading and elution curve of synthetic hydrolysate solution with CS16GC resin in acid form at a temperature of 50 °C. A = the empirical sorption model; B = the AS theory. Feed composition: see caption of Fig. 6 in Paper IV. For details, see captions of Figs. 15 and 18.

The computational effort required to calculate the pulse elution profiles shown in Fig. 18 with the dynamic column model using the two sorption equilibrium models studied here was also investigated [171]. With an average laptop computer (Intel Core i5 M 540, 4.0 GB RAM, Windows 7 64-bit), the computation times required using the empirical approach and the AS theory were 2 s and 110 s, respectively. The large difference in the computational effort is due to different approaches used to calculate the sorbed amount of components. In the empirical model, this is done explicitly using Eqs. (23)-(25) while in the AS theory a group of ordinary differential equations is solved. Naturally, the latter is a more time consuming method.

The effect of the modelling of resin volume changes on the correlation between the experimental and calculated elution profiles of the concentrated acid hydrolysates on a gel type resin is demonstrated in Fig. 20. Exclusion of the resin volume changes from the model leads to clearly erroneous prediction (Fig. 20). In the case of the constant resin volume, the predicted elution profile of sulfuric acid is steeper and less dilute than according to the experimental results. However, the breakthrough of sulfuric acid is not affected by the omission of the resin volume changes from the column model (Fig. 20). The infinitely low sulfuric acid concentration at the sulfuric acid front does not cause resin shrinking and, therefore, the breakthrough of sulfuric acid is independent of the resin volume changes.

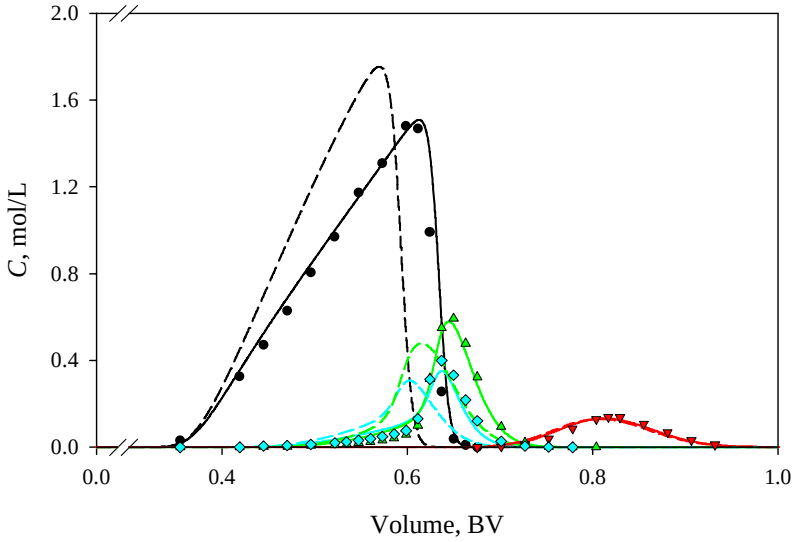

Figure 20. Effect of the modelling of resin volume changes on the prediction of the elution of a pulse of concentrated acid hydrolysate on CS16GC resin in acid form. Lines: calculated results; line colors correspond to the symbol colors, see caption of Fig. 15; solid = changing resin volume; dashed = constant resin volume. Symbols: experimental results, see caption of Fig. 15. Sorption model: the empirical approach; model parameters are given in Paper III.

The erroneous prediction of the sulfuric acid profile in the case of constant resin volume also affects the prediction of the elution of the monosaccharides (Fig. 20). The main parts of the monosaccharide profiles elute too early and the focusing of the monosaccharides is not as strong as according to the experimental results. The latter is caused by the faster propagation of the rear parts of the sulfuric acid profile which decreases the accumulation of the monosaccharides to the rear of the sulfuric acid profile.

The exclusion of the resin volume changes from the column model does not affect the prediction of the acetic acid profile in the case shown in Fig. 20. This is due to the relatively

strong sorption of acetic acid: it elutes so far behind sulfuric acid that the changes in the resin volume do not affect the elution of acetic acid.

On the basis of the results showed in this Chapter, the empirical approach was chosen to be used in predicting the multi-component sorption equilibria in this thesis work. In addition, it was deemed necessary to model the resin volume changes in order to obtain good correlation between the experimental and simulated results.

8.2.3 Effect of resin crosslinking degree on the fractionation

In paper I, the effect of the crosslinking degree of the gel type strong cation exchange resins (for resin details, see Table 3) on the chromatographic fractionation of concentrated acid hydrolysates was investigated experimentally. Authentic spruce and birch hydrolysates (30 wt. % sulfuric acid) were used as feed solutions. In this Chapter, the effects of the crosslinking on the elution behavior will be reviewed. The effects of resin crosslinking on the separation process performance will be discussed in Chapter 8.2.4.

The degree of resin crosslinking was found to have a strong impact on the fractionation task at hand (Fig. 21). As the degree of resin crosslinking decreases the sorption of sulfuric acid increases. This is due to lower charge density of the less crosslinked resins and, thus, also weaker electrolyte exclusion. The breakthrough of sulfuric acid is unaffected by the resin crosslinking due to complete electrolyte exclusion at infinite dilution and due to the fact that resin shrinking does not occur at infinite dilution (Fig. 21).

Sorption of the monosaccharides and acetic acid was also found to increase with decreasing resin crosslinking (Fig. 21) due to diminished size exclusion effect with less crosslinked resins. HMF and furfural, present in small quatities in the authentic hydrolysates, are completely separated from the other components (Fig. 21). The degree of resin crosslinking has only a minor effect on their elution.

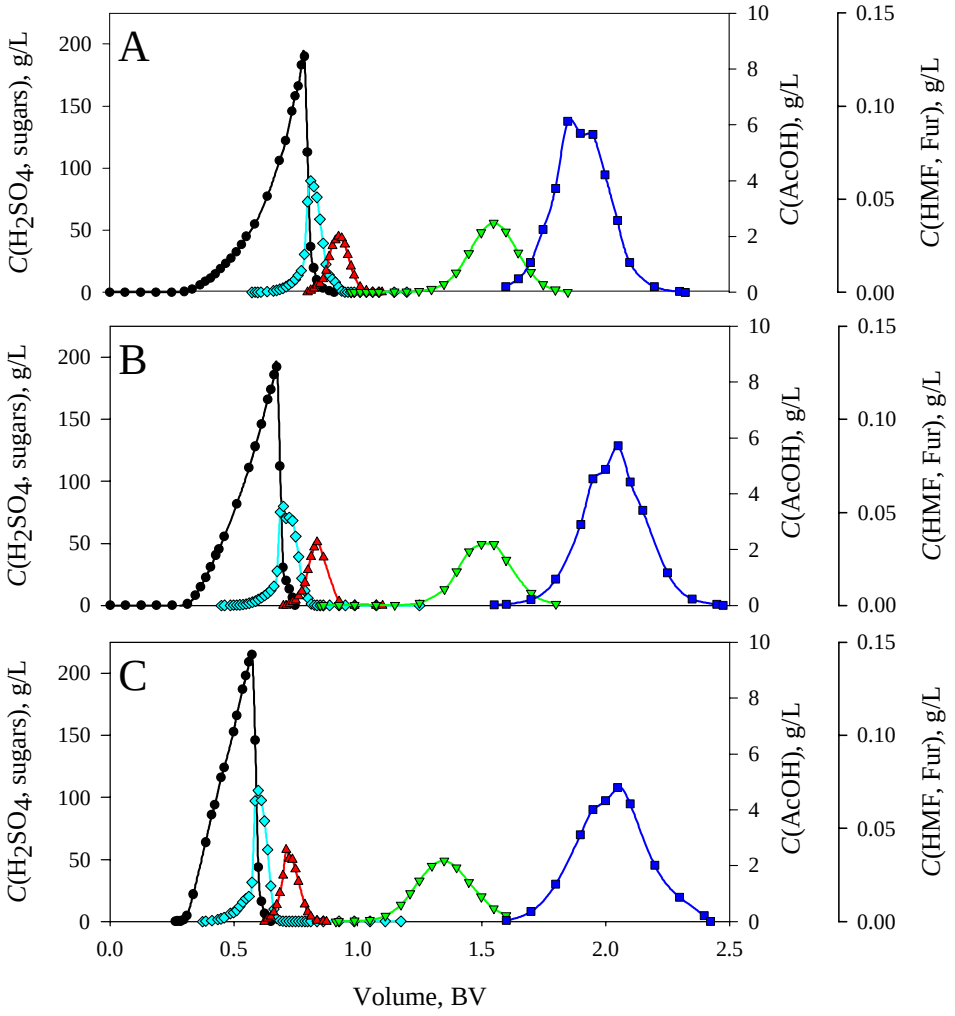

Figure 21. Effect of the crosslinking degree (wt. % DVB) of a gel type strong acid cation exchange resin in acid form on the fractionation of concentrated acid spruce hydrolysate at a temperature of 50 °C. Degree of resin crosslinking: 4.5 wt. % (A), 6.0 wt. % (B), and 8.0 wt. % (C). The monosaccharides are shown as one pseudocomponent. For feed composition and experimental details, see Paper I. Symbols: black ● = sulfuric acid; cyan ◆ = monosaccharides; red ▲ = acetic acid; green ▼ = HMF; blue ■ = furfural. Lines are presented to guide the eye.

8.2.4 Process performance

The separation performance of the single-column batchwise chromatographic fractionation was investigated both experimentally and by simulations. The experimental investigation was

limited to the investigation of the effects of resin crosslinking on the separation performance. A detailed description of this investigation is given in Paper I.

Numerical simulations were used to investigate the performance of both a stand-alone chromatographic fractionation and a chromatographic fractionation coupled with biomass hydrolysis and recycling of sulfuric acid. Stand-alone means here that recycling of fractions from the chromatographic separation step to the hydrolysis reactor was not considered. This investigation was done with one resin, CS16GC (8 wt. % DVB), for which the model was derived. A detailed description of this investigation is given in Paper III.

Effect of resin crosslinking degree

The effects of resin crosslinking on the monosaccharide yield Y_{sugar} and productivity Pr_{sugar} in the batchwise fractionation are shown in Fig. 22. The constraints used for the cut points of the monosaccharide fraction were the sulfuric acid yield Y_{H2SO4} and the maximum acetic acid concentration in the monosaccharide fraction $c_{AcOH}^{product}$. For details, see Paper I.

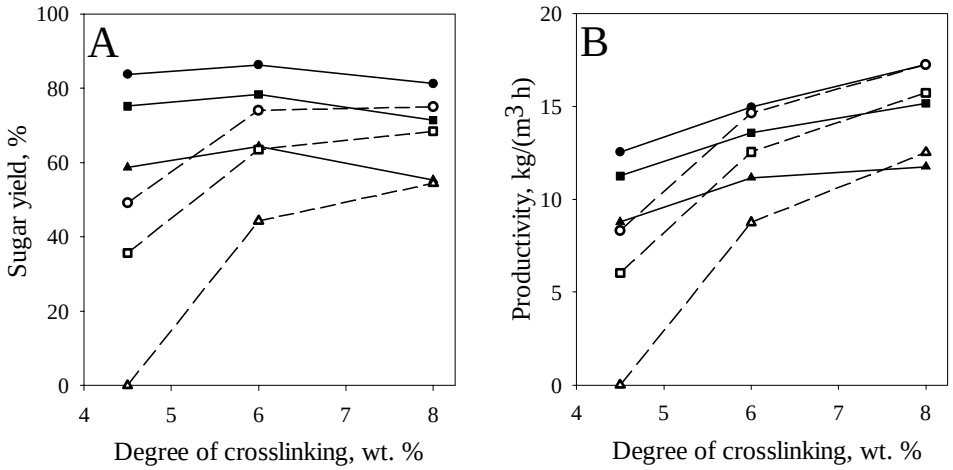

Figure 22. Effect of resin crosslinking degree on Y_{sugar} (A) and Pr_{sugar} (B). Y_{H2SO4} is varied and $c_{AcOH}^{product}$ is kept constant at 1.0 g/L: (●) = 90 %, (■) = 95 %, and (▲) = 98 % H_2SO_4 yield. Filled symbols = spruce hydrolysate; open symbols = birch hydrolysate. Lines are presented to guide the eye. For details, see Paper I.

It was found out that acetic acid concentration of the hydrolysate has a strong effect on the separation performance (Fig. 22). With the spruce hydrolysates which contained only a low amount of acetic acid (see Paper I for details), Y_{sugar} depended only slightly on the resin crosslinking (Fig. 22A). On the other hand, with the birch hydrolysate which contained larger amount of acetic acid, the effect of resin crosslinking on Y_{sugar} is considerable (Fig. 22A). This results from the fact that the sorption of the monosaccharides is more strongly affected by size

exclusion than that of acetic acid. The size exclusion effect becomes weaker with decreasing resin crosslinking and, thus, the sorption of acetic acid increases only slightly while the sorption of the monosaccharides increases considerably (see Fig. 21). As a consequence of the size exclusion effect, the monosaccharide–acetic acid separation efficiency and Y_{sugar} increases when the degree of crosslinking increases (Fig. 22A).

Pr_{sugar} was found to increase with increasing degree of resin crosslinking (Fig. 22B). This is due to a shorter cycle time resulting from the smaller overall sorption with resins with higher degree of crosslinking (see Fig. 21). This decrease in the overall sorption results from the stronger electrolyte exclusion and size exclusion effects. The effect of acetic acid on Y_{sugar} is also seen in the productivity (Fig. 22B): Pr_{sugar} depends on the resin crosslinking more in the case of the birch hydrolysate than in the case of the spruce hydrolysate.

Separation performance of the stand-alone fractionation process

Numerical simulations were used to evaluate the separation performance of the stand-alone fractionation process. It was found out that the sulfuric acid concentration of the hydrolysate has a significant effect on the separation. Decrease in the acid concentration increases the productivity of the separation process and the yield of the monosaccharides, and decreases the eluent consumption. For example, Pr_{sugar} is approximately doubled when the sulfuric acid concentration is decreased from 30 wt. % to 20 wt. % (Fig. 23).

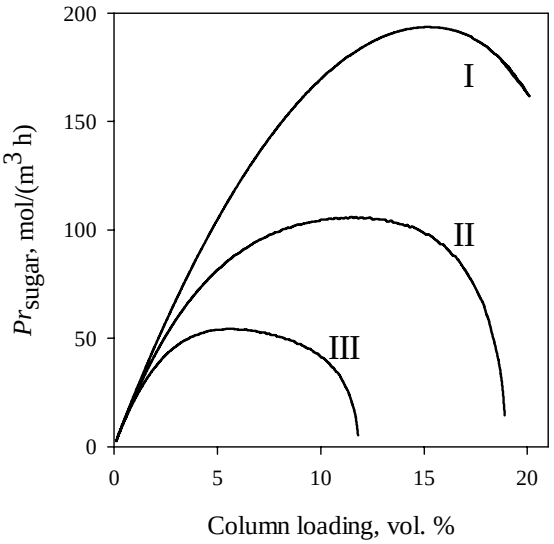

Figure 23. Effects of column loading and sulfuric acid concentration on Pr_{sugar}. Feed composition: 10 wt. % (I), 20 wt. % (II), or 30 wt. % (III) sulfuric acid; for other components see caption of Fig. 6 in Paper III. Operating conditions: flow rate = 1.5 BV/h; for other details, see Paper III.

The column loading has also a strong effect on the separation performance. This is illustrated for Pr_{sugar} in Fig. 23. Pr_{sugar} goes through a wide maximum with increasing column loading. The optimal loading also depends on the sulfuric acid concentration in the hydrolysate. For example for Pr_{sugar}, the optimal loading with 20 wt. % sulfuric acid is approximately two times larger than with 30 wt. % acid (Fig. 23). A detailed discussion of the effects of the sulfuric acid concentration and the column loading on the performance is given in Paper III.

The effects of the flow rate and the column loading on the performance of the stand-alone single-column batchwise fractionation process were investigated outside the appended publications. The fractionation constraints given in Paper III were used. The results are shown in Fig. 24. Approximately 30 000 simulations were done to obtain the results.

The monosaccharide yield was found to decrease with increasing flow rate and column loading (Fig. 24A) due to increasing overlapping of the components, especially sulfuric acid and the monosaccharides. The effect of the loading on the monosaccharide yield is more pronounced than that of the flow rate (Fig. 24A). High monosaccharide yield in the single-column batchwise fractionation can only be obtained with very low column loadings. In this region, however, the values of other performance parameters are unsatisfactory (Fig. 24).

On the contrary to the monosaccharide yield, the sulfuric acid yield Y_{H2SO4}, increases with increasing column loading and flow rate (Fig. 24B). With increasing loading and flow rate, a larger part of the rear shock layer is taken into the sulfuric acid fraction due to the definition of the cut point between the sulfuric acid and monosaccharide fractions (for details, see Paper III). The changes in Y_{H2SO4} are not nearly as significant as the changes in Y_{sugar}. Also in this case, the effect of the column loading on the yield is more pronounced (Fig. 24B).

The productivity of the separation process has a well-defined maximum (Fig. 24C). With low column loadings and flow rates, increase in both variables increase Pr_{sugar} although the monosaccharide yield decreases rapidly (Fig. 24A) as the amount of monosaccharides treated in one cycle increases. Maximum Pr_{sugar} 481.2 mol/(m^3 h) was obtained with flow rate 9.03 BV/h and column loading 7.68 vol. %. At this point, Y_{sugar} was only 42.2 %. After a certain point, further increase in column loading or flow rate leads to decrease in Pr_{sugar} as Y_{sugar} becomes very small (Fig. 24). The column loading affects Pr_{sugar} more than the flow rate as column loading has a more pronounced effect on the monosaccharide yield (Fig. 24A).

Eluent consumption *EC*, depends also strongly on the column loading and the flow rate (Fig. 24D). The flow rate obviously has a stronger effect on *EC* than column loading. The minimum *EC* 13.85 L/mol was obtained with flow rate 2.36 BV/h and column loading 14.1 vol. % (Fig. 24D). At this point, Pr_{sugar} was approximately 50 % lower than the maximum value. However, at the point giving the maximum Pr_{sugar}, *EC* was two times higher than the minimum *EC* value. Obviously compromises must be made regarding the process performance, as is usually the case in process industry.

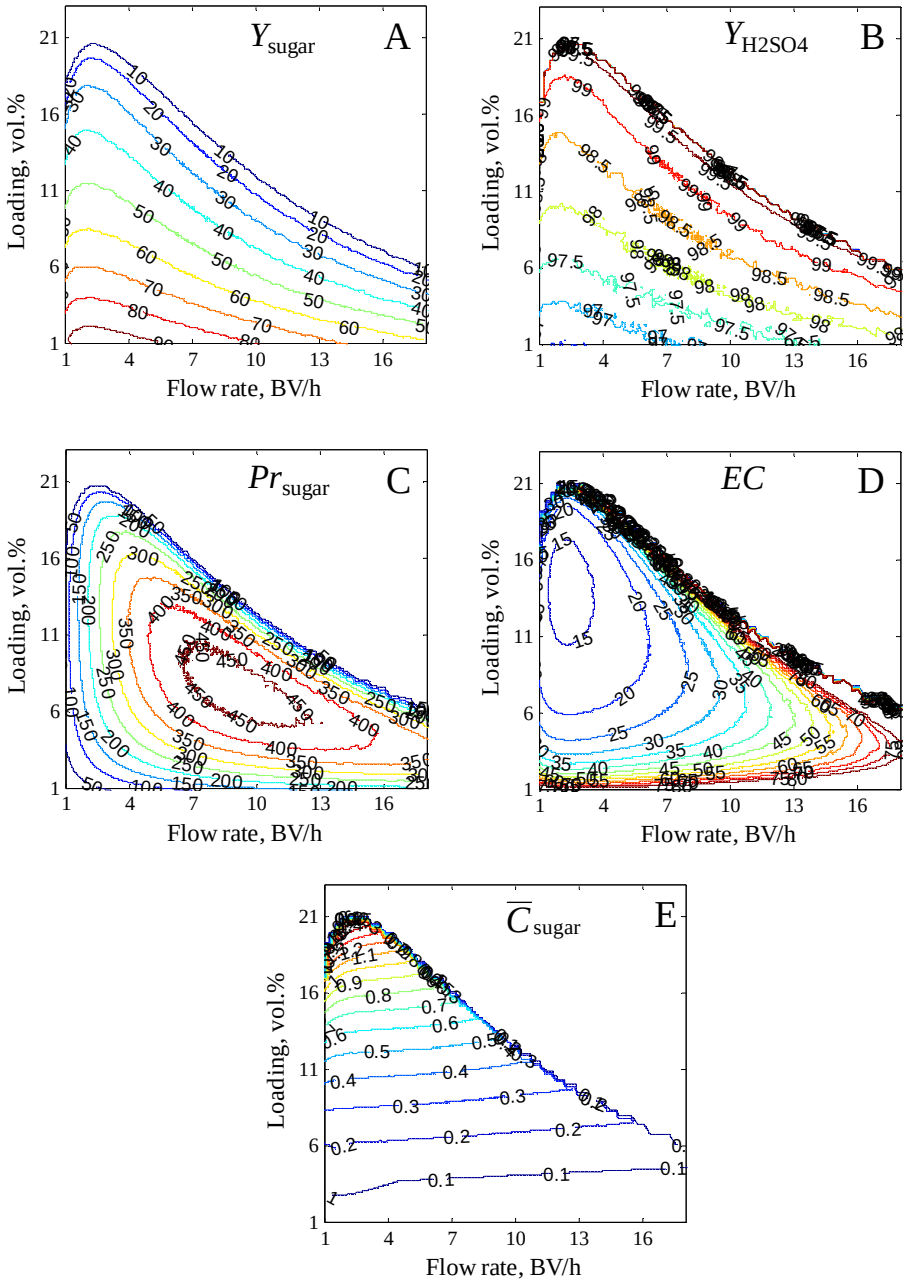

Figure 24. Effects of flow rate and column loading on the performance of a single-column batchwise chromatographic fractionation of concentrated acid lignocellulosic hydrolysates. Feed: 2.32 mol/L (20 wt. %) sulfuric acid, 0.35 mol/L glucose, 0.35 mol/L xylose, and 0.16 mol/L acetic acid. Operational conditions, model parameters, and fractionation constraints are given in Paper III.

Increase in the column loading was found to increase the average monosaccharide concentration in the monosaccharide fraction (Fig. 24E). On the other hand, the flow rate had only a minor effect on the monosaccharide concentration. This is due to the effect of the flow rate on the separation performance. With increasing flow rate the strength of the focusing decreases as the component profiles become more diffuse due to mass transfer limitations (Fig. 25). The cut points have to be adjusted accordingly. The cut point between the monosaccharide and acetic acid fractions is shifted to the left, and the cut point between the sulfuric acid and monosaccharide fractions is shifted to the right (Fig. 25). As a result, the amount of monosaccharides in their target fraction decreases. However, at the same time the volume of this fraction decreases and, thus, the average monosaccharide concentration remains approximately constant as the flow rate is increased and the loading is kept constant.

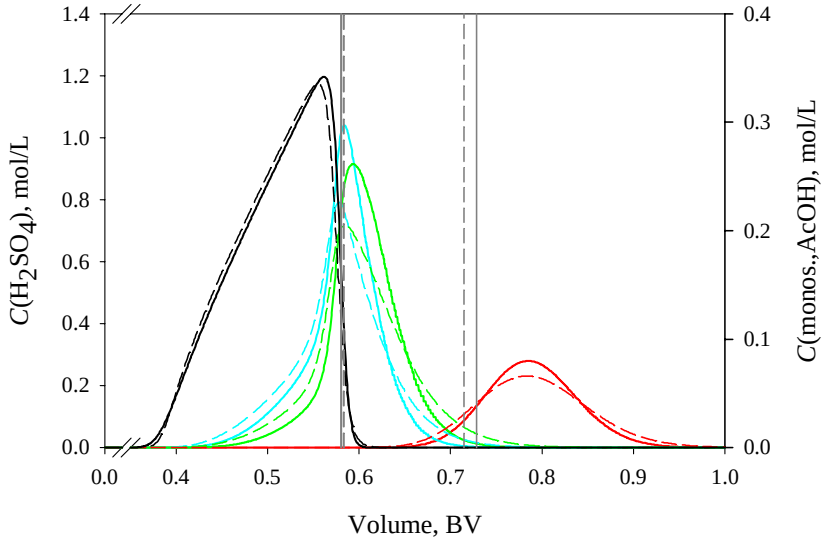

Figure 25. Effect of flow rate on the elution profiles of the main components of concentrated acid hydrolysates. Flow rates: 5.98 mL/min (solid lines); 11.25 mL/min (dashed lines); line colors correspond to the symbol colors in Fig. 15; vertical lines mark the cut points of the monosaccharide fraction. For other details, see caption of Fig. 24 and Paper III.

Chromatographic fractionation coupled with the recycling of sulfuric acid to biomass hydrolysis

The performance of the single-column batchwise chromatographic fractionation in a process consisting of a two-step concentrated acid hydrolysis, chromatographic separation, and sulfuric acid recycling steps was also investigated in this work by numerical simulations. The studied process is shown in Fig. 1 in Paper III. In this investigation, the feed concentration of sulfuric acid was 20 wt. %. The monosaccharides in the sulfuric acid fraction obtained in the

chromatographic separation were recycled back to the hydrolysis reactor and were not treated as lost product. The formation of HMF and furfural in the hydrolysis was omitted from here: these were assumed to be removed by adsorption [33,52-56]. A detailed description of the studied process and the parameters used in the performance evaluation are given in Paper III.

It was found out that with the recycling of the sulfuric acid fraction, the column loading giving the maximum productivity (18.2 vol. % in steady state) is considerably higher than in the single pass operation (13.0 vol. %) (Fig. 26). In addition, significant increase to maximum Pr_{sugar} was obtained with the recycling (Table 4). This is due to increased amount of monosaccharides in the feed: monosaccharides in the sulfuric acid fraction are recycled from the chromatographic separation back to the hydrolysis reactor (see Fig. 1 in Paper III).

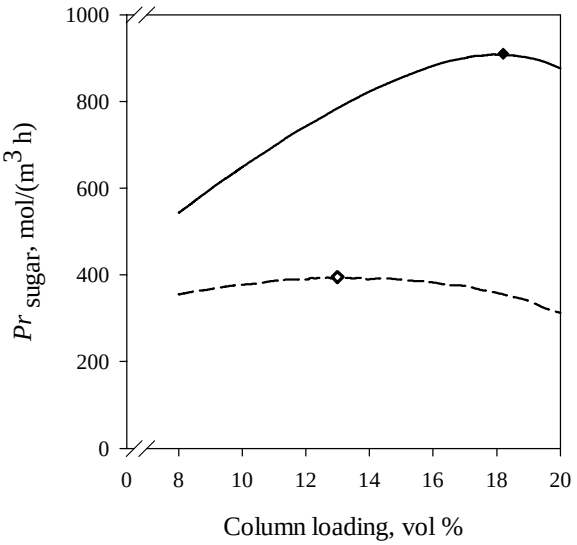

Figure 26. Pr_{sugar} in the chromatographic frctionation step in a process shown in Fig. 1 of Paper III without sulfuric acid fraction recycling (dashed line) and in steady state with sulfuric acid fraction recycling (solid line). Symbols: open diamond = maximum Pr_{sugar} without recycling; filled diamond = maximum Pr_{sugar} with recycling. Details are given in Paper III.

After the chromatographic separation step the sulfuric acid has to be concentrated to 70 wt. % [23,24] to be reused in the hydrolysis. In the case studied here, this means that approximately 90 % of the water in the sulfuric acid fraction has to be removed for example using multiple effect evaporator [92,109] or vapor compression distillation [23,24,109]. In the studied system, the recycling of sulfuric acid decreased the fresh acid consumption of the two-step concentrated acid hydrolysis by approximately 91 %. The water removed from the sulfuric acid fraction can be used to replace fresh eluent water in the chromatographic separation: 61 % decrease in the fresh water consumption was reached in this example case.

Table 4. Performance of the chromatographic fractionation step in a process shown in Fig. 1 of Paper III without H_2SO_4 fraction recycling (single pass) and with H_2SO_4 fraction recycling in steady state. Details are given in Paper III.

	Separation with a single pass	Separation with recycling
Pr_{sugar}, mol/(m^3 h)	354.82	910.20
Y_{sugar}, %	32.0	90.6
Y_{H2SO4}, %	99.0	97.0
EC, L/mol	13.91	5.42

The monosaccharide yield was also increased significantly by the recycling of the sulfuric acid fraction (Table 4): over 90 % of the monosaccharides that are fed to the separation column end up to the monosaccharide fraction. The rest of the monosaccharides are taken out from the process in the acetic acid fraction. With a rough calculation, the monosaccharide yield from the whole process (yield in the hydrolysis: 80 %) with the recycling in the studied case was 72.5 %. In addition to the increased Pr_{sugar} and Y_{sugar}, considerable decrease in the eluent consumption is achieved with the recycling of the sulfuric acid fraction (Table 4).

8.2.5 Fermentability of chromatographically purified hydrolysates

The effectiveness of the chromatographic fractionation was verified by fermentative production of ethanol from chromatographically purified monosaccharide fractions (see Paper II for details). CS12GC resin in acid form was used as a stationary phase and authentic concentrated acid (30 wt. %) spruce and birch hydrolysates were used as feed solutions.

The chromatographically purified monosaccharide fractions were fermented at VTT Biotechnology (Technical Research Centre of Finland, Espoo, Finland) using *S.cerevisiae* and *P. stipitis* yeasts. Fermentation of $Ca(OH)_2$ neutralized hydrolysate was used as a reference. Of the studied yeasts, *S. cerevisiae* was found to give considerably higher ethanol productivity than *P. stipitis*. Only the results obtained with *S. cerevisiae* are shown here, a detailed discussion is given in Paper II.

It was found out that the chromatographic purification provides a notable increase in the ethanol yield over the $Ca(OH)_2$ neutralization (Table 5) although the ethanol productivity from both solutions were comparable (Fig. 27). The improvement in the ethanol yield results from the removal of all HMF and furfural and most of acetic acid with chromatography (see Table 2 in Paper II). $Ca(OH)_2$ neutralization, on the other hand, does not remove all of these by-products [33,34].

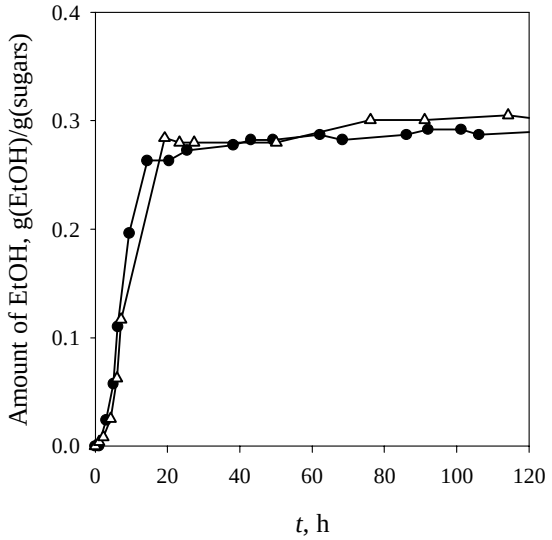

Figure 27. Ethanol production from concentrated acid spruce hydrolysate with *S. cerevisiae*. Experimental conditions: see Paper II. Symbols: ● = chromatographically purified hydrolysate; final pH adjustment with $Ca(OH)_2$; ▵ = $Ca(OH)_2$ neutralized hydrolysate. Lines are presented to guide the eye.

Table 5. Ethanol yields obtained from purified concentrated acid lignocellulosic hydrolysates using *S. cerevisiae*.

	Chrom. purified		$Ca(OH)_2$ neutralized	
Yeast	Spruce	Birch	Spruce	Birch
Y / total sugars	74.3 %	64.7 %	61.3 %	60.5 %
C_{EtOH}, g/L	14.9	13.3	14.8	14.5

8.3 Fractionation using multi-column chromatographic processes

The use of multi-column chromatographic separation processes for the fractionation of concentrated acid lignocellulosic hydrolysates was also investigated in this work. Two multi-column process schemes were chosen for the investigation: the Multi-Column Recycling Chromatography (MCRC) process, i.e., the Sequential SMB (Chapter 5.3), and the Japan Organo (JO) process (Chapter 5.2). The most important results obtained in the investigation of these multi-column process schemes will be reviewed here.

8.3.1 Multi-Column Recycling Chromatography

Use of the MCRC process for the chromatographic fractionation of concentrated acid lignocellulosic hydrolysates was investigated in Paper V. Using the design method based on the ideal model of chromatography, distance–time diagram, and numerical simulations, (see

Paper V for details), a four-column MCRC scheme shown in Fig. 28 was chosen for this separation task. The selected process scheme allows the introduction of a feed pulse into the process before the mass of the preceding feed pulse has been completely taken out. This reduces the eluent consumption as part of the eluent is replaced with the fresh feed.

In the selected four-column MCRC process scheme, sulfuric acid is collected at outlet of each column in order to minimize dilution and spreading of the profile. In total, four sulfuric acid fractions are collected in one cycle (Fig. 28). On the other hand, monosaccharides and acetic acid are collected at one column outlet only. Collection of the monosaccharides occurs at the outlet of the last column. This is because the separation between sulfuric acid and the monosaccharides is difficult, but greatly improved by the co-operative effect of sulfuric acid on the sorption of the monosaccharides (see Chapter 8.2). Therefore, a long elution path is favorable for good monosaccharide recovery. Acetic acid collection is done from the outlet of the third column after it has been completely separated from the other components.

To improve the monosaccharide and sulfuric acid yields, the unresolved parts of the profiles of these components are recycled as a prefeed fraction in the chosen process scheme (Fig. 28). After this recycling operation, fresh feed is introduced to column one.

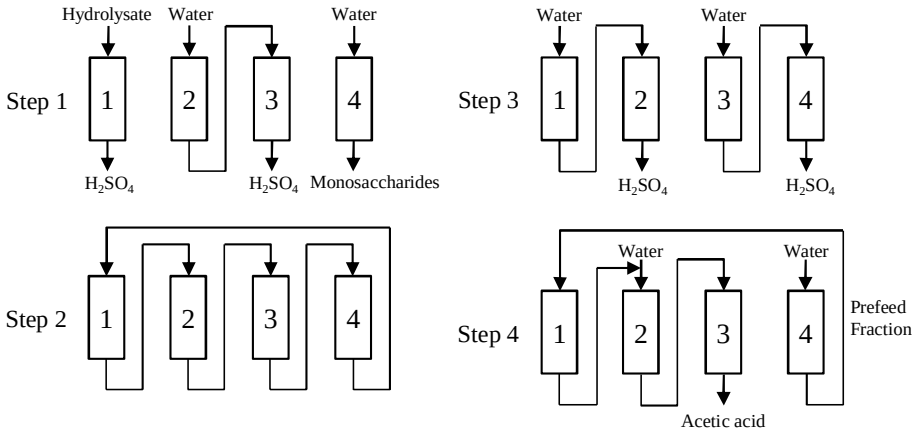

Figure 28. Four-column MCRC process for the chromatographic fractionation of concentrated acid lignocellulosic hydrolysates.

Fractionation of concentrated acid hydrolysates using the four-column MCRC scheme (Fig. 28) was studied experimentally using both synthetic feed solution and authentic softwood hydrolysate. The maximum flow rates used were calculated using Eq. (42) by setting the maximum feasible pressure drop from process inlet to outlet to 2 bar. However, such a limit would allow very high flow rates in the small laboratory scale columns (d_{bed} = 2.5 cm, h_{bed} = 20 cm, d_p = 246µm) used in this work and render the results irrelevant for large scale applications. Therefore, the actual flow rates were chosen by considering an industrial scale column (d_{bed} = 1.5 m, h_{bed} = 3.0 m, d_p = 246µm), applying a pressure limit of

2 bar, and scaling down while keeping the volumetric flow rate proportional to the bed volume constant.

The characteristic features of the outlet profiles obtained with the MCRC process (Fig. 29) are similar to those obtained in the single-column batchwise fractionation (see Fig. 15). With the selected MCRC scheme (Fig. 28), high total purity of sulfuric acid was achieved with the synthetic feed solution (Table 6). For details, see Paper V.

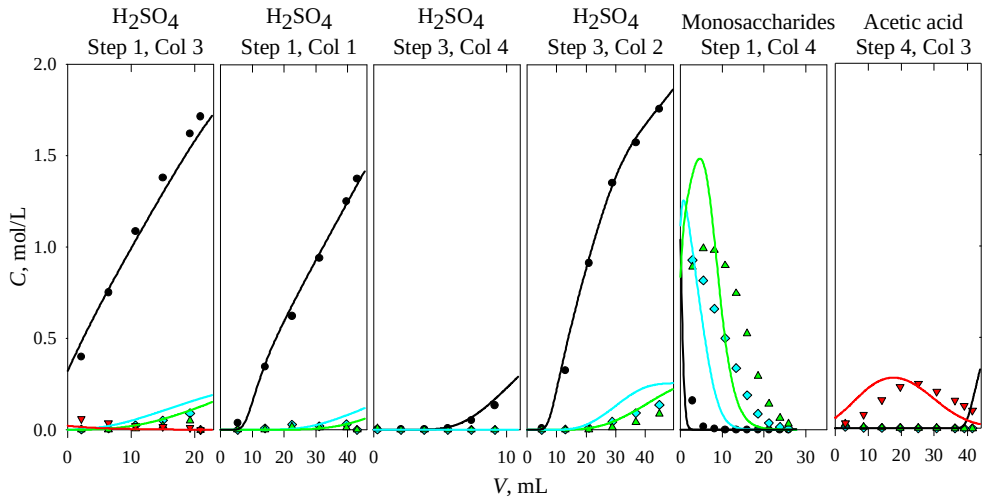

Figure 29. Outlet profiles in steady state in the fractionation of concentrated acid hydrolysate with the four-column MCRC process (Fig. 28). For feed composition and operating parameters, see caption of Fig. 6 in Paper V. Symbols: experimental results; see caption of Fig. 15. Lines = calculated results; line colors correspond to the symbol colors.

Table 6. Performance of the four-column MCRC process (Fig. 28) in the fractionation of synthetic and authentic concentrated acid hydrolysate. Data from experiments. For details, see Paper V.

	Hydrolysate type	
	Synthetic	Authentic
Pr_{sugar}, mol/(m^3 h)	235.93	142.48
Y_{H2SO4}, %	97.95	95.78
Y_{sugar}, %	80.77	72.09
Y_{AcOH}, %	88.09	83.12
Pu_{H2SO4}, %	93.69	95.89
Pu_{sugar}, %	96.40	93.77
Pu_{AcOH}, %	91.46	41.04
EC_{Sugar}, L/mol	5.56	10.47

All monosaccharides eluting after the sulfuric acid profile could be collected to their target fraction in the selected MCRC scheme (Fig. 29: step 1, col 4). Approximately 96.4 % pure monosaccharide fraction could be obtained with the synthetic feed solution (Table 6). The yield of the monosaccharides was also relatively high.

Focusing of the monosaccharides is also evident in the MCRC process (Fig. 29). Due to this highly beneficial phenomenon, the maximum monosaccharide concentrations in their target fraction were significantly higher (0.94 mol/L glucose; 1.0 mol/L xylose) than in the feed solution (0.32 mol/L glucose; 0.4 mol/L xylose). Due to the focusing, also the average monosaccharide concentrations in their target fraction (0.36 mol/L glucose; 0.56 mol/L xylose) were higher than the feed concentrations. This clearly demonstrates the beneficial effect of the focusing on the process economy.

Acetic acid purity and yield were also high when the synthetic feed solution was used (Table 6) (Fig. 29). On the contrary to the single-column batchwise fractionation (see Fig. 15), in the MCRC process the focusing of acetic acid due to co-operative effect of sulfuric acid on acetic acid sorption (Fig. 29). Maximum concentration of acetic acid, 0.23 mol/L, is higher than the feed concentration, 0.16 mol/L. However, the focusing is too weak to prevent the dilution of the acid fraction: the average acetic acid concentration in its target fraction was 0.13 mol/L whereas the feed concentration was 0.16 mol/L.

Fractionation of authentic concentrated acid softwood hydrolysate (for the composition, see Table 1 in Paper V) using the MCRC process (Fig. 28) was also investigated experimentally. Also in this case a good separation performance was achieved (Table 6). Only acetic acid purity was very low, which is reasonable considering its low acetic acid concentration of the feed solution (see Table 1 in Paper V). The small amounts of HMF and furfural in the authentic hydrolysate did not cause any problems to the separation performance.

The model derived in this work for the separation task at hand gave a good correlation between the experimental and calculated profiles also in the case of the MCRC process (Fig. 29). Some minor differences were noted between the results due to the simple resin shrinking model used (Eq. (30)). For details, see Paper V.

Comparison of MCRC and single-column batch chromatography

To obtain a better picture of the separation performance of the four-column MCRC scheme (see Fig. 28), the results obtained in the experimental work were compared with simulated results obtained with a single-column batchwise fractionation of concentrated acid hydrolysates using four parallel columns (h_{bed} = 20 cm, d_{bed} = 2.5 cm). Full optimization of the MCRC process was not attempted in this work.

The batch process was found to give significantly higher Pr_{sugar} (1925 mol/(m^3 h)) than the MCRC process (235.9 mol/(m^3 h)). Without paying any attention to eluent consumption and monosaccharide yield, the batch process seems more feasible option. However, at the point giving the maximum Pr_{sugar}, EC of the traditional batch process was approximately 20 times higher than that of the MCRC process (5.6 L/mol). In addition, Y_{sugar} obtained with the batch process was considerably lower (42.2 %) than with the MCRC process (80.8 %). This clearly demonstrates the efficiency of the MCRC concept in reducing the eluent consumption. Low eluent consumption is beneficial especially in such biorefinery applications as investigated here as it is directly related to energy consumption and CO_2 emissions.

8.3.2 Japan Organo process

Outside the appended publication, the use of the Japan Organo (JO) process for the fractionation of concentrated acid hydrolysate was investigated by numerical simulations. The results presented here are taken from Ref. [2]. Same purity constraints were used as in the process performance evaluation of the single-column batchwise fractionation process (see Paper III). Purity constraints were given only for the monosaccharide outlet stream. In the studied system, sulfuric acid as the least sorbed component and acetic acid as the most sorbed component elute as raffinate and extract, respectively (see Fig. 9). Monosaccharides are collected to the intermediate outlet stream.

Investigation of the eluent consumption was excluded from this study, and, therefore, internal recycling stream was not utilized. Due to this, the process was operated without zone IV (see Fig. 9). Five columns were connected in configuration 1:2:2. The inlet flow rates to the system in steps one and two were defined as the maximum feasible flow rates when the pressure loss from the system inlet to the system outlet was set to 4 bar. Industrial scale columns (d_{bed} = 2.5 cm, h_{bed} = 20 cm, d_p = 246µm) were used in this investigation.

As no zone IV and recycle stream was utilized, the outlet flow rates in step one of the JO process were equal to the inlet flow rates in the corresponding section of the process (see Fig. 9). The maximum possible flow rates were used in step one. The effect of the duration of this step t_1 (1.0-2.2 min), on the separation performance was investigated here.

In step two, only eluent is fed to the process while two outlet streams exist (extract and raffinate). Here, the effect of raffinate and extract stream flow rates on the separation performance was evaluated by changing the ratio of these streams υ. In addition, the effect of the duration of step two t_2 (3.0-3.7 min) on the performance was investigated.

With the selected JO scheme steady state was reached in 15 cycles. The spatial profiles in steady state obtained with the Japan Organo process at an operating point the highest separation performance are shown in Fig. 30. The characteristic features of the spatial profiles are similar to the outlet profiles obtained with the single-column batch process (Fig. 15) and

the four-column MCRC scheme (Fig. 29). Like in the case of the MCRC process, focusing of the monosaccharides at the rear of the sulfuric acid profile is very strong: the maximum concentrations are approximately three times larger than those in the feed solution. Also in this case, acetic acid is well separated from sulfuric acid and the monosaccharides (Fig. 30).

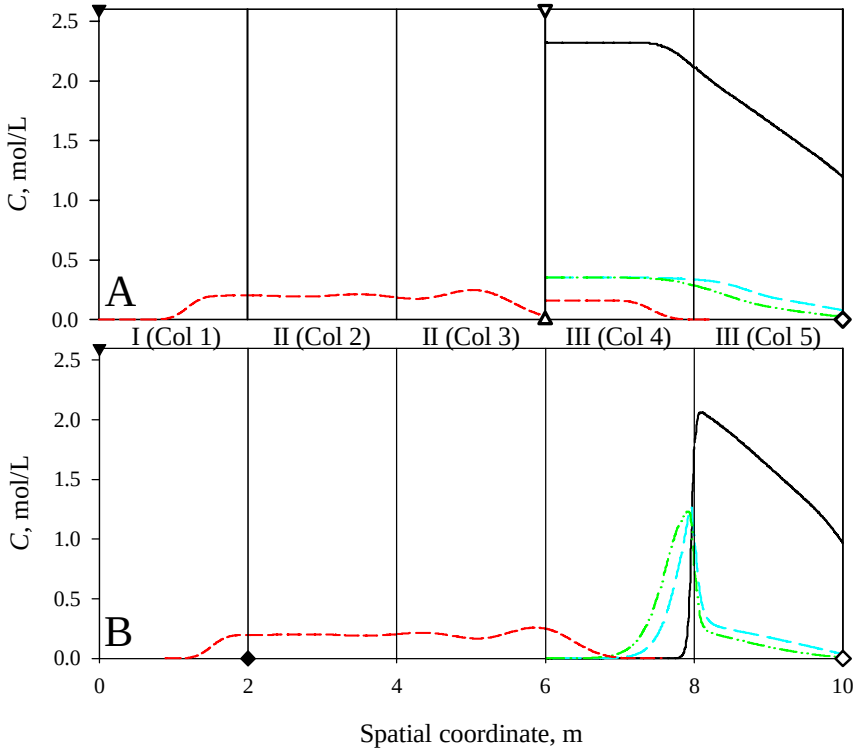

Figure 30. Spatial steady state profiles of a five-column Japan Organo process at the end of the first step (A) and at the end of the second step (B). Feed composition: see caption of Fig. 24. Operating parameters: h_{bed} = 2 m, d_{bed} = 2 m, $t_{step,1}$ = 2.0 min, $t_{step,2}$ = 3.59 min, $\dot{V}_{feed,1}$ = 123.1 m^3/h, $\dot{V}_{eluent,1}$ = 82.1 m^3/h, $\dot{V}_{eluent,2}$ = 73.5 m^3/h, and υ = 0.216. Lines: black solid = sulfuric acid; cyan dash = glucose; green dash-dot-dot = xylose; red dash = acetic acid. Symbols: ▼ and ▽ indicate the inlet positions of eluent and feed streams, respectively; ◆, ◇, and △ indicate the outlet positions of extract, raffinate, and intermediate streams, respectively. Roman numerals indicate the zone.

Pr_{sugar} in the JO process was found to increase with increasing duration of step 1 until t_1 was so large that the acetic acid front reached the inlet of the second column zone III. Increasing t_1 beyond this threshold quickly decreased Pr_{sugar} to zero with the given purity constraints. This is because the amount of acetic acid in the monosaccharide outlet stream becomes too large.

Highest Pr_{sugar} was obtained with t_1 = 2.0 min. Interestingly, Pr_{sugar} was found to stay on a relatively constant level as υ is increased (i.e., the flow rate through zones II and III decreases

in step two) and t_2 is increased. With t_2 = 3.59 min and φ = 0.216 (Fig. 30), Pr_{sugar} was 283 mol/(m^3 h) which was approximately two times larger than obtained in a single-column batchwise fractionation (145 mol/(m^3 h) using one column with similar dimensions (h_{bed} = 2 m, d_{bed} = 2 m, d_p = 246µm). However, when the single-column batchwise fractionation was done using five parallel columns, the JO process was found to be less effective than the batch process with respect to the productivity. Comparison with the four-column MCRC process scheme was be done here due to different column dimensions used in the investigations of these two processes.

Good yields were obtained for the sulfuric acid and acetic acid fractions: 97.3 % and 93.5 %, respectively. The monosaccharide yield was relatively low, 61.7 %, due to the co-elution of the monosaccharides with sulfuric acid (Fig. 30). Purities of the product streams with t_2 = 3.59 min and φ = 0.216 were 89.0 %, 88.7 %, and 100 % for sulfuric acid, monosaccharides, and acetic acid, respectively.

Average concentrations in each outlet streams in steady state are given in Table 7. All components in their target outlet streams were diluted: the most diluted component was sulfuric acid (Table 7). For the monosaccharides and acetic acid, the dilution is much smaller due to the co-operative effect of sulfuric acid on their sorption.

Table 7. Average concentrations in the feed solution and the outlet streams of the five-column Japan Organo process in steady state. For details, see caption of Fig. 30.

	Concentration, mol/L			
	Feed	Extract	Intermediate	Raffinate
H_2SO_4	2.32	0	0.08	0.44
Sugars	0.7	0	0.65	0.05
Acetic acid	0.16	0.13	$3.36 \cdot 10^{-3}$	$1.6 \cdot 10^{-3}$

9 CONCLUSIONS

In this thesis, *a systematic experimental and model-based study of the use of the electrolyte exclusion chromatography (EEC) for the fractionation of concentrated acid lignocellulosic hydrolysates* was conducted. Such hydrolysates are formed in the conversion of lignocellulosic biomasses (e.g., wood) to monosaccharides using sulfuric acid as a catalyst. Also other valuable chemicals are obtained in this process as by-products. Fractionation of the acidic lignocellulosic hydrolysates can be accomplished in one or two steps. In here, the two-step option was investigated. In the first step, some of the hydrolysis by-products, i.e., furans and phenols, are removed by adsorption. This step was not investigated in here as deep knowledge regarding this unit operation already exists. Instead, this work focused on the second step of the two-step fractionation process in which EEC is used for the fractionation of the furan- and phenol-free concentrated acid hydrolysates into sulfuric acid, monosaccharide, and acetic acid fractions. *Sulfonated gel type strong acid polystyrene–divinylbenzene cation exchange resins in acid (H^+) form* were used as a stationary phase in this work.

The main objective of this thesis was to determine the *phenomena affecting the fractionation* of the concentrated acid hydrolysates, and to *develop a simple model that takes these phenomena correctly into account*. Performance of the chromatographic fractionation was investigated experimentally and by simulations. The *effect of the resin crosslinking degree* on the separation was studied as well as the *effects of the hydrolysate composition* and *the operating conditions*. In addition, *different process options* available were investigated.

It was found out that the fractionation of concentrated acid lignocellulosic hydrolysates is well accomplished using the electrolyte exclusion chromatography. However, the separation task is far from simple due to the nature of the studied system. Interesting phenomena were observed; these complicate the separation, but also have beneficial effects on the separation performance. It was found out that sulfuric acid has a strong co-operative on the sorption of the other components present in the system. This effect is especially beneficial for the separation of sulfuric acid and the monosaccharides. Also other strong electrolytes were found to have this kind of co-operative effect on the sorption of nonelectrolytes.

The observed phenomena complicate the modelling of the separation task at hand. However, these phenomena could be taken into account with simple empirical models. The use of the Adsorbed Solution theory for the modelling of the sorption equilibria was also investigated, but the nature of this model resulted in slightly inaccurate predictions of the sorption equilibria. A simple and fast dynamic column model which takes into account the volume changes of the gel type resins used in this work as a stationary phase was also derived. Due to the simplicity of the derived model it is well suited for process design and optimization purposes. This model is also applicable for the modelling of the chromatographic fractionation of dilute acid lignocellulosic hydrolysates.

The investigation of the performance of the fractionation process revealed that in order to obtain good separation efficiency in the studied case, the concentrated acid hydrolysis should be done with as low sulfuric acid concentration as possible. This is due to increased separation efficiency obtained with lower sulfuric acid concentrations. Also, high degree of resin crosslinking (e.g., 8 wt. % DVB) was found to lead to increased separation performance, especially when the hydrolysates contain high amounts of acetic acid. This is the case, for example, if birch is used as raw material in the hydrolysis. The column loading and the flow rate also have large effects on the performance: the optimal values, naturally, depend on the objectives set for the separation. Compromises must be made when choosing the process parameters as is often the case in process industry: for example, minimum eluent consumption and maximum productivity cannot usually be obtained with the same parameters.

In this work, it was demonstrated that when the fractions obtained in the chromatographic fractionation are recycled to the preceding unit operations, these unit operations should be taken into account in the performance evaluation of the fractionation process. By using this kind of approach for a single-column batchwise fractionation, the need of fresh sulfuric acid in the hydrolysis could be reduced by 90 % with the recycling of the sulfuric acid. Considerable savings in the chemical costs related to the hydrolysis could be achieved. Also the need for fresh eluent water in the chromatographic fractionation decreased significantly.

Three process options for the fractionation of concentrated acid hydrolysates were investigated here (traditional single-column batch process, the Japan Organo (JO) process, and the Multi-Column Recycling Chromatography (MCRC) process). Of these, the single-column batch process gave the highest productivity with respect to the monosaccharides. However, when the eluent consumption and the monosaccharide yield were also taken into account, the MCRC was found to be superior to the batch process. It is especially efficient in reducing the eluent consumption which is very important for process industry.

Currently new renewable sources for chemical production are investigated extensively. Via the concentrated sulfuric acid hydrolysis, monosaccharides and other valuable platform chemicals can be produced efficiently from lignocellulosic biomasses. So far, the concentrated acid hydrolysis has been neglected mainly due to high chemical consumption. This work clearly shows that this chemical consumption can be decreased considerably by using the electrolyte exclusion chromatography for the fractionation of the hydrolysates obtained in the acidic hydrolysis. This method enables the recycling of the hydrolysis acid as well as the selective recovery of all components present in the obtained hydrolysates. The efficient fractionation of the hydrolysates depends naturally on the selection of the process scheme for the chromatographic separation. With a proper operation mode, very high separation efficiency and, thus, a high increase to the feasibility of the concentrated acid hydrolysis can be achieved.

REFERENCES

1 Blommel, P.G., Cortright, R.D., *Production of Conventional Liquid Fuels from Sugars*, http://www.biofuelstp.eu/downloads/Virent_Technology_Whitepaper.pdf, accessed, 24.3.2012.

2 Heinonen, J., Sainio, T., Chromatographic Fractionation of Lignocellulosic Hydrolysates, in *Advances in Chemical Engineering Vol. 42 – Chemical Engineering for Renewables Conversion* (Murzin, D.Y., ed.), Academic Press, San Diego, USA, 2013, pp. 261-350.

3 Parikka, M., Global Biomass Fuel Resources, *Biomass Bioenerg.* 27 (2004), 613-620.

4 Duff, S.J.B., Murray, W.D., Bioconversion of Forest Products Industry Waste Cellulosics to Fuel Ethanol: A Review, *Bioresource Technol.* 55 (1996), 1-33.

5 Galbe, M., Zacchi, G., A Review of the Production of Ethanol from Softwood, *Appl. Microbiol. Biotechnol.* 59 (2002), 618-628.

6 Hamelinck, C.N., von Hooijdonk, G., Faaij, A.P.C., Ethanol from Lignocellulosic Biomass: Techno-Economic Performance in Short-, Middle- and Long-Term, *Biomass Bioenerg*. 28 (2005), 384-410.

7 Sun, Z.-Y., Tang, Y.-Q., Iwanaga, T., Sho, T., Kida, K., Production of Fuel Ethanol From Bamboo by Concentrated Sulfuric Acid Hydrolysis Followed by Continuous Ethanol Fermentation, *Bioresource Technol.* 102 (2011), 10929-10935.

8 Sun, Y., Cheng, J., Hydrolysis of Lignocellulosic Materials for Ethanol Production: A Review, *Bioresource Technol*. 83 (2002), 1-11.

9 Takerzadeh, M.J., Karimi, K., Acid-Based Hydrolysis Processes for Ethanol from Lignocellulosic Materials: A Review, *Bioresources* 2 (2007), 472-499.

10 Taherzadeh, M.J., Karimi, K., Bioethanol: Market and Production Processes, in *Biofuels Refining and Performance* (Nag, A., ed.), McGraw-Hill, Fairfield, USA, 2008, pp. 69-106.

11 *International Energy Outlook 2013*, U.S. Energy Information Administration, http://www.eia.gov/forecasts/ieo/pdf/0484%282013%29.pdf, accessed 12.11.2013

12 Burk, M.J., Sustainable Production of Industrial Chemicals from Sugars, *Int. Sugar J.* 112 (2010), 30-35.

13 van Leeuwen, B.N.M., van der Wulp, A.M., Duijnstee, I., van Maris, A.J.A., Straathof, A.J.J., Fermentative Production of Isobutene, *Appl. Microbiol. Biotechnol.* 93 (2012), 1377-1387.

14 Luo, L., van der Voet, E., Huppes, G., Biorefining of Lignocellulosic Feedstock – Technical, Economic and Environmental Considerations, *Bioresource Technol.* 101 (2010), 5023-5032.

15 Kunkes, E.L., Simonetti, D.A., West, R.M., Serrano-Ruiz, J.C., Gärtner, C.A., Dumesic, J.A., Catalytic Conversion of Biomass to Monofunctional Hydrocarbons and Targeted Liquid-Fuel Classes, *Science* 333 (2008), 417-421.

16 Vogel, A., Mueller-Langer, F., Kaltschmitt, M., Analysis and Evaluation of Technical and Economic Potentials of BtL-Fuels, *Chem. Eng. Technol.* 31 (2008), 755-764.

17 Schaub, G., Vetter, A., Biofuels for Automobiles – An Overview, *Chem. Eng. Technol.* 31 (2008), 721-729.

18 Hamelinck, C.N., Faaij, A.P.C., den Uil, H., Boerrigter, H., Production of FT Transportation Fuels From Biomass: Technical Options, Process Analysis and Optimisation, and Development Potential, *Energy* 29 (2004), 1743-1771.

19 Fernando, S., Adhikari, S., Chandrapal, C., Murali, N., Biorefineries: Current Status, Challenges, and Future Direction, *Energ. Fuel.* 20 (2006), 1727-1737.
20 Wettstein, S., Alonso, D.M., Gürbüz, E.I., Dumesic, J.A., A Roadmap for Conversion of Lignocellulosic Biomass to Chemicals and Fuels, *Curr. Opin. Chem. Eng.* (2012), 218-224.
21 McMurry, J., *Organic Chemistry*, 7th ed., Thomson Learning, London, United Kingdom, pp. 973-1015.
22 Pedersen, S., Chemicals from Sugars, www.topsoe.com/sitecore/shell/Applications/~/media/PDF%20files/topsoe_catalysis_Forum/2008/pedersen.ashx, accessed 9.8.2013.
23 Farone, W.A., Cuzens, J.E., Method of Producing Sugars Using Strong Acid Hydrolysis of Cellulosic and Hemicellulosic Materials, U.S. Patent No. 5,562,777, October 8, 1996.
24 Farone, W.A., Cuzens, J.E., Strong Acid Hydrolysis of Cellulosic and Hemicellulosic Materials, U.S. Patent No. 5,597,714, January 28, 1997.
25 Iranmahboob, J., Nadim, F., Monemi, S., Optimizing Acid-Hydrolysis: A Critical Step for Production of Ethanol from Mixed Wood Chips, *Biomass Bioenerg.* 22 (2002), 401-404.
26 Gurgel, L.V.A., Marabezi, K., Zambon, M.D., Curvelo, A.A.S., Dilute Acid Hydrolysis of Sugarcane Bagasse at High Temperatures – A Kinetic Study of Cellulose Saccharification and Glucose Decomposition. Part II: Sulfuric Acid as Catalyst, *Ind. Eng. Chem. Res.* 51 (2012), 1173-1185.
27 Torget, R.W., Padukone, N., Hatzis, C., Wyman, C.E., Hydrolysis and Fractionation of Lignocellulosic Biomass, U.S. Patent 6,022,419, February 8, 2000.
28 Camacho, F., González-Tello, P., Jurado, E., Robles, A., Microcrystalline-Cellulose Hydrolysis with Concentrated Sulphuric Acid, *J. Chem. Tech. Biotechnol.* 67 (1996), 350-356.
29 Kristensen, J.B., Felby, C., Jørgensen, H., Yield-Determining Factors in High-Solids Enzymatic Hydrolysis of Lignocellulose, *Biotechnol. Biofuels* 2 (2009).
30 Clausen, E.C., Caddy, J.L., Concentrated Sulfuric Acid Process for Converting Lignocellulosic Materials to Sugars, U.S. Patent 5,118,673, February 23, 1993.
31 Heinonen, J., Tamminen, A., Uusitalo, J., Sainio, T., Ethanol Production from Wood via Concentrated Acid Hydrolysis, Chromatographic Separation, and Fermentation, *J. Chem. Technol. Biotechnol.* 87 (2012), 689-696.
32 Janga, K.K., Hägg, M.-B., Moe, S.T., Influence of Acid Concentration, Temperature, and Time on Decrystallization in Two-Stage Concentrated Sulfuric Acid Hydrolysis of Pinewood and Aspenwood: A Statistical Approach, *Bioresources* 7 (2012), 391-411.
33 Chandel, A.K., Rajeev, K.K., Singh, A., Kuhad, R.C., Detoxification of Sugarcane Bagasse Hydrolysate Improves Ethanol Production by *Candida Shehatae* NCIM 3501, *Bioresource Technol.* 98 (2007), 1947-1950.
34 Palmqvist, E., Hahn-Hägerdahl, B., Fermentation of Lignocellulosic Hydrolysates. I: Inhibition and Detoxification, *Bioresource Technol*. 74 (2000), 17-24.
35 Guichon, G., Preparative Liquid Chromatography, *J. Chromatogr. A* 965 (2002), 129-161.
36 Guiochon, G., Shirazi, S.G., Katti, A.M., *Fundamentals of Preparative and Non-Linear Chromatography*, Elsevier Academic Press, San Diego, USA, 2006.
37 Wheaton, R.M., Bauman, W.C., Ion Exclusion – A Unit Operation Utilizing Ion Exchange Materials, *Ind. Eng. Chem.* 45 (1953), 228-233.

38 Dorfner, K., Introduction to Ion Exchange and Ion Exchangers, in *Ion Exhangers* (Dorfner, K., ed.), Walter de Gruyter, Berlin, Germany, 1991, pp. 7-189.
39 Helfferich, F., *Ion Exchange*, Dower Publications Inc., Mineola, New York, USA, 1995.
40 Neuman, R.P., Rudge, S.R., Ladisch, M.R., Sulfuric Acid–Sugar Separation by Ion Exclusion, *React. Polym.* 5 (1987), 55-61.
41 Nanguneri, S.R., Hester, R.D., Acid/Sugar Separation Using Ion Exclusion Resins: A Process Analysis and Design, *Separ. Sci. Technol.* 25 (1990), 1829-1842.
42 Wooley, R., Ma, Z., Wang, N.-H.L., A Nine-Zone Simulating Moving Bed for the Recovery of Glucose and Xylose from Biomass Hydrolyzate, *Ind. Eng. Chem. Res.* 37 (1998), 3699-3709.
43 Sprinfield, R.M., Hester, R.D., Continuous Ion-Exclusion Chromatography System for Acid/Sugar Separation, *Separ. Sci. Technol.* 34 (1999), 1217-1241.
44 Sprinfield, R.M., Hester, R.D., Development and Modelling of a Continuous Simulated Moving Bed Ion Exclusion Process for the Separation of Acid and Sugar, *Separ. Sci. Technol.* 36 (2011), 911-930.
45 Kearney, M., *Industrial Membrane Filtration and Short-Bed Fractal Separation Systems for Separating Monomers from Heterogeneous Plant Material – Final Report*, Amalgamated Research Inc.,2004, http://www.arifractal.com/ARi%202004%20DOE%20biomass%20processing%20report.pdf, accessed 30.10.2013.
46 Xie, Y., Phelps, D., Lee, C.-H., Sedlak, M., Ho, N., Wang, N.-H.L., Comparison of Two Adsorbents for Sugar Recovery from Biomass Hydrolysate, *Ind. Eng. Chem. Res.* 44 (2005), 6816-6823.
47 Kochergin, V., Kearney, M., Existing Biorefinery Operations that Benefit from Fractal-Based Process Intensification, *Appl. Biochem. Biotech.* 129-132 (2006), 349-360.
48 *Nedo's Application of Arkenol's Concentrated Acid Hydrolysis Technology for the Conversion of Biomass to Ethanol*, 2004, http://bfreinc.com/docs/IZUMI_Status_2004_for_BlueFire_051606.pdf, accessed 30.10.2013.
49 Laatikainen, M., Heinonen, J., Sainio, T., Modeling of Chromatographic Separation of Concentrated-Acid Hydrolysates, *Sep. Purif. Technol.* 80 (2011), 610-619.
50 Hellstén, S, Sainio, T., Steady State Recycling Chromatography in Acid–Sugar Separation on an Ion-Exchange Resin, *Sep. Sci. Technol.* 47 (2012), 2358-2365.
51 Hester, R.D., Farina, G.E., Exclusion Chromatographic Separation of Ionic from Nonionic Solutes, U.S. Patent 5,667,693, September 16, 1997.
52 Nilvebrant, N.-O., Reimann, A., Larsson, S., Jönsson, L.J., Detoxification of Lignocellulose Hydrolysates with Ion-Exchange Resins, *Appl. Biochem. Biotech.* 91-93 (2001), 35-49.
53 Weil, J.R., Dien, B., Bothast, R., Hendrickson, R., Mosie, N.S., Ladisch, M.R., Removal of Fermentation Inhibitors Formed During Pretreatment of Biomass by Polymeric Adsorbents, *Ind. Eng. Chem. Res.* 41 (2002), 6132-6138.
54 Villarreal, M.L.M., Prata, A.M.R., Felipe, M.G.A., Almeida E Silva, J.B., Detoxification Procedures of Eucalyptus Hemicellulose Hydrolysate for Xylitol Production by *Candida Quilliermondii*, *Enzyme Microb. Tech.* 40 (2006), 17-24.
55 Ranjan, R., Thust, S., Gounaris, C.E., Woo, M., Floudas, C.A., von Keitz, M., Valentas, K.J., Wei, J., Tsapatsis, M., Adsorption of Fermentation Inhibitors from Lignocellulosic Biomass Hydrolyzates for Improved Ethanol Yield and Value-Added Product Recovery, *Micropor. Mesopor. Mat.* 122 (2009), 143-148.

56 Sainio, T., Turku, I., Heinonen, J., Adsorptive Removal of Fermentation Inhibitors from Concentrated Acid Hydrolysates of Lignocellulosic Biomass, *Bioresource Technol.* 102 (2011), 6048-6057.
57 Do, D.D., *Adsorption Analysis: Equilibria and Kinetics*, Imperial College Press, London, Great Britain, 1998.
58 Myers, A.L., Prausnitz, J.M., Thermodynamics of Mixed-Gas Adsorption, *AIChE J.* 11 (1965), 121-127.
59 Radke, C.J., Prausnitz, J.M., Thermodynamics of Multi-Solute Adsorption from Dilute Liquid Solutions, *AIChE J*. 18 (1972), 761-768.
60 Masuda, T., Sonobe, T., Matsuda, F., Horie, M., Process for Fractional Separation of Multi-Component Fluid Mixture, U.S. Patent 5,198,120, March 30, 1993.
61 Heikkilä, H., Hyöky, G., Kuisma, J., Method for the Recovery of Betaine from Molasses, European patent 0345511 A2, December 13, 1989.
62 Clark, T.A., Mackie, K.L., Fermentation Inhibitors in Wood Hydrolysates Derived from the Softwood *Pinus radiate*, *J. Chem. Tech. Biotechnol.* 34B (1984), 101-110.
63 Palmqvist, E., Hahn-Hägerdahl, B., Fermentation of Lignocellulosic Hydrolysates. II: Inhibitors and Mechanisms of Inhibition, *Bioresource Technol*. 74 (2000), 25-33.
64 Lee, J.W., Wankat, P.C., Design of Pseudo-Simulated Moving Bed Process with Multi-Objective Optimization for the Separation of a Ternary Mixture: Linear Isotherms, *J. Chromatogr. A* 1217 (2010), 3418-3426.
65 Mata, V.G., Rodrigues, A.E., Separation of Ternary Mixtures by Pseudo-Simulated Moving Bed Chromatography, *J. Chromatogr. A* 939 (2001), 23-40.
66 Arslan, Y., Takac, S., Eken-Saracoglu, N., Kinetic Study of Hemicellulosic Sugar Production from Hazelnut Shells, *Chem. Eng. J.* 185-186 (2012), 23-28.
67 Xiang, Q., Kim, J.S., Lee, Y.Y., A Comprehensive Kinetic Model for Dilute-Acid Hydrolysis of Cellulose, *Appl. Biochem. Biotechnol.* 105-108 (2003A), 337-352.
68 Xiang, Q., Lee, Y.Y., Pettersson, P.O., Torget, R.W., Heterogeneous Aspects of Acid Hydrolysis of α-Cellulose, *Appl. Biochem. Biotechnol.* 105-108 (2003B), 505-514.
69 Gonzáles, G., López-Santín, J., Caminal, G., Solá, C., Dilute Acid Hydrolysis of Wheat Straw Hemicelluloses at Moderate Temperature: A Simplified Kinetic Model, *Biotechnol. Bioeng.* 28 (1986), 288-293.
70 Melin, K., Hurme, M., Evaluation of Lignocellulosic Biomass Upgrading Routes to Fuels and Chemicals, *Cell. Chem. Technol.* 44 (2010), 117-137.
71 Cheungm H., Tanke, R.S., Torrence, G.P., Acetic Acid, in *Ullmann's Encyclopedia of Industrial Chemistry* (Elvers, B., ed.), 2013, online edition, http://onlinelibrary.wiley .com/book/10.1002/14356007.
72 Li, Y., Liu, H., Song, C., Gu, X., Li, H., Zhu, W., Yin, S., Han, C., The Dehydration of Fructose to 5-Hydroxymethylfurfural Efficiently Catalyzed by Acidic Ion-Exchange Resin in Ionic Liquid, *Bioresource Technol.* 133 (2013), 347-353.
73 Gallo, J.M.R., Alonso, D.M., Mellmer, M.A., Yeap, J.H., Wong, H.C., Dumesic, J.A., Production of Furfural from Lignocellulosic Biomass Using Beta Zeolite and Biomass-Derived Solvent, *Top. Catal.* 56 (2013), 1775-1781.
74 Werpy, T.A., Petersen, G., Top Value Added Chemicals from Biomass, U.S. Department of Energy, 2004, http://www1.eere.energy.gov/bioenergy/pdfs/35523.pdf, 24.7.2013.
75 Saari, P., Häkkä, K., Jumppanen, J., Heikkilä, H., Hurme, M., Study on Industrial Scale Chromatographic Separation Methods of Galactose from Biomass Hydrolysates, *Chem. Eng. Technol.* 33 (2010), 137-144.

76 Tong, X., Ma, Y., Li, Y., Biomass into chemicals: Conversion of sugars to furan derivatives by catalytic processes, *Appl. Catal. A-Gen.* 385 (2010), 1-13.
77 Ezeji, T., Qureshi, N., Blaschek, H.P., Butanol Production from Agricultural Residues: Impact of Degradation Products on *Clostridium beijerinskii* Growth and Butanol Fermentation, *Biotechnol. Bioeng.* 97 (2007) 1460-1469.
78 Nghiem, N.P., Hicks, K.B., Johnston, D.B., Integration of Succinic Acid and Ethanol Production with Potential Application in a Corn Barley Biorefinery, *Appl. Biochem. Biotechnol.*, 162 (2010), 1915-1928.
79 Cardona, C.A., Sánchez, Ó.J., Fuel Ethanol Production: Process Design Trends and Integration Opportunities, *Bioresource Technol.* 98 (2007), 2415-2457.
80 Kim, S.R., Ha, S.-J., Wei, N., Oh, E.J., Yu, Y.-S., Simultaneuous Co-Fermentation of Mixed Sugars: A Promising Strategy for Producing Cellulosic Ethanol, *Trends Biotechnol.* 30 (2012), 274-282.
81 Blaschek, H.P., Ezeji, T.C., Scheffran, J., Biofuels from Agricultural Wastes and By-Products: An Introduction, in *Biofuels from agricultural wastes and by-products* (Blaschek, H.P., Ezeji, T.C., Scheffran, J., eds.), Blackwell Publishing, 2010.
82 Qureshi, N., Hughes, S., Ezeji, T.C, Production of Liquid Biofuels from Biomass: Emerging Technologies, in *Biofuels from Agricultural Wastes and By-Products* (Blaschek, H.P., Ezeji, T.C., Scheffran, J., eds.), Blackwell Publishing, 2010.
83 Ezeji, T.C., Blaschek, H.P., Butanol Production from Lignocellulosic Biomass, in *Biofuels from Agricultural Wastes and By-Products* (Blaschek, H.P., Ezeji, T.C., Scheffran, J., eds.), Blackwell Publishing, 2010.
84 Weber, C., Farwick, A., Benisch, F., Brat, D., Dietz, H., Subtil, T., Boles, E., Trends and Challenges in the Microbial Production of Lignocellulosic Bioalcohol Fuels, *Appl. Microbiol. Biotechnol.* 87 (2010), 1303-1315.
85 Shapovalov, O.I., Ashkinazi, L.A., Biobutanol: Biofuel of Second Generation. *Russ. J. Appl. Chem.* 81 (2008), 2232-2236.
86 Xiong, M., Deng, J., Woodruff, A.P., Zhu, M., Zhou, J., Park, S.W., Li, H., Fu, Y., Zhang, K., A Bio-Catalytic Approach to Aliphatic Ketones, *Scientific Reports* 2 (2012).
87 Scholten, E., Dägele, D., Succinic Acid Production by a Newly Isolated Bacterium, *Biotehcnol. Lett.* 30 (2008), 2143-2146.
88 Yu, J., Li, Z., Ye, Q., Yang, Y., Chen, S., Development of Succinic Acid Production from Corncob Hydrolysate by *Actinobacillus succinogenes*, *J. Ind. Microbiol. Biotechnol.* 37 (2010), 1033-1040.
89 Kamm, B., Kamm, M., Biorefinies – Multi Product Processes, *Adv. Biochem. Engin./Biotechnol.* 105 (2007), 175-204.
90 Colmenares, J.C., Magdziarz, A., Bielejewska, A., High-Value Added Chemicals Obtained from Selective Photo-Oxidation of Glucose in the Presence of Nanostructured Titanium Photocatalysts, *Bioresource Technol.* 102 (2011), 11254-11257.
91 Heinonen, J., Sainio, T., Chromatographic Recovery of Monosaccharides for the Production of Bioethanol from Wood, *Ind. Eng. Chem. Res.* 49 (2010), 3713-3729.
92 Hoshino, C., Yamada, T., Taneda, D., Nagata, Y., Fujii, T., Mase, T., Ueno, Y., Method for Producing Monosaccharides from Biomass and Monosaccharide Producing Device, U.S. Patent 0,148,750, June 28, 2007.
93 Lee, Y.Y., Iyer, P., Torget, R.W., Dilute-Acid Hydrolysis of Lignocellulosic Biomass, Advances in Biochemical Engineering, *Adv. Biochem. Eng. Biot.* 65 (1999), 93-115.

94 Lenihan, P., Orozco, A., O'Neill, E., Ahmad, M.N.M., Rooney, D.W., Walker, G.M., Dilute Acid Hydrolysis of Lignocellulosic Biomass, *Chem. Eng. J.* 156 (2010), 395-403.
95 Baniel A., Eyal, A., Process for the Production of HCl Gas from Chloride Salts and for the Production of Carbohydrates, U.S. Patent No. 2011/0178290 A1, July 21, 2011.
96 Mussatto, S.I., Roberto, I.C., Alternatives for Detoxification of Diluted-Acid Lignocellulosic Hydrolyzates for Use in Fermentative Processes: A Review, *Bioresource Technol.* 93 (2004), 1-10.
97 Rinaldi, R., Schüth, F., Acid Hydrolysis of Cellulose as the Entry Point Into Biorefinery Schemes, *ChemSusChem* 2 (2009), 1096-1107.
98 Rafiqul, I.S.M., Sakinah, A.M.M., Kinetic Studies on Acid Hydrolysis of *Meranti* Wood Sawdust for Xylose Production, *Chem. Eng. Sci.* 71 (2012), 431-437.
99 Binder, J.B., Blank, J.J., Cefali, A.V., Raines, R.T., Synthesis of Furfural from Xylose and Xylan, *ChemSusChem* 3 (2010), 1268-1272.
100 Lima, S., Antunes, M.M., Fernandes, A., Pillinger, M., Ribeiro, M.F., Valente, A.A., Acid-Catalysed Conversion of Saccharides into Furanic Aldehydes in the Presence of Three-Dimensional Mesoporous Al-TUD-1, *Molecules* 15 (2010), 3863-3877.
101 Lewkowski, J., Synthesis, Chemistry and Applications of 5-hydroxymethylfurfural and Its Derivatives, *Arkivoc* (2001), 17-54.
102 Delgenes, J.P., Moletta, R., Navarro. J.M., Effect of Lignocellulose Degradation Products on Ethanol Fermentations of Glucose and Xylose by *Saccharomyces cerevisiae*, *Zymomonas mobilis*, *Pichia stipitis*, and *Candida shehatae*, *Enzyme Microb. Tech.* 19 (1996), 220-225.
103 Uçar, G., Balaban, M., Hydrolysis of Polysaccharides with 77 % Sulfuric Acid for Quantitative Saccharification, *Turk. J. Agric. For.* 27 (2003), 361-365.
104 Alén, R., Sjöström, E., Vaskikari, P., Carbon Dioxide Precipitation of Lignin from Alkaline Pulping Liquors, *Cell. Chem. Technol.* 19 (1985), 537-541.
105 Fuhrmann, A., Kleen, M., Koljonen, K., Österberg, M., Stenius, P., *Precipitation of Lignin and Extractives from Bleaching Filtrates – Effects on Pulp Properties*, TAPPI International Bleaching Conference, 2002.
106 Koljonen, K., Österberg, M., Kleen, M., Fuhrmann, A., Stenius, P., Precipitation of Lignin and Extractives on Kraft Pulp: Effect on Surface Chemistry, Surface Morphology and Paper Strength, *Cellulose* 11 (2004), 209-224.
107 Heinonen, J., Sainio, T., Modelling and Performance Evaluation of Chromatographic Monosaccharide Recovery from Concentrated Acid Lignocellulosic Hydrolysates, *J. Chem. Technol. Biotechnol.* 87 (2012), 1676-1686.
108 Glód, B.K., Ion Exclusion Chromatography: Parameters Influencing Retention, *Neurochem. Res.* 22 (1987), 1237-1248.
109 Gsell, G., Water Systems Utilizing Multiple Effect and Vapor Compression Technologies Compared, *Pharm. Eng.* 24 (2004), 1-7.
110 Katsuo, S., Mazzotti, M., Intermittent Simulated Moving Bed Chromatography: 1. Design Criteria and Cyclic Steady-State, *J. Chromatogr. A* 1217 (2010), 1354-1361.
111 Sainio, T., Kaspereit, M., Analysis of Steady State Recycling Chromatography Using Equilibrium Theory, *Sep. Purif. Technol.* 66 (2009), 9-18.
112 Kaspereit, M., Sainio, T., Simplified Design of Steady-State Recycling Chromatography under Ideal and Nonideal Conditions, *Chem. Eng. Sci.* 66 (2011), 5428-5438.
113 *BlueFire Renewables*, http://bfreinc.com/, accessed 30.10.2013.

114 Wankat, P.C., *Rate-Controlled Separations*, Elsevier Science Publishers Ltd, Essex, Great Britain, 1990.
115 Wang, B., Feng, H., Detoxification of Lignocellulosic Hydrolysates, in *Biofuels from Agricultural Wastes and By-Products* (Blaschek, H.P., Ezeji, T.C., Scheffran, J., eds.), Blackwell Publishing, 2010.
116 Abrams, I.M., Millar, J.R., A History of the Origin And Development of Macroporous Ion-Exchange Resins, *React. Funct. Polym.* 35 (1997), 7-22.
117 Rieman III, W., Salting-Out Chromatography – A Review, *J. Chem Educ.* 38 (1961), 338-343.
118 Ching, C.B., Ho, C., Hidajat, K., Ruthven, D.M., Experimental Study of a Simulated Counter-Current Adsorption System – V. Comparison of Resin and Zeolite Absorbents for Fructose-Glucose Separation at High Concentration, *Chem. Eng. Sci.* 42 (1987), 2547-2555.
119 Nowak, J., Gedicke, K., Antos, D., Piatkowski, W., Seidel-Morgenstern, A., Synergistic Effects in Competitive Adsorption of Carbohydrates on an Ion-Exchange Resin, *J. Chromatogr. A* 1164 (2007), 224-234.
120 Nowak, J., Poplewska, I., Antos, D., Seidel-Morgenstern, A., Adsorption Behaviour of Sugars versus Their Activity in Single and Multicomponent Liquid Solutions, *J. Chromatogr. A* 1216 (2010), 8697-8704.
121 Vente, J.A., Bosch, H., de Haan, A.B., Bussmann, P.J.T., Evaluation of Sugar Sorption Isotherm by Frontal Analysis under Industrial Processing Conditions, *J. Chromatogr. A* 1066 (2005), 71-79.
122 *IUPAC Goldbook*, IUPAC, goldbook.iupac.org/P04436.html, 23.7.2013.
123 Sargent, R., Rieman III, W., Salting-Out Chromatography, *J. Phys. Chem.* 61 (1956), 354-358.
124 Baldwin, R.L., How Hofmeister Ion Interactions Affect Protein Stability, *Biophys. J.* 71 (1996), 2056-2063.
125 Shimizu, S., McLaren, W.M., Matubayasi, N., The Hofmeister Series and Protein-Salt Interactions, *J. Chem. Phys.* 124 (2006).
126 Zhang, Y., Cremer, P.S., Interactions Between Macromolecules and Ions: The Hofmeister Series, *Curr. Opin. Chem. Biol.* 10 (2006), 658-663.
127 Gao, Y.Q., Simple Theory for Salt Effects on the Solubility of Amide, *J. Phys. Chem. B* 116 (2012), 9934-9943.
128 Friedman, R., Electrolyte Solutions and Specific Ion Effects on Interfaces, *J. Chem. Educ.* 90 (2013), 1018-1023.
129 Schwierz, N., Horinek, D., Netz, R.R., Anionic and Cationic Hofmeister Effects on Hydrophobic and Hydrophilic Surfaces, *Langmuir* 29 (2013), 260-2614.
130 Kaspereit, M., Advanced Operating Concepts for Simulated Moving Bed Processes, in *Advances in Chromatography, Vol. 47* (Grushka, E., Grinberg, N., eds.), CRC Press, Boca Raton, USA, 2009, pp. 165-192.
131 Broughton, D., Gerhold, C.G., Continuous Sorption Process Employing Fixed Bed of Sorbent and Moving Inlets And Outlets, U.S. Patent 2,985,589, May 23, 1961.
132 Ando, M., Tanimura, M., Tamura, M., Method for Chromatographic Separation, U.S. Patent 4,970,002, November 13, 1990.
133 Giacobello, S., Storti, G., Tola, G., Design of a Simulated Moving Bed Unit for Sucrose-Betaine Separations, *J. Chromatogr. A* 872 (2000), 23-35.
134 Barreto Jr., A.G., da Silva Jr., I.J., dos Santos, M.A.G., de Veredas, V., Santana, C.C., Modeling, Simulation, and Experimental Evaluation of Continuous Chromatographic

Separation of Ketamine Enantiomers on MCTA, *J. Liq. Chromatogr. R. T.* 31 (2008), 3057-3076.
135 Goncalves, C.V., Carpes, M.J.S., Correia, C.R.D., Santana, C.C., Purification of *n*-Boc-Rolipram Racemate on Chiral Stationary Phase Using Simulated Moving Bed Chromatography under Linear Conditions, *Biochem. Eng. J.* 40 (2008), 526-536.
136 Juza, M., Mazzotti, M., Morbidelli, M., Simulated Moving-Bed Chromatography and Its Application to Chirotechnology, *Trends Biotechnol.* 18 (2000), 108-118.
137 Lee, E., Kim, J.M.., Kim, W.S., Kim, I.H., Simulation and Operation Performance of Simulated Moving Bed for Enantioseparation of Mandelic Acid, *Biotechnol. Bioproc. E.* 15 (2010), 103-109.
138 Lehoucq, S., Verhève, D., Wouwer, A.V., Cavoy, E., SMB Enantioseparation: Process Development, Modeling, and Operating Conditions, *AIChE J.* 46 (2000), 247-256.
139 Pais, L.S., Loureiro, J.M., Rodrigues, A.E., Modeling Strategies for Enantiomers Separation by SMB Chromatography, *AIChE J.* 44 (1998), 561-569.
140 Ribeiro, A.E., Gomes, P.S., Pais, L.S., Rodrigues, A.E., Chiral Separation of Ketoprofen Enantiomers by Preparative and Simulated Moving Bed Chromatography, *Sep. Sci. Technol.* 46 (2011), 1726-1739.
141 Schulte, M., Strube, J., Preparative Enantioseparation by Simulated Moving Bed Chromatography, *J. Chromatogr. A* 906 (2001), 399-416.
142 Agrawal, G., Kawajiri, Y., Comparison of Various Ternary Simulated Moving Bed Separation Schemes by Multi-Objective Optimization, *J. Chromatogr. A.* 1238 (2012), 105-113.
143 Kurup, A.S., Hidajat, K., Ray, A.K., Optimal Operation of a Pseudo-SMB Process for Ternary Separation under Non-Ideal Conditions, *Sep. Purif. Technol.* 51 (2006), 387-403 (2006).
144 Heikkilä, H., Hyöky, G., Kuisma, J., A Method for the Fractionation of Molasses, International patent WO 94/17213, August 4, 1994.
145 Heikkilä, H., Hyöky, G., Kuisma, J., Method for Fractionation of a Solution by a Chromatographic Simulated Moving Bed Process, International patent WO 97/45185, December 4, 1997.
146 Heikkilä, H., Hyöky, G., Kuisma, J., Method for the Fractionation of Molasses, U.S. Patent 6,093,326, July 25, 2000.
147 Heikkilä, H., Lewandowski, J., Kuisma, J., Chromatographic Separation Method, U.S. Patent, 7,229,558 B2, June 12, 2007.
148 Airaksinen, J., Heikkilä, H., Lewandowski, J., Laiho, K., Separation Process, U.S. Patent 2010/0212662 A1, August 26, 2010.
149 Harned, H.S., Ehlers, R.W., The Dissociation Constant of Acetic Acid from 0 to 60 °C centigrade, *J. Am. Chem. Soc.* 55 (1953), 652-656.
150 Costa, E., Sotelo, J.L., Calleja, G., Marrón, C., Adsorption of Binary and Ternary Hydrocarbon Gas Mixtures on Activated Carbon: Experimental Determination and Theoretical Prediction of the Ternary Equilibrium Data, *AIChE J.* 27 (1981), 5-12.
151 Myers, A.L., Activity Coefficients of Mixtures Adsorbed on Heterogeneous Surfaces, *AIChE J.* 29 (1983), 691-693.
152 Talu, O., Zwiebel, I., Multicomponent Adsorption Equilibria of Nonideal Mixtures, *AIChE J.* 32 (1986), 1263-1276.
153 Steffan, D.G., Akgerman, A., Thermodynamic Modeling of Binary and Ternary Adsorption on Silica Gel, *AIChE J.* 47 (2001), 1234-1246.

154 Sochard, S., Fernandes, N., Reneaume, J.-M., Modeling of Adsorption Isotherm of a Binary Mixture with Real Adsorbed Solution Theory and Nonrandom Two-Liquid Model, *AIChE J.* 56 (2010), 3109-3119.
155 Erto, A., Lancia, A., Musmarra, D., A Real Adsorbed Solution Theory Model for Competitive Multi-Component Liquid Adsorption onto Granular Activated Carbon, *Micropor. Mesopor. Mat.* 154 (2012), 45-50.
156 Rubiera Landa, H.O., Flockerzi, D., Seidel-Morgenstern, A., A Method for Efficiently Solving the IAST Equations with an Application to Adsorber Dynamics, *AIChE J.* 59 (2013), 1263-1277.
157 Pitzer, K.S., Thermodynamics of Electrolytes. I. Theoretical Basis and General Equations, *J. Phys. Chem.-US.* 77 (1972), 268-277.
158 Pitzer, K.S., Ion Interaction Approach: Theory and Data Correlation, in *Activity Coefficients in Electrolyte Solutions* (Pitzer, K.S., ed.), CRC Press, Boca Raton, USA, 1991, pp. 75-154.
159 Fernández-Mérida, L., Rodríguez-Raposo, R., García-García, G.E., Esteso, M.A., Modification of the Pitzer Equations for Application to Electrolyte + Polar Non-Electrolyte Mixtures, *J. Electroanal. Chem.* 379 (1994), 63-69.
160 Durão, M.I., Costa, C.A.V., Rodrigues, A.E., Saturation and Regeneration of Ion Exchangers with Volume Changes, *Ind. Eng. Chem. Res.* 31 (1992), 2564-2572.
161 Marra, R.A., Cooney, D.O., Multicomponent Sorption Operations: Bed Shrinking and Swelling in an Ion Exclusion Case, *Chem. Eng. Sci.* 33 (1978), 1597-1601.
162 Mazzotti, M., Neri, B., Gelosa, D., Morbidelli, M., Dynamics of a Chromatographic Reactor: Esterification Catalyzed by Acidic Resins, *Ind. Eng. Chem. Res.* 36 (1997), 3163-3172.
163 Sainio, T., Paatero, E., Mass Coordinates for Dynamic Simulation of Column Operations Involving Dimensional Changes of Packing Material, *Comput. Chem. Eng.* 31 (2007), 374-383.
164 Tiihonen, J., Sainio, T., Kärki, A., Paatero, E., Co-eluent Effect in Partition Chromatograhy. Rhamnose–Xylose Separation with Strong and Weak Cation-Exchangers in Aqueous Ethanol, *J. Chromatogr. A* 982 (2002), 69-84.
165 Mackie, J.S., Meares, P., The Diffusion of Electrolytes in a Cation-Exchange Resin Membrane. I. Theoretical., *Proc. Royal Soc.* A232 (1955), 498-509.
166 Schiesser, W.E., *The Numerical Method of Lines*, Academic Press, San Diego, USA, 1991.
167 McCabe, W.L., Smith, J.C., Harriott, P., *Unit Operations of Chemical Engineering*, 7th Ed., McGraw-Hill, New York, USA, 2005, pp. 163-167.
168 Heuer, C., Küsters, E., Plattner, T., Seidel-Morgenstern, A., Design of the Simulated Moving Bed Process Based On Adsorption Isotherm Measurements Using a Perturbation Method, *J. Chromatogr. A* 827 (1998), 175-191.
169 Seidel-Morgenstern, A., Experimental Determination of Single Solute and Competitive Adsorption Isotherms, *J. Chromatogr. A* 1037 (2004), 255-272.
170 Sainio, T., Laatikainen, M., Paatero, E., Phase Equilibria in Solvent Mixture–Ion Exchange Resin Systems, *Fluid Phase Equilib.* 218 (2004), 269-283.
171 Heinonen, J., Laatikainen, M., Sainio, T., Separation of Electrolytes and Organic Solutes on Elastic Ion Exchange Resins: Modelling Approaches, in *IEX 2012 – The International Ion Exchange Conference*, (Cox, M., ed.), Cambridge, United Kingdom, September 19-21, 2012.

PAPER I

Chromatographic Recovery of Monosaccharides for the Production of Bioethanol from Wood

Jari Heinonen and Tuomo Sainio*

Laboratory of Industrial Chemistry, Lappeenranta University of Technology, Skinnarilankatu 34, FIN-53850 Lappeenranta, Finland

Chromatographic recovery of monosaccharides from concentrated-acid hydrolysates of spruce and birch was investigated for the production of bioethanol from lignocellulose. The effects of resin cross-linkage, column loading, and hydrolysate composition on the yield of monosaccharides and the productivity of the process were of particular interest. Three strong acid cation-exchange resins (gel type) were used. Chromatographic separation experiments were done in a batch column. Monosaccharides were recovered as a "center cut" between sulfuric acid and acetic acid. Hydroxymethyl furfural and furfural, which inhibit the fermentation of monosaccharides, were completely separated from the other components. The highest H_2SO_4−monosaccharide separation efficiency was obtained with a 6 wt % cross-linked resin. The monosaccharide−acetic acid separation efficiency was found to improve with increasing resin cross-linkage. In the case of high amounts of acetic acid in the hydrolysate, a resin with a high cross-link density is needed for a good yield of monosaccharides. With hydrolysates containing small amounts of acetic acid, a 6 wt % cross-linked resin was found to give the highest yield. The productivity of the process was found to increase with the resin cross-linkage (up to 8 wt %). The optimum column loading depends on whether a high monosaccharide yield or high productivity is desired. The highest yield is obtained with a low loading. As to the productivity, the optimum loading was found to be approximately 10 vol % of the bed volume.

1. Introduction

This article focuses on the chromatographic recovery of monosaccharides from concentrated-acid hydrolysates for the production of second-generation, i.e., lignocellulosic, bioethanol. It is a candidate for a biofuel that can be used to replace gasoline. It can be used as a mixture with gasoline or pure in modern internal combustion engines (ICEs) without or with modifications, respectively.[1,2] Addition of ethanol to gasoline increases octane number and lowers the CO_2, volatile organic carbon, and particulate emissions of the engines.[1]

The manufacturing process of lignocellulosic bioethanol is a complex process containing many unit operations. This is because lignocellulosic materials contain, instead of directly fermentable monosaccharides (glucose, xylose, etc.), cellulose and hemicellulose that must be hydrolyzed to monosaccharides before fermentation to ethanol can occur.[1−3] The monosaccharides can also be converted via fermentation to biobutanol,[4−6] or via catalytic upgrading to different biofuels and biochemicals.[7] In addition to fuel usage, ethanol can also be used for the manufacturing of chemicals such as hydrogen, acetaldehyde, ethylene, butadiene, and acetic acid.[8]

One possible route to manufacture lignocellulosic bioethanol is via concentrated-acid catalyzed hydrolysis, in which usually sulfuric acid is used to catalyze the breakdown of the polysaccharide (cellulose and hemicellulose) chains.[1−4,9] The hydrolysis is done in two steps at normal atmospheric pressure and at temperatures below 100 °C. In the first step lignocellulosic raw material is pretreated with 70−80 wt % H_2SO_4. In the second step the acid is diluted to 20−30 wt %, and the actual hydrolysis is carried out.[10−13]

With the concentrated-acid hydrolysis, high monosaccharide yields are obtained: even 90% or higher.[9,11,12] The disadvantages of the concentrated-acid hydrolysis are corrosion problems and high acid consumption. The latter is because the used hydrolysis acid must be removed after hydrolysis in order to be able to ferment the monosaccharides. Traditionally, the acid is removed by neutralization with lime ($Ca(OH)_2$), which increases the costs of the process considerably. Also a high amount of $CaSO_4$ is generated.[1,3,9,11,12] In order to make the concentrated-acid process economically viable, the hydrolysis acid must be recycled.[9,13] Electrodialysis,[14] precipitation/extraction process with ethanol,[15] and chromatographic separation[11,12,16,17] have been studied for the recycling of the hydrolysis acid, and for the recovery monosaccharides. However, the first two have disadvantages when compared to the chromatographic separation process. The disadvantage of electrodialysis is the cost of the process. The ethanol precipitation/extraction process, on the other hand, is a complex process and consists of multiple steps.[17] The chromatographic separation process is a relatively inexpensive and simple process consisting of only one step. When the ion-exchange resin is used in the H^+ form, not even regeneration of the resin is required. For these reasons, this study focuses on the chromatographic hydrolysis acid recycling and monosaccharide recovery.

Electrolyte exclusion chromatography has been studied for the separation of monosaccharides from dilute-acid lignocellulosic hydrolysates.[16,17] Xie et al.[16] compared two ion-exchange resins (strong acid cation-exchange resin, Dowex 99, and weak anion-exchange resin, Reillex HP) for the chromatographic separation of monosaccharides from corn-stover hydrolysates (dilute-acid hydrolysate, 13.6 g/L sulfuric acid). According to Xie et al.,[16] with both resins monosaccharide separation efficiency was good. Neuman et al.[17] have investigated chromatographic glucose−sulfuric acid separation with synthetic solution (dilute 7.7 wt % H_2SO_4, 1.0 wt % glucose) using a strong cation-exchange resin (Amberlite IR-118). They found that the best separation was achieved when the temperature was 55 or 68 °C and the column loading was low.[17] The monosaccharide recovery from concentrated-acid hydrolysates has not

* To whom correspondence should be addressed. Tel.: +358-5-6212269. Fax: +358-5-6212199. E-mail: tuomo.sainio@lut.fi.

10.1021/ie901598z
Published on Web 02/17/2010

Table 1. Composition of the Concentrated-Acid Hydrolysates

	c, g/L	
	spruce	birch
H_2SO_4	340.75	329.77
glucose	47.16	48.73
xylose	7.40	29.03
galactose	4.70	1.01
mannose	16.20	3.73
arabinose	2.42	6.44
monosaccharides	77.88	88.94
acetic acid	2.04	9.07
HMF	0.10	0.12
furfural	0.30	1.28

Table 2. Properties of the Resins[a]

	CS09GC	CS12GC	CS16GC
matrix	PS−DVB	PS−DVB	PS−DVB
functional groups	sulfonic acid	sulfonic acid	sulfonic acid
degree of cross-linking, %	4.5	6.0	8.0
mean particle diameter, μm	211.0	217.0	217.5
vol capacity (H^+), mequiv/mL	1.07	1.51	1.93

[a] Volume capacities were measured by using standard methods.

been investigated much publicly. Few patents have been made regarding the separation: Farone and Cuzens[11,12] have investigated the recovery of monosaccharides (23.0 wt %) from concentrated-acid hydrolysate (33.6 wt % H_2SO_4) using the Finex GS-16 strong cation-exchange resin. They got 90% pure acid and 94% pure monosaccharide streams in their experiments.[11,12] In the previous studies concerning the recovery of monosaccharides from dilute- or concentrated-acid hydrolysates, the productivity of the process has not been investigated. The productivity is an important factor when evaluating the process performance and should also be investigated.

In this article, the chromatographic recovery of monosaccharides from concentrated-acid hydrolysates (approximately 30 wt % H_2SO_4) of spruce and birch, with different compositions, is investigated systematically. Batch column experiments are done. The effects of resin cross-linkage, column loading, and hydrolysate composition on the monosaccharide yield and the productivity of the process are of particular interest. Three strong acid polystyrene−divinylbenzene (PS−DVB) resins are used. The monosaccharide yield and the productivity of the process with respect to the monosaccharides are calculated from the experimental results and used for the evaluation of the process.

2. Materials and Methods

Chromatographic recovery of monosaccharides from concentrated-acid hydrolysates was studied in a batch column. Experiments were done in order to investigate the effects of resin cross-linkage, column loading, and hydrolysate composition on the separation. Authentic concentrated-acid spruce and birch hydrolysates were used (Table 1). The hydrolysates were prepared by stepwise treating wood chips with 70 wt % sulfuric acid at 50 °C and 30 wt % sulfuric acid at 80 °C in a 1 L glass reactor. Nine components were monitored: five monosaccharides (glucose, xylose, arabinose, galactose, and mannose), sulfuric acid, acetic acid, hydroxymethyl furfural (HMF), and furfural.

Three strong acid PS−DVB cation-exchange resins (gel type) in H^+ form were used: CS09GC, CS12GC, and CS16GC (Finex Oy, Finland). The specifications of the resins are listed in Table 2.

The experimental setup consisted of two HPLC pumps for eluent and feed (Waters 515 series pumps), a chromatographic column (XK 26, Pharmacia Biotech) with 26 mm inner diameter and water heating jacket, a water circulation thermostat for column heating (Lauda C6CS), an on-line conductivity detector (conductivity monitor, Pharmacia Biotech), an on-line refractive index (RI) detector (Schambeck RI-2000F), an on-line UV detector (Waters 2487 Dual λ Absorbance Detector with 3 mm semiprep flow cell), and a fraction collector (Pharmacia LKB FRAC-100). The sampling interval used in the experiments was 30 s. LabView program (version 8.2, National Instruments) was used to control the valves and collect the online data.

2.1. Resin Pretreatment and Column Packing. Before the separation experiments the resins were converted into hydrogen form with 1 M hydrochloric acid. The resin bed volume was 106 cm^3 (bed height 20 cm). The resin was packed to the column so that the bed height was 21.4 cm, and then the bed was compressed to the desired bed height.

2.2. Resin Shrinking Measurements. The effect of sulfuric acid concentration on the resin shrinking was measured with batch experiments, with each of the resins. A 6.0 g sample of dry resin was put into glass containers with 50 mL of H_2SO_4 solution. Sulfuric acid concentrations ranged from 5 to 30 wt %. Batches were equilibrated for 24 h, and the resin shrinking was determined by measuring the volumes of the shrunken resins and comparing these values to the initial states.

2.3. Separation Experiments with Authentic Hydrolysates. All batch chromatography experiments were done using top-down flow at 50 °C temperature, and with purified and degassed water as eluent. Water was pumped with a 0.5 cm/min superficial velocity through the column (corresponds to the flow rate of 2.655 mL/min in XK 26 column). Three resin cross-linkages (4.5, 6, and 8 wt %) and three column loadings (feed volumes 4.7, 9.4, and 18.8 vol % of resin bed volume) were studied.

2.4. Sample Analyses. The concentrations of the monosaccharides, acetic acid, hydroxymethyl furfural (HMF), and furfural were measured with an off-line HPLC system (HP 1100 equipped with RI and UV detectors, Hewlett-Packard/Agilent). A Bio-Rad Aminex HPX-87H column was used. The HPLC analyses were conducted at 60 °C, with 10 μL injection volumes, and with 0.005 M H_2SO_4 as an eluent. The calibration curves were linear with an index of determination above 0.999. In the following, all monosaccharides are treated as a single pseudocomponent, because of their practically simultaneous elution in the chromatographic experiments. The separation of monosaccharides from each other was not attempted in this study, because in the fermentation step following the monosaccharide recovery, the goal is to ferment all monosaccharides to ethanol simultaneously.

Sulfuric acid concentrations were calculated from the on-line conductivity detector signal when monosaccharides were not present and H_2SO_4 concentration was below 50 g/L. Otherwise titration was used. The reason for this is that monosaccharides increase the viscosity of the solution, which causes the conductivity to decrease. In other words, sulfuric acid concentration calculated from the conductivity detector signal is lower than the actual H_2SO_4 concentration when monosaccharides elute from the column at the same time. The same occurs also when pure and very concentrated sulfuric acid elutes from the column.

Typically, only a single column experiment was done for each pulse width (loading) with each resin. This was justified by results from preliminary experiments where three consecutive injections of same size (6 wt % cross-link density, 9.4 vol % loading) resulted in practically identical signals of the on-line detectors. Since no replicate experiments were done, no error estimates or confidence intervals can be given.

2.5. Evaluation of the Feasibility of the Resins. On the basis of the experimental results, the effects of resin cross-linkage, column loading, and hydrolysate composition on the monosaccharide yield and the productivity of the process with respect to monosaccharides were evaluated. The constraint that determined the first cut point (beginning) for the monosaccharide fraction was the yield of H_2SO_4 in the first fraction, i.e., sulfuric acid fraction, $Y_{H_2SO_4}$ (from 90 to 98%). If lower than 90% H_2SO_4 yield is used, too much sulfuric acid is lost in the separation process. Also, if H_2SO_4 yield higher than 98% yield is used, the economy of the separation process will suffer.

The constraint that determined the second cut point (end) for the monosaccharide fraction was the maximum allowed concentration of inhibitors (acetic acid, HMF, and furfural) in the monosaccharide fraction, $c_{AcOH}^{product}$ (from 0.5 to 1.5 g/L). In practice, the second constraint included only acetic acid, because HMF and furfural were strongly sorbed to the resins, and thus were completely separated from the other components (this aspect will be discussed in more detail in section 3). If the allowed concentration is higher than 1.5 g/L, the amount of acetic acid in the monosaccharide fraction will be harmful for the fermentation. On the other hand, a small amount of acetic acid is not harmful for the fermentation, so the lower limit for acetic acid was chosen to be 0.5 g/L. In addition, if acetic acid were to be removed completely from the monosaccharide fraction, the costs of the separation process would increase.

The productivity of the process with respect to monosaccharides (Pr) can be calculated with the following equation

$$\mathrm{Pr} = \frac{Y_m c_m^{feed} V^{feed}}{t_{cycle}} \quad (1)$$

where Y_m is the monosaccharide yield, c_m^{feed} is the concentration of monosaccharides in feed, V^{feed} is the feed volume, and t_{cycle} is the cycle time. The beginning of a cycle was set to the breakthrough point of H_2SO_4. When calculating the productivities, three presumptions were made. First, the monosaccharides that elute before the first cut point (with H_2SO_4) were treated as lost product for the sake of simplicity. Second, HMF and furfural are presumed to be removed before the monosaccharide recovery due to their high sorption (this aspect will be discussed in more detail in section 3). Third, the cycle ends when the acetic acid concentration decreases below 0.05 g/L. This is because the acetic acid eluting after this point is recovered in the sulfuric acid fraction in the next cycle. In addition, if the cycle were to end when acetic acid concentration reaches zero, the cycle time of the separation process would again be increased at the cost of productivity.

3. Results and Discussion

The chromatographic recovery of monosaccharides from concentrated-acid hydrolysates was studied with batch column experiments. The effects of resin cross-linkage (4.5, 6.0, and 8 wt %), column loading (4.7, 9.4, and 18.8 vol %), and hydrolysate composition on the yield of monosaccharides and the productivity of the process were investigated. Experiments were done with authentic spruce and birch hydrolysates (see Table 1). The suitability of the resins for the recovery process was evaluated from the experimental results. Evaluation was done by calculating the monosaccharide yield and productivity with respect to monosaccharides (see section 2.5 for details).

A typical elution chromatogram of concentrated-acid lignocellulosic hydrolysate with the studied resins (see Table 2) is shown in Figure 1. Sulfuric acid elutes first, and is soon followed by monosaccharides and acetic acid, respectively. The separation between these components is not complete. All monosaccharides are treated as a single pseudocomponent, because of their simultaneous elution. This is due to similarities in molecular structures when compared to each other. The separation of the monosaccharides from each other was not attempted in this study. HMF and furfural, which inhibit the subsequent fermentation, are quite strongly sorbed to the resin and are completely separated from the other components (Figure 1).

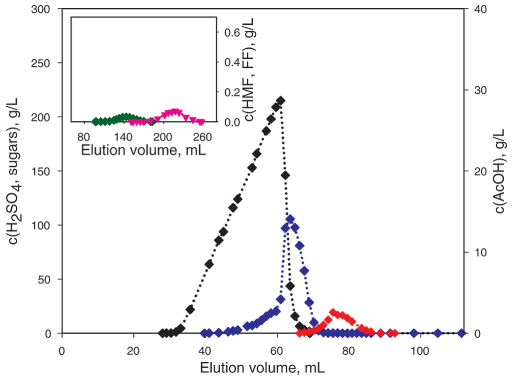

Figure 1. Example of chromatographic treatment of concentrated-acid hydrolysate (spruce, see Table 1). Resin: CS16GC. All monosaccharides are treated as one pseudocomponent. Experimental conditions: column loading 9.4 vol %, column diameter 2.6 cm, bed height 20 cm, purified water as eluent, superficial velocity = 0.5 cm/min, top-down flow, and temperature 50 °C. Colors: black = H_2SO_4, blue = monosaccharides, red = acetic acid, green = hydroxymethyl furfural (HMF), and pink = furfural (FF). Lines are presented to guide the eye.

The breakthrough point of the sulfuric acid peak is very close to the void volume of the resin bed (Figure 1); only a little difference caused by dispersion is noted. Electrolyte exclusion influences the sorption of sulfuric acid. At very low H_2SO_4 concentrations, electrolyte exclusion is strong enough to prevent all HSO_4^- and SO_4^{2-} ions from entering the pores of the resin. Because the anions of sulfuric acid cannot enter the resin, neither can the cations, due to electroneutrality condition. Therefore, sulfuric acid is not sorbed to the resin, and it elutes at the void volume of the resin bed. With higher sulfuric acid concentrations electrolyte exclusion is not strong enough to keep all HSO_4^- and SO_4^{2-} anions from entering the resin's pores (the amount in the solid phase increases as H_2SO_4 concentration increases), and H_2SO_4 elutes slower. This results in the diffuse front of the sulfuric acid peak.

A sharp shock layer is formed to the rear of the sulfuric acid peak (Figure 1). Low H_2SO_4 concentrations move faster than the high ones, but cannot pass them, and a shock layer is formed. The shape of the H_2SO_4 peak is typical for a component with an anti-Langmuirian sorption isotherm. Some tailing can be seen at the end of the H_2SO_4 peak. Tailing is caused by large dispersion due to resin shrinking. Sulfuric acid causes resin to shrink (this aspect will be discussed in more detail later on).

The monosaccharide peak has an extensive front under the sulfuric acid peak (Figure 1). This stems from the influence of H_2SO_4 on the sorption equilibrium of the monosaccharides in the resin. Sulfuric acid slows the propagation of the monosaccharides: the higher the acid concentration, the slower the monosaccharides' propagation. This results in the extensive fronting seen in Figure 1. The phenomenon is opposite to the tagalong effect, which is common in chromatography.

The influence of sulfuric acid on the sorption isotherms of the monosaccharides leads also to another interesting phenomenon: a steep increase in the concentration of monosaccharides after the wide and shallow front (Figure 1). In Figure 1, the maximum monosaccharide concentration is approximately 106 g/L, while in the feed it is approximately 78 g/L (see Table 1). As was mentioned above, the propagation of the front of the monosaccharide peak is slowed by sulfuric acid. On the other hand, the propagation of the rear of the monosaccharide peak is not affected by sulfuric acid, because no H_2SO_4 is present in the rear of the monosaccharide peak. Because the propagation velocity of the front of the monosaccharide peak is slower than the velocity of the rear, the peak squeezes and the monosaccharide concentration increases above the feed value. This phenomenon is not caused by the acetic acid, because it was also observed in the absence of it. The concentration of the later eluting component is uncommon for chromatographic systems, and may have a great effect on the economy of the monosaccharide recovery process.

The mechanism of how sulfuric acid slows the propagation of monosaccharides, i.e., increases their sorption, is explained in the following. The presence of monosaccharides in the aqueous sulfuric acid solution leads to an increase in the total energy of the system. A decrease in the total energy, which is desired, is achieved if one of the components is "salted out". Water molecules prefer to solvate sulfuric acid molecules instead of the monosaccharide molecules, which leads to a decrease in the solubility of the monosaccharides. They are "salted out" to the resin phase, and the total energy of the system decreases, and the sorption of the monosaccharides increases.

Acetic acid elutes right after the monosaccharides, and is not completely separated from them (Figure 1). From the shape of the acetic acid peak, it can be seen that the sorption isotherm of this component is linear, or at least very close to linear. However, the sorption of acetic acid is also influenced by H_2SO_4, due to the close-by elution of the sulfuric acid and acetic acid peaks.

Hydroxymethyl furfural and furfural are completely separated from the other components in the hydrolysates (Figure 1). The shapes of the HMF and furfural peaks indicate that their sorption isotherms are linear. They are quite strongly sorbed to the resin and propagate slowly. Similarities in the molecular structures of HMF and furfural cause them to propagate close to each other. Because of the long retention times of HMF and furfural, the cycle time of the separation process is quite long. This affects the economy of the separation process severely. A large amount of eluent is needed to elute HMF and furfural from the column, and a low amount of hydrolysate can be purified in a time unit. Without HMF and furfural, the cycle time of the batch process would be much shorter. It would be beneficial for the process that HMF and furfural were removed before the acid−monosaccharide separation.

3.1. Effect of Resin Cross-Linkage on the Process Performance. The effect of the resin cross-linkage on the recovery of monosaccharides from concentrated-acid hydrolysates is presented in Figure 2A (spruce hydrolysate, see Table 1) and Figure 2B (birch hydrolysate, see Table 1). The elution profiles presented in Figure 2 are similar and are fairly independent of the composition of the hydrolysates. This is as expected, because the main difference in the hydrolysates is in the amount of acetic acid, which does not affect the elution of the other components.

The breakthrough point of sulfuric acid is not affected by the resin cross-linkage (≈30 mL for each resin), because of complete electrolyte exclusion at very low H_2SO_4 concentrations

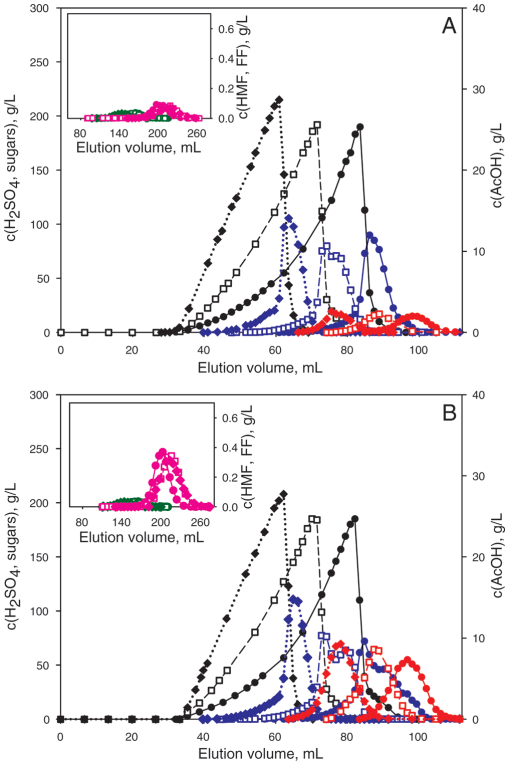

Figure 2. Effect of resin cross-linkage on the chromatographic recovery of monosaccharides from concentrated-acid spruce (A) and birch (B) hydrolysates. Feed composition: see Table 1. All monosaccharides are treated as one pseudocomponent. Experimental conditions: see caption of Figure 1. (●) 4.5 wt %, (□) 6.0 wt %, and (◆) 8.0 wt % cross-linked resin. Colors: black = H_2SO_4, blue = monosaccharides, red = acetic acid, green = hydroxymethyl furfural (HMF), and pink = furfural (FF). Lines are presented to guide the eye.

(Figure 2). However, the resin cross-link density has an effect on the H_2SO_4 peak when the concentration of H_2SO_4 is higher. As the resin cross-linkage decreases, the charge density in the resin decreases, causing electrolyte exclusion also to decrease. With less-cross-linked resins, sulfuric acid sorption is higher at the same acid concentration, than with more-cross-linked resins, and H_2SO_4 propagates slower (Figure 2). Therefore, as the resin cross-linkage decreases, the H_2SO_4 peak spreads and the peak maximum decreases, i.e., H_2SO_4 dilutes. Also the tailing of the H_2SO_4 peak increases as the resin cross-linkage decreases. This is because the resin shrinking, caused by sulfuric acid, increases substantially and leads to an increase in dispersion. The effect of the resin cross-linkage on the resin shrinking is discussed in more detail later on.

The extensive fronting of the monosaccharide peak can be seen with each degree of cross-linkage (Figure 2). The width of the front is not affected by the resin cross-link density, but the breakthrough point of the front increases as the resin cross-linkage decreases (Figure 2). Also, the other parts of the monosaccharide peak propagate slower with less-cross-linked resins. This is due to higher sorption: with looser resins the monosaccharides are not as strongly excluded from the resin by size exclusion as with tighter resins.

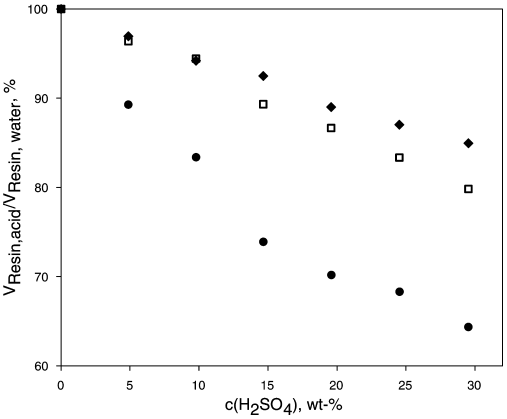

Figure 3. Effect of resin cross-linkage on resin shrinking with varying H_2SO_4 concentration. Experimental conditions: batch experiments at 50 °C temperature; 6 g of dried resin in each batch. $V_{resin,acid}/V_{resin,water}$ = resin volume in acid compared to resin volume in pure water. (●) 4.5 wt %, (□) 6.0 wt %, and (◆) 8.0 wt % cross-linked resin. Lines are presented to guide the eye.

Decrease in the resin cross-linkage has also a weakening influence on the concentration effect of the monosaccharides (Figure 2). This is also because of the higher sorption of the monosaccharides. The rear of the monosaccharide peak propagates slower with looser resins than with the tighter resins, and the squeezing of the monosaccharide peak is smaller.

Also acetic acid sorption increases as the resin cross-link density decreases (Figure 2). The acetic acid sorption isotherm is not as much influenced by the resin cross-linkage as the monosaccharide isotherms, because of smaller molecular dimensions; i.e., the sorption of acetic acid is not much influenced by size exclusion. Decrease in the resin cross-link density has a disadvantageous influence on the monosaccharide−acetic acid separation efficiency (Figure 2). From Figure 2 it can also be seen that the concentration of monosaccharides in the feed does not influence the retention of acetic acid.

Hydroxymethyl furfural and furfural are completely separated from other components of the hydrolysates regardless of the resin cross-linkage (Figure 2). The sorption of HMF and furfural increases as the resin cross-linkage increases from 4.5 to 6.0 wt % (Figure 2). A change in resin cross-link density from 6.0 to 8.0 wt % has no effect on HMF and furfural sorption.

The effect of the resin cross-linkage on the resin shrinking is presented in Figure 3. Resin shrinking increases substantially when the resin cross-link density decreases (Figure 3). This is because the less-cross-linked resins are looser than more-cross-linked resins, and can therefore swell and shrink more. The resin shrinking increases as the sulfuric acid concentration increases, and the effect of the H_2SO_4 concentration is quite significant (Figure 3). Resin shrinking cannot be avoided with gel-type ion-exchange resins at high electrolyte concentrations, and it causes large dispersion in the chromatographic column.

3.1.1. Monosaccharide Yield. The effect of the resin cross-linkage on the monosaccharide recovery from concentrated-acid hydrolysates was evaluated from the experimental results by calculating the monosaccharide yield. The constraints used to determine the cut points of the monosaccharide fraction were the desired sulfuric acid yield in the H_2SO_4 fraction (first fraction), $Y_{H_2SO_4}$, and the maximum allowed inhibitor concentration in the monosaccharide fraction (middle fraction), $c_{AcOH}^{product}$.

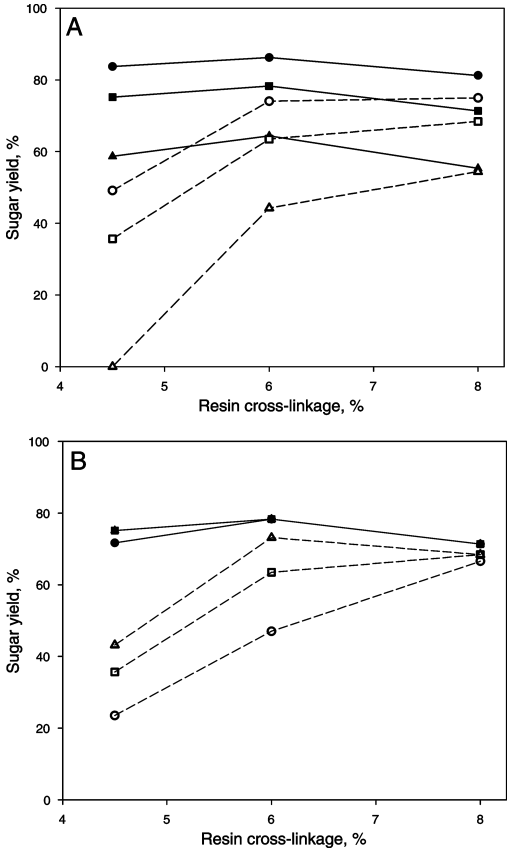

Figure 4. Effect of resin cross-linkage on the monosaccharide yield. (A) $Y_{H_2SO_4}$ is varied and $c_{AcOH}^{product}$ is kept constant at 1.0 g/L: (○, ●) 90%, (□, ■) 95%, and (△, ▲) 98% H_2SO_4 yield. (B) $c_{AcOH}^{product}$ is varied and $Y_{H_2SO_4}$ is kept constant at 95%: (○, ●) 0.5 g/L, (□, ■) 1.0 g/L, and (△, ▲) 1.5 g/L acetic acid. Filled symbols = spruce and open symbols = birch hydrolysate. Lines are presented to guide the eye.

In practice, the only inhibitor eluting near the monosaccharides is acetic acid (see Figures 1 and 2). Therefore, the inhibitor concentration corresponds to the acetic acid concentration. The constraints were varied between 90 and 98% for $Y_{H_2SO_4}$, and between 0.5 and 1.5 g/L for $c_{AcOH}^{product}$.

The effect of the resin cross-linkage on the monosaccharide yield is presented in Figure 4A (constant $c_{AcOH}^{product}$) and Figure 4B (constant $Y_{H_2SO_4}$). With the spruce hydrolysate (Figure 4), the effect on the monosaccharide yield is small, although a weak maximum is observed at 6.0 wt % cross-link density. With the birch hydrolysate, the effect is more significant, especially when the resin cross-link density is low. In all cases, the yield of monosaccharides decreases as $Y_{H_2SO_4}$ increases (at constant $c_{AcOH}^{product}$, Figure 4A) or as $c_{AcOH}^{product}$ decreases (at constant $Y_{H_2SO_4}$, Figure 4B).

When the cross-linkage increases, electrolyte exclusion becomes stronger due to higher charge density in the resin. This leads to lower sorption of sulfuric acid (see Figure 2), and the separation efficiency of H_2SO_4 from the monosaccharides should increase. However, at the same time, the sorption of monosaccharides decreases. This is due to higher size exclusion of

monosaccharides with tighter resins. As a consequence, the monosaccharide yield obtained with the spruce hydrolysate with the 6.0 wt % cross-linked resin is somewhat higher than with the other resins (Figure 4). Because of the low amount of acetic acid in the spruce hydrolysate (see Table 1 for details), separation of monosaccharides and acetic acid does not significantly affect the yield. This is clearly seen in Figure 4B, where the constraint $c_{AcOH}^{product}$ is varied at constant $Y_{H_2SO_4}$.

The birch hydrolysate contained a relatively high amount of acetic acid (see Table 1), and the monosaccharide yield depended also on the monosaccharide−acetic acid separation efficiency. Sorption of acetic acid decreases as the resin cross-linkage increases (see Figure 2) due to increasing size exclusion. However, the sorption of acetic acid is not as much affected by size exclusion as the sorption of the monosaccharides because of the smaller molecular dimensions. Due to this the monosaccharide−acetic acid separation efficiency increases as the resin cross-linkage increases. This explains the improvement of the monosaccharide yields obtained with the birch hydrolysate with increasing cross-link density (Figure 4).

The conclusions made regarding the influence of cross-link density on the yield do not depend on the choice of the constraints used (Figure 4). However, it should be noted that no confidence intervals could be presented due to the lack of replicate experiments.

3.1.2. Productivity. The effect of the resin cross-linkage on the productivity of the batch process with respect to the monosaccharides was evaluated using the same constraints as in the calculation of the monosaccharide yield (see section 2.5 for details). When evaluating the cycle time, the beginning of a cycle was set to the breakthrough point of sulfuric acid. It was presumed that the cycle ends when the acetic acid concentration decreases below 0.05 g/L. Acetic acid eluting after this point is recovered in the H_2SO_4 fraction in the following cycle. In addition, monosaccharides eluting before the first cut point were treated as lost product. HMF and furfural are strongly sorbed to the resin (see Figures 1 and 2), and prolong the cycle time of the batch process considerably. Obviously, if they were not removed before the acid−monosaccharide separation, the process would be economically unfeasible. HMF and furfural can be removed from the hydrolysates for example with polymeric adsorbents such as XAD-8,[18] or with other separation methods.[19,20]

As seen in Figure 5, the productivity of the separation process increases as the resin cross-linkage increases because the cycle time of the batch process decreases. This is caused by decreased sorption of all components, which makes them propagate faster through the column. The highest productivity is obtained with the 8.0 wt % cross-linked resin (Figure 5), for which the cycle time was approximately 21 min. An almost 50% longer cycle time was obtained for the 4.5 wt % cross-linked resin (approximately 30 min).

The differences in the productivity between different resin cross-linkages are smaller with the spruce hydrolysate than with the birch hydrolysate (Figure 5). This is due to the smaller differences in the monosaccharide yield between different resin cross-linkages with the spruce hydrolysate than with the birch hydrolysate (see Figure 4). The productivity of the batch process decreases as $Y_{H_2SO_4}$ increases (at constant $c_{AcOH}^{product}$, Figure 5A) or as $c_{AcOH}^{product}$ decreases (at constant $Y_{H_2SO_4}$, Figure 5B) due to the lower monosaccharide yield obtained.

3.2. Effect of Column Loading on the Process Performance. The effect of column loading (feed volume to resin bed volume ratio) on the recovery of monosaccharides from concentrated-acid hydrolysates was also investigated. Three column loadings were used: 4.7, 9.4, and 18.8 vol %.

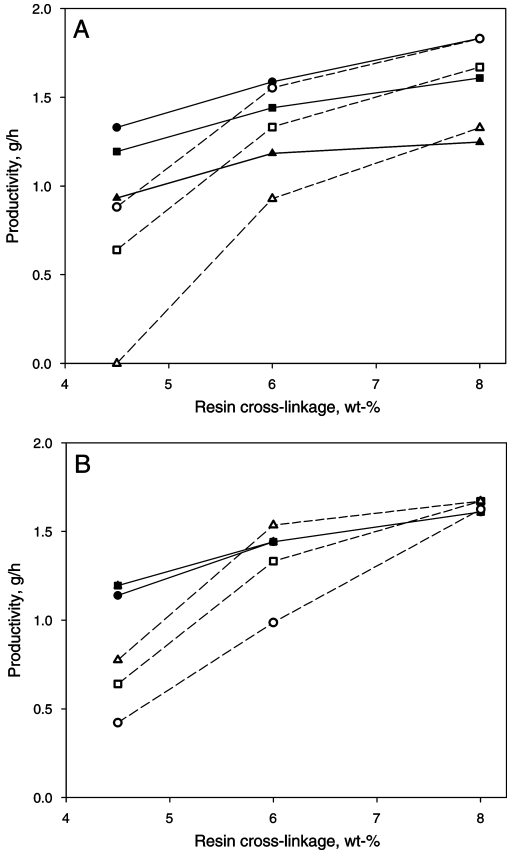

Figure 5. Effect of resin cross-linkage on productivity. (A) $Y_{H_2SO_4}$ is varied and $c_{AcOH}^{product}$ is kept constant at 1.0 g/L: (○, ●) 90%, (□, ■) 95%, and (△, ▲) 98% H_2SO_4 yield. (B) $c_{AcOH}^{product}$ is varied and $Y_{H_2SO_4}$ is kept constant at 95%: (○, ●) 0.5 g/L, (□, ■) 1.0 g/L, and (△, ▲) 1.5 g/L acetic acid. Filled symbols = spruce and open symbols = birch hydrolysate. Lines are presented to guide the eye.

In Figure 6A (spruce hydrolysate, see Table 1 for details) and Figure 6B (birch hydrolysate, see Table 1 for details), the effect of column loading on the monosaccharide recovery with the 6.0 wt % cross-linked resin is shown. With the other resins, similar chromatograms were obtained. As was expected, the effects of the column loading on the elution chromatograms are fairly independent of the composition of the hydrolysates (Figure 6). As was mentioned before, the main difference in the hydrolysates is in the amount of acetic acid, which does not affect the elution of the other components.

As the column loading increases, the sulfuric acid peak shape remains essentially the same; only the size of the peak increases (Figure 6). The breakthrough point of H_2SO_4 is not influenced by the column loading, due to complete electrolyte exclusion at very low H_2SO_4 concentrations. The amount of tailing of the H_2SO_4 peak increases as the column loading increases due to higher dispersion (resin shrinking). The higher the column loading, the higher the amount of sulfuric acid, and the higher the resin shrinking.

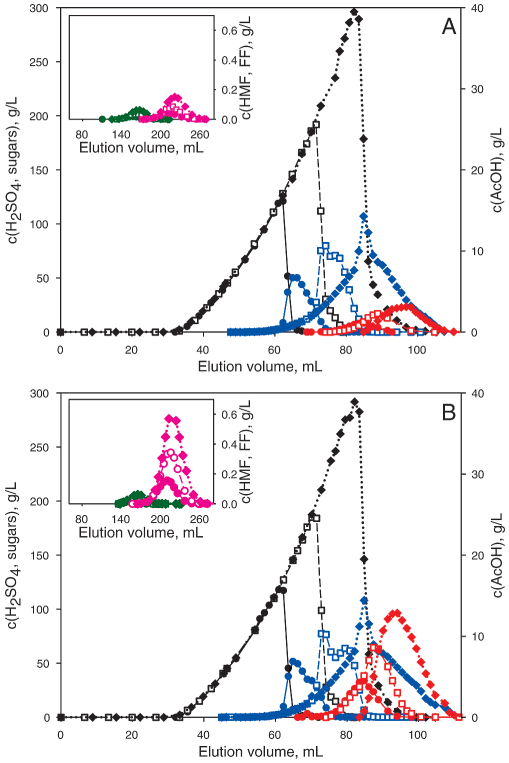

Figure 6. Example of the effect of column loading on the chromatographic recovery of monosaccharides from concentrated-acid spruce (A) and birch (B) hydrolysates. Resin: CS12GC. Feed composition: see Table 1. All monosaccharides are treated as one pseudocomponent. Experimental conditions: see the caption of Figure 1. (●) 4.7 vol %, (□) 9.4 vol %, and (◆) 18.8 vol % cross-linked resin. Colors: black = H_2SO_4, blue = monosaccharides, red = acetic acid, green = HMF, and pink = FF. Lines are presented to guide the eye.

The monosaccharide peak's breakthrough point does not increase when the column loading increases (Figure 6) because the H_2SO_4 concentration is the same at the monosaccharide peak's breakthrough point with each loading. The front of the monosaccharide peak is similar with each column loading for 15 mL from the breakthrough point (approximately 47 mL with the 6.0 wt % cross-linked resin). On the contrary, the retention time of the maximum concentration of the monosaccharide peak increases as the column loading increases (Figure 6). This is because more H_2SO_4 is present, and therefore the monosaccharide sorption is higher (the higher the H_2SO_4 concentration, the slower the propagation of the monosaccharides). Sulfuric acid affects the shape of the monosaccharide peak through resin shrinking and because it influences the sorption of monosaccharides (Figure 6). When the column loading increases, the amount of monosaccharides eluting in the extensive front increases. With the 18.8 vol % column loading, the extensive front contains a large portion of the monosaccharides, the monosaccharide peak is very dispersed, and consecutively the separation of monosaccharides from H_2SO_4 is very poor. Also the separation of monosaccharides from acetic acid with the highest loading is poor (Figure 6).

The retention of acetic acid increases as the column loading increases. This is due to the influence of sulfuric acid on the sorption of acetic acid, as well as the increase in the void volume, which is caused by the shrinking of the resin (Figure 6). The increase in the breakthrough point of acetic acid is approximately the same as the change in the volume of the feed. For the increase of loading from 4.7 to 9.4 vol % the difference was approximately 5 mL, and for the increase of loading from 9.4 to 18.8 vol % the difference was approximately 10 mL. The shape of the acetic acid peak is not affected by column loading, which indicates that the sorption isotherm of acetic acid is linear or at least very close to linear (Figure 6).

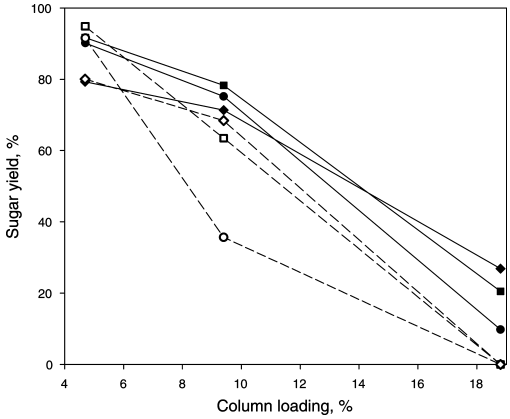

Figure 7. Effect of column loading on the monosaccharide yield. $Y_{H_2SO_4}$ and $c_{AcOH}^{product}$ are kept constant at 95% and 1.0 g/L, respectively. (○, ●) 4.5 wt %, (□, ■) 6.0 wt %, and (◇, ◆) 8.0 wt % cross-linked resin. Filled symbols = spruce and open symbols = birch hydrolysate. Lines are presented to guide the eye.

Hydroxymethyl furfural and furfural are not significantly influenced by the column loading (Figure 6). Their breakthrough points and peak shapes remain essentially the same (due to linear isotherms) when column loading is changed.

3.2.1. Monosaccharide Yield. The effect of column loading on the recovery of monosaccharides from concentrated-acid hydrolysates was evaluated by calculating the monosaccharide yield from the experimental results (see section 2.5 for details).

The effect of column loading on the monosaccharide yield with the studied resins is presented in Figure 7. The monosaccharide yield decreases with each resin as column loading increases (Figure 7). This result is in accordance with earlier results obtained by Neuman et al.[17] It is due to the reduced separation of the monosaccharides from sulfuric and acetic acids at higher loadings, because of higher peak overlapping (higher amount of feed) and dispersion (see section 3.2).

The differences in the monosaccharide yield obtained with different resins are small at the lowest column loading, but increase as the column loading increases (Figure 7). With the lowest loading, the monosaccharide yield is somewhat independent of the hydrolysate composition with each resin. However, with the higher loadings (9.4 and 18.8 vol %) the spruce hydrolysate tends to give higher monosaccharide yields than the birch hydrolysate. This is due to the lower amount of acetic acid in the spruce hydrolysate (see Table 1). With 18.8 vol % loading the monosaccharide yields obtained with each resin are 0 for the birch hydrolysate, and below 40% for the spruce hydrolysate (Figure 7).

The conclusions made regarding the influence of column loading on the yield do not depend on the resin used (Figure

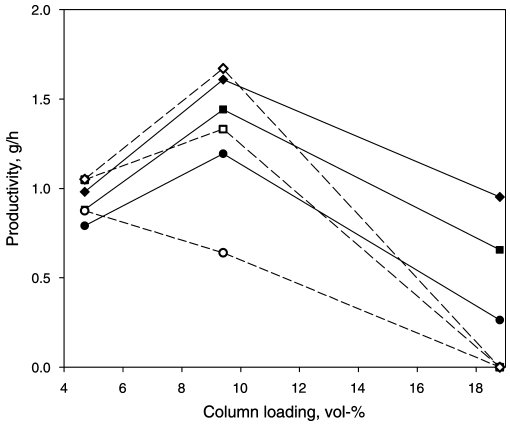

Figure 8. Effect of column loading on productivity. $Y_{H_2SO_4}$ and $c_{AcOH}^{product}$ are kept constant at 95% and 1.0 g/L, respectively. (○, ●) 4.5 wt %, (□, ■) 6.0 wt %, and (◇, ◆) 8.0 wt % cross-linked resin. Filled symbols = spruce and open symbols = birch hydrolysate. Lines are presented to guide the eye.

7). However, it should be noted again that no confidence intervals could be presented due to lack of replicate experiments.

3.2.2. Productivity. The effect of column loading on the productivity of the batch process with respect to monosaccharides was evaluated with the same constraints and presumptions as in the calculation of monosaccharide yield (see section 2.5 for details).

The highest productivity was obtained with the 9.4 vol % column loading (Figure 8). The only exception was the loosest resin with the birch hydrolysate, because of the low monosaccharide yield due to poor separation efficiency (see Figure 7). The 9.4 vol % column loading gave higher productivity than the lowest loading (Figure 8), although a higher monosaccharide yield was obtained with the latter (see Figure 7). This is because, with the higher loading, a higher amount of feed is treated in a cycle. In addition, with the 9.4 vol % loading the monosaccharide yield is quite close to the yield obtained with the 4.7 vol % loading for all other resins except the 4.5 wt % cross-linked resin with the birch hydrolysate (see Figure 7).

When the column loading increases from 9.4 vol %, the productivity decreases again (Figure 8). The amount of feed handled in a cycle increases as the loading increases, but the yield decreases (see Figure 7). This causes the productivity to decrease as the loading increases from 9.4 vol %.

The differences in the productivities with each resin are rather small at the lowest column loading, but increase as the loading increases (Figure 8). The 8.0 wt % cross-linked resin gave the highest productivity with 9.4 vol % column loading, because of the short cycle time (Figure 8). Although the 6.0 wt % cross-linked resin gave a higher yield (see Figure 7) than the 8.0 wt % cross-linked resin, the productivity is lower due to longer cycle time (Figure 8).

4. Conclusions

Chromatographic recovery of monosaccharides from authentic concentrated-acid lignocellulosic hydrolysates and recycling of hydrolysis acid was investigated batchwise. Hydrolysates contained sulfuric acid, five monosaccharides, acetic acid, hydroxymethyl furfural (HMF), and furfural. The effects of resin cross-linkage, column loading, and the composition of the hydrolysate on the monosaccharide yield and the productivity of the separation process were of particular interest. Three strong acid PS−DVB ion-exchange resins with different cross-linkages were used.

With the PS−DVB resins, sulfuric acid, monosaccharides, and acetic acid elute first from the column close to each other, in respective order. HMF and furfural elute after acetic acid, and are completely separated from the other components. Complex interactions of different origins influence the separation: electrolyte exclusion, size exclusion, sorption, and salting out.

It was found that the dilution of sulfuric acid decreases with increasing resin cross-linkage due to stronger electrolyte exclusion. Also, the monosaccharide−acetic acid separation efficiency increases as the resin cross-link density increases. On the other hand, the 6.0 wt % cross-linked resin had the highest H_2SO_4−monosaccharide separation efficiency. Productivity of the process improves as the resin cross-link density increases because of shorter cycle time.

The composition of the hydrolysate also affects the choice of resin. With hydrolysates containing high amounts of acetic acid, a resin with a high monosaccharide−acetic acid separation efficiency gives generally better results. With hydrolysates containing low amounts of acetic acid, the H_2SO_4−monosaccharide separation efficiency has a large effect on the monosaccharide yield. Generally, higher monosaccharide yield and productivity can be obtained with hydrolysates containing low amounts of acetic acid.

The optimum column loading (feed volume to resin bed volume ratio) depends also on whether high monosaccharide yield or productivity is desired. High monosaccharide yield can be obtained with low column loading, but a higher loading should be used to obtain high productivity. The optimum column loading for high productivity was found to be around 10 vol %.

Acknowledgment

Financial support from the Academy of Finland (Grant SA/121280) is gratefully acknowledged. J.H. thanks the Graduate School in Chemical Engineering (Finland), Finnish Cultural Foundation/South Karelia Regional Fund, Emil Aaltonen Foundation (Finland), and LUT Research Foundation for personal grants. The authors wish to thank Ms. Katrin Müller for her experimental assistance.

Nomenclature

c_m^{feed} = monosaccharide concentration in feed (g/L)
$c_{AcOH}^{product}$ = maximum allowed concentration of inhibitors (g/L)
Pr = productivity (g/h)
t_{cycle} = cycle time (h)
V^{feed} = feed volume (L)
$Y_{H_2SO_4}$ = yield of H_2SO_4 in the sulfuric acid fraction (%)
Y_m = yield of monosaccharides (%)

Literature Cited

(1) Hamelinck, C. N.; van Hooijdonk, G.; Faaij, A. P. C. Ethanol from Lignocellulosic Biomass: Techno-Economic Performance in Short-, Middle- and Long-term. *Biomass Bioenergy* **2005**, *28*, 384–410.

(2) Galbe, M.; Zacchi, G. A Review of the Production of Ethanol from Softwood. *Appl. Microbiol. Biotechnol.* **2002**, *59*, 618–628.

(3) Taherzadeh, M. J.; Karimi, K. Bioethanol: Market and Production Processes. In *Biofuels Refining and Performance*; Nag, A., Ed.; McGraw-Hill: Fairfield, 2008; pp 69−106.

(4) From 1st- to 2nd-Generation Biofuel Technologies—An Overview of Current Industry and RD&D Activities. International Energy Agency, November 2008; http://www.iea.org/textbase/papers/2008/2nd_Biofuel_Gen.pdf.

(5) Shapovalov, O. I.; Ashkinazi, L. A. Biobutanol: Biofuel of Second Generation. *Russ. J. Appl. Chem* **2008**, *81*, 2232–2236.

(6) Kumar, P.; Barrett, D. M.; Delwiche, M. J.; Stroeve, P. Methods for Pretreatment of Lignocellulosic Biomass for Efficient Hydrolysis and Biofuel Production. *Ind. Eng. Chem. Res.* **2009**, *48*, 3713–3729.

(7) Kunkes, E. L.; Simonetti, D. A.; West, R. M.; Serrano-Ruiz, J. C.; Gärtner, C. A.; Dumesic, J. A. Catalytic Conversion of Biomass to Monofunctional Hydrocarbons and Targeted Liquid-Fuel Classes. *Science* **2008**, *322*, 417–421.

(8) Rass-Hansen, J.; Falsig, H.; Jørgensen, B.; Christensen, C. H. Bioethanol: Fuel or Feedstock. *J. Chem. Technol. Biotechnol.* **2007**, *82*, 329–333.

(9) Hamelinck, C. N.; van Hooijdonk, G.; Faaij, A. P. C. Ethanol from Lignocellulosic Biomass: Techno-Economic Performance as Development Progresses. Universiteit Utrecht/Copernicus Institute, November 2003; https://www.senternovem.nl/mmfiles/ 149043_tcm24-280055.pdf.

(10) Iranmahboob, J.; Nadim, F.; Monemi, S. Optimizing Acid-Hydrolysis: A Critical Step for Production of Ethanol from Mixed Wood Chips. *Biomass Bioenergy* **2002**, *22*, 401–404.

(11) Farone, W. A.; Cuzens, J. E. Strong Acid Hydrolysis of Cellulosic and Hemicellulosic Materials. U.S. Patent 5,597,714, June 7, 1995.

(12) Farone, W. A.; Cuzens, J. E. Method of Producing Sugars Using Strong Acid Hydrolysis of Cellulosic and Hemicellulosic Materials. U.S. Patent 5,562,777, March 26, 1993.

(13) Clausen, E. C.; Gaddy, J. L. Concentrated Sulfuric Acid Process for Converting Lignocellulosic Materials to Sugars. U.S. Patent 5,188,673, Oct 12, 1988.

(14) Huang, T.-C.; Juang, R.-S. Recovery of Sulfuric Acid with Multicompartment Electrodialysis. *Ind. Eng. Chem. Process Des. Dev.* **1986**, *25*, 537–542.

(15) Lightner, G. E. Method to Produce Fermentable Sugars from A Lignocellulose Material. U.S. Patent 6,258,175, Nov 3, 1999.

(16) Xie, Y.; Phelps, D.; Chong-Ho, L.; Sedlak, M.; Ho, N.; Wang, N.-H. L. Comparison of Two Adsorbents for Sugar Recovery from Biomass Hydrolyzate. *Ind. Eng. Chem. Res.* **2005**, *44*, 6816–6823.

(17) Neuman, R. P.; Rudge, S. R.; Ladisch, M. R. Sulfuric Acid-Sugar Separation by Ion Exclusion. *React. Polym.* **1987**, *5*, 55–61.

(18) Nilvebrant, N.-O.; Reimann, A.; Larsson, S.; Jönsson, L. J. Detoxification of Lignocellulose Hydrolysates with Ion-exhange Resins. *Appl. Biochem. Biotechnol.* **2001**, *91*−*93*, 35–49.

(19) Palmqvist, E.; Hahn-Hägerdal, B. Fermentation of Lignocellulosic Hydrolysates. I: Inhibition and Detoxification. *Bioresour. Technol.* **2000**, *74*, 17–24.

(20) Mussatto, S. I.; Roberto, I. C. Alternatives for Detoxification of Diluted-Acid Lignocellulosic Hydrolysates for Use in Fermentative Processes: a Review. *Bioresour. Technol.* **2004**, *93*, 1–10.

Received for review October 13, 2009
Revised manuscript received December 22, 2009
Accepted January 23, 2010

IE901598Z

PAPER II

Research Article

Received: 31 July 2011 Revised: 20 October 2011 Accepted: 22 October 2011 Published online in Wiley Online Library: 7 December 2011

(wileyonlinelibrary.com) DOI 10.1002/jctb.2766

Ethanol production from wood via concentrated acid hydrolysis, chromatographic separation, and fermentation

Jari Heinonen,[a] Anu Tamminen,[b] Jaana Uusitalo[b] and Tuomo Sainio[a]*

Abstract

BACKGROUND: Production of bioethanol from wood using concentrated acid hydrolysis has received less attention than the dilute acid hydrolysis route. The feasibility of producing lignocellulosic bioethanol from spruce and birch via concentrated acid hydrolysis was studied experimentally. Hydrolysis with sulfuric acid, chromatographic purification of the hydrolysate, and fermentation of the monosaccharides were investigated.

RESULTS: Monosaccharide yields of 70% were obtained in the hydrolysis of spruce and birch. Only low amounts of by-products were formed. With chromatographic purification of the hydrolysate, over 90% of the hydrolysis acid was recovered for recycling, and furfural and HMF were removed completely. Most of the acetic acid was recovered in a separate fraction. The monosaccharide yield in a single pass separation was approximately 70%. In the fermentation, *S. cerevisiae* produced higher amounts of ethanol and more efficiently than *P. stipitis*. Chromatographically purified hydrolysates gave higher ethanol productivities and yields than $Ca(OH)_2$ neutralized hydrolysates.

CONCLUSIONS: Chromatographic purification of concentrated acid lignocellulosic hydrolysates has advantages when compared with neutralization with $Ca(OH)_2$. With chromatography, most of the inhibitory compounds can be removed from the hydrolysates. In addition, due to the recycling of the hydrolysis acid, the economy of the bioethanol manufacturing process is increased considerably.

Keywords: lignocellulose; bioethanol; concentrated acid hydrolysis; chromatographic separation; detoxification; fermentation

INTRODUCTION

Lignocellulosic bioethanol production via dilute acid hydrolysis has been studied extensively.[1–4] Also hydrolysate detoxification methods are well known.[5–11] Another possible route, the concentrated acid hydrolysis, has received less attention. This is because of high acid consumption in the early process schemes, where detoxification and pH adjustment were done by overliming. Using lime results in the generation of large amounts of gypsum.[2,3,12,13] In addition, ethanol yield in fermentation has been low because overliming does not remove all the toxic compounds from the hydrolysates.[7,14] Open literature on the fermentation of concentrated acid lignocellulose hydrolysates is scarce.

A modern process scheme for lignocellulosic bioethanol production via concentrated acid hydrolysis is presented in Fig. 1.[12,13,15,16] Acid hydrolysis is done in two steps at normal atmospheric pressure and at temperatures below 100 °C.[2,3,17,18] In the first step, the raw material is pretreated with 70–80 wt% H_2SO_4 in order to break down the crystalline parts of the cellulose chains. In the second step, the acid is diluted to 20–30 wt%, and hydrolysis is carried out.

The benefits of the concentrated acid hydrolysis route include very high monosaccharide yield (up to 90%) and only a small amount of by-products formed.[2,14,15] The main by-products are acetic acid (from acetyl groups in hemicelluloses), furans (monosaccharide degradation products), and phenolic compounds (from lignin).[5,14,19]

In order to make the concentrated acid process economically viable, the hydrolysis acid must be recycled. This can be done by using chromatography with ion exchange resins, as has been shown in earlier works.[12,13,20,21,22] A rigorous thermodynamic model for the separation was recently presented by Laatikainen *et al*.[23] Fermentation inhibitors can be removed at the same time as the hydrolysis acid[20] or in a separate step.[24]

Fermentation of the purified concentrated acid lignocellulosic hydrolysates is not straightforward because these solutions contain monosaccharides from both cellulose and hemicelluloses. Softwoods (e.g. spruce) contain around 42–45% cellulose, 20–26% hemicellulose and up to 28% lignin. The hemicelluloses consist of mannose (hexose sugar), only 6–7% of hemicelluloses are pentose sugars. Hardwoods (e.g. birch) contain around 40% cellulose, 39%

* *Correspondence to: Tuomo Sainio, Lappeenranta University of Technology, Laboratory of Industrial Chemistry, Skinnarilankatu 34, FIN-53850 Lappeenranta, Finland. E-mail: tuomo.sainio@lut.fi*

a *Lappeenranta University of Technology, Laboratory of Industrial Chemistry, Skinnarilankatu 34, FIN-53850 Lappeenranta, Finland*

b *VTT Technical Research Centre of Finland, P.O.Box 1000, FIN-02044 VTT, Finland*

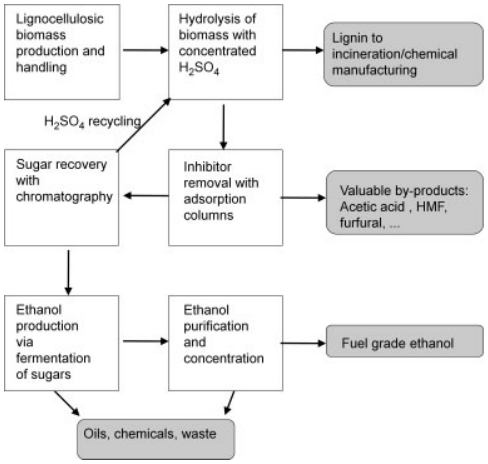

Figure 1. Lignocellulosic bioethanol production by concentrated acid hydrolysis using chromatography for hydrolysate purification.

hemicellulose and 21% lignin. The content of pentoses is around 25% of the total wood.[1,9]

Saccharomyces cerevisiae is widely used for ethanol production from hexose sugars because of its high ethanol productivity and tolerance to ethanol and inhibitors. Unfortunately, wild type *S. cerevisiae* cannot utilize xylose, which is the dominant pentose sugar in the hydrolysates of lignocellulosic biomass. Naturally occurring yeasts such as *Pichia stipitis* are able to ferment both glucose and xylose to ethanol. *P. stipitis* can utilize very efficiently xylose on non-toxic conditions but cannot tolerate inhibiting conditions. *P. stipitis* is also quite sensitive to ethanol.[25,26,27]

In this study, the feasibility of a concentrated acid lignocellulosic bioethanol production process is investigated experimentally through the three main unit operations of the process (see Fig. 1): hydrolysis, chromatographic monosaccharide recovery and detoxification, and fermentation. Two wood species, spruce and birch, are used as raw materials. Fermentation of the purified hydrolysates is carried out with two yeasts: *S. cerevisiae* which is genetically modified to utilize xylose and naturally xylose utilizing *P. stipitis*. The goal of this work was to find a feasible combination of pH adjustment and detoxification methods and fermentation yeasts. No process optimization is considered here, however.

EXPERIMENTAL

Concentrated acid hydrolysis

Concentrated acid hydrolysis experiments were conducted in a 1 L jacketed glass reactor equipped with a reflux condenser. Mechanical stirring was used to mix the contents of the reactor. The reactor was heated to the desired temperature with a water circulation thermostat (C6CS, Lauda). Prior to hydrolysis, raw materials were ground with a hammer mill to a particle size between 1 mm and 5 mm and dried overnight in oven at 50 °C.

Pretreatment of the wood chips was done at 50 °C. 100 g of dried wood chips were added gradually (in 20 min) into 321 g of 70 wt% preheated sulfuric acid (diluted from pro analysis grade 95–97 wt% sulfuric acid (Merck KGaA) with purified water). The mixture was stirred manually during the addition of the chips. A homogeneous black paste formed when the chips were added to sulfuric acid solution. The paste was kept at 50 °C for 2 h from the beginning of addition of the chips to H_2SO_4. The paste was stirred manually to promote breakdown of the wood chips.

The actual hydrolysis was initiated after pre-treatment. 429 g of purified and heated water (50 °C) was added to the reactor in order to dilute the sulfuric acid to approximately 30 wt%. After adding the water to the reactor, the mixture was heated to 80 °C (heating time: 20 min). The mixture was stirred continuously with a mechanical stirrer. The hydrolysis was carried out for 6 h. Samples from the liquid phase were taken for analysis.

After 6 h, the hydrolysis reactions were stopped by cooling the reaction mixture in a freezer (−18 °C). Afterwards, the remaining solids in the hydrolysate were separated from the solution using a pressure filter. Samples were taken from the filtered solutions to see if any monosaccharide losses occurred during the filtering.

Chromatographic monosaccharide recovery

Chromatographic recovery of monosaccharides from the concentrated acid hydrolysates (spruce and birch) was done in a batch column. The aim of these runs was to produce purified monosaccharide solution for the fermentation. Gel type strong acid cation exchange resin with polystyrene–divinylbenzene matrix (CS12GC, d_p 217 µm, Q_v 1.51 mequiv mL^{-1}, Finex Oy, Finland) was chosen for use in fractionation based on earlier results.[20] CS12GC was chosen because it gives good monosaccharide yield with both hydrolysates (spruce and birch).

The experimental setup for chromatographic separations consisted of two HPLC pumps for eluent and feed (515 series pumps, Waters), a chromatographic column (XK 26, Pharmacia Biotech) with 26 mm inner diameter and water heating jacket, a water circulation thermostat for column heating (C6CS, Lauda), an online conductivity detector (Conductivity monitor, Pharmacia Biotech), an on-line refractive index (RI) detector (RI-2000F, Schambeck), and an on-line UV detector (2487 dual λ Absorbance Detector with 3 mm semiprep flow cell, Waters). LabView program (version 8.2, National Instruments) was used to control the valves and collect the online data.

The resin bed volume was 106 cm^3 (bed height 20 cm). The resin was packed in the column in H^+ form so that the bed height was 21.4 cm, and then the bed was compressed to the desired height. The chromatographic fractionations were done using top-down flow at 50 °C temperature, and with purified water as eluent at a flow rate of 2.655 mL min^{-1} (corresponds to a linear velocity of 0.5 cm min^{-1} in the XK 26 column). Based on earlier results,[20] 10 mL injection volume was chosen to be used in the fractionation. The monosaccharide fractions were collected at 74.2–86.3 mL and 74.2–85.0 mL for spruce and birch, respectively. 100 runs were performed to purify approximately 1 L of concentrated acid hydrolysates from spruce and birch using this procedure.

Fermentation

The fermentability of purified concentrated acid hydrolysates and ethanol production capability of two different yeasts were investigated. The yeasts were a genetically engineered *Saccharomyces cerevisiae* (VTT B-08 014), developed at Technical Research Centre of Finland, and *Pichia stipitis* (VTT C-10 876) capable of natural xylose utilization. The fermentation experiments were carried out in anaerobic shake flask cultivations.

In addition to chromatographically purified hydrolysates, fermentation of $Ca(OH)_2$ neutralized hydrolysates was studied

as a reference. Also neutralization with NaOH was tested in a preliminary experiment. Since neither yeast was able to produce ethanol because of very high dissolved salt concentration (ionic strength), this option was not studied further.

Microorganisms and culture medium

Genetically modified xylose utilizing *S. cerevisiae* VTT B-08014 yeast was preserved on agar plate containing yeast nitrogen base (YNB, Difco) + 2% xylose. *Pichia stipitis* VTT C10876 was used as the natural xylose-utilizing yeast. *Pichia stipitis* was preserved on yeast peptone dextrone (YPD)-agar plates. The yeast cells were precultured aerobically in 5 mL YPD medium (yeast extract 1%, peptone 2% and glucose 2%) overnight at 30 °C in a rotary shaker (New Brunswick Scientific, USA) set to 200 rpm. After 24 h incubation time the cells were transferred to 45 mL YP medium supplemented with 5% glucose. *S. cerevisiae* and *P. stipitis* cells were grown overnight to optical density at 600 nm (OD_{600}) values of approximately 25 and 35, respectively. The cells were then harvested, washed on Na-phosphate buffer (pH 7.0) and resuspended in 10 times concentrated YNB medium, giving initial OD_{600} of 3.5 (equals 1 g L^{-1} dry weight concentration of cells) in 50 mL.

Fermentation of the purified hydrolysates

The pH of the unpurified and chromatographically purified hydrolysates was adjusted to 5.0 with $Ca(OH)_2$ powder prior to the fermentation. The $CaSO_4$ precipitate formed in the pH adjustment was removed by filtration. The filtered hydrolysates were sterilized prior to yeast inoculation.

The fermentation studies were performed for approximately 250 h in anaerobic conditions using 100 mL glycerol lock flasks, working volume of 50 mL in orbital shaker (HT Infors Minitron, Infors AG) at 100 rpm and 30 °C. Initial cell dry weight mass was 0.05 g in 50 mL.

Sample analyses

Hydrolysis and chromatographic separation

Concentrations of monosaccharides, acetic acid, hydroxymethyl furfural (HMF), and furfural were measured with an off-line HPLC system (HP 1100 Hewlett-Packard/Agilent, Bio-Rad Aminex HPX-87H column, RI and UV detectors). From monosaccharides, only glucose and xylose can be analysed with HPX-87H column because other monosaccharides elute under xylose peak. Therefore, the composition at the end of the hydrolysis was analysed also with Varian Metacarb 87P column in order to obtain the concentrations of all individual monosaccharides. HPLC analyses with HPX-87H and Metacarb 87P columns were conducted at 60 °C and 85 °C, respectively, with 10 µL injection volume, and with 0.005 mol L^{-1} H_2SO_4 and purified water as an eluent, respectively.

Sulfuric acid concentration was determined with potentiometric titration. For more details, see our previous study.[20]

Fermentation

During the fermentation experiments, the amount of ethanol produced was determined by measuring the weight loss of the fermentation flasks. The weight loss is caused by CO_2 release, and the mole amount of released CO_2 equals the mole amount of ethanol produced. The weight loss was measured daily. In addition, the ethanol production was analysed with HPLC using an Aminex HPX-87H column at 55 °C, with 20 µL injection volume, with 2.5 mmol L^{-1} H_2SO_4 as an eluent, and with a flow rate of 0.3 mL min^{-1}. HPLC samples were centrifuged before the analyses. Cell growth during the fermentation experiments was followed optically by spectrophotometer (UV-1201 UV-VIS, Shimadzu) at 600 nm.

The quantitative analysis of carbohydrates (rhamnose, arabinose, galactose, glucose, mannose and xylose) was carried out with high performance anion exchange chomatography (Dionex ICS-3000, Dionex) with a pulse amperometric detector (HPAEC-PAD) using a CarboPac PA-1 (Dionex) column at 30 °C. Purified water was used as eluent.

RESULTS AND DISCUSSION

Concentrated acid hydrolysis

The kinetics of concentrated acid hydrolysis of spruce and birch is shown in Fig. 2. Only the hydrolysis step (i.e. after dilution to 30 wt%) is shown. Xylose, galactose, mannose, and arabinose are shown as one pseudocomponent, whereas glucose is presented separately. The final concentrations of each major component (also each monosaccharide) in the hydrolysates are presented in Table 1. The values in the table are taken from the analyses conducted

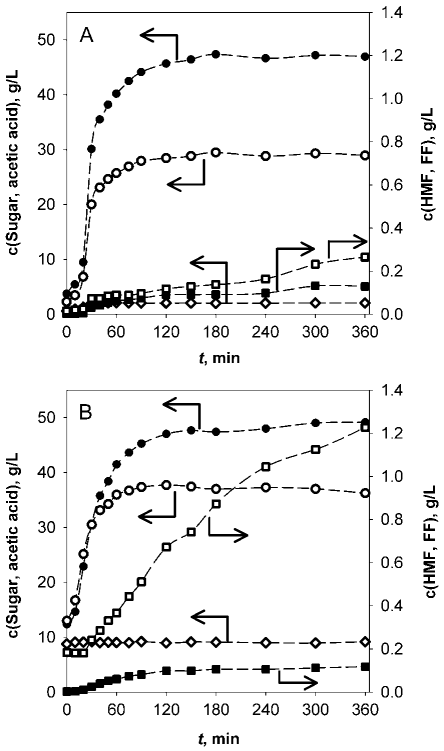

Figure 2. Concentrated sulfuric acid hydrolysis of spruce (A) and birch (B) chips. Experimental conditions: 1 L glass reactor, T = 50 °C. Dilution water was added to the paste at t = 0 min. Symbols: ● = glucose, ○ = other monosaccharides (xylose, arabinose, galactose, and mannose), ◊ = acetic acid, ■ = hydroxymethyl furfural (HMF), and □ = furfural (FF). Lines are presented to guide the eye.

Table 1. Compositions of concentrated acid lignocellulosic hydrolysates of spruce and birch after 8 h of hydrolysis (2 h pretreatment and 6 h hydrolysis). XGMA = combined amount of xylose, galactose, mannose, and arabinose

	c, g/L	
	Spruce	Birch
H_2SO_4	340.8	329.8
Glucose	47.2	48.7
Xylose	7.4	29.0
Galactose	4.7	1.0
Mannose	16.2	3.7
Arabinose	2.4	6.4
XGMA	30.7	40.2
Acetic acid	2.0	9.1
HMF	0.1	0.1
Furfural	0.3	1.3

after filtration of the hydrolysate. However, no differences were detected between the concentration values obtained before and after filtration.

From the first data points in Fig. 2(A) and 2(B) it is seen that only a small amount of monosaccharides was released from spruce (6 g L^{-1} in total, Fig. 2(A)) but a significant amount from birch (25 g L^{-1}, Fig. 2(B)) during the pretreatment (70 wt% H_2SO_4). This difference is mainly due to different particle sizes obtained when grinding the wood (larger particles for spruce). With smaller particle size, the hydrolysis acid impregnates the wood particles faster, and the release of monosaccharides is faster.

Hydrolysis occurs relatively rapidly and concentrations level off at approximately 2 h (Fig. 2). After this point, the rates of monosaccharide formation and their breakdown into furfural and hydroxymethyl furfural are equal. The amount of glucose in both hydrolysates is approximately the same at the end of the hydrolysis (Fig. 2 and Table 1) although spruce contains more cellulose, from which glucose is mainly released.[9] On the other hand, birch hydrolysate contains a higher concentration of xylose, galactose, mannose, and arabinose due to its higher hemicelluloses content.[9] The monosaccharide yields from spruce and birch were 69.2% and 69.4%, respectively (cellulose and hemicelluloses contents of spruce and birch were 69% and 79%, respectively).[9]

Acetic acid concentration remains constant in the hydrolysis of birch (Fig. 2(B)). In spruce hydrolysis, its concentration increases at the beginning of hydrolysis, but levels off after 30 min. Lower formation rate in the case of spruce stems from different particle sizes of the starting materials. Acetic acid is released from the acetyl groups of hemicelluloses that are easily cleaved off. Birch hydrolysate therefore has approximately three times higher concentration of acetic acid than spruce hydrolysate (Fig. 2 and Table 1). Acetic acid is not thought to be a very harmful inhibitor at low concentration, and a low acetic acid concentration can even be beneficial for the hydrolysis depending on the fermentation conditions.[8,28]

In addition to acetic acid, the only by-products detected in the hydrolysates were hydroxymethyl furfural (HMF) and furfural. No phenolic lignin degradation products were detected. HMF concentration increases slowly during hydrolysis (Fig. 2). It is a degradation product of hexoses (glucose, mannose, and galactose). The concentration of HMF in both hydrolysates is relatively low (Table 1). Birch hydrolysate has a somewhat higher concentration of HMF than spruce hydrolysate. This is because birch contains more hemicellulose hexoses that are more easily released than glucose from cellulose, and are therefore exposed for a longer time for degradation reactions.

The furfural concentration increases steadily during hydrolysis (Fig. 2). Furfural is a degradation product of pentoses (xylose and arabinose). Birch hydrolysate contains approximately four times higher concentration of furfural than spruce hydrolysate (Table 1) due to the higher amount of pentose monosaccharides in the former. The concentration of furfural in both hydrolysates is quite small compared with the total monosaccharide concentrations. However, even small concentrations of HMF and furfural have a detrimental effect on fermentation,[5,8,19] although at least one study[10] reported that very small furfural concentrations may have a positive effect on fermentation.

Chromatographic fractionation

The hydrolysates obtained from concentrated acid hydrolysis were purified chromatographically batchwise using a gel type strong acid cation exchange resin (CS12GC). Chromatograms obtained with concentrated acid spruce and birch hydrolysates are

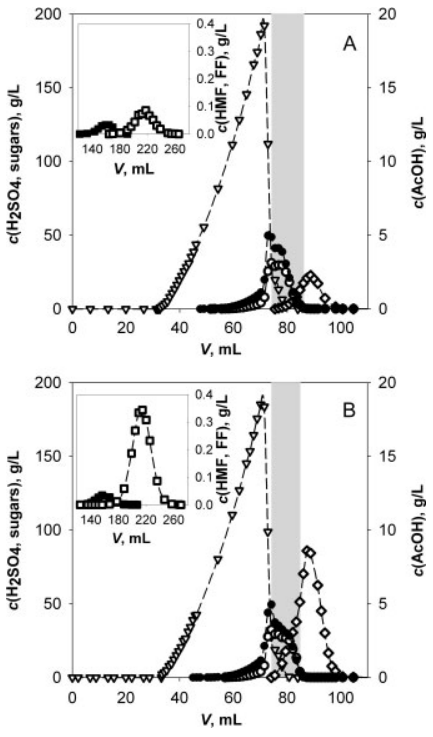

Figure 3. Batchwise chromatographic fractionation of concentrated acid spruce (A) and birch hydrolysates (B) with CS12GC resin. Feed composition: see Table 1. Experimental conditions: V_{inj} = 10 mL, d_{col} = 2.5 cm, h_{bed} = 20 cm, purified water as eluent, $\dot{V}$ = 2.655 mL min^{-1}, top–down flow, and T = 50 °C. Symbols: ▽ = H_2SO_4, ● = glucose, ○ = XGMA, ◊ = acetic acid, ■ = HMF, and □ = FF. Shaded area represents the monosaccharide fraction. Lines are presented to guide the eye.

Table 2. Composition of the monosaccharide fraction of spruce and birch hydrolysates before and after chromatographic purification

		Spruce	Birch
		c, g L^{-1}	c, g L^{-1}
Feed to the separation	H_2SO_4	340.8	329.8
	Glucose	47.2	48.7
	X+G+M+A	30.7	40.2
	AcOH	2.0	9.1
	HMF	0.1	0.1
	Furfural	0.3	1.3
First run	H_2SO_4	6.4	7.3
	Glucose	24.0	27.3
	Xylose	18.2	23.8
	AcOH	0.5	2.0
	HMF	0.0	0.0
	Furfural	0.0	0.0
Average (100 runs)	H_2SO_4	14.7	24.2
	Glucose	33.7	33.6
	Xylose	22.3	27.2
	AcOH	0.3	0.8
	HMF	0.0	0.0
	Furfural	0.0	0.0

presented in Fig. 3. The positions of the monosaccharide fractions are also shown. The compositions of the hydrolysates prior to and after chromatographic purification are shown in Table 2.

The concentration profile of sulfuric acid has a clearly anti-Langmuirian shape (Fig. 3), and its breakthrough occurs at the void volume. This is due to complete electrolyte exclusion at small H_2SO_4 concentrations. The monosaccharide profiles have extensive front parts under the H_2SO_4 profile (Fig. 3). This is due to a salting out effect: the presence of H_2SO_4 slows down the propagation of the monosaccharides and an extensive front is formed (see earlier work[20,23] for details). Another interesting phenomenon resulting from the salting out is the focusing[29] of monosaccharides during elution (Fig. 3). Such focusing prevents erosion of the maximum monosaccharide concentration. With the spruce hydrolysate (Fig. 3(A)), for example, the maximum monosaccharide concentration is the same as the feed concentration (50 g L^{-1} glucose and 30 g L^{-1} other monosaccharides). While the propagation of the front parts of the monosaccharide profiles are slowed down by sulfuric acid, the rear parts of the profiles, where sulfuric acid is not present, are not affected. Consequently, the profiles are 'squeezed in' and the concentration of the monosaccharides increases. This kind of focusing is rare in chromatography and has a significant positive effect on process economics.

Acetic acid elutes after the monosaccharides (Fig. 3) but is not completely separated from them. HMF and furfural, on the other hand, are strongly adsorbed to the resin and are completely separated from the other compounds. Their retention time is so long that it would be beneficial to remove them from the hydrolysates in a separate process step before acid–sugar separation, as indicated in Fig. 1.

The first cut point of the monosaccharide fraction (Fig. 3) was chosen such that the pH in the target fraction (monosaccharide fraction) was approximately 0.8. The second cut point was chosen so that most of the monosaccharides were recovered but the acetic acid concentration in the monosaccharide fraction remained low. The small difference in the volumes of the monosaccharide fractions in spruce and birch hydrolysates stems from higher initial acetic acid concentration in the birch hydrolysate.

The compositions of the original and purified hydrolysates are shown in Table 2. The 100 run average concentrations differ in some cases from the concentrations after the first run (Table 2). This is because of changes in the resin bed packing due to resin shrinking and swelling, which is substantial under the conditions of these experiments (see earlier work[20] for details).

With respect to HMF and furfural, chromatographic detoxification was complete (Table 2). Furfural and HMF were completely separated from the other components due to their higher sorption (Fig. 3). The yields of glucose from the chromatographic purification (see Tables 1 and 2) of spruce and birch hydrolysates were 74% and 73%, respectively. For xylose, galactose, mannose, and arabinose, combined yields of 69% and 68% were obtained with spruce and birch hydrolysates. The yields are relatively low because part of the monosaccharides elute under the sulfuric acid peak (Fig. 3) and are lost in a single-pass procedure. The slightly lower monosaccharide yields with birch hydrolysate stem from the higher amount of acetic acid in the hydrolysate because the acetic acid concentration was used as a design constraint in the separation.

Approximately 95% and 92% of the sulfuric acid in the spruce and birch hydrolysates, respectively, was recovered for reuse. For the spruce hydrolysate, the weight fraction of sulfuric acid in the chromatographically purified hydrolysate is 84% lower than in the original hydrolysate. More sulfuric acid could be removed from the monosaccharide solution at this level of monosaccharide yield only by sacrificing productivity (i.e. by decreasing the feed volume to the column).

Most of the acetic acid was also removed from the hydrolysates with the chromatographic separation (Table 2): 80% for spruce and 90% for birch hydrolysate.

In summary, a large increase in the monosaccharide weight fraction, combined with complete detoxification, was achieved in just a single batch process step. This indicates that chromatographic separation is well suited to the purification of concentrated acid hydrolysates of lignocellulose. Productivity and monosaccharide yield can be further increased by applying recycling or continuous multicolumn units.

Fermentation

Ethanol production from the concentrated acid lignocellulosic hydrolysates was studied with two yeasts: *Saccharomyces cerevisiae,* which was genetically modified to utilize xylose, and natural xylose-utilizing *Pichia stipitis*. The hydrolysates used in the fermentation studies were purified chromatographically ('100 run average' in Table 2) and the final pH adjustment to 5.0 was done with $Ca(OH)_2$. The fermentability of the chromatographically purified hydrolysates was compared with that of $Ca(OH)_2$-neutralized hydrolysates.

Ethanol production from spruce hydrolysate

The effects of yeast strain and purification method on ethanol production from concentrated acid spruce hydrolysate are presented in Fig. 4. Table 3 shows hexose and pentose concentrations in the fermentation experiments at the beginning and the end (250 h from inoculum).

S. cerevisiae was able to produce ethanol more efficiently from chromatographically purified spruce hydrolysate than *P. stipitis*

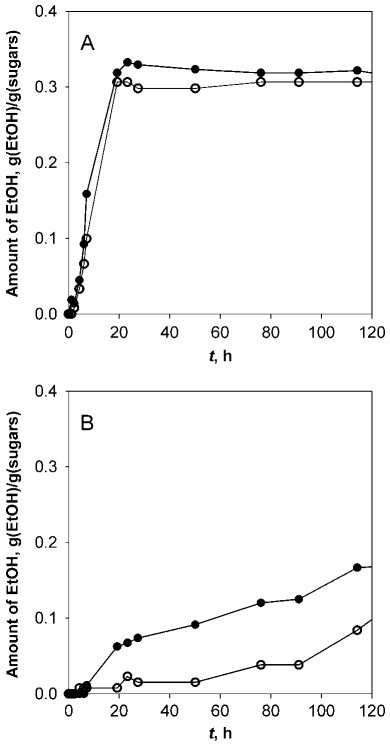

Figure 4. Ethanol production from concentrated acid spruce hydrolysates in shake flask cultivations with *S. cerevisiae* (A) and *P. stipitis* (B). Experimental conditions: c_{yeast} = 1.0 g L^{-1}, $V_{solution}$ = 50 mL, T = 30 °C. Symbols: ● = chromatographically purified hydrolysate, final pH adjustment with $Ca(OH)_2$; ○ = $Ca(OH)_2$ neutralized hydrolysate. Concentrations are average values from two parallel experiments. Lines are presented to guide the eye.

(Fig. 4). With *S. cerevisiae*, $Ca(OH)_2$-neutralized hydrolysate gave slightly lower ethanol production than the chromatographically purified hydrolysate (Fig. 4(A)). The maximum amount of ethanol was achieved in both cases after approximately 20 h. The reason for the lower amount of ethanol at the end of the fermentation with $Ca(OH)_2$-neutralized hydrolysate is that $Ca(OH)_2$ neutralization does not efficiently remove inhibitory compounds from the hydrolysates.[7] In particular, acetic acid is unaffected by $Ca(OH)_2$ neutralization.[14] *S. cerevisiae* is not very sensitive to the inhibitory compounds present in the neutralized hydrolysates (HMF, furfural, and acetic acid), as seen in Fig. 4(A). During 250 h fermentation, *S. cerevisiae* was able to consume all the hexose sugars, but only a fraction of the pentose sugars (Table 3).

The ethanol productivity of *P. stipitis* was much lower than that of *S. cerevisiae* (Fig. 4) although *P. stipitis* produced biomass more quickly than *S. cerevisiae* (data not shown). The reason for the lower ethanol productivity with *P. stipitis* is its sensitivity to inhibitory compounds. The chromatographically purified hydrolysate contained only small amounts of acetic acid, whereas the $Ca(OH)_2$-neutralized hydrolysate contained HMF and furfural and high amounts of acetic acid (Tables 1 and 2). This explains the clear differences in ethanol production with *P. stipitis* from chromatographically purified and $Ca(OH)_2$-neutralized hydrolysates (Fig. 4(B)). Chandel *et al.*[7] obtained similar results in fermentation experiments with *Candida Shehatae* when they compared chromatographic purification of dilute acid hydrolysate with direct neutralization of the hydrolysate. *P. stipitis* is known to be sensitive to ethanol,[25,26,27] which also explains the slow ethanol productivity obtained.

Ethanol production by *P. stipitis* continued throughout the fermentation experiments. After 120 h, the ethanol concentration was much lower than with *S. cerevisiae* (Figs 4(A) and 4(B)). After 250 h, the amount of ethanol had reached the same level as with *S. cerevisiae* (approximately 0.3 g(EtOH) g^{-1}(monosaccharides)). After 250 h, *P. stipitis* had consumed almost all the hexose and pentose sugars, as seen in Table 3. In other words, natural xylose-utilizing *P. stipitis* can use pentose sugars more efficiently than *S. cerevisiae,* which is genetically modified to utilize xylose, but it requires an excessive residence time.

Ethanol yields (percentage of the theoretical yield, 0.51 g(EtOH) g^{-1}(monosaccharides)) and concentrations from spruce hydrolysates treated with different purification methods are presented in Table 4. With both yeast strains, chromatographic treatment provides a significant increase in ethanol yield over $Ca(OH)_2$ treatment. The ethanol concentrations after 120 h of fermentation ranged from 5.1 g L^{-1} to 14.9 g L^{-1}.

The yield of ethanol from the whole process (hydrolysis, chromatographic separation, and fermentation) was 18.7% when *S. cerevisiae* was used to ferment chromatographically purified spruce hydrolysate.

Ethanol production from birch hydrolysate

The effects of yeast strain and purification method on concentrated acid hydrolysate from birch are presented in Fig. 5. Table 3

Table 3. Hexose (C6) and pentose (C5) concentrations at the beginning of fermentation and the end of fermentation (250 h from inoculum)

		Chromatographically purified		$Ca(OH)_2$ neutralized	
	Yeast	Spruce	Birch	Spruce	Birch
t = 0 h		C6/C5, g L^{-1}	C6/C5, g L^{-1}	C6/C5, g L^{-1}	C6/C5, g L^{-1}
	S. cerevisiae	38.6/4.7	25.5/16.3	44.5/3.8	35.9/12.0
	P. stipitis	37.7/3.9	29.8/15.0	48.7/3.7	36.7/11.3
t = 250 h		C6/C5, g L^{-1}	C6/C5, g L^{-1}	C6/C5, g L^{-1}	C6/C5, g L^{-1}
	S. cerevisiae	0.1/3.0	0.0/6.2	0.1/1.4	0.1/8.3
	P. stipitis	0.1/1.6	0.0/5.1	0.1/0.6	1.2/8.5

Table 4. Ethanol yields from total sugars and ethanol concentrations from differently purified spruce and birch hydrolysates after 120 h fermentation. Yields are expressed as percentage of theoretical ethanol yield: 0.51 g(EtOH) g^{-1}(monosaccharides).[3]

	Chromatographically purified		$Ca(OH)_2$ neutralized	
Yeast	Spruce	Birch	Spruce	Birch
S. cerevisiae				
Y(EtOH), %	74.3	64.7	61.3	60.5
C(EtOH), g L^{-1}	14.9	13.3	14.8	14.5
P. stipitis				
Y(EtOH), %	34,1	46.5	19.4	36.7
C(EtOH), g L^{-1}	7.1	10.4	5.1	8.8

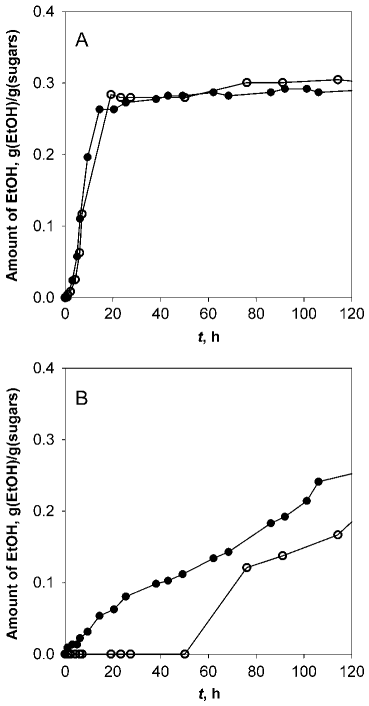

Figure 5. Ethanol production from concentrated acid birch hydrolysates with *S. cerevisiae* (A) and *P. stipitis* (B) in shake flask cultivations. For experimental conditions and symbols, see caption to Fig. 4. Concentrations are average values from two parallel experiments. Lines are presented to guide the eye.

shows hexose and pentose concentrations in the fermentation experiments at the beginning and the end (250 h from inoculum).

In the case of birch hydrolysate, *S. cerevisiae* produced ethanol similarly from chromatographically purified and $Ca(OH)_2$-neutralized hydrolysates (Fig. 5(A)). The maximum amount of ethanol was achieved in approximately 20 h. The final amount of ethanol per gram of monosaccharides was slightly higher from $Ca(OH)_2$-neutralized hydrolysate than from chromatographically purified hydrolysate (Table 4). This is due to the higher C5 monosaccharide content of the chromatographically purified hydrolysate.

The fermentation of birch hydrolysates with *P. stipitis* follows similar trends to the fermentation of spruce hydrolysate (Figs 4(B) and 5(B)). $Ca(OH)_2$ neutralization did not remove the inhibitory compounds, which resulted in lower ethanol productivity than with chromatographically purified hydrolysate.

The ethanol yield (percentage of theoretical yield, 0.51 g(EtOH) g^{-1} (monosaccharides)) and concentrations with chromatographically purified and $Ca(OH)_2$-neutralized birch hydrolysates are presented in Table 4 for *S. cerevisiae* and *P. stipitis*. With birch hydrolysate, the ethanol concentrations ranged from 8.8 g L^{-1} to 14.8 g L^{-1}. As in the case of spruce hydrolysate, chromatographic purification results in higher ethanol yield (Table 4). The ethanol yield from the total process with *S. cerevisiae* fermented chromatographically purified (final pH adjustment with $Ca(OH)_2$) birch hydrolysate was 16.1%.

When comparing the two wood species, it is observed that the spruce hydrolysate gives higher ethanol yield than the birch hydrolysate because of the higher hexose concentration in the former (Table 3).

Although the ethanol productivities with chromatographically purified hydrolysates and $Ca(OH)_2$-neutralized hydrolysates are similar when using *S. cerevisiae*, chromatographic separation has certain advantages. The most significant is that chromatographic purification increases the ethanol yield. This is because most of the inhibitory compounds can be removed from the hydrolysates. Chromatographic purification of the hydrolysates also decreases considerably the total chemical consumption of the lignocellulosic bioethanol manufacturing process when compared with $Ca(OH)_2$ neutralization. This is because the hydrolysis acid can be recycled. Moreover, $Ca(OH)_2$ neutralization produces a significant amount of solid waste (gypsum).

CONCLUSIONS

The feasibility of lignocellulosic bioethanol production using concentrated acid hydrolysis was studied experimentally using authentic hydrolysates. Two wood species, spruce and birch, were used as raw materials. The hydrolysates were purified chromatographically or neutralized with $Ca(OH)_2$ prior to fermentation of the monosaccharides to ethanol.

Both raw materials were effectively hydrolysed in the concentrated acid hydrolysis. Approximately 70% yield was obtained for the monosaccharides from both spruce and birch. Only small amounts of harmful by-products were formed in the hydrolysis. The only by-products detected were acetic acid, hydroxymethyl furfural, and furfural.

Chromatographic separation provided considerable increase in the purity of hydrolysates in a single process step. More than 90% of the sulfuric acid in the hydrolysates was removed. The monosaccharide purity increased from 20% to 80%, but the yield in the separation was relatively low (approximately 70%).

Fermentation of the chromatographically purified and $Ca(OH)_2$-neutralized hydrolysates was investigated with two different yeast strains: *Saccharomyces cerevisiae,* which was genetically modified to utilize xylose, and natural xylose-utilizing *Pichia stipitis*. *S. cerevisiae* produced higher amounts of ethanol at a higher rate than *P. stipitis*. In all cases, higher ethanol yields were obtained with chromatographically purified hydrolysates than with $Ca(OH)_2$-neutralized hydrolysates. This is because simple neutralization

does not remove acetic acid and other inhibitory compounds but chromatographic treatment does. The difference was largest with *P. stipitis*, which is more sensitive to inhibitors.

Chromatographic separation was shown to be a good option for the purification of biomass hydrolysates. High purity with respect to fermentation inhibitors is obtained, and the hydrolysis acid can be removed and recycled back to the hydrolysis step. This decreases the total chemical consumption of a lignocellulosic bioethanol process considerably, if the concentrated acid hydrolysis route is chosen for the production of ethanol.

ACKNOWLEDGEMENTS

Financial support from the Academy of Finland (Grants SA/121280 and SA/123376) is gratefully acknowledged. J.H. thanks the Graduate School in Chemical Engineering (Finland) for personal grants.

REFERENCES

1 Galbe M and Zacchi G, A review of the production of ethanol from softwood. *Appl Microbiol Biotechnol* **59**:618–628 (2002).
2 Hamelinck CN, van Hooijdonk G and Faaij APC, Ethanol from lignocellulosic biomass: techno-economic performance as development progresses. November 2003; https://www.senternovem.nl/mmfiles/149043_tcm24-280055.pdf [accessed 23 June 2011].
3 Taherzadeh MJ and Karimi K, Bioethanol: market and production processes, in *Biofuels Refining and Performance*, ed by Nag A. McGraw-Hill, Fairfield, USA, pp 69–106 (2008).
4 Larsson S, Palmqvist E, Hahn-Hägerdahl B, Tengborg C, Stenberg K, Zacchi G, *et al*, The generation of fermentation inhibitors during dilute acid hydrolysis of softwood. *Enzyme Microb Technol* **24**:151–159 (1999).
5 Delgenes JP, Moletta R and Navarro JM, Effect of lignocellulose degradation products on ethanol fermentations of glucose and xylose by *Saccharomyces cerevisiae, Zymomonas mobilis, Pichia stipitis*, and *Candida shehatae*. *Enzyme Microb Technol* **19**:220–225 (1996).
6 Xie Y, Phelps D, Lee C-H, Sedlak M, Ho N and Wang N-HL, Comparison of two adsorbents for sugar recovery from biomass hydrolysate. *Ind Eng Chem Res* **44**:6816–6823 (2005).
7 Chandel AK, Rajeev KK, Singh A and Kuhad RC, Detoxification of sugarcane bagasse hydrolysate improves ethanol production by *Candida shehatae* NCIM 3501. *Bioresource Technol* **98**:1947–1950 (2007).
8 Mussatto SI and Roberto IC, Alternatives for detoxification of diluted-acid lignocellulosic hydrolyzates for use in fermentative processes: a review. *Bioresource Technol* **93**:1–10 (2004).
9 Olsson L and Hahn-Hägerdahl B, Fermentation of lignocellulosic hydrolysates for ethanol production. *Enzyme Microb Technol* **18**:312–331 (1996).
10 Roberto IC, Lacis LS, Barbosa MFS and de Mancilha IM, Utilization of sugar cane bagasse hemicellulosic hydrolysate by *Pichia stipitis* for the production of ethanol. *Process Biochem* **26**:15–21 (1991).
11 Nilvebrant N-O, Reimann A, Larsson S and Jönsson LJ, Detoxification of lignocellulose hydrolysates with ion-exchange resins. *Appl Biochem Biotechnol* **91–93**:35–49 (2001).
12 Farone WA and Cuzens JE, Method of producing sugars using strong acid hydrolysis of cellulosic and hemicellulosic materials. US Patent No. 5562777, March 26, 1993.
13 Farone WA and Cuzens JE, Strong acid hydrolysis of cellulosic and hemicellulosic materials. US Patent No. 5597714, June 7, 1995.
14 Palmqvist E and Hahn-Hägerdahl B, Fermentation of lignocellulosic hydrolysates. I: Inhibition and detoxification. *Bioresource Technol* **74**:17–24 (2000).
15 Clausen EC and Gaddy JL, Concentrated sulfuric acid process for converting lignocellulosic materials to sugars. US Patent No. 5188673, October 12, 1988.
16 Hoshino C, Yamada T, Taneda D, Nagata Y, Fujii T, Mase T, *et al*, Method for producing monosaccharides from biomass and monosaccharide production device. US Patent No. 0148750, June 28, 2007.
17 Sims R, Taylor M, Saddler J and Mabee W, From 1st- to 2nd-generation biofuel technologies – An overview of current industry and RD&D activities, November 2008; http://www.iea.org/papers/2008/2nd_Biofuel_Gen.pdf [accessed 23 June 2011].
18 Carrez D, Biofuels in Europe – Europabio position and specific recommendations, June 2007; http://www.europabio.org/positions/Biofuels_EuropaBio%20position_Final.pdf [accessed 23 June 2011].
19 Palmqvist E and Hahn-Hägerdahl B, Fermentation of lignocellulosic hydrolysates. II: inhibitors and mechanisms of inhibition. *Bioresource Technol* **74**:25–33 (2000).
20 Heinonen J and Sainio T, Chromatographic recovery of monosaccharides for the production of bioethanol from wood. *Ind Eng Chem Res* **49**:3713–3729 (2010).
21 Sprinfield RM and Hester RD, Continuous ion-exclusion chromatography system for acid/sugar separation. *Separ Sci Technol* **34**:1217–1241 (1999).
22 Neuman RP, Rudge SR and Ladisch MR, Sulfuric acid–sugar separation by ion exclusion. *React Polym* **5**:55–61 (1987).
23 Laatikainen M, Heinonen J and Sainio T, Modeling of chromatographic separation of concentrated-acid hydrolysates. *Sep Purif Technol* **80**:610–619 (2011).
24 Turku I, Heinonen J and Sainio T, Adsorptive removal of fermentation inhibitors from concentrated acid hydrolysates of lignocellulosic biomass. *Bioresource Technol* **102**:6048–6057 (2011).
25 Du L, Li S and Zhao H, Discovery and characterization of novel D-xylose-specific transporters from *Neurospora crassa* and *Pichia stipitis*. *Mol BioSyst* **6**:1–7 (2010).
26 Ladisch M and Svarczkopf J, Ethanol production and the cost of fermentable sugars from biomass. *Bioresource Technol* **36**:83–95 (1991).
27 Matsushika A, Inoue H, Murakami K, Takimuru O and Sawayama S, Bioethanol production performance of five recombinant strains of laboratory and industrial xylose-fermenting Saccharomyces cerevisiae. *Bioresource Technol* **100**:2392–2398 (2009).
28 Palmqvist E, Grage H, Meinander NQ and Hahn-Hägerdahl B, Main and interaction effects of acetic acid, furfural, and *p*-hydroxybenzoic acid on growth and ethanol productivity of yeasts. *Biotechnol Bioeng* **63**:46–55 (1999).
29 Wankat PC, *Rate-controlled Separations*. Elsevier Science Publishers, Essex (1990).

PAPER III

Research Article

Received: 1 July 2011 Revised: 14 December 2011 Accepted: 8 March 2012 Published online in Wiley Online Library: 10 May 2012

(wileyonlinelibrary.com) DOI 10.1002/jctb.3816

Modelling and performance evaluation of chromatographic monosaccharide recovery from concentrated acid lignocellulosic hydrolysates

Jari Heinonen and Tuomo Sainio*

Abstract

BACKGROUND: Chromatographic fractionation of concentrated acid lignocellulosic hydrolysates was investigated. The goal was to present a model that can be used in designing and performance evaluation of the fractionation process. Simple models were fitted to the experimental sorption data of the main components of the hydrolysates (sulfuric acid, monosaccharides, and acetic acid) on CS16GC resin. A column model which takes into account resin shrinking was derived.

RESULTS: Simulation results were found to be in good agreement with the experimental results. The isotherm models predicted correctly the co-operative effect of H_2SO_4 on the sorption of the other adsorbates. The effect of column loading on the productivity of the separation process was studied with simulations. With 20 wt% H_2SO_4, the highest productivity was obtained with 11.5 vol% column loading. In addition, a process consisting of concentrated acid lignocellulose hydrolysis, batchwise chromatographic separation, and H_2SO_4 recycling was investigated. With the recycling, the maximum productivity was obtained with 18.2 vol% column loading.

CONCLUSIONS: It was demonstrated that the entire reactor-separation process with internal recycling must be considered when evaluating the performance of the monosaccharide-acid separation step. Process performance was found to decrease with increasing feed concentration of sulfuric acid.

Keywords: chromatographic separation; lignocellulosic hydrolysate; electrolyte exclusion; salting out; focusing effect; resin swelling; process performance

NOTATION

A_{col}	column cross-sectional area, m^2
C_i	liquid phase concentration, mol L^{-1}
$D_{ax,i}$	axial dispersion coefficient, m^2 s^{-1}
D_i^P	pore diffusion coefficient, m^2 s^{-1}
d_{col}	column diameter, cm
d_p	particle diameter, m
EC	eluent consumption, L mol^{-1}
h_{col}	resin bed/column height, cm
$k_{m,i}$	intraparticle mass transfer coefficient, s^{-1}
N	number of components
n	molar amount, mol
Pr_{sugar}	productivity of the separation process with respect to the monosaccharides, mol (m^{-3} h^{-1})
q_i	solid phase concentration, mol L^{-1}
q_i^*	solid phase concentration at equilibrium with liquid phase concentration C_i, mol L^{-1}
$\overline{q}_i$	average solid phase concentration, mol L^{-1}
T	temperature, °C
t	time, s
t_{cycle}	cycle time, h
u	superficial flow rate, cm min^{-1}
V	volume, mL
V_m	molar volume, L mol^{-1}
V_{bed}	resin bed volume, mL
V^{feed}	feed (injection) volume, mL
$\dot{V}$	volumetric flow rate, mL min^{-1}
Y_{sugar}	monosaccharide yield in the monosaccharide fraction, -
Y_{H2SO4}	sulfuric acid yield in the sulfuric acid fraction, -
z	spatial coordinate, m

Greek letters

α, β, γ	positive constants
ε	resin bed porosity, -
θ	extent of resin shrinking, -
ψ_p	volume fraction of polymer, -

* *Correspondence to: Tuomo Sainio, Lappeenranta University of Technology, Laboratory of Industrial Chemistry, Skinnarilankatu 34, FIN-53850 Lappeenranta, Finland. E-mail: tuomo.sainio@lut.fi*

Lappeenranta University of Technology, Laboratory of Industrial Chemistry, Skinnarilankatu 34, FIN-53850 Lappeenranta, Finland

Subscripts and superscripts

acid	in acid
ax	axial
col	column cross-section
bed	resin bed
feed	feed value
i, j, k	component
in	at column inlet
m	mass transfer
P	pore
p	polymer matrix or particle
ref	reference state
sugar	all monosaccharides
water	in water

INTRODUCTION

Lignocellulosic biomasses, e.g. wood, straw, and reed canary grass, can be used as raw materials to manufacture biofuels such as lignocellulosic bioethanol. This can be used as a mixture with gasoline or as pure in modern internal combustion engines with or without modifications to the engine.[1] Addition of ethanol into gasoline increases octane number and lowers CO_2, VOC, and particulate emissions of the engines.[1] Bioethanol can also be used for the manufacturing of chemicals such as acetic acid, acetaldehyde, ethylene, butadiene and hydrogen.[2,3]

Unlike the manufacturing of bioethanol from plants containing sucrose (e.g. sugarcane), the manufacturing process of lignocellulosic bioethanol consists of many unit operations. This is because the lignocellulosic raw materials contain, instead of directly fermentable monosaccharides (glucose, xylose, etc.), polysaccharides (cellulose and hemicelluloses) that must be hydrolysed to monosaccharides before the fermentation to ethanol can occur.[1,4]

One possible route to manufacture lignocellulosic bioethanol is via concentrated acid hydrolysis, in which concentrated sulfuric acid is used to catalyze the breakdown of the polysaccharide chains.[1,2,4,5] High monosaccharide yield, 80% or even higher, can be achieved. In addition, only small amounts of by-products are formed.[5–8] The disadvantages of concentrated acid hydrolysis are corrosion problems and high hydrolysis acid consumption. The hydrolysis acid must be removed before fermentation. This is traditionally done by neutralization with lime ($Ca(OH)_2$) which increases the costs of the process considerably. In addition, large amounts of $CaSO_4$ are generated[4–7] and the ethanol yield obtained in the fermentation is relatively low.[9] In order to make the concentrated acid process economically viable, the hydrolysis acid must be recycled. This can be done by using chromatography.[6,7,10–13] With chromatography using strong acid cation exchange resins, the monosaccharides in the hydrolysates can be separated from sulfuric acid and by-products formed during the hydrolysis (mainly acetic acid, hydroxymethyl furfural, and furfural). Although this can be accomplished in one step, it would be more economical to remove the by-products in an additional adsorption step prior to the chromatographic monosaccharide–acid separation.[10,14] After the purification, the monosaccharides are fermented into ethanol and concentrated to fuel grade (≥99.9%). The monosaccharides can also be used to produce other chemicals and biofuels, such as biobutanol.[15,16]

Chromatographic monosaccharide recovery from concentrated acid hydrolysates has not been widely investigated according to the academic literature. Heinonen and Sainio[10] made an experimental study, in which they compared three strong acid PS–DVB resins for the fractionation of concentrated acid hydrolysates. Heinonen *et al.*[13] demonstrated that chromatographically purified concentrated acid spruce and birch hydrolysates are readily fermentable to ethanol. Laatikainen *et al.*[17] presented a thermodynamic model that accurately describes the phase equilibrium phenomena as well as column dynamics in the purification of concentrated acid hydrolysates of lignocelluloses. Such a rigorous model employing liquid and solid phase mixing models as well as swelling pressure and electrostatic interaction contributions is not well suited to process design and optimization.

Few patents have been applied regarding the recovery of monosaccharides from concentrated acid hydrolysates: Farone and Cuzens[6,7] have investigated the recovery of monosaccharides (23.0 wt%) from concentrated acid hydrolysate (33.6 wt% H_2SO_4) using Finex CS16 strong cation exchange resin.

The goal of this study is to present a model that can be used in process design of chromatographic monosaccharide recovery from concentrated acid hydrolysates. A crucial part of the model is the adsorption isotherms of the components in the system. Simple empirical isotherm models were fitted to the experimental sorption data obtained in this study and in our previous study.[17] A dynamic model for the chromatographic column that takes into account resin shrinking is also presented. The model is then used to study the performance of the batchwise chromatographic monosaccharide recovery process. In practice, the sulfuric acid fraction collected in the chromatographic separation step is recycled back to the hydrolysis reactor. Since the recycled fraction contains also monosaccharides, the performance evaluation of the separation step should be based on investigation of the complete concentrated acid hydrolysis and monosaccharide recovery process. This often neglected aspect is included in this study.

EXPERIMENTAL

Materials and methods

Gel type strong acid polystyrene–divinylbenzene (PS–DVB) type cation exchange resin CS16GC (Finex Oy, Finland) with 8 wt% cross-linking (DVB content) was used as an adsorbent. The resin was converted to hydrogen form with 1 mol L^{-1} hydrochloric acid (37%, pro analysi, Merck KGaA) using standard methods. The volumetric capacity of the resin in hydrogen form was 1.93 mequiv L^{-1}, and average particle size was 246 μm.

Pro analysis grade sulfuric acid (95–97%, pro analysi, Merck KGaA), α-D-glucose (≥99.5% (GC), Sigma-Aldrich Co.), D-(+)-xylose (min. 99%, Sigma-Aldrich Co.), acetic acid (100%, pro analysi, Merck KGaA), and purified and degassed water were used in the experiments.

Experimental setup for the column experiments consisted of two HPLC pumps for eluent and feed (515 series pumps, Waters), an eluent degasser unit (Degassex DG-4400, Phenomenex), a chromatographic column (ECO SR 25/200, Kronlab) with 25 mm inner diameter and water heating jacket, a water circulation thermostat for column heating (C6CS, Lauda), an on-line conductivity detector (Conductivity monitor, Pharmacia Biotech), an on-line RI-detector (RI-2000F, Schambeck), an on-line UV-detector (2487 Dual λ Absorbance Detector with 3 mm semi-prep flow cell, Waters), automatic valves (seven port motor valve MV-7 and solenoid valve PSV-50, Pharmacia), and a fraction collector (LKB FRAC-100, Pharmacia). The sampling interval used in the experiments was 30 s. All valves in the system were controlled

with, and all on-line data collected with LabView program (version 8.2, National Instruments).

Adsorption isotherm measurements

The determination of the adsorption isotherms of the main components of concentrated acid lignocellulosic hydrolysates (sulfuric acid, monosaccharides, and acetic acid) at 50 °C temperature for CS16GC resin is presented in our previous study.[17] The isotherms were measured using pulse on a plateau (sulfuric acid), frontal analysis (acetic acid), and batch equilibrium methods (glucose and xylose). Glucose and xylose were the only monosaccharides used in this study because with CS16GC other monosaccharides in the system behave similarly as these. The Henry constants of the glucose and xylose isotherms were measured in this study by injecting small dilute pulses into the column (same experimental setup as with H_2SO_4 isotherm measurement).[17] Measurements were done in water and in H_2SO_4 solutions with concentrations corresponding to the equilibrium concentrations of sulfuric acid in the batch experiments.

Resin shrinking

The adsorbent used in this study was a gel type resin. It is a well known fact that resin swelling and shrinking due to changes in liquid phase composition can be significant with gel type resins.[18,19] Therefore, the extent of shrinking of CS16GC resin was determined experimentally. Preliminary experiments were done with each adsorbate separately at concentrations exceeding the concentration range of the actual separation experiments. Practically no shrinking of the resin was observed with other compounds than sulfuric acid (data not shown). The resin shrinking data used in this work was obtained by measuring the resin bed height in a column (initial h_{col} in pure water 20 cm) equilibrated with a H_2SO_4 solution of known concentration (from 0.25 to 4.0 mol L^{-1}).

Model validation experiments

To validate the model, dynamic column experiments with synthetic solutions were made at 50 °C. Column loadings in the experiments were 0.102, and 0.204 bed volumes. Synthetic solution containing sulfuric acid (2.22 mol L^{-1}), glucose (0.24 mol L^{-1}), xylose (0.38 mol L^{-1}), and acetic acid (0.16 mol L^{-1}) was used. Resin bed diameter was 2.5 cm and height 20 cm. The superficial velocity was 0.5 cm min^{-1} (corresponding to flowrate 2.45 mL min^{-1} with ECO SR 25/200 column). Top-down flow was used, and the eluent was purified and degassed water.

Sample analyses

Glucose, xylose and acetic acid concentrations were determined with HPLC (HP1100, Hewlett-Packard/Agilent) using Metacarb 87H column (Varian/Agilent). Potentiometric titration was used for sulfuric acid concentration measurements. For more details, see our previous study.[10]

MODELLING AND CALCULATIONS

Isotherms of the main components of concentrated acid lignocellulosic hydrolysates (H_2SO_4, glucose, xylose, and acetic acid) and resin shrinking were correlated with empirical models. A column model that can be used in the designing of chromatographic recovery of monosaccharides from lignocellulosic hydrolysates was derived.

Adsorption isotherm and resin shrinking models

Sorption of electrolytes on a strong acid cation exchange resin is affected by electrolyte exclusion. In fact, the sorbed amount of H_2SO_4 as well as the first derivative of the isotherm must be zero at infinite dilution because of complete electrolyte exclusion.[19] The simplest expression that could be used to describe the H_2SO_4 sorption accurately was;

$$q_{H2SO4} = \alpha_{H2SO4}(C_{H2SO4})^{\beta_{H2SO4}}, \quad (1)$$

where q and C are solid phase and liquid phase concentrations, respectively, and α and β are positive constants. Physical constraints (finite volume of eluent during column regeneration) require that β is larger than unity.

Glucose and xylose sorption was found to depend on sulfuric acid concentration, and the isotherms were found to be slightly concave upward type. For these reasons, the following isotherm model with linear dependency of the Henry constant on sulfuric acid concentration was used to describe glucose and xylose sorption;

$$q_k = \frac{(\alpha_k + \beta_k C_{H2SO4})C_k}{1 - \sum_{j=1}^{N} \gamma_j C_j} \quad (2)$$

where subscript k stands for glucose and xylose, γ is a positive constant, and the sum in the denominator denotes total monosaccharide concentration.

Acetic acid sorption was also found to depend on sulfuric acid concentration. A linear isotherm with the Henry constant depending on sulfuric acid concentration was used for acetic acid:

$$q_{AcOH} = (\alpha_{AcOH} + \beta_{AcOH} C_{H2SO4})C_{AcOH} \quad (3)$$

The extent of resin shrinking was related to the adsorbed amount of sulfuric acid;

$$\theta = \frac{V_{bed,acid}}{V_{bed,water}} = 1 - \frac{\alpha_\theta q_{H2SO4}}{\beta_\theta + q_{H2SO4}} \quad (4)$$

where θ is extent of resin shrinking, i.e. the ratio of resin bed volume (V_{bed}) in acid to resin bed volume in water. Equation (4) is scaled so that θ is unity in pure water, and decreases with increasing q_{H2SO4}.

Dynamic column model

A column model that takes into account resin shrinking as changing bed porosity was derived. The resin particles are assumed to be attached to a fixed two-dimensional grid.[20] When C_{H2SO4} changes the particle diameter and therefore also the void volume (bed porosity) changes.

Mass balance for component i over a small volume element of length Δz in the chromatographic column can be written as

$$\frac{\partial}{\partial t}(C_i\varepsilon)A_{col}\Delta z + \frac{\partial}{\partial t}(q_i(1-\varepsilon))A_{col}\Delta z = -\frac{\partial}{\partial z}(\dot{V}C_i)\Delta z + D_{ax,i}A_{col}\varepsilon\frac{\partial}{\partial z}\left(\varepsilon\frac{\partial C_i}{\partial z}\right)\Delta z \quad (5)$$

where ε is local bed porosity, $\dot{V}$ is volumetric flow rate, A_{col} is column cross-sectional area, D_{ax} is axial dispersion coefficient, t and z are temporal and spatial coordinates, respectively.

In principle, the volumetric flow rate is also a locally varying property according to Equation (6):

$$\frac{\partial \dot{V}}{\partial z}\Delta z = \sum_{j=1}^{N+1} V_{m,j}\frac{\partial n_j}{\partial t} \tag{6}$$

where V_m is molar volume and n is the total amount of component i in the liquid and solid phases within the volume element. Note that the summation in Equation (6) includes also the eluent (component $N+1$). Use of Equation (6) thus requires modelling also the sorption of the eluent. For the sake of simplicity, the sorption of eluent was not taken into account here, and the volumetric flow rate was assumed constant. With this assumption, applying the chain rule to Equation (5) yields the final form of the column mass balance equation:

$$\frac{\partial C_i}{\partial t} = -\frac{\dot{V}}{\varepsilon A_{col}}\frac{\partial C_i}{\partial z} + \frac{q_i - C_i}{\varepsilon}\frac{\partial \varepsilon}{\partial t} - \frac{1-\varepsilon}{\varepsilon}\frac{\partial q_i}{\partial t} + \frac{D_{ax,i}}{\varepsilon}\frac{\partial}{\partial z}\left(\varepsilon\frac{\partial C_i}{\partial z}\right) \tag{7}$$

The second term on the right-hand side of Equation (7) takes into account the influence of changing phase ratio on the liquid phase concentration.

Danckwert's boundary conditions were used at the column inlet and outlet:

$$\frac{\partial C_i}{\partial z} = \frac{\dot{V}}{A_{col}\varepsilon}\frac{(C_i^{in} - C_i)}{D_{ax,i}}, z = 0 \tag{8}$$

$$\frac{\partial C_i}{\partial z} = 0, z = h_{col} \tag{9}$$

where C_i^{in} is the concentration at the column inlet and h_{col} is the column height. Resin bed porosity ε was calculated from

$$\varepsilon = 1 - \theta(1 - \varepsilon_{ref}) \tag{10}$$

where ε_{ref} is bed porosity in reference state, which was in this case a column equilibrated with pure water. The rate of bed porosity change is obtained through differentiation of Equation (10) with respect to time:

$$\frac{\partial \varepsilon}{\partial t} = -\frac{\partial \theta}{\partial t}(1 - \varepsilon_{ref}) \tag{11}$$

from which, using the chain rule and Equation (4), an equation for the rate of bed porosity change depending on the rate of sulfuric acid sorption is obtained:

$$\frac{\partial \varepsilon}{\partial t} = \frac{\alpha_\theta \beta_\theta}{(\beta_\theta + q_{H2SO4})^2}\frac{\partial q_{H2SO4}}{\partial t}(1 - \varepsilon_{ref}) \tag{12}$$

By relating the extent of resin shrinking to the adsorbed amount of sulfuric acid, the effect of adsorption kinetics on the shrinking is also taken into account.

The solid film linear driving force model was used to describe mass transfer between the phases:

$$\frac{\partial \bar{q}_i}{\partial t} = k_{m,i}(q_i^* - \bar{q}_i) + \frac{\bar{q}_i}{1-\varepsilon}\frac{\partial \varepsilon}{\partial t} \tag{13}$$

where $k_{m,i}$ is intraparticle mass transfer coefficient, q_i^* is solid phase concentration of i at equilibrium with liquid phase concentration C_i, and $\bar{q}_i$ is average solid phase concentration of i. The second term on the right in Equation (13) originates from a change in the phase ratio due to resin shrinking.

The intraparticle mass transfer coefficient was calculated from

$$k_{m,i} = \frac{60 D_i^P}{d_p^2} \tag{14}$$

where D_i^P is diffusion coefficient, which depends on resin shrinking. It was calculated from the correlation of Mackie and Meares:[17,21]

$$D_i^P = D_{i,ref}^P\left[\frac{(1-\psi_p)(1+\psi_{p,ref})}{(1+\psi_p)(1-\psi_{p,ref})}\right]^2 \tag{15}$$

where $D_{i,ref}^P$ is diffusion coefficient in the reference state, ψ_p volume fraction of the polymer, and $\psi_{p,ref}$ volume fraction of the polymer in reference state. Water swollen CS16GC was taken here as a reference state and $\psi_{p,ref} = 0.391$.[17] Particle diameter d_p can be calculated from

$$d_p = d_{p,ref}\left(\frac{1-\varepsilon}{1-\varepsilon_{ref}}\right)^{1/3} \tag{16}$$

where $d_{p,ref}$ is particle diameter in the reference state.

The method of lines[22] was used to solve the partial differential equations in Equation (7). The diffusion coefficients in reference state in Equation (15) and the axial dispersion coefficients (same value for all components) in Equation (7) were estimated by fitting the simulated elution profiles to the experimentally obtained profiles.

Evaluation of process performance

Stand-alone chromatographic separation

Process performance of the batchwise chromatographic recovery of monosaccharides from lignocellulosic hydrolysates was investigated with simulations. In order to elucidate the effect of hydrolysis acid concentration on process performance, the feed composition was varied as follows: 10 wt% (1.087 mol L^{-1}), 20 wt% (2.324 mol L^{-1}), or 30 wt% (3.729 mol L^{-1}) sulfuric acid together with 0.3 mol L^{-1} of glucose, 0.3 mol L^{-1} of xylose, and 0.16 mol L^{-1} of acetic acid. Same column and flow parameters were used as in the model validation (see section Experimental).

The effect of column loading on the productivity of the separation process with respect to the monosaccharides was studied using the constraints given below. Also, the monosaccharide and H_2SO_4 yields in their target fractions, eluent consumption, and average sulfuric acid and monosaccharide concentrations in their target fractions were investigated.

The monosaccharides elute as a middle fraction between H_2SO_4 and acetic acid, and the cut points for the fractionation were chosen as follows. The first cut point (beginning of the H_2SO_4 fraction) was set to the point of sulfuric acid breakthrough. The second cut point (beginning of the monosaccharide fraction) was defined so that $n_{sugar}/n_{H2SO4} \geq 8$ in the monosaccharide fraction while maximizing the productivity. In this way, the n_{sugar}/n_{H2SO4} obtained was always close to 8. The monosaccharide yield was not set as a constraint for the cut points. This is because most of the monosaccharides that are not collected in the monosaccharide fraction are collected in the H_2SO_4 fraction, which is recycled back to the lignocellulose hydrolysis reactor. Therefore, these monosaccharides are not lost product.

The third cut point (end of the monosaccharide fraction) was chosen by defining the maximum allowed acetic acid concentration in the monosaccharide fraction to be 0.4 g L^{-1} (6.7 mmol L^{-1}). For this reason, a small portion of the monosaccharides are collected in the acetic acid fraction and are regarded as lost product. End of the acetic acid fraction (fourth cut point) was set to the point where acetic acid concentration decreases below 0.01 g L^{-1} (0.2 mmol L^{-1}). The cycle time was defined as the difference between first and fourth cut points.

The productivity of the separation process with respect to the monosaccharides (Pr_{sugar}) was calculated from

$$Pr_{sugar} = \frac{Y_{sugar} C_{sugar}^{feed} V^{feed}}{V_{bed} t_{cycle}} \quad (17)$$

where Y_{sugar} is monosaccharide yield, C_{sugar}^{feed} is monosaccharide concentration in the feed, V^{feed} is feed (injection) volume, and t_{cycle} is cycle time. Eluent consumption was calculated from

$$EC = \frac{t_{cycle}\dot{V} - V^{feed}}{Y_{sugar} C_{sugar}^{feed} V^{feed}}. \quad (18)$$

Chromatographic separation coupled with biomass hydrolysis and recycling of sulfuric acid

In order to obtain a more realistic picture of the performance of the chromatographic separation step, a hypothetical process consisting of concentrated acid hydrolysis, chromatographic monosaccharide recovery, and H_2SO_4 concentration and recycling was also investigated with simulations. Figure 1 shows the streams and the unit operations of the system.

The concentrated acid hydrolysis is conducted in two steps.[6,7,23] First, the wood chips are treated with 70 wt% H_2SO_4 (pretreatment) after which the acid is diluted to 20 wt% and the actual hydrolysis is done. After the hydrolysis, the hydrolysate is separated from the remaining solids by filtration and then taken to the chromatographic separation. In this step, the hydrolysate is separated into three fractions: H_2SO_4, monosaccharide, and acetic acid fractions. The monosaccharide and acetic acid fractions are taken to downstream processing, but the H_2SO_4 fraction is recycled back to the hydrolysis reactor through a concentration step. H_2SO_4 is concentrated to 70 wt%[6] for example by using a multiple effect evaporator or vapor compression distillation.[6,24] Also the other components in the H_2SO_4 fraction are recycled back to the hydrolysis reactor.

The following values were used when evaluating the process performance: 1 ton of wood chips and 70 wt% sulfuric acid were mixed so that at the end of hydrolysis (after the second hydrolysis step) the wood to liquid mass ratio was 1 : 6 (same for each hydrolysis). In the second hydrolysis step, H_2SO_4 was diluted to 20 wt% concentration with water. Wood was assumed to contain 70 wt% polysaccharides (40% cellulose and 30% hemicelluloses). In the hydrolysis, polysaccharides were cleaved only into glucose (cellulose) and xylose (hemicelluloses) with 80 wt% yield.[6,7,23] In addition to the monosaccharides, acetic acid was also formed during hydrolysis in such amounts that the concentration of acetic acid after hydrolysis was 0.16 mol L^{-1} (concentration of acetic acid in concentrated acid birch hydrolysate).[10] The formation of other by-products (mainly furfural and hydroxymethyl furfural) was neglected in the calculations because their amounts are expected to be low and they can effectively be removed in a separate adsorption unit.[14] The volume of the hydrolysate was calculated

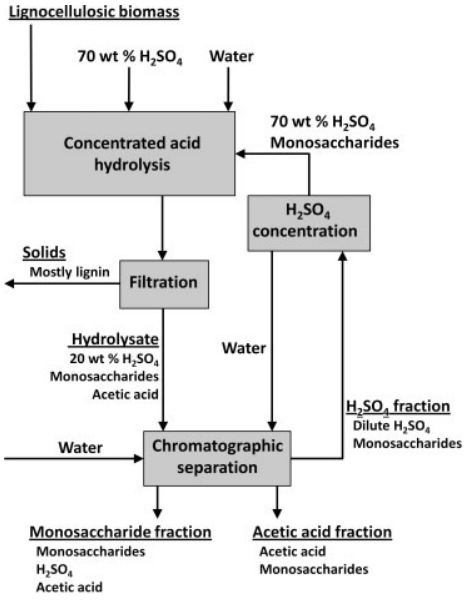

Figure 1. The streams and main unit operations of a process consisting of two-step concentrated acid hydrolysis, batchwise chromatographic separation, and concentration and recycling of sulfuric acid fraction.

with the density of 20 wt% H_2SO_4(aq). After the hydrolysis, the solids were separated from the hydrolysate with filtration, in which 6.5 vol% of the hydrolysate was lost (concentrations remained constant). The amount of hydrolysate obtained was 5000 L and remained constant throughout the process.

The chromatographic separation was done batchwise using a 4 m high column and a flow rate of 4 BV h^{-1}. Flow rate and column were chosen for demonstration purposes and were not optimized. The effect of column loading on the productivity of the separation process with respect to the monosaccharides in steady state was investigated. The changes in the performance of the chromatographic separation process upon reaching steady state were evaluated with the loading giving the maximum Pr_{sugar}. The cut points for the separation process were defined in the same manner as in the investigation of the stand-alone chromatographic separation.

RESULTS AND DISCUSSION

Adsorption isotherms and resin shrinking

Empirical isotherm models were fitted to the adsorption isotherms of sulfuric acid, glucose, xylose, and acetic acid on a gel type CS16GC resin in hydrogen form at 50 °C temperature (sorption data obtained in this and in our previous study).[17] The experimental results with the corresponding isotherm models (Equations (1)–(3)) are shown in Figs 2–4. Resin shrinking due to sulfuric acid was also measured, and an empirical model (Equation (4)) was used to correlate the data (Fig. 2(B)). The parameters used for the isotherm and resin shrinking models are given in Table 1.

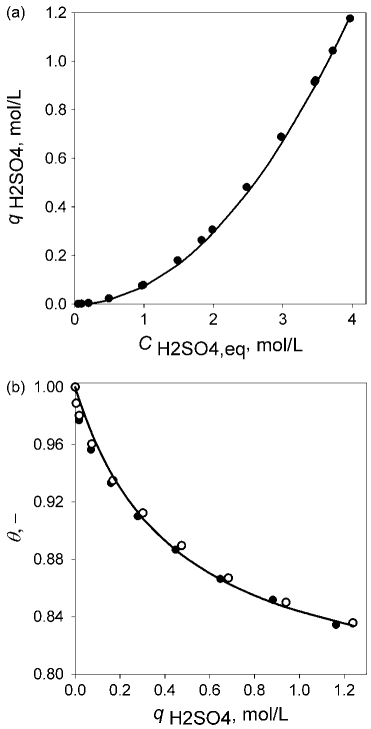

Figure 2. (A) Sorption of sulfuric acid from water on CS16GC resin. Experimental details: pulse on a plateau method, $u = 0.2$ cm min^{-1}, $d_{col} = 2.5$ cm, $h_{col} = 20$ cm, top-down flow, and $T = 50\,^{\circ}$C. Line is the isotherm model fit (Equation (1)). (B) Effect of q_{H2SO4} on the shrinking of CS16GC resin. Results from two independent experiments are presented (filled and open symbols). Experimental details: equilibrium measurements in a column, $T = 50\,^{\circ}$C, h_{col} in pure water $= 20$ cm, $d_{col} = 2.5$ cm. Line is the model fit (Equation (4)). Model parameters are given in Table 1.

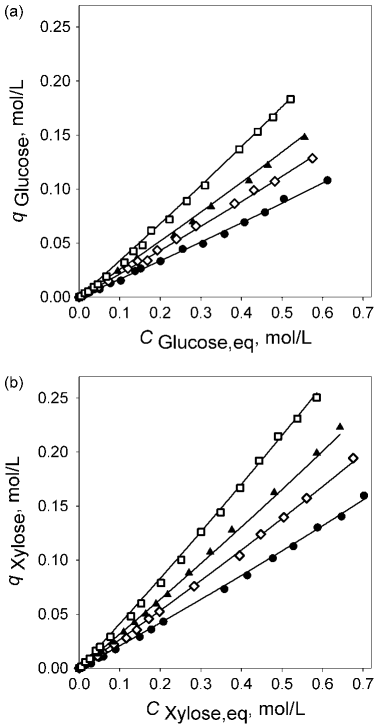

Figure 3. Sorption of glucose (A) and xylose (B) from water and from various sulfuric acid solutions on CS16GC resin. Experimental details: batch method, $m_{resin} = 5$ g, $V_{solution} = 7$ mL, $T = 50\,^{\circ}$C. Symbols: (●) water, (◊) 0.97 mol L^{-1} H_2SO_4, (▲) 1.84 mol L^{-1} H_2SO_4, and (□) 3.46 mol L^{-1} H_2SO_4. Lines are the model fits (Equation (2)). Model parameters are given in Table 1.

The sulfuric acid isotherm is clearly concave upward (Fig. 2(A)). The Henry constant of the isotherm at infinite dilution is zero: electrolyte exclusion is strong enough to prevent all HSO_4^- and SO_4^{2-} ions from entering the pores of the resin. Because the anions cannot enter the resin pores, H_2SO_4 is completely excluded from the resin at infinite dilution due to electroneutrality condition.

As the H_2SO_4 concentration increases, the effect of electrolyte exclusion on H_2SO_4 sorption diminishes and eventually vanishes. Due to this, the shape of the sulfuric acid isotherm approaches linear at high concentrations (Fig. 2(A)). The fit of the isotherm model Equation (1) to the experimental H_2SO_4 sorption data is good and it predicts correctly the Henry constant of the isotherm at infinite dilution.

The effect of sulfuric acid concentration on the shrinking of CS16GC is significant (Fig. 2(B)): at the last experimental point ($C_{H2SO4} \approx 4$ mol L^{-1}) the volume of the resin is approximately 16 vol% smaller than in pure water. Obviously, such a large volume change must be taken into account both in modelling and interpretation of the experimental sorption equilibrium data. If it was neglected when analysing the raw data from the phase equilibrium measurements, the sorption of glucose and xylose from sulfuric acid solutions would be up to twice that in reality (data not shown). In addition, excluding the resin shrinking from the dynamic column model would lead to erroneous elution profiles (not shown). Errors in the elution of H_2SO_4 would directly lead to errors in the elution of the other adsorbates because their sorption depends on the concentration of H_2SO_4. As observed in Fig. 2(B), the shrinking of the resin due to H_2SO_4 is well described by Equation (4).

The sorption isotherms of glucose and xylose on CS16GC are shown in Fig. 3. The isotherms of the monosaccharides are only slightly concave upward and sulfuric acid has a significant effect on the sorption of these neutral components (Fig. 3). For both monosaccharides, the sorption on CS16GC resin is almost doubled when water is changed to 3.5 mol L^{-1} H_2SO_4. For glucose, this kind of behavior has also been observed earlier.[12] The co-operative effect of sulfuric acid on monosaccharide sorption is due to an effect similar to salting out. This can be explained as follows: in an aqueous solution of an electrolyte (e.g. sulfuric acid), the water molecules are organized with the electrolyte in an energetic way. Addition of neutral components (e.g. monosaccharides) to the water–electrolyte system disturbs this organization and leads to an increase in the total energy of the system. The total energy of the system is decreased if the neutral molecules are 'salted out' from the liquid phase. Therefore, in the presence of H_2SO_4,

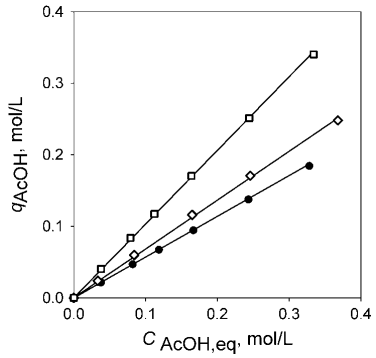

Figure 4. Sorption of acetic acid from water and from various sulfuric acid solutions on CS16GC resin. Experimental details: frontal analysis method, see caption of Fig. 2 (A) for other details. Symbols: (●) water, (◊) 0.96 mol L^{-1} H_2SO_4, and (□) 3.92 mol L^{-1} H_2SO_4. Lines are the model fits (Equation (3)). Model parameters are given in Table 1.

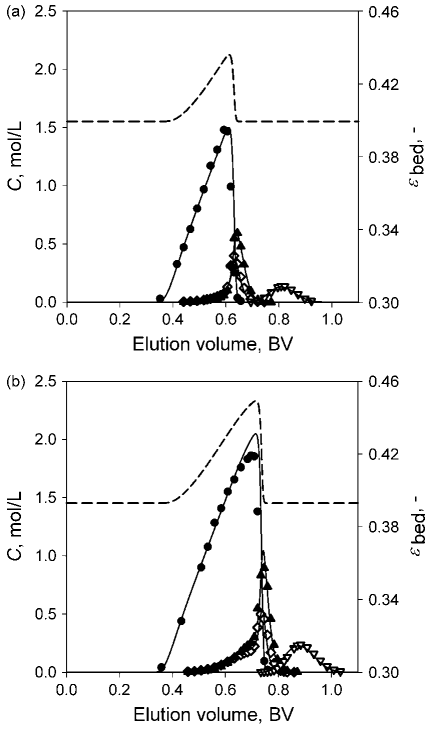

Figure 5. Elution profiles of 0.101 BV (A) and 0.204 BV (B) pulses of synthetic hydrolysate solution with CS16GC resin. Feed composition: 2.22 mol L^{-1} sulfuric acid, 0.24 mol L^{-1} glucose, 0.38 mol L^{-1} xylose, and 0.16 mol L^{-1} acetic acid. Experimental details: $T = 50\ ^{\circ}C$, $u = 0.5$ cm min^{-1}, $\varepsilon = 0.395$, for other details see caption of Fig. 2(A). Symbols: sulfuric acid (●), glucose (◊), xylose (▲), and acetic acid (▽). Lines are the simulation results; dashed line is the simulated ε. Model parameters are given in Table 1.

the monosaccharides are salted out to the resin phase and their sorption increases.

The monosaccharide isotherms were fitted with concave upward isotherm model Equation (2) which takes into account the influence of sulfuric acid on the monosaccharide sorption. The fit of the model to the experimental data is good with both monosaccharides (Fig. 3). The linear dependency of the Henry constant on H_2SO_4 concentration in Equation (2) adequately describes the co-operative effect of sulfuric acid on monosaccharide sorption.

The sorption isotherm of acetic acid is shown together with the model fit in Fig. 4. Also in the case of acetic acid sorption, a co-operative effect of H_2SO_4 due to salting out can be seen clearly. The sorption is doubled in 4 mol L^{-1} H_2SO_4 compared with pure water (Fig. 4). The fit of the linear isotherm model Equation (3) to the experimental data is good, and the linear dependency of the Henry constant on sulfuric acid concentration is adequate (Fig. 4).

Model validation

The column model presented in this study, including the empirical isotherm and resin shrinking models (see section Modelling and calculations), was validated with pulse injection experiments using synthetic hydrolysate solutions.

Two experimental elution profiles obtained with 0.101 BV and 0.204 BV pulses are shown in Fig. 5 with the model predictions. The values of diffusion coefficients, and axial dispersion coefficients are given in Table 1.

The simulation results are in good accordance with the experimental data (Fig. 5). The modelling of resin shrinking as changing resin bed porosity describes adequately the effects of resin shrinking on the elution profiles. In reality, a gap forms between the upper end of the resin bed and the upper adapter due to resin shrinking. This could be described by using mass coordinates instead of axial coordinates,[25] but was found to be not necessary in this case.

The breakthrough of sulfuric acid occurs approximately at column void volume due to complete electrolyte exclusion (Fig. 5). The concave upward shape of the sulfuric acid isotherm can clearly be seen from the diffuse front and from the shock layer at the back of the sulfuric acid profile (Fig. 5). The model predicts quite accurately the breakthrough of sulfuric acid, and also the other parts of the sulfuric acid outlet profile (Fig. 5). A slight difference

Table 1. Model parameters used in the simulations. $D_{ax} = 6 \times 10^{-8}$ m^2 s^{-1} for all components

	H_2SO_4	Glucose	Xylose	Acetic acid	Swelling
α	0.072	0.164	0.205	0.57	0.226
β	2.03	4.854×10^{-2}	5.812×10^{-2}	0.117	0.442
γ	–	0.114	0.114	–	–
D^P, m^2 s^{-1}	3.0×10^{-10}	1.5×10^{-10}	1.5×10^{-10}	4.0×10^{-10}	–

between the experimental and calculated results can be seen towards the end of the H_2SO_4 profile. This is because the points represent the average concentrations at certain sampling interval.

Figure 5 also shows the calculated change in resin bed porosity. The profile of resin bed porosity is similar to the profile of sulfuric acid since it is linked to the sorption of sulfuric acid.

The monosaccharides elute between sulfuric acid and acetic acid (Fig. 5). The outlet profiles of the monosaccharides are elongated due to the salting out effect: sulfuric acid slows down the propagation of the monosaccharides. The front parts of the monosaccharide profiles spread and become diffuse. The model predicts correctly the elongation of the monosaccharide profiles (Fig. 5).

Another interesting phenomenon arising from the salting out is the focusing of the monosaccharides during the elution (Fig. 5). The outlet profiles of the monosaccharides have a steep rise in concentrations at the end of the H_2SO_4 profile after the elongated front parts. This kind of focusing effect can occur when some thermodynamic variable (in this case, H_2SO_4 concentration) is changed causing a large change in sorption of the adsorbates.[26] After some separation has been achieved, the front parts of the monosaccharide profiles are still slowed down by sulfuric acid, but the rear parts of the profiles are not affected, and therefore propagate faster than the front parts. This results in focusing of the monosaccharides at the end of the H_2SO_4 profile. This is also well described by the model (Fig. 5). The focusing effect is beneficial for process efficiency, but is rarely seen in chromatography.

The focusing effect is slightly stronger for xylose than for glucose due to the slightly higher sorption of xylose (see Fig. 3). In other words, a (relatively) lower amount of xylose elutes under the H_2SO_4 profile and higher amount at the rear of the H_2SO_4 profile, when compared with glucose.

Acetic acid elutes after the monosaccharides (Fig. 5). Acetic acid is quickly separated from sulfuric acid and the effects of salting out on its profile are small and no focusing of acetic acid can be seen (Fig. 5). The acetic acid profile is also well described by the model.

Process performance

The process performance of the chromatographic separation of concentrated acid lignocellulosic hydrolysates was studied with simulations on two levels. The performance of the stand-alone batchwise chromatographic separation step was investigated using different performance parameters. However, due to the recycling of the H_2SO_4 fraction, the investigation of the sole separation step is not sufficient for the evaluation of process performance. For this reason, also the performance of a complete concentrated acid hydrolysis and monosaccharide recovery process with hydrolysis acid recycling was investigated.

Stand-alone chromatographic separation

The effects of column loading and the concentration of hydrolysis acid on the chromatographic separation were investigated with simulations using the column model presented above. The column loading was varied from 0.01 to 0.2 BV and C_{H2SO4} from 10 to 30 wt%. The effects of column loading and hydrolysis acid concentration on the productivity of the process with respect to the monosaccharides (Pr_{sugar}), the monosaccharide yield (Y_{sugar}) and the sulfuric acid yield (Y_{H2SO4}) in their target fractions, eluent consumption (*EC*), and sulfuric acid and monosaccharide concentrations in their target fractions were investigated. The results from this investigation are shown in Fig. 6.

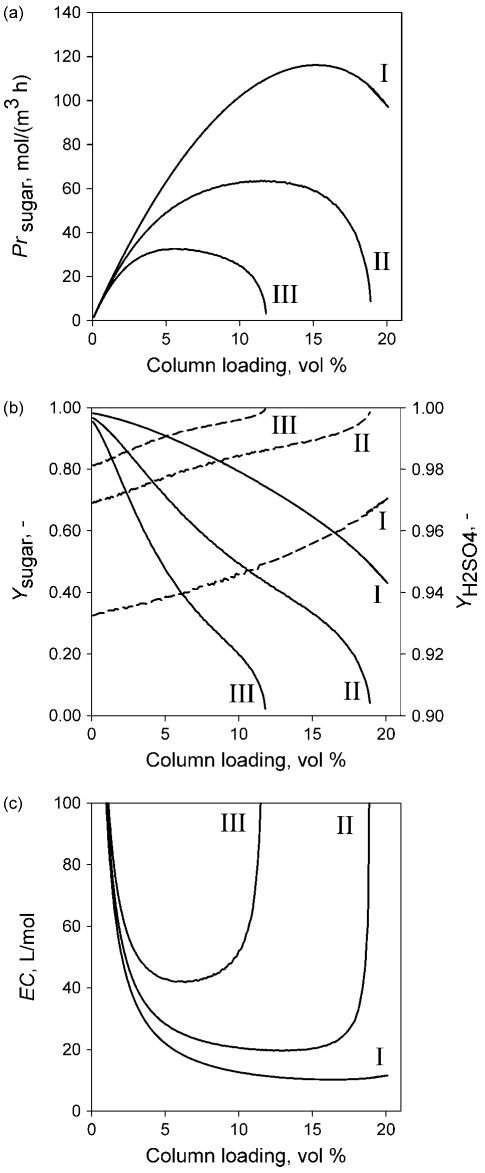

Figure 6. The effects of column loading and $C_{H2SO4,feed}$ on Pr_{sugar} (A), Y_{sugar} (solid) and Y_{H2SO4} (dashed) in their target fractions (B), and *EC* (C). Feed composition: 10 wt% (I), 20 wt% (II), or 30 wt% (III) sulfuric acid, and 0.3 mol L^{-1} glucose, 0.3 mol L^{-1} xylose, and 0.16 mol L^{-1} acetic acid. Model parameters are given in Table 1. See Figs 2(A) and 5 for column and flowrate parameters. For fractionation constraints see section Modelling and calculations.

Pr_{sugar} goes through a maximum when the column loading is increased. The loadings giving the maximum Pr_{sugar} for 10 wt%, 20 wt%, and 30 wt% hydrolysis acid concentrations were 15.1 vol%, 11.5 vol%, and 5.5 vol%, respectively (Fig. 6(A)). Pr_{sugar} is nearly independent of the column loading over a wide range of loadings around the maximum (Fig. 6(A)). For example, with 20 wt% H_2SO_4, the productivity is close to the maximum value when the column loading is between 8 and 15 vol%.

With increasing loading, the amount of monosaccharides treated during one cycle increases and so does Pr_{sugar} until a certain limit (11.5 vol% loading with 20 wt% H_2SO_4), although Y_{sugar} decreases (Fig. 6(B)). At column loadings above a certain limit (15 vol% with 20 wt% H_2SO_4) Y_{sugar} becomes so low that Pr_{sugar} begins to decrease rapidly and eventually reaches zero. With column loadings smaller than a certain limit (8 vol% with 20 wt% H_2SO_4) Pr_{sugar} is lower than the maximum value, due to small amounts of monosaccharides treated per cycle, although Y_{sugar} is higher than with the loading giving the maximum Pr_{sugar} (Fig. 6(B)).

Hydrolysis acid concentration has also a significant effect on Pr_{sugar} (Fig. 6(A)). Higher productivity of monosaccharides can be achieved with lower $C_{H2SO4,feed}$. As $C_{H2SO4,feed}$ increases, larger fraction of the monosaccharides elute under the H_2SO_4 profile and are collected in the H_2SO_4 fraction. This lowers Y_{sugar} (Fig. 6(B)) and therefore also Pr_{sugar}. In addition, the column loading giving the maximum Pr_{sugar} decreases with increasing H_2SO_4 concentration (Fig. 6(A)). Also increase in cycle time with increasing column loading and $C_{H2SO4,feed}$ has a negative effect on Pr_{sugar}, but its influence is smaller than that of the column loading and $C_{H2SO4,feed}$.

It is interesting to note that the maximum productivity is achieved at relatively low monosaccharide yield (Y_{sugar} = 64.3%, 44.5%, and 41.3% in the order of increasing H_2SO_4 concentration). Y_{sugar} decreases when column loading is increased (Fig. 6(B)) because more and more of the monosaccharides elute under the H_2SO_4 profile and are collected in the H_2SO_4 fraction.

The dependence of Y_{H2SO4} on the column loading is opposite to that of Y_{sugar} (Fig. 6(B)). With increasing column loading, the overlapping of monosaccharide and H_2SO_4 profiles increases and the second cut point has to be moved to the right so that the limiting n_{sugar}/n_{H2SO4} value in monosaccharide fraction is achieved. Y_{H2SO4} increases as a larger part of the H_2SO_4 shock layer is taken into the H_2SO_4 fraction due to the limiting n_{sugar}/n_{H2SO4}. Y_{H2SO4} with the column loading giving the maximum Pr_{sugar} is (in the order of increasing H_2SO_4 feed concentration) 95.6%, 98.6%, and 99.2%. High Y_{H2SO4} is beneficial for the process economy, because a lower amount of fresh sulfuric acid is needed for the hydrolysis of lignocellulosic biomass.

The effects of column loading and hydrolysis acid concentration on *EC* are shown in Fig. 6(C). *EC* decreases first with increasing column loading because the amount of monosaccharides collected in the monosaccharide fraction increases. However, as Y_{sugar} approaches zero, *EC* begins to increase rapidly (Fig. 6(C)). A decrease in $C_{H2SO4,feed}$ has a positive effect also on eluent consumption, due to better separation. The *EC* around the minimum value is only little affected by column loading. For this reason, with each hydrolysis acid concentration, *EC* at the column loading giving the maximum Pr_{sugar} is only a little higher than the minimum value (Fig. 6(C)).

Sulfuric acid is diluted during elution regardless of the column loading due to the thermodynamics of the system. However, this unwanted dilution decreases with decreasing $C_{H2SO4,feed}$ and increasing column loading.

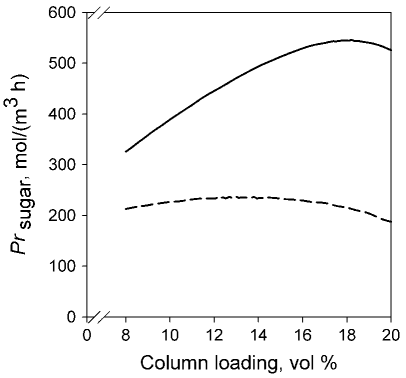

Figure 7. Pr_{sugar} in chromatographic separation in the process shown in Fig. 1 as a function of column loading: without H_2SO_4 fraction recycling (dashed) and with H_2SO_4 fraction recycling (solid). Model parameters are given in Table 1. For details see section Modelling and calculations.

At low column loadings, dilution of the monosaccharide fraction also occurs. The concentration of the monosaccharides in their target fraction increases with increasing column loading and eventually a concentrated monosaccharide fraction is obtained. This is due to the focusing effect of the monosaccharides.

It can be concluded that the hydrolysis acid concentration has a significant effect on the performance of the chromatographic monosaccharide–acid separation: higher performance can be obtained with lower hydrolysis acid concentration. Also the column loading has a significant effect on the performance. The loading giving the maximum Pr_{sugar} was associated with a relatively low Y_{sugar}. However, due to the internal recycling of the H_2SO_4 fraction, the performance of the entire lignocellulosic hydrolysis–separation process should be investigated when evaluating the performance of the separation step.

Chromatographic separation coupled with biomass hydrolysis and recycling of sulfuric acid

The investigation of the stand-alone chromatographic separation of concentrated acid lignocellulosic hydrolysates is not sufficient for the optimization and evaluation of the process performance. Therefore, the separation performance of an entire concentrated acid lignocellulosic hydrolysis–separation process (see Fig. 1) was investigated with simulations. Details of the investigation procedure can be found in section Modelling and calculations. The effect of column loading on the productivity of the chromatographic separation process with respect to the monosaccharides in steady state was investigated. The separation process performance (Pr_{sugar}, Y_{sugar}, Y_{H2SO4}, and *EC*) was then evaluated with the loading giving the maximum Pr_{sugar} in steady state.

The process with recycling reached steady state in six cycles with each column loading. With recycling of the H_2SO_4 fraction, the column loading giving the maximum Pr_{sugar} (18.2 vol%) is considerably higher than when no recycling of the sulfuric acid fraction is used (13.0 vol%) (Fig. 7). Without the recycling Pr_{sugar} is quite close to the maximum value over a wide range of column loadings (10–16 vol%). With recycling, maximizing the productivity requires more careful optimization: a change in column loading from 18.2 vol% quickly decreases Pr_{sugar} considerably. The productivity with H_2SO_4 fraction recycling

Table 2. Performance of chromatographic separation in the process shown in Fig. 1 with 18.2 vol% column loading without H_2SO_4 fraction recycling and with H_2SO_4 fraction recycling in steady state. Model parameters are given in Table 1

	Separation with a single pass	Separation with recycling
Pr_{sugar}, mol (m^{-3} h^{-1})	212.89	546.31
Y_{sugar}, %	32.0	90.6
Y_{H2SO4}, %	99.0	97.0
EC, L mol^{-1}	13.91	5.42

(546.3 mol (m^{-3} h^{-1})) is approximately 157% higher than without recycling (Table 2). The large increase in Pr_{sugar} was due to the higher monosaccharide concentration in the feed to the separation column due to the recycling of the H_2SO_4 fraction (Table 3).

In the sulfuric acid concentration step, the acid was concentrated into 70 wt% (11.5 mol L^{-1}, Table 3) by removing water: approximately 90% of the water had to be removed. This water was recycled to be used as eluent for the chromatographic separation. In this way, the fresh water consumption decreased by approximately 61%. 92.3% of the acid needed for hydrolysis was obtained through recycling.

The H_2SO_4 concentration in the feed to the separation column was not affected by the recycling (Table 3) because a constant amount of H_2SO_4 was used in the hydrolysis on each cycle. However, the amount of monosaccharides in the feed to the separation column increased due to the recycling of the H_2SO_4 fraction (Table 3) because the recycle fraction contains monosaccharides. This affected the position of the second cut point in the separation. Y_{H2SO4} (Table 2) and H_2SO_4 concentration in the H_2SO_4 fraction decreased slightly while the H_2SO_4 concentration in the monosaccharide fraction was doubled (Table 3).

With H_2SO_4 fraction recycling, Y_{sugar} in the chromatographic separation was much higher than without recycling (Table 2). This is because most of the monosaccharides which are not collected in the monosaccharide fraction are recycled back to the process in the H_2SO_4 fraction. With the recycling, 90.6% of the monosaccharides that are produced in the concentrated acid hydrolysis are taken out from the separation column for downstream processing (fermentation, etc.). Therefore, the yield of monosaccharides from wood over the whole process (monosaccharide yield in the hydrolysis is 80%) with the recycling is 72.5%.

By recycling the H_2SO_4 fraction, the total glucose and xylose concentrations in the product fraction were increased approximately by a factor of 2.9 and 1.8, respectively, (Table 3). The increase in monosaccharide concentrations would be highly beneficial for subsequent fermentation or other unit operation. The cycle time remained constant because the amounts of the first and last eluting components (H_2SO_4 and acetic acid) remained unchanged in the feed to the separation column, and because the sorption of acetic acid is not affected by the amount of monosaccharides in the feed solution.

Acetic acid was removed completely from the process in the monosaccharide and acetic acid fractions. Therefore, recycling has no effect on its concentration in the hydrolysate.

CONCLUSIONS

A dynamic column model, which can be used for process design, was derived for the chromatographic separation of concentrated acid lignocellulosic hydrolysates. The elution of four main components of such hydrolysates (sulfuric acid, glucose, xylose, and acetic acid) were modelled. A gel type strong acid cation exchange resin, for which shrinking due to sulfuric acid is considerable, was used as an adsorbent. The column model takes into account resin shrinking as changing bed porosity and particle size.

Simple empirical models were fitted to the experimental adsorption isotherm and resin shrinking data. The fit of these models to the experimental data was found to be very good. The models were able to describe the co-operative effect of sulfuric acid on the sorption of the other adsorbates, as well as the extent of resin shrinking.

The model was validated with experimental column data. The simulation results were found to be in good agreement with the experimental results. The use of changing bed porosity to describe the effects of resin shrinking on the elution of the components was found to be adequate in this case.

Performance of the batchwise chromatographic separation as a function of hydrolysis acid concentration and column loading was investigated with simulations. The performance of the separation

Table 3. Volumes and concentrations in a lignocellulosic biomass conversion and purification process (see Fig. 1) with 18.2 vol% column loading without H_2SO_4 fraction recycling and with H_2SO_4 fraction recycling in steady state. Model parameters are given in Table 1

	Feed to separation column	H_2SO_4 fraction	H_2SO_4 fraction after concentration	Monosaccharide fraction	Acetic acid fraction
Separation with a single pass					
V, L	5000	9897	1000	1259	8096
C_{H2SO4}, mol L^{-1}	2.379	1.162	11.494	0.099	0
$C_{Glucose}$, mol L^{-1}	0.332	0.121	1.2	0.338	4.2×10^{-3}
C_{Xylose}, mol L^{-1}	0.299	0.081	0.8	0.476	11.7×10^{-3}
C_{AcOH}, mol L^{-1}	0.16	0	0	6.6×10^{-3}	97.6×10^{-3}
Separation with H_2SO_4 fraction recycling					
V, L	5000	9767	982	1434	8050
C_{H2SO4}, mol L^{-1}	2.379	1.156	11.494	0.228	0
$C_{Glucose}$, mol L^{-1}	0.742	0.224	2.229	0.978	13.7×10^{-3}
C_{Xylose}, mol L^{-1}	0.474	0.096	0.953	0.854	25.9×10^{-3}
C_{AcOH}, mol L^{-1}	0.16	0	0	6.6×10^{-3}	98.2×10^{-3}

was found to decrease with increasing concentration of H_2SO_4. The loading giving the maximum productivity of the separation process with respect to the monosaccharides was also found to decrease with increasing H_2SO_4 concentration. The maximum productivity was associated with a low monosaccharide yield. However, the low yield of monosaccharides is not a problem, as most of the monosaccharides that are not collected in the monosaccharide fraction are recycled back to the process in the sulfuric acid fraction. From the investigation of the stand-alone separation process, it can be concluded that the concentrated acid hydrolysis should be done with as low an acid concentration as possible in order to obtain high separation performance.

Due to the recycling of the sulfuric acid fraction, the separation performance in a process consisting of concentrated acid lignocellulosic hydrolysis, chromatographic separation, and sulfuric acid fraction recycling and concentration was also investigated with simulations. The recycling of the sulfuric acid increases the performance of the chromatographic separation process considerably. Also, the column loading giving the maximum productivity with respect to the monosaccharides is considerably higher than without the recycling. The increase in performance is due to the monosaccharides which are also recycled back to the hydrolysis step with the sulfuric acid.

ACKNOWLEDGEMENTS

Financial support from the Academy of Finland (Grant SA/121280) is gratefully acknowledged. J.H. thanks the Graduate School in Chemical Engineering (Finland) and Walter Ahlström Foundation (Finland) for personal grants.

REFERENCES

1 Taherzadeh MJ and Karimi K, Bioethanol: market and production processes, in *Biofuels Refining and Performance*, ed by Nag A. McGraw-Hill, Fairfield, USA, pp 69–106 (2008).
2 Sims R, Taylor M, Saddler J and Mabee W, *From 1st to 2nd Generation Biofuel Technologies – An Overview of Current Industry and RD&D Activities*, November 2008; http://www.iea.org/papers/2008/2nd_Biofuel_Gen.pdf [accessed 23 June 2011].
3 Rass-Jansen J, Falsig H, Jørgensen B and Christensen CH, Bioethanol: fuel or feedstock? *J Chem Technol Biotechnol* **82**:329–333 (2007).
4 Galbe M and Zacchi G, A review of the production of ethanol from softwood. *Appl Microbiol Biotechnol* **59**:618–628 (2002).
5 Hamelinck CN, van Hooijdonk G and Faaij APC, *Ethanol from Lignocellulosic Biomass: Techno-Economic Performance as Development Progresses*, November 2003; https://www.senternovem.nl/mmfiles/149043_tcm24-280055.pdf [accessed 23 June 2011].
6 Farone WA and Cuzens JE, Strong Acid Hydrolysis of Cellulosic and Hemicellulosic Materials. US Patent No. 5,597,714, June 7, 1995.
7 Farone WA and Cuzens JE, Method of Producing Sugars Using Strong Acid Hydrolysis of Cellulosic and Hemicellulosic Materials. US Patent No. 5,562,777, March 26, 1993.
8 Clausen EC and Gaddy JL, Concentrated Sulfuric Acid Process for Converting Lignocellulosic Materials to Sugars. US Patent No. 5,188,673, October 12, 1988.
9 Palmqvist E and Hahn-Hägerdahl B, Fermentation of lignocellulosic hydrolysates. II: inhibitors and mechanisms of inhibition. *Bioresource Technol* **74**:25–33 (2000).
10 Heinonen J and Sainio T, Chromatographic recovery of monosaccharides for the production of bioethanol from wood. *Ind Eng Chem Res* **49**:3713–3729 (2010).
11 Sprinfield RM and Hester RD, Continuous ion-exclusion chromatography system for acid/sugar separation. *Sep Sci Technol* **34**:1217–1241 (1999).
12 Neuman RP, Rudge SR and Ladisch MR, Sulfuric acid–sugar separation by ion exclusion. *React Polym* **5**:55–61 (1987).
13 Heinonen J, Tamminen A, Uusitalo J and Sainio T, Ethanol production from wood via concentrated acid hydrolysis, chromatographic separation, and fermentation. *J Chem Technol Biotechnol* **87**:689–696 (2012).
14 Sainio T, Turku I and Heinonen J, Adsorptive removal of fermentation inhibitors from concentrated acid hydrolysates of lignocellulosic biomass. *Bioresource Technol* **102**:6048–6057 (2011).
15 Shapovalov OI and Ashkinazi LA, Biobutanol: biofuel of second generation. *Russ J Appl Chem* **81**:2232–2236 (2008).
16 Kunkes EL, Simonetti DA, West RM, Serrano-Ruiz JC, Gärtner CA and Dumesic JA, Catalytic conversion of biomass to monofunctional hydrocarbons and targeted liquid-fuel classes. *Science* **333**:417–421 (2008).
17 Laatikainen M, Heinonen J and Sainio T, Modeling of chromatographic separation of concentrated-acid hydrolysates. *Sep Purif Technol* **80**:610–619 (2011).
18 Sainio T, Laatikainen M and Paatero E, Phase equilibria in solvent mixture–ion exchange resin systems. *Fluid Phase Equilib* **218**:269–283 (2004).
19 Helfferich F, *Ion Exchange*, Dower Publications Inc., Mineola, New York, USA (1995).
20 Mazzotti M, Neri B, Gelosa D and Morbidelli M, Dynamics of a chromatographic reactor: esterification catalyzed by acidic resins. *Ind Eng Chem Res* **36**:3163–3172 (1997).
21 Mackie JS and Meares P, The diffusion of electrolytes in a cation-exchange resin membrane. I. *Theoretical Proc Royal Soc* **A232**:498–509 (1955).
22 Schiesser WE, *The Numerical Method of Lines*. Academic Press, San Diego, USA (1991).
23 Hoshino C, Yamada T, Taneda D, Nagata Y, Fujii T, Mase T, *et al*, Method for Producing Monosaccharides from Biomass and Monosaccharide Production Device. US Patent No. 0,148,750, June 28, 2007.
24 Gsell G, Water systems utilizing multiple effect and vapor compression technologies compared. *Pharm Eng* **24**:1–7 (2004).
25 Sainio T and Paatero E, Mass coordinates for dynamic simulation of column operations involving dimensional changes of packing material. *Comput Chem Eng* **31**:374–383 (2007).
26 Wankat PC, *Rate-Controlled Separations*. Elsevier Science, Essex (1990).

PAPER IV

Separation and Purification Technology 95 (2012) 235–247

Contents lists available at SciVerse ScienceDirect

Separation and Purification Technology

journal homepage: www.elsevier.com/locate/seppur

Use of Adsorbed Solution theory to model competitive and co-operative sorption on elastic ion exchange resins

Jari Heinonen [a], Héctor Octavio Rubiera Landa [b], Tuomo Sainio [a,*], Andreas Seidel-Morgenstern [b]

[a] Lappeenranta University of Technology, Laboratory of Industrial Chemistry, Skinnarilankatu 34, FIN-53850 Lappeenranta, Finland
[b] Max Planck Institute for Dynamics of Complex Technical Systems, Sandtorstrasse 1, DE-39106 Magdeburg, Germany

ARTICLE INFO

Article history:
Received 5 November 2011
Received in revised form 30 March 2012
Accepted 2 May 2012
Available online 12 May 2012

Keywords:
Adsorbed Solution theory
Ion exchange resin
Electrolyte
Non-electrolyte
Chromatographic separation

ABSTRACT

An Adsorbed Solution theory which takes into account non-idealities in both the adsorbed and the liquid phase was applied for the prediction of multi-component adsorption equilibria based on single component and binary mixture data. A novel non-iterative solution method was applied for the solution of the set of partly implicit model equations. The Pitzer activity coefficient model was used for the liquid phase and an empirical model for the adsorbed phase activity coefficients. Separation of concentrated acid lignocellulosic hydrolysates on an elastic strong acid cation exchange resin was used as a test system. The application is relevant in biorefineries when polysaccharides in wood are hydrolyzed to monosaccharides using concentrated sulfuric acid.

It was found that the novel solution method for the equilibrium model can be applied successfully for complex multi-component systems; it is fast and easy to implement. The predictions of the thermodynamic model were validated with dynamic column experiments (pulse injections and loading/elution curves). Hereby, in the column mass balances, porosity fluctuations were taken explicitly into account. Satisfactory correlation between the calculated and experimental results was obtained. It was observed that the predictions of the model can be quite sensitive with respect to even minor inaccuracies in the calculated multi-component adsorption isotherms.

1. Introduction

Multi-component adsorption equilibria can be predicted using different models [1]. One popular approach that exploits in a thermodynamically consistent way pure component isotherms is the Ideal Adsorbed Solution (IAS) theory [1–3] developed by Myers and Prausnitz [2], and Radke and Prausnitz [3]. In the IAS theory, in addition to the assumption that the fluid phase (liquid or gas) behaves ideal, also the adsorbed phase is treated as ideal. When this assumption is not valid, a more general model, the Real Adsorbed Solution (RAS) theory where adsorbed phase activity coefficients are taken into account, can be used instead [1,4–9]. A further hardly applied approach to reality can be made by assuming that both adsorbed and liquid phases are nonideal.

Conventionally, the implicit algebraic equations of the IAS theory and also of the extended models are solved iteratively [1,5–9]. This approach is rather slow due to the need to calculate as intermediate information the spreading pressure on the adsorbed phase. Recently Rubiera Landa et al. [10,11] presented a novel non-iterative solution method for the IAS theory equations in which the intermediate calculation of the spreading pressure is avoided. The novel solution method developed is easy to implement and fast to compute [10,11].

In this study, the more realistic theory assuming that both adsorbed and fluid phases can be real is used together with the new solution method [10,11] to predict the sorption of strong and weak electrolytes and neutral species on an elastic ion exchange resin. Due to the complexity of the system studied, both liquid and adsorbed phase activities are taken into account. Liquid phase activity coefficients are calculated using the well-known Pitzer activity coefficient model [12,13] as modified by Fernández-Mérida et al. [14]. This activity coefficient model can be applied to systems containing electrolytes and non-electrolytes. The adsorbed phase activity coefficients for sulfuric acid are calculated using an empirical model. For the sake of simplicity, the adsorbed phase activity coefficients of the other components are taken as unity.

To test the applicability of the multi-component equilibrium isotherm model for the aforementioned system, modelling of adsorption of concentrated acid lignocellulosic hydrolysates on a strong acid cation exchange resin is studied experimentally. These hydrolysates contain mainly sulfuric acid, acetic acid, monosaccharides, and furfural. Sorption of sulfuric acid (strong electrolyte) on ion exchange resin is affected by electrolyte exclusion [15,16], whereas acetic acid (weak electrolyte) can be treated as a

* Corresponding author. Tel.: +358 40 3578683; fax: +358 5 6212199.
E-mail address: tuomo.sainio@lut.fi (T. Sainio).

1383-5866/$ - see front matter © 2012 Published by Elsevier B.V.
http://dx.doi.org/10.1016/j.seppur.2012.05.003

Nomenclature

A	Pitzer activity coefficient model constant
a	liquid phase activity, mol/L
b	Pitzer activity coefficient model constant
C_i	liquid phase concentration, mol/L
C^*_{H2O}	concentration of water in pure water, mol/L
$D_{ax,i}$	axial dispersion coefficient, m^2/s
D_i^p	pore diffusion coefficient, m^2/s
d_{bed}	column diameter, m or cm
d_p	particle diameter, m
h_{bed}	resin bed height, m or cm
I_m	molal ionic strength of the electrolyte solution, mol/L
$k_{m,i}$	intraparticle mass transfer coefficient, 1/s
M_i	molar mass, g/mol
m_i	molal concentration, mol/kg solvent
n	mole amount, mol
p	ionic charge, –
p^{tot}	total pressure of the system, Pa
p_i^{sat}	saturation pressure, Pa
q_i	adsorbed phase concentration, mol/L
q_i^*	concentration in adsorbed phase when in equilibrium with liquid phase concentration C_i, mol/L
$\bar{q}_i$	average adsorbed phase concentration, mol/L
$q_{sat,i}$	saturation capacity, mol/L
q^{tot}	total adsorbed concentration in a mixture, mol/L
S_{col}	column cross-sectional area, m^2
T	temperature, °C
t	temporal coordinate, s
u	superficial flow rate, cm/min
V_{bed}	resin bed volume, mL
V^{feed}	feed (injection) volume, mL
$\dot{V}$	volumetric flow rate, mL/min
$V^*_{m,i}$	molar volume of the pure component, cm^3/mol
w_i	weight fraction, –
x_i	liquid phase mole fraction, –
$\bar{x}_i$	adsorbed phase mole fraction, –
y_i	gas phase mole fraction, –
z	spatial coordinate, m

Greek letters

α	Pitzer model interaction constant
β_0, β_1	constants of Pitzer model for pure electrolyte
γ	activity coefficient, –
δ_1, δ_2	resin shrinking model constants
ε	resin bed porosity, –
θ	extent of resin shrinking, –
κ_1^S, κ_2^S	adsorbed phase activity coefficient model constants
$\lambda^{(0)}$, $\lambda^{(1)}$	Pitzer model parameters for interactions between similar neutral components
ν	stoichiometric number of ion, –
ξ	integration variable, –
π_{mix}	reduced spreading pressure, –
ρ	density, g/cm^3
τ	isotherm model constant
ϕ_N	osmotic coefficient, –
$\chi^{(0)}$, $\chi^{(1,0)}$, $\chi^{(1,1)}$	Pitzer model constants for interactions between neutral component and electrolyte
ψ_p	volume fraction of polymer, –
ω_1, ω_2	isotherm model constants

Subscripts and superscripts

0	hypothetical pure component value
*	pure component value; equilibrium value
±	ionic mean activity
acid	in acid
ax	axial
bed	resin bed
c	molarity scale
col	column cross-section
cycle	cycle
feed	feed value
i, j, k	component
in	inlet
MX	electrolyte
m	mass transfer; molar volume; molality scale
mix	mixture
N	neutral component
P	pore
p	polymer matrix; particle
ref	reference state
S	adsorbed phase
sat	saturation
Soln	solution
Solvent	solvent
sugar	all monosaccharides
sym	symmetrical
tot	total
unsym	unsymmetrical
water	in water
x	mole fraction scale
θ	resin shrinking
∞	infinite dilution

non-electrolyte [15]. Sulfuric acid is known to have an interesting co-operative effect on the sorption of the monosaccharides, acetic acid, and furfural on strong acid cation exchange resin [15,16].

The elasticity of the adsorbent used in this study further complicates the modelling: elastic ion exchange resins shrink and swell depending on the degree of cross-linking, the concentration of functional groups, and the liquid phase composition [17–20]. Many approaches have been presented to take into account resin volume changes in adsorption processes [17–22]. Recently, Heinonen and Sainio [16] demonstrated that the volume of resin particles can be directly related to the amount of sorbed sulfuric acid. This simple correlation is used also in this study.

The predictions of the multi-component adsorption model are validated with dynamic column experiments using both pulse injections and loading/elution curve data. Synthetic solutions containing sulfuric acid, glucose, xylose, acetic acid, and furfural are used instead of authentic concentrated acid lignocellulosic hydrolysates.

2. Materials and methods

Gel type strong acid (sulfonated) polystyrene–divinylbenzene (PS–DVB) type cation exchange resin CS16GC (Batch No. 4394, Finex Oy, Finland) with 8 wt.% cross-linking (DVB content) was used as an adsorbent. The resin was converted to hydrogen form with 1 M hydrochloric acid (37%, pro analysi, Merck KGaA) with standard methods. The volumetric capacity of the resin in hydrogen form was 1.93 mequiv/L, and average particle size was 246 μm.

Pro analysis grade sulfuric acid (95–97%, pro analysi, Merck KGaA), α-D-glucose (min. 99.5%, Sigma–Aldrich Co.), D-(+)-xylose (min. 99%, Sigma–Aldrich Co.), acetic acid (100%, pro analysi, Merck KGaA), furfural (min. 98%, Merck KGaA), and purified and degassed water were used in the experiments.

Glucose, xylose, acetic acid, and furfural concentrations were determined with HPLC (HP1100, Hewlett–Packard/Agilent) using Metacarb 87H column (Varian/Agilent). Potentiometric titration

was used for sulfuric acid concentration measurements. For more details, see our previous studies [16,23].

A chromatographic column with 25 mm inner diameter (ECO SR 25/200 with a water heating jacket, Kronlab) was used. Details of the experimental setup are also reported in our previous study [16].

2.1. Adsorption isotherm measurements

The adsorption isotherm of furfural on CS16GC resin was measured for this study in water at a temperature of 50 °C with frontal analysis [24] using ECO SR 25/200 column (h_{bed} 20 cm). Superficial velocity was 0.5 cm/min. The adsorption isotherms of sulfuric acid, glucose, xylose, and acetic acid were available [25].

2.2. Model validation experiments

To validate the model, column experiments with synthetic solutions were conducted at a temperature of 50 °C. Both pulse injections and loading and elution curve experiments were done. The resin bed height was 20 cm. The superficial velocity was 0.5 cm/min (2.45 mL/min with ECO SR 25/200 column). Top-down flow was used. The eluent was purified and degassed water.

In the pulse experiments, column loadings were 0.102, and 0.204 bed volumes. A synthetic injection solution containing sulfuric acid (2.22 mol/L), glucose (0.24 mol/L), xylose (0.38 mol/L), acetic acid (0.16 mol/L), and furfural (0.02 mol/L) was used.

Loading experiments were done with two synthetic solutions containing 1.05 mol/L or 2.28 mol/L sulfuric acid together with 0.27 mol/L glucose, 0.31 mol/L xylose, and 0.18 mol/L acetic acid. For both solutions, subsequent elution was performed with purified and degassed water.

3. Modelling and calculations

3.1. Phase equilibrium model

It is well known from the literature [26–29] that concentrated sugar solutions behave nonideally and a description of such systems requires the consideration of liquid phase activities instead of liquid phase concentrations. In addition, it has been shown [16] that sulfuric acid affects the sorption of neutral components through interactions in liquid phase. In order to incorporate these facts into our description of the adsorption equilibria, liquid phase activity coefficients were calculated using the Pitzer model [13–15].

To be able to describe possible non-idealities in the adsorbed phase, adsorbed phase activity coefficients were introduced following the approach used in the Real Adsorbed Solution (RAS) theory [1,4–9]. This was done exclusively for sulfuric acid for which the largest nonideality was expected (due to considerably higher liquid phase concentration compared to other components and highly nonideal behavior in the liquid phase) using a simple empirical model, whereas for the other components these adsorbed phase activity coefficients were taken as unity.

Thus, the predictions of the multi-component adsorption equilibria are based in this work on the well-known framework provided by the IAS theory. However, regarding both phases involved, extensions accounting for non-idealities are incorporated.

3.1.1. Pure component adsorption equilibria

In order to take nonideal behavior of the liquid phase into account, the liquid phase concentration C was substituted by the liquid phase activity a by introducing liquid phase activity coefficients γ_i:

$$a_i = \gamma_i C_i. \tag{1}$$

These activities were used in standard single component adsorption isotherm models directly by just exchanging C_i by a_i. No detailed discussion regarding the physical relevance of the original and the modified single component isotherm models is attempted here. The connection between specific activity coefficient models used (here the Pitzer model) and possible changes in the structure of an isotherm model switching from ideal to real phase description is a difficult task outside the scope of this paper. For the purpose of the present study the single component isotherm models given below are seen as a tool to quantify the single component behavior sufficiently accurate.

Sorption of acetic acid and furfural was described with a model analogous to the single component Langmuir isotherm [24]

$$q_i = \frac{q_{sat,i}\omega_{1,i}a_i}{1+\omega_{1,i}a_i}, \quad i = \text{acetic acid, furfural}, \tag{2}$$

where $q_{sat,i}$ is the saturation capacity, and ω_1 is a constant.

Sorption of glucose and xylose is known to behave more complex: the isotherms are slightly unfavorable shaped due to nonidealities in the liquid phase resulting from small distribution coefficients [26–29]. This was also confirmed in our own preliminary experiments. Thus, a more complex second order model (analogous to the "quadratic isotherm" [24]) was applied to describe the equilibrium data for these components

$$q_i = \frac{q_{sat,i}(\omega_{1,i}a_i + 2\omega_{2,i}a_i^2)}{1+\omega_{1,i}a_i+\omega_{2,i}a_i^2}, \quad i = \text{glucose, xylose}, \tag{3}$$

where q_i is the adsorbed phase concentration and ω_2 is a constant. The experimental data presented later do not reveal inflection points in the concentration range studied. Therefore, in principle, the simple anti-Langmuir isotherm could be used instead of the quadratic isotherm, but it is not thermodynamically consistent due to the discontinuity at a finite liquid phase concentration. In addition, of course a better correlation of the data was obtained with the more flexible quadratic isotherm.

A characteristic feature of electrolyte sorption on a strong acid cation exchange resin is electrolyte exclusion. The isotherms are unfavorable (concave upward) and the sorbed amount as well as the first derivative of the isotherm must be zero at infinite dilution because of complete electrolyte exclusion [15]. Experimental sulfuric acid sorption data were correlated using the liquid phase activities in a model analogous to the Redlich–Peterson isotherm model [24]

$$q_{H2SO4} = \frac{\omega_{1,H2SO4}a_{H2SO4}}{1+\omega_{2,H2SO4}(a_{H2SO4})^{\tau_{H2SO4}}}, \tag{4}$$

where τ is a constant.

3.1.2. Multi-component adsorption equilibria

3.1.2.1. Adsorbed Solution theory. The Adsorbed Solution theory can be used to predict multi-component isotherms from thermodynamically consistent single component isotherms [1,4–9]. It is used when the adsorbed phase cannot be treated as ideal. The fundamental equations of the theory are analogous to the IAS theory with addition of certain adsorbed phase activity coefficients [1,4–9].

The reduced spreading pressure of a mixture of n components π_{mix} is calculated from the following integrals

$$\pi_{mix} = \int_0^{a_i^0} \frac{q_1^0(a_1^0)}{a_1^0}da_1^0 = \cdots = \int_0^{a_n^0} \frac{q_n^0(a_n^0)}{a_n^0}da_n^0, \quad i = 1, n, \tag{5}$$

where the superscript 0 designates hypothetical pure component values.

Adsorbed phase mole fraction of component i $\bar{x}_i$ is calculated with an equation analogous to Raoult's law including an adsorbed phase activity coefficient γ_i^S:

$$\bar{x}_i = \frac{a_i}{\gamma_i^S a_i^0}, \quad i = 1, n. \tag{6}$$

The sum of the adsorbed phase mole fractions must equal unity:

$$\sum_{i=1}^{n} \bar{x}_i = 1. \tag{7}$$

With the frame of the RAS theory, the total adsorbed phase concentration q^{tot} can be calculated from [1,6–8]

$$\frac{1}{q^{tot}} = \sum_{i=1}^{n} \frac{\bar{x}_i}{q_i^0(a_i^0)} + \sum_{i=1}^{n} \bar{x}_i \frac{\partial \ln \gamma_i^S}{\partial \pi_{mix}}. \tag{8}$$

The second term on the right hand side of Eq. (8) can be neglected if the adsorbed phase activity coefficients are not a function of the spreading pressure [8]. This leads then to the simple equation applied within the IAS theory:

$$\frac{1}{q^{tot}} = \sum_{i=1}^{n} \frac{\bar{x}_i}{q_i^0(a_i^0)}. \tag{9}$$

The adsorbed concentrations of the individual components in a mixture are finally calculated from

$$q_i = \bar{x}_i q^{tot}, \quad i = 1, n. \tag{10}$$

3.1.2.2. Solution of the Adsorbed Solution theory equations. Recently Rubiera Landa et al. [10,11] presented a novel method to solve the IAS theory equations. The approach is simple and fast to compute and does not require the calculation of the reduced spreading pressure. This method was used here to solve the multi-component adsorption equilibrium model equations (Eqs. (4)–(9)). It should be emphasized that the use of liquid or adsorbed phase activities does not change the essential features of the solution method proposed in [10,11].

In this novel solution method, the equation for the reduced spreading pressure (Eq. (4)) is first written as $n-1$ equalities:

$$\begin{aligned} &\pi_1(a_1^0) = \pi_2(a_2^0) \\ &\vdots \\ &\pi_1(a_1^0) = \pi_n(a_n^0). \end{aligned} \tag{11}$$

Assuming a solution of the form $a_i^0(a_1^0),\ i = 2, \ldots, n$, we proceed to differentiate each $\pi_i(a_i^0),\ i = 1, \ldots, n$ in Eq. (11) with respect to their arguments, yielding the following equalities:

$$\pi_1' = \pi_i'(a_i^0(a_1^0)) \frac{da_i^0(a_1^0)}{da_1^0}, \quad i = 2, \ldots, n. \tag{12}$$

From this expression we construct the initial value problem

$$\begin{aligned} &\frac{da_2^0}{da_1^0} = \frac{\pi_1'}{\pi_2'} \\ &\vdots \\ &\frac{da_n^0}{da_1^0} = \frac{\pi_1'}{\pi_n'} \quad a_i^0(0) = 0, \quad i = 2, \ldots, n. \end{aligned} \tag{13A}$$

For i = 1 holds

$$\frac{da_1^0}{da_1^0} = 1, \quad a_1^0(0) = 0. \tag{13B}$$

For the implementation, we introduce the integration variable ξ and the initial value problem, Eq. (13), is expressed as

$$\frac{da_1^0}{d\xi} = 1, \tag{14A}$$

$$\begin{aligned} &\frac{da_2^0}{d\xi} = \frac{\pi_1'}{\pi_2'} = \frac{q_1^0/a_1^0}{q_2^0/a_2^0} \\ &\vdots \\ &\frac{da_n^0}{d\xi} = \frac{\pi_1'}{\pi_n'} = \frac{q_1^0/a_1^0}{q_n^0/a_n^0}, \end{aligned} \tag{14B}$$

$$a_i^0(0) = 0, \quad i = 1, \ldots, n. \tag{14C}$$

Particular solution for given a_i is obtained from the closure condition presented in Eq. (7), written conveniently (i.e. avoid divisions by zero when integrating Eq. (14)) in the following form:

$$W(a_i^0 \ldots a_n^0, a_1 \ldots a_n) = \left(\prod_{i=1}^{n} a_i^0 \right) \left(\sum_{i=1}^{n} \frac{a_i}{\gamma_i^S a_i^0} - 1 \right). \tag{15}$$

The integration of Eq. (14) is continued as long as the value of W is positive. The values of a_i^0 obtained at the end of the integration (i.e. at $W = 0$) provide the solution required to solve explicitly the remaining part of the thermodynamic isotherm model.

Now the adsorbed phase mole fractions can be obtained directly from Eq. (6), after which the total adsorbed concentration can be calculated with Eq. (8) (or Eq. (9) in case the adsorbed phase activity coefficients are not a function of the reduced spreading pressure). Finally, the adsorbed concentrations of individual components are obtained from Eq. (10).

3.1.3. Resin shrinking

The extent of swelling of ion exchange resins depends on the degree of cross-linking, concentration of functional groups, temperature as well as the solution environment. In aqueous electrolyte solutions, the activity of water is the main solution property of interest [15]. However, it was demonstrated by Heinonen and Sainio [16] that the volume of resin particles can be directly related to the sorbed amount of sulfuric acid if such experimental data is available. Therefore, a simple empirical correlation was used here

$$\theta = \frac{V_{bed,acid}}{V_{bed,water}} = 1 - \frac{\delta_1 q_{H2SO4}}{\delta_2 + q_{H2SO4}}, \tag{16}$$

where θ is the extent of resin shrinking, i.e. the ratio of resin bed volume (V_{bed}) in acid to resin bed volume in water, and δ_1 and δ_2 are positive constants. Eq. (16) is scaled so that θ is unity in pure water, and decreases with increasing amount of sorbed sulfuric acid.

3.2. Liquid and adsorbed phase activity coefficients

3.2.1. Liquid phase activity coefficients

The studied test system consists of a strong electrolyte (sulfuric acid), a weak electrolyte (acetic acid), and neutral components (glucose, xylose, and furfural). This kind of mixed system sets limitations to the choice of the activity coefficient model.

Pitzer activity coefficient model [12] is widely used for mixtures of electrolytes. A generalized Pitzer model [13] can be used to calculate activity coefficients in mixtures of electrolytes and non-electrolytes. Fernández-Mérida et al. [14] further modified the generalized Pitzer equation to be better suited for polar neutral components. This modified equation with some simplifying assumptions was used in this study to calculate the activity coefficients of each component. The estimation of Pitzer activity coefficient model parameters and unit conversions are presented in Appendices A and B.

3.2.1.1. Sulfuric acid. Sulfuric acid is a diprotic acid. Three different ions exist in an aqueous solution (H^+, HSO_4^-, and SO_4^{2-}). The experiments in this study were done at a temperature of 50 °C

where the value of the second dissociation constant is very small ($\approx 5.3 \times 10^{-3}$ mol/L [30]). It was thus assumed that the first dissociation of sulfuric acid is complete and the second dissociation is negligible. Therefore, the only ionic species of sulfuric acid were H^+ and HSO_4^- (1:1 salt). In addition, it was assumed that the other components do not affect the H_2SO_4 activity in liquid phase. The mean ionic activity coefficient of sulfuric acid in the liquid phase was calculated with the basic Pitzer equation for a single strong electrolyte omitting ternary interactions [13]

$$\ln \gamma_{\pm}^{(m)} = -A_p |p_+ p_-| + B_p m_{MX} \frac{2\nu_+\nu_-}{\nu_+ + \nu_-} + C_p (m_{MX})^2 \frac{2(\nu_+\nu_-)^{3/2}}{\nu_+ + \nu_-}, \quad (17A)$$

$$A_p = A\left[\frac{\sqrt{I_m}}{1 + b\sqrt{I_m}} + \frac{2}{b}\ln(1 + b\sqrt{I_m})\right], \quad (17B)$$

$$B_p = 2\beta_0 + \frac{2\beta_1}{(\alpha_{MX})^2 I_m}\left[1 - \left(1 + \alpha_{MX}\sqrt{I_m} - \frac{(\alpha_{MX})^2 I_m}{2}\right) \times \exp(-\alpha_{MX}\sqrt{I_m})\right], \quad (17C)$$

where $\gamma_{\pm}^{(m)}$ is ionic mean activity coefficient on molality scale, p is ionic charge, m_{MX} is molality of the electrolyte, ν is stoichiometric number of the ion, I_m is molal ionic strength of the electrolyte solution, and A, b, α_{MX}, β_0, β_1, and C_p are constants. Values of b and α_{MX} are 1.2 $kg^{1/2}/mol^{1/2}$ and 2.0 $kg^{1/2}/mol^{1/2}$ (1:1 salts), respectively [13,14]. The values of A, β_0, β_1, and C_p at a temperature of 50 °C were obtained by fitting Eq. (17) to the H_2SO_4 activity coefficient data published by Clegg et al. [31].

3.2.1.2. Other components. The activity coefficients of the other components in the system (glucose, xylose, acetic acid, and furfural) were calculated using the modified general Pitzer equation of Fernández-Mérida (Eq. (17) in [14]). Acetic acid was treated as a neutral molecule, due to its small dissociation constant ($\approx 1.6 \times 10^{-5}$ mol/L at 50 °C [32]) and the high concentration of strong acids (sulfuric acid and sulfonic acid groups in the resin). It was further assumed that there were no interactions between different neutral species.

It has been shown that sulfuric acid increases the sorption of the other components in the system through a salting out effect [16]. Due to this, the interactions between sulfuric acid and the neutral components were taken into account. The activity coefficients of glucose, xylose, acetic acid, and furfural were calculated with

$$\ln \gamma_N^{(m)} = 2m_N\left\{\lambda_{NN}^{(0)} + \frac{\lambda_{NN}^{(1)}}{(\alpha_{NN})^2 m_N}\left[1 - \left(1 + \alpha_{NN}\sqrt{m_N} - \frac{(\alpha_{NN})^2 m_N}{2}\right)\exp(-\alpha_{NN}\sqrt{m_N})\right]\right\} + 2m_{MX}\left\{\chi^{(0)} + \frac{2\chi^{(1,0)}}{(\alpha_{NMX})^2 I_m}\left[1 - \left(1 + \alpha_{NMX}\sqrt{I_m}\right)\exp(-\alpha_{NMX}\sqrt{I_m})\right]\right\} + m_N\left\{\frac{4\chi^{(1,1)}}{(\alpha_{NMX})^2 I_m}\left[1 - \left(1 + \alpha_{NMX}\sqrt{I_m}\right)\exp(-\alpha_{NMX}\sqrt{I_m})\right]\right\}, \quad (18)$$

where $\gamma_N^{(m)}$ is activity coefficient of neutral component N on molality scale, m_N is molality of neutral component; $\lambda_{NN}^{(0)}$, $\lambda_{NN}^{(1)}$, and α_{NN} are parameters for interactions between similar neutral components; and $\chi^{(0)}$, $\chi^{(1,0)}$, $\chi^{(1,1)}$, and α_{NMX} are parameters for interactions between neutral component and electrolyte. Ternary interactions are omitted in Eq. (18). For α_{NN}, a value of 0.5 $kg^{1/2}/mol^{1/2}$ was used [14].

3.2.2. Adsorbed phase activity coefficients

Sulfuric acid sorption is affected by electrolyte exclusion. According to Ref. [15] and our previous results [16], the sorption of sulfuric acid in the presence of neutral components should be in the studied concentration range the same as the sorption in pure sulfuric acid solution. However, it was found that the Adsorbed Solution theory predicts an increase in the H_2SO_4 sorption in the presence of the other components if the adsorbed phase activity coefficient is unity. This originates from the unfavorable isotherm of sulfuric acid. In order to describe the sulfuric acid sorption in the mixture more correctly, the following empirical adsorbed phase activity coefficient model was used

$$\gamma_{H2SO4}^S = 1 + \kappa_1^S \sum_{i=2}^{n} a_i \exp\left[\kappa_2^S \sum_{i=2}^{n} a_i\right], \quad (19)$$

where γ_{H2SO4}^S is adsorbed phase activity coefficient of sulfuric acid on molarity scale, κ_1^S and κ_2^S are constants, and the sum of the liquid phase activities excludes sulfuric acid (i = 1). Thus, for pure H_2SO_4, the value of γ_{H2SO4}^S is unity. The constants in Eq. (19) were estimated from experimental binary sorption data.

The adsorbed phase activity coefficients of the other components were taken as unity for all reduced spreading pressures. Eq. (9) was used to calculate the total adsorbed concentration because the activity coefficient described by Eq. (19) is not a function of the reduced spreading pressure [8].

3.3. Dynamic column model

A column model that takes into account resin shrinking and corresponding changes in bed porosity was used. The resin particles were assumed to be attached to a fixed two-dimensional grid [20]. When q_{H2SO4} changes the particle diameter and therefore also the local void volume (bed porosity) changes.

Conventional column mass balance including changes in the bed porosity can be written as:

$$\frac{\partial C_i}{\partial t} = -\frac{\dot{V}}{\varepsilon S_{col}}\frac{\partial C_i}{\partial z} + \frac{q_i - C_i}{\varepsilon}\frac{\partial \varepsilon}{\partial t} - \frac{1-\varepsilon}{\varepsilon}\frac{\partial q_i}{\partial t} + \frac{D_{ax,i}}{\varepsilon}\frac{\partial}{\partial z}\left(\varepsilon\frac{\partial C_i}{\partial z}\right), \quad (20)$$

where $\dot{V}$ is volumetric flow rate, S_{col} is column cross-sectional area, ε is bed porosity, D_{ax} is axial dispersion coefficient, t and z are temporal and spatial coordinates, respectively, and subscript i stands for component i. In Eq. (20), C_i, q_i, and ε are functions of both t and z. Danckwert's boundary conditions were used at the column inlet and outlet:

$$\frac{\partial C_i}{\partial z} = \frac{\dot{V}}{\varepsilon S_{col}}\frac{(C_i^{in} - C_i)}{D_{ax,i}}, \quad z = 0, \quad (21A)$$

$$\frac{\partial C_i}{\partial z} = 0, \quad z = h_{bed}, \quad (21B)$$

where V_i^{in} is the concentration at the column inlet and h_{bed} is the resin bed height. Resin bed porosity ε was calculated from

$$\varepsilon = 1 - \theta(1 - \varepsilon_{ref}), \quad (22)$$

where ε_{ref} is bed porosity in reference state, which was in this case a column equilibrated with pure water. The corresponding rate of bed porosity change is:

$$\frac{\partial \varepsilon}{\partial t} = -\frac{\partial \theta}{\partial t}(1 - \varepsilon_{ref}). \quad (23)$$

Applying the model formulated above (Eq. (16) and using the chain rule yields:

$$\frac{\partial \varepsilon}{\partial t} = \frac{\delta_1\delta_2}{(\delta_2 + q_{H2SO4})^2}\frac{\partial q_{H2SO4}}{\partial t}(1 - \varepsilon_{ref}). \quad (24)$$

By relating the extent of resin shrinking to the change in the amount of sulfuric acid adsorbed as expressed by Eq. (24), the effect of finite adsorption kinetics on the shrinking is taken into account.

The solid film linear driving force model was used to describe the mass transfer between the phases:

$$\frac{\partial \bar{q}_i}{\partial t} = k_{m,i}(q_i^* - \bar{q}_i) + \frac{\bar{q}_i}{1-\varepsilon}\frac{\partial \varepsilon}{\partial t}, \quad (25)$$

where $k_{m,i}$ is intraparticle mass transfer coefficient, q_i^* is adsorbed phase concentration of i at equilibrium with liquid phase concentration C_i, and $\bar{q}_i$ is the average adsorbed phase concentration of i. The second term on the right hand side of Eq. (25) originates from changes in porosity due to resin swelling.

The intraparticle mass transfer coefficient was calculated from

$$k_{m,i} = \frac{60 D_i^p}{(d_p)^2}, \quad (26)$$

where D_i^p is diffusion coefficient which depends on resin shrinking according to the correlation of Mackie and Meares [25,33]:

$$D_i^p = D_{i,ref}^p \left[\frac{(1-\psi_{p,ref}/\theta)(1+\psi_{p,ref})}{(1+\psi_{p,ref}/\theta)((1-\psi_{p,ref})}\right]^2, \quad (27)$$

where $D_{i,ref}^p$ is diffusion coefficient in the reference state and $\psi_{p,ref}$ volume fraction of the polymer in the reference state. Water swollen resin was taken here again as a reference state, i.e. $\psi_{p,ref} = 0.391$ [25]. Particle diameter d_p was calculated from

$$d_p = d_{p,ref}\left(\frac{1-\varepsilon}{1-\varepsilon_{ref}}\right)^{1/3}, \quad (28)$$

where $d_{p,ref}$ is particle diameter in the reference state.

Method of lines [34] was used to solve the partial differential equations in Eq. (20). The diffusion coefficients in reference state in Eq. (27) and the axial dispersion coefficients (same value for all components) in Eq. (20) were estimated by fitting simulated elution profiles to the experimentally obtained profiles.

4. Results and discussion

The applicability of the proposed phase equilibrium model was investigated with a system consisting of concentrated acid lignocellulosic hydrolysate (sulfuric acid, glucose, xylose, acetic acid, and furfural) and gel type strong acid PS–DVB cation exchange resin in hydrogen form. The model was validated with dynamic column data (pulse injection and loading/elution curve data).

4.1. Phase equilibrium

4.1.1. Single component adsorption and resin shrinking

Redlich–Peterson (Eq. (4)), quadratic (Eq. (3)), and Langmuir (Eq. (2)) isotherm models were fitted to the single component adsorption equilibrium data of sulfuric acid, glucose, xylose, acetic acid, and furfural on gel type CS16GC resin available at 50 °C. These sorption data were obtained in this and in our previous studies [16,25]. Liquid phase concentrations were converted into activities with Pitzer activity coefficient model. The pure component isotherms with model fits are shown in Fig. 1. The isotherm model parameters are given in Table 1.

The isotherm models used in this study for the pure components give a good fit to the experimental sorption data (Fig. 1). On activity scale, the experimental sulfuric acid isotherm is slightly S-shaped (Fig. 1A) because the experimental H_2SO_4 activity coefficient as a function of concentration first decreases then passes through a minimum and finally begins to increase [31]. The Redlich–Peterson isotherm model is not able to reproduce the observed inflection in the H_2SO_4 isotherm, but the correlation is still satisfactory for the present purpose.

Glucose and xylose isotherms are slightly unfavorable on activity scale in the studied concentration range (Fig. 1B). The sorption of these components is accurately described with the quadratic isotherm model.

The isotherms of acetic acid and furfural appear to be only slightly nonlinear. Use of two-parameter Langmuir isotherms instead of linear isotherms is justified because of the better fit obtained with such a model. Nonlinearity is most pronounced at low concentration range, and was found to affect retention of furfural in chromatographic separation when dilution is significant. In addition, for components with linear isotherms, the phase equilibrium model predicts no interactions between the components. This led to erroneous dynamic profiles with respect to furfural (data not shown).

The fit of the Langmuir isotherm model to acetic acid and furfural sorption isotherms is very good (Fig. 1C). As frequently encountered with the Langmuir model, in the case of almost linear isotherms the individual parameter values q_{sat} and β_1 are not well identified, although their product is.

The effect of sulfuric acid concentration on the shrinking of CS16GC is shown in Fig. 2. This effect is significant and must be taken into account in the modelling. At the last experimental point ($C_{H2SO4} \approx 4$ mol/L, $q_{H2SO4} \approx 1.2$ mol/L), the volume of the resin is approximately 16 vol.% smaller than in pure water. The shrinking due to H_2SO_4 is well described by Eq. (16), by which it is directly related to the concentration of H_2SO_4 inside the resin particles, instead of correlating it to the activity of water. The values for the constants δ_1 and δ_2 used in Eq. (16) were determined to be 0.226 and 0.442, respectively [16].

4.1.2. Binary adsorption equilibria with Adsorbed Solution theory

Binary interaction parameters between sulfuric acid and the other components (χ-parameters) needed in the Pitzer model were acquired by fitting the phase equilibrium model results to the binary sorption data of H_2SO_4 and the other components. The results are shown in Fig. 3 (glucose and xylose) and 4 (acetic acid). Pitzer model interaction parameters for pure components (λ_{NN}) and for neutral–electrolyte (χ) interactions are listed in Table 2.

For mixtures of neutral components and sulfuric acid, the phase equilibrium model predicts too strong sorption for H_2SO_4 on a strong acid cation exchange resin (as will be shown below). This is because of the fundamental nature of the theory: it predicts co-operative sorption for components with unfavorable isotherms. Sulfuric acid sorption, however, is influenced by electrolyte exclusion which is independent of the concentrations of neutral components (as long as the resin swelling is unaffected by the neutral components) [15]. Therefore, H_2SO_4 sorption on a strong acid cation exchange resin from a mixture with neutral components should be same as in the case of sorption from pure aqueous H_2SO_4 solution. As a consequence, an adsorbed phase activity coefficient (Eq. (19)) had to be used to correct the erroneous sorption predicted by the model. The values of the constants κ_1^S and κ_2^S in Eq. (19) were adjusted to 0.45 and −0.64, respectively.

Sulfuric acid has a co-operative effect on the sorption of glucose, xylose, acetic acid, and furfural through a phenomenon similar to salting out (see [16] for details). The sorption of glucose and xylose is approximately 50% larger in 1.84 mol/L H_2SO_4 than in water (Fig. 3). It can be seen from the experimental sorption data that in the presence of sulfuric acid, glucose and xylose isotherms remain slightly unfavorable (Fig. 3).

Without using the liquid phase activities, the fit of the calculated results to the experimental data was poor with the monosaccharides isotherms in the presence of H_2SO_4 (Fig. 3, dotted lines). A better correlation was obtained by using activities for the liquid phase (Fig. 3, solid lines). However, in this case, an inflection point can be observed in the calculated monosaccharide isotherms in the

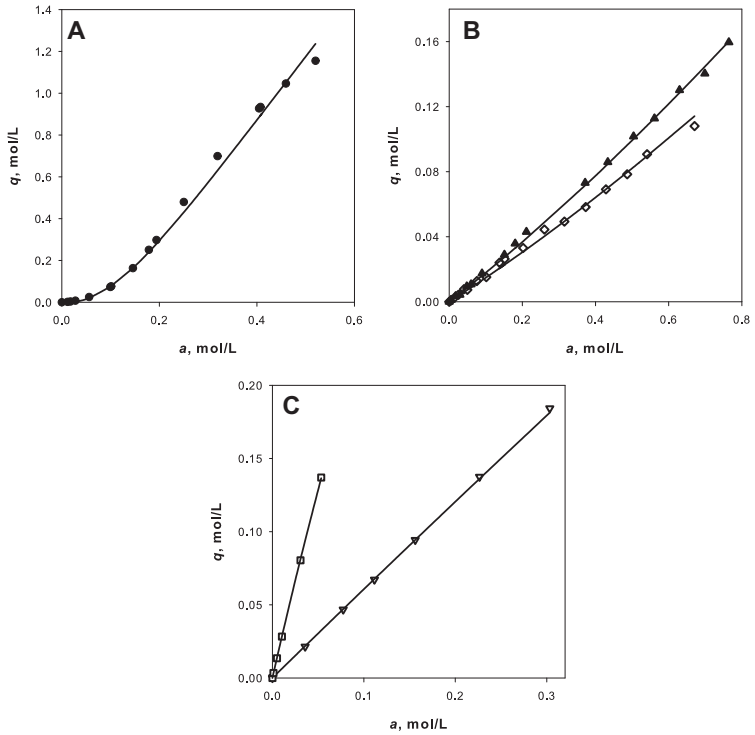

Fig. 1. Sorption of sulfuric acid (●) (A), glucose (◇) and xylose (▲) (B), and acetic acid (▽) and furfural (□) (C) from water on CS16GC resin at a temperature of 50 °C. Experimental data from this study and from Refs. [16,25]. Lines are the model fits; parameters are given in Table 1.

Table 1
Single component isotherm model parameters.

	H_2SO_4	Glucose	Xylose	Acetic acid	Furfural
q_{sat} or τ	−1.75	1.1	1.26	8.28	1.82
ω_1	2.75	0.13	0.14	0.076	1.52
ω_2	0.06	0.03	0.03	0	0

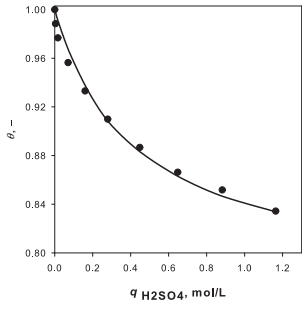

Fig. 2. Effect of q_{H2SO4} on the shrinking of CS16GC resin at a temperature of 50 °C. Experimental data from Ref. [16]. Line is the model fit (Eq. (16)).

presence of H_2SO_4 (Fig. 3 inset): the slopes of the calculated monosaccharide isotherms (q_i/C_i values) first decrease then pass through a minimum and finally begin to increase in the presence of H_2SO_4. This property does not originate from using the quadratic isotherm model (which can generate inflection points). Instead, the phase equilibrium predicts favorable isotherms for the monosaccharides unless the shape is shifted to unfavorable behavior using liquid phase activity coefficients. At low monosaccharide concentrations this correction effect disappears because the system becomes nearly ideal. As a result, the calculated isotherms are favorable at low concentrations and unfavorable at higher concentrations (Fig. 3).

The inflection points in the monosaccharide isotherms become less notable as the sulfuric acid concentration increases (Fig. 3). To eliminate these completely, adsorbed phase activity coefficients of the monosaccharides different from unity could be used. This, however, would increase the amount of parameters considerably, and was therefore omitted from this study.

Acetic acid sorption also increases considerably with increasing sulfuric acid concentration (Fig. 4). The fits of the isotherms calculated with the phase equilibrium model to the experimental sorption data are excellent in this binary system when the liquid phase activities are taken into account.

Salting out due to H_2SO_4 also increases the sorption of furfural. However, due to the largely different sorption strengths of H_2SO_4 and furfural, zero values were used for the interaction parameters of this pair. As will be shown below, the prediction of the furfural elution in the pulse injection cases was good even without these parameters.

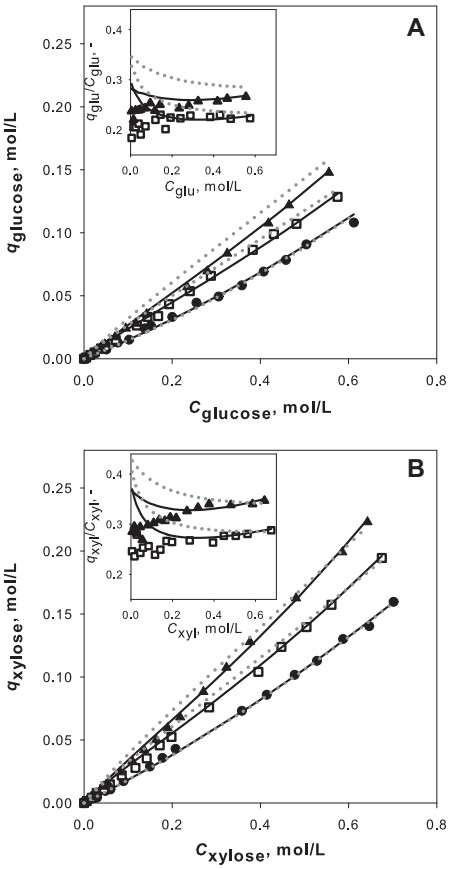

Fig. 3. Sorption of glucose (A) and xylose (B) from water and from sulfuric acid solutions on CS16GC resin at a temperature of 50 °C. Experimental data from Refs. [16,25]. Symbols: (●) water, (□) 0.97 mol/L H_2SO_4, and (▲) 1.84 mol/L H_2SO_4. Black solid lines are calculated with liquid phase activities; gray dotted lines are calculated without liquid phase activities. Inset: Slopes of the calculated monosaccharide isotherms in the presence of H_2SO_4. Model parameters are given in Tables 1 and 2.

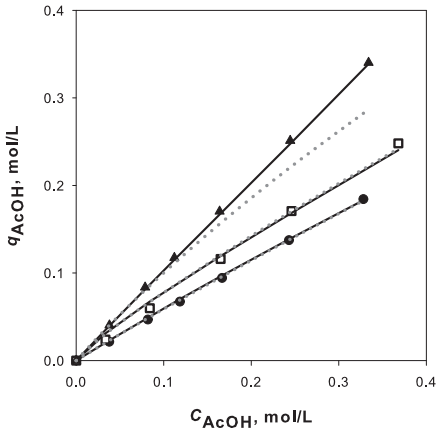

Fig. 4. Sorption of acetic acid from water and from sulfuric acid solutions on CS16GC resin at a temperature of 50 °C. Experimental data from Refs. [16,25]. Symbols: (●) water, (□) 1.0 mol/L H_2SO_4, and (▲) 4.0 mol/L H_2SO_4. Black solid lines are calculated with liquid phase activities; gray dotted lines are calculated without liquid phase activities. Model parameters are given in Tables 1 and 2.

4.2. Multi-component adsorption equilibria and column dynamics with the phase equilibrium model

Predictions of the phase equilibrium model in four and five component systems were validated with experimentally determined responses to pulse injections (five components) as well as with loading and elution curves (four components).

The values of dispersion and diffusion coefficients were obtained by fitting the calculated column profiles to the experimental ones. The averaged value of dispersion coefficient was 6.0×10^{-8} m^2/s for all components. Estimated diffusion coefficients were 3×10^{-10} m^2/s, 5×10^{-10} m^2/s, 4×10^{-10} m^2/s, 5×10^{-10} m^2/s, and 1×10^{-10} m^2/s for sulfuric acid, glucose, xylose, acetic acid, and furfural, respectively.

4.2.1. Pulse injections

Pulse injection experiments were done with a synthetic solution containing sulfuric acid, glucose, xylose, acetic acid, and furfural. Column loadings in the experiments were 0.102, and 0.204 bed volumes. The experimental and calculated chromatograms are shown in Fig. 5.

The fit of the model to the experimental profiles is good considering the complexity of the system (Fig. 5). The dotted line in Fig. 5 represents the H_2SO_4 sorption predicted by the IAS theory. The rear shock of the H_2SO_4 profile lies to the right of the experimental data, which means that the sulfuric acid sorption calculated with IAS theory is too strong. The solid line is the H_2SO_4 sorption calculated with the proposed phase equilibrium model using Eq. (19) for the adsorbed phase activity coefficient of H_2SO_4. In this case, the correlation between the model results and the experimental data is good (Fig. 5).

The front of the sulfuric acid profile is correctly predicted by the model: the break through point of sulfuric acid is approximately at the void volume of the column, and the diffuse front is similar to

Table 2
Parameters for the Pitzer activity coefficient model.

	H_2SO_4	Glucose	Xylose	Acetic acid	Furfural
A or λ_0	3.36	0.03	0.017	0.003	−0.427
β_0 or λ_1	0.46	−0.008	−0.002	−0.168	0.334
β_1 or $\chi^{(0)}$	6.37	0.113	0.097	0.084	0.0
C_ϕ or $\chi^{(1,0)}$	−0.03	−0.299	−0.234	−0.201	0.0
$\chi^{(1,1)}$	–	0.037	0.054	0.082	0.0
α_{NMX}	–	0.65	0.65	0.65	0.65

the one in the experimental profile (Fig. 5). At high sulfuric acid concentrations there exists some deviation between the experimental and simulated results. These deviations are partly due to inaccuracies in the chemical analyses.

Without using the H_2SO_4 adsorbed phase activity coefficient model (i.e., with the IAS theory), the sorption of glucose and xylose would also be predicted as too strong (data not shown). This stems from the strong co-operative effect of sulfuric acid on their sorption. With the adsorbed phase activity coefficient model for H_2SO_4, the glucose and xylose profiles are well predicted (Fig. 5).

The co-operative effect of H_2SO_4 on the sorption of the monosaccharides affects their elution profiles. The fronts of the monosaccharide profiles are elongated because sulfuric acid slows down their propagation and the effect is the stronger the higher the acid concentration. However, the model predicts that a somewhat too high amount of the monosaccharides elutes in the elongated fronts (Fig. 5). This can be seen more clearly for glucose than for xylose. The reason for this is the inflection point in the calculated monosaccharide isotherms (see Fig. 3): the isotherms are favorable (competitive sorption) at low concentrations and unfavorable (co-operative sorption) at higher concentrations. As a result the model predicts too large amount of monosaccharides in the elongated fronts of the corresponding profiles.

The co-operative effect of H_2SO_4 on the monosaccharide sorption causes focusing of the monosaccharides at the rear of the H_2SO_4 profile (Fig. 5). This kind of focusing effect can occur when the change of some thermodynamic variable (in this case, H_2SO_4 concentration) causes a large change in the sorption of the adsorbates [35]. After some separation has been achieved, the front parts of the monosaccharide profiles still elute under sulfuric acid and are slowed down, but the rear parts of the profiles are not affected anymore and therefore propagate faster than the fronts. This results in the focusing of the monosaccharide profiles (Fig. 5). In this case the focusing effect is beneficial for the process efficiency (higher concentration of products). The observed and described effect has been rarely seen in chromatography.

The focusing of xylose is well predicted by the model (Fig. 5). However, for glucose, the model predicts slightly weaker focusing than obtained in the experiments (Fig. 5). This is probably due to the slightly erroneous prediction of the front part of the glucose profile.

The elution of acetic acid is accurately predicted by the model (Fig. 5). Acetic acid does not have an elongated front part of the profile due to H_2SO_4 like the monosaccharides, and focusing of acetic acid does not occur (Fig. 5). Acetic acid is so quickly separated from sulfuric acid that the co-operative effect of sulfuric acid basically only increases the retention time of acetic acid. The anomalies seen in the calculated monosaccharide profiles (Fig. 5) do not stem from acetic acid because it is quickly separated from the monosaccharides.

Furfural elution is also accurately predicted by the model without the χ-parameters for furfural–H_2SO_4 pair (Fig. 5). The retention time of furfural in the pulse injections is same as when furfural is injected as a sole component (data not shown). This is because furfural is quickly separated from the other components and because the effects of the other components on furfural sorption compensate each other. The co-operative effect of sulfuric acid and monosaccharides on furfural sorption is compensated by the competitive effect introduced by acetic acid.

If shrinking of the resin is not included in the model, the calculated sorption is too strong and the calculated profiles are shifted to the right. In practice, shrinking of resin is problematic because

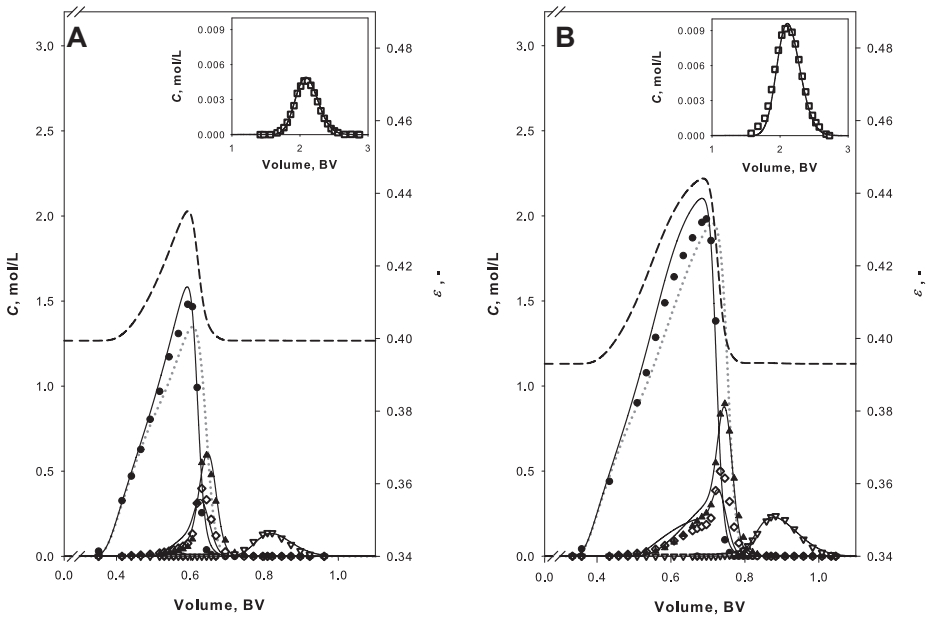

Fig. 5. Elution profiles of 0.102 BV (A) and 0.204 BV (B) pulses of synthetic hydrolysate solution with CS16GC resin at a temperature of 50 °C. Feed composition: 2.22 mol/L sulfuric acid, 0.24 mol/L glucose, 0.38 mol/L xylose, 0.16 mol/L acetic acid, and 0.022 mol/L furfural. Experimental conditions: u = 0.5 cm/min, ε_{ref} = 0.395, for other details see Ref. [16]. Symbols: see caption of Fig. 1. Black solid lines are calculated with the RAS theory; gray dotted line is the sulfuric acid profile calculated with the IAS theory; black dashed line is calculated ε at column outlet. Inset: elution profile of furfural. Model parameters are given in Tables 1 and 2.

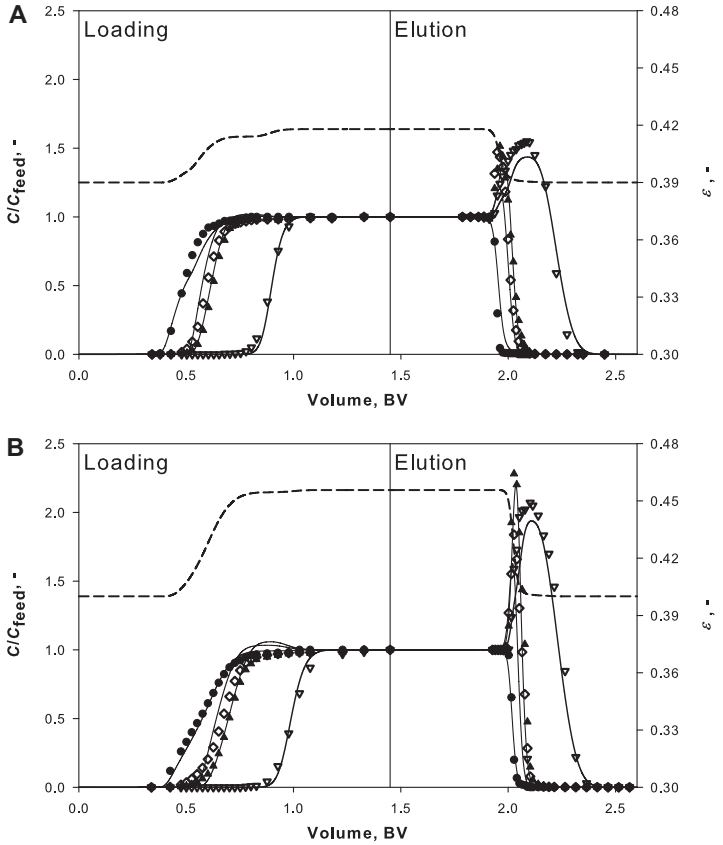

Fig. 6. Loading and elution curves of synthetic hydrolysate solution with CS16GC resin at a temperature of 50 °C. Feed composition: 1.05 mol/L (10 wt.%) (A) or 2.28 mol/L (20 wt.%) (B) sulfuric acid together with 0.27 mol/L glucose, 0.31 mol/L xylose, and 0.18 mol/L acetic acid. Experimental conditions and symbols: See captions of Figs. 1 and 5. Model parameters are given in Tables 1 and 2.

it increases dispersion in particular at the top of the column. In the present case, however, self-sharpening of the rear of the sulfuric acid profile decreases this effect to some extent.

4.2.2. Loading and elution curves

In addition to pulse injections, loading and elution curves were measured to validate predictions of the multi-component adsorption equilibria. In the loading step, solutions containing sulfuric acid, glucose, xylose, and acetic acid were fed to the column. The adsorbed components were eluted from the column with pure water in the elution step. Measured and calculated loading and elution curves are shown in Fig. 6.

The experimental loading curves do not have overshoots during the loading steps as is typical for components having unfavorable isotherms (Fig. 6). Breakthrough of sulfuric acid is at the void volume of the column because of complete electrolyte exclusion. By comparing the loading curves obtained for 10 wt.% (Fig. 6A) and 20 wt.% (Fig. 6B) H_2SO_4, the co-operative effect of sulfuric acid on the sorption of the other components can clearly be seen: their sorption increases with increasing C_{H2SO4} in the feed solution. In the loading step, the separation between the monosaccharides and sulfuric acid is poor. However, acetic acid is well separated from the other components (Fig. 6), due to the clearly higher sorption compared to the other components.

From the experimental elution profiles (Fig. 6) it can be seen that also during elution acetic acid is well separated from the other components. In the elution step, sulfuric acid concentration decreases to zero while, simultaneously, focusing of the other components occurs (Fig. 6). Contrary to the pulse injection profiles (see Fig. 5), focusing of acetic acid at the rear of the sulfuric acid profile can be clearly seen in both elution curves (Fig. 6). Also in the case of acetic acid, the focusing stems from the co-operative effect of H_2SO_4 on the sorption of acetic acid (see previous section).

Similar overshoots in an elution profile have been observed for monosaccharides on a gel type cation exchange resin in calcium form [28], and during chromatographic separation of salts on nanoporous non-ionic adsorbents and correlated with a thermodynamic model [36,37]. In the latter systems, two cations of different hydrated size, but with a common anion, are separated according to the size exclusion effect if their common anion can access the pores of the packing material freely. A strong overshoot in the elution profile of the smaller cation is formed because it is concentrated into the pores of the packing material in the same manner as the monosaccharides and acetic acid are concentrated in the

resin in the presence of sulfuric acid. The main difference between the two systems is that enhanced sorption in the electrolyte separation stems from steric exclusion of one of the cations whereas here it stems from molecular interactions in the liquid phase.

The characteristic features of the loading and elution profiles are well reproduced with the proposed dynamic model using the phase equilibrium model (Fig. 6). However, there are some anomalies in the calculated curves that cannot be seen in the experimental profiles. Firstly, the predicted loading curves of sulfuric acid become less steep than the experimental curves at the breakthrough point of the monosaccharides. This is more clearly seen with the lower feed concentration of sulfuric acid (Fig. 6A) and stems from the influence of monosaccharides on the adsorbed phase activity coefficient of H_2SO_4. Secondly, the calculated monosaccharide profiles are too steep at low concentrations and exhibit slight overshooting before reaching the feed concentration level (Fig. 6). These features originate from the nature of the phase equilibrium model: it predicts competitive sorption between the monosaccharides and acetic acid. This competition results in displacement of the monosaccharides from the adsorbed phase by acetic acid and is seen as overshoots in the calculated monosaccharide profiles after the fronts (Fig. 6). However, sorption on an elastic adsorbent can occur without competition and therefore the experimental loading profiles lack these overshoots (Fig. 6).

Use of linear isotherm model for acetic acid does not eliminate the competition between the monosaccharide and acetic acid sorption (data not shown). However, it can be erased by taking into account interactions between different neutral species in the Pitzer model or by using adsorbed phase activity coefficients for these species. This approach was not followed here because it would drastically increase the amount of adjustable parameters.

5. Conclusions

The co-operative and competitive sorption of strong and weak electrolytes and non-electrolytes on an elastic ion exchange resin was studied. An Adsorbed Solution theory, with a novel method to solve the corresponding equations, which takes into account non-idealities in both the adsorbed and the liquid phase, was used to calculate the multi-component adsorption equilibria. Adsorption of concentrated acid lignocellulosic hydrolysates (mainly sulfuric acid, monosaccharides, acetic acid, and furfural) on a strong acid cation exchange resin was used as a test case in this study. Due to the complexity of the system studied, activities for both liquid and adsorbed phases were used. Liquid phase activity coefficients were calculated using the well-known Pitzer model. Adsorbed phase activity coefficients were calculated for sulfuric acid with an empirical equation. For other components, adsorbed phase activity coefficients were taken as unity.

The predictions of the phase equilibrium model were applied in a dynamic model which takes bed porosity changes into account and validated with experimental column data. It was shown that the novel method to solve the Adsorbed Solution theory equations can be applied to complex systems. It is easy to code, and it is considerably faster than the traditional iterative solution method.

The studied phase equilibrium model could represent relatively well but not precisely the adsorption equilibria considered. Firstly, the predictions can be quite sensitive with respect to even minor inaccuracies in the calculated multi-component adsorption isotherms, and therefore even small anomalies in the isotherms can reduce the prediction accuracy. This could be seen with the monosaccharide sorption in presence of H_2SO_4: the Adsorbed Solution theory with the liquid phase activities gave a good fit of the calculated results to the experimental data, but for both monosaccharides the model predicted an inflection point in the binary isotherms with H_2SO_4. Secondly, the Adsorbed Solution theory tended to predict competitive sorption between different species. However, in the case of elastic adsorbents, sorption can also occur without competition which leads to slightly erroneous predictions with the model. In the test system studied here, the model predicted falsely competitive sorption between the monosaccharides and acetic acid resulting in slightly erroneous predictions in some cases.

The predictions of the phase equilibrium model could be improved by taking into account the interactions between neutral species, and by using adsorbed phase activities for the neutral species. This, however, would drastically increase the amount of parameters. When taken into account the simplifying assumptions, the complexity of the studied system, and the nature of the Adsorbed Solution theory, the predictions were satisfactory in the studied test case.

Acknowledgements

The authors are grateful for the support of Prof. D. Flockerzi in solving the equations of the multi-component phase equilibrium model. Financial support from the Academy of Finland (Grant SA/121280) is gratefully acknowledged. J.H. thanks the Graduate School in Chemical Engineering (Finland) for personal Grant.

Appendix A. Estimation of Pitzer model interaction parameters

A.1. Neutral–neutral parameters

For glucose and xylose, the pure component λ_{NN} parameters (Eq. (18)) were obtained by fitting equation [14]

$$\phi_N - 1 = (\lambda_{NN}^{(0)} + \lambda_{NN}^{(1)} \exp(1 - \alpha_{NN}\sqrt{m_N}) m_N, \quad (A.1)$$

to experimental osmotic coefficient ϕ_N data at a temperature of 25 °C from Refs. [38,39]. λ_{NN} parameters for acetic acid and furfural were obtained by fitting Eq. (18) (m_{MX} = 0 mol/kg H_2O) to activity coefficient data. Acetic acid activity coefficient data was obtained from Refs. [40,41]. The activity coefficient data for furfural was calculated from vapor liquid equilibrium (VLE) data from Ref. [42] by using Raoult's law (assumption of ideal gas phase)

$$y_{Furfural} p^{tot} = \gamma_{Furfural}^{(x)} x_{Furfural} p_{Furfural}^{sat}, \quad (A.2)$$

where $y_{Furfural}$ and $x_{Furfural}$ are gas and liquid phase mole fractions, respectively, p^{tot} is the total pressure of the system, $\gamma_{Furfural}^{(x)}$ is activity coefficient on mole fraction scale, and $p_{Furfural}^{sat}$ is saturation (pure component) pressure. $p_{Furfural}^{sat}$ at a temperature of 50 °C was calculated using the Antoine equation (parameters from Ref. [43]).

Activity coefficients obtained from VLE data are on symmetrical scale (γ_i approaches unity as x_i approaches unity) while Eq. (18) is on unsymmetrical scale (γ_i approaches unity as x_i approaches zero; i is not solvent) [44]. The change from symmetrical to unsymmetrical scale was done with

$$\gamma_{i,unsym.}^{(x)} = \frac{\gamma_{i,sym.}^{(x)}}{\gamma_i^{(x),\infty}}, \quad i = 1, n, \quad (A.3)$$

where $\gamma_i^{(x),\infty}$ is activity coefficient at infinite dilution and subscripts unsym. and sym. stand for unsymmetrical and symmetrical, respectively [44]. $\gamma_{AcOH}^{(x),\infty}$ was obtained from Ref. [41], and $\gamma_{Furfural}^{(x),\infty}$ by extrapolating the activity coefficient data calculated from data in Ref. [42].

Finally, $\gamma_{i,unsym.}^{(x)}$ was changed from mole fraction scale to molality scale with

$$\gamma_{i,unsym.}^{(m)} = \frac{\gamma_{i,unsym.}^{(x)}}{1 + 0.001 M_{Solvent} m_i}, \quad (A.4)$$

where $M_{Solvent}$ is molar mass of solvent [45]. The molal concentration m_i was calculated from

$$m_i = \frac{w_i 1000}{M_i(1 - w_i)}, \quad (A.5)$$

where w_i is weight fraction of component i in the solution [46]:

$$w_i = \frac{x_i M_i}{M_s - x_i M_s + x_i M_i}. \quad (A.6)$$

A.2. Neutral-electrolyte parameters

χ and α_{NMX} interaction parameters (Eq. (18)) were estimated by fitting the predictions of the phase equilibrium model for binary mixtures of neutral component and sulfuric acid to corresponding experimental sorption data. However, for furfural χ parameters were set to zero due to the largely different sorption strengths of H_2SO_4 and furfural.

Appendix B. Other unit conversions

Calculation of activity coefficients with the Pitzer equations were done on molality scale. The activity coefficients obtained with the Pitzer equations were converted to molarity scale with [45]

$$\gamma_i^{(c)} = \frac{m_i \rho_{Solvent}}{C_i} \gamma_i^{(m)}, \quad (B.1)$$

where m_i and C_i are molal and molar concentrations of i, respectively and $\rho_{Solvent}$ is the density of the solvent (water: 0.988 g/cm^3 at 50 °C [47]).

Molality of component i in solution was calculated from the molar concentration with

$$m_i = \frac{C_i}{\rho_{Soln} - \frac{\sum_{i=1}^{n} C_i M_i}{1000}}, \quad (B.2)$$

where ρ_{Soln} is density of the solution, and M_i is molar mass (Table B.1). Density of the solution was calculated with

$$\rho_{Soln} = \frac{\sum x_i M_i + x_S M_S}{\sum x_i V^*_{m,i} + x_S V^*_{m,S}}, \quad (B.3)$$

where $V^*_{m,i}$ is the molar volume of the pure component i:

$$V^*_{m,i} = \frac{M_i}{\rho^*_i}, \quad (B.4)$$

where ρ^*_i is the density of pure component i. The pure component densities used in this study are given in Table B.1. The following equation was derived for x_i needed in Eq. (B.3)

$$x_i = \frac{C_i}{C_{H2O^*} - 15.3676(\sum_i^n C_i)^{0.3567}}, \quad (B.5)$$

where C^*_{H2O} is the concentration of water in pure water (i.e. 54.84 mol/L at 50 °C temperature). The constants in Eq. (B.5) were estimated using experimental density data.

Table B.1
Molar masses and densities of pure components at a temperature of 50 °C [47].

Component	M, g/mol	ρ^0, g/cm^3
Sulfuric acid	98.079	1.801
Glucose	180.155	1.562
Xylose	150.130	1.525
Acetic acid	60.052	1.048
Furfural	96.085	1.159

References

[1] D.D. Do, Adsorption Analysis: Equilibria and Kinetics, Imperial College Press, London, Great Britain, 1998.
[2] A.L. Myers, J.M. Prausnitz, Thermodynamics of mixed-gas adsorption, AIChE J. 11 (1965) 121–127.
[3] C.J. Radke, J.M. Prausnitz, Thermodynamics of multi-solute adsorption from dilute liquid solutions, AIChE J. 18 (1972) 761–768.
[4] E. Costa, J.L. Sotelo, G. Calleja, C. Marrón, Adsorption of binary and ternary hydrocarbon gas mixtures on activated carbon: experimental determination and theoretical prediction of the ternary equilibrium data, AIChE J. 27 (1981) 5–12.
[5] A.L. Myers, Activity coefficients of mixtures adsorbed on heterogeneous surfaces, AIChE J. 29 (1983) 691–693.
[6] O. Talu, I. Zwiebel, Multicomponent adsorption equilibria of nonideal mixtures, AIChE J. 32 (1986) 1263–1276.
[7] D.G. Steffan, A. Akgerman, Thermodynamic modeling of binary and ternary adsorption on silica gel, AIChE J. 47 (2001) 1234–1246.
[8] S. Sochard, N. Fernandes, J.-M. Reneaume, Modeling of adsorption isotherm of a binary mixture with real adsorbed solution theory and nonrandom two-liquid model, AIChE J. 56 (2010) 3109–3119.
[9] A. Erto, A. Lancia, D. Musmarra, A Real Adsorbed Solution theory model for competitive multi-component liquid adsorption onto granular activated carbon, Micropor. Mesopor. Mater. 154 (2012) 45–50.
[10] H.O. Rubiera Landa, D. Flockerzi, A. Seidel-Morgenstern, Prediction of competitive adsorption equilibria for general single component adsorption isotherm shapes using the ideal adsorbed solution theory, in: Lecture Nr. L213, 24th International Symposium on Preparative Chromatography, 10–13.7.2011, Boston, USA.
[11] H.O. Rubiera Landa, D. Flockerzi, A. Seidel-Morgenstern, A method for efficiently solving the IAST equations with an application to adsorber dynamics, AIChE J., submitted for publication.
[12] K.S. Pitzer, Thermodynamics of electrolytes. I. Theoretical basis and general equations, J. Phys. Chem. US 77 (1972) 268–277.
[13] K.S. Pitzer, Ion interaction approach: theory and data correlation, in: K.S. Pitzer (Ed.), Activity Coefficients in Electrolyte Solutions, CRC Press, Boca Raton, United States, 1991, pp. 75–154.
[14] L. Fernández-Mérida, R. Rodríguez-Raposo, G.E. García-García, M.A. Esteso, Modification of the Pitzer equations for application to electrolyte + polar non-electrolyte mixtures, J. Electroanal. Chem. 379 (1994) 63–69.
[15] F. Helfferich, Ion Exchange, Dower Publications Inc., Mineola, New York, United States, 1995.
[16] J. Heinonen, T. Sainio, Modelling and performance evaluation of chromatographic monosaccharide recovery from concentrated acid lignocellulosic hydrolysates, J. Chem. Technol. Biotechnol. (2012), http://dx.doi.org/10.1002/jctb.3816.
[17] M.I. Durão, C.A.V. Costa, A.E. Rodrigues, Saturation and regeneration of ion exchangers with volume changes, Ind. Eng. Chem. Res. 31 (1992) 2564–2572.
[18] J. Tiihonen, T. Sainio, A. Kärki, E. Paatero, Co-eluent effect in partition chromatography. Rhamnose–xylose separation with strong and weak cation-exchangers in aqueous ethanol, J. Chromatogr. A 982 (2002) 69–84.
[19] T. Sainio, E. Paatero, Mass coordinates for dynamic simulation of column operations involving dimensional changes of packing material, Comput. Chem. Eng. 31 (2007) 374–383.
[20] M. Mazzotti, B. Neri, D. Gelosa, M. Morbidelli, Dynamics of a chromatographic reactor: esterification catalyzed by acidic resins, Ind. Eng. Chem. Res. 36 (1997) 3163–3172.
[21] R.A. Marra, D.O. Cooney, Equilibrium theory for sorption accompanied by sorbent bed shrinking or swelling, AIChE J. 19 (1973) 181–183.
[22] R.A. Marra, D.O. Cooney, Multicomponent sorption operations: bed shrinking and swelling in an ion exclusion case, Chem. Eng. Sci. 33 (1978) 1597–1601.
[23] J. Heinonen, T. Sainio, Chromatographic recovery of monosaccharides for the production of bioethanol from wood, Ind. Eng. Chem. Res. 49 (2010) 3713–3729.
[24] G. Guiochon, S.G. Shirazi, A.M. Katti, Fundamentals of Preparative and Non-Linear Chromatography, Academic Press Inc., London, Great Britain, 1994.
[25] M. Laatikainen, J. Heinonen, T. Sainio, Modeling of chromatographic separation of concentrated-acid hydrolysates, Sep. Purif. Technol. 80 (2011) 610–619.
[26] C.B. Ching, C. Ho, K. Hidajat, D.M. Ruthven, Experimental study of a simulated counter-current adsorption system-V. Comparison of resin and zeolite absorbents for fructose–glucose separation at high concentration, Chem. Eng. Sci. 42 (1987) 2547–2555.
[27] J.A. Vente, H. Bosch, A.B. de Haan, P.J.T. Bussmann, Evaluation of sugar sorption isotherm by frontal analysis under industrial processing conditions, J. Chromatogr. A 1066 (2005) 71–79.
[28] J. Nowak, K. Gedicke, D. Antos, W. Piatkowski, A. Seidel-Morgenstern, Synergistic effects in competitive adsorption of carbohydrates on an ion-exchange resin, J. Chromatogr. A 1164 (2007) 224–234.
[29] J. Nowak, I. Poplewska, D. Antos, A. Seidel-Morgenstern, Adsorption behaviour of sugars versus their activity in single and multicomponent liquid solutions, J. Chromatogr. A 1216 (2010) 8697–8704.
[30] Y.C. Wu, D. Feng, The second dissociation constant of sulfuric acid at various temperatures by the conductometric method, J. Solut. Chem. 24 (1995) 133–144.

[31] S.L. Clegg, J.A. Rard, K.S. Pitzer, Thermodynamic properties of 0–6 mol kg^{-1} aqueous sulfuric acid from 273.15 to 328.15 K, J. Chem. Soc. Faraday Trans. 90 (1994) 1875–1894.
[32] H.S. Harned, R.W. Ehlers, The dissociation constant of acetic acid from 0 to 60 °C centigrade, J. Am. Chem. Soc. 55 (1933) 652–656.
[33] J.S. Mackie, P. Meares, The diffusion of electrolytes in a cation-exchange resin membrane. I. Theoretical., Proc. Roy. Soc. A232 (1955) 498–509.
[34] W.E. Schiesser, The Numerical Method of Lines, Academic Press Inc., San Diego, United States, 1991.
[35] P.C. Wankat, Rate-Controlled Separations, Elsevier Science Publishers Ltd., Essex, Great Britain, 1990.
[36] M. Laatikainen, T. Sainio, V. Davankov, M. Tsyurupa, Z. Blinnikova, E. Paatero, Chromatographic separation of a concentrated HCl–$CaCl_2$ solution on non-ionic hypercrosslinked polystyrene, React. Funct. Polym. 67 (2007) 1589–1598.
[37] M. Laatikainen, T. Sainio, V. Davankov, M. Tsyurupa, Z. Blinnikova, E. Paatero, Modeling of size-exclusion chromatography of electrolytes on non-ionic nanoporous adsorbents, J. Chromatogr. A 1149 (2007) 245–253.
[38] K. Miyajima, M. Sawada, M. Nakagaki, Studies on aqueous solutions of saccharides. I. Activity coefficients of monosaccharides in aqueous solutions at 25 °C, Bull. Chem. Soc. Jpn. 56 (1983) 1620–1623.
[39] H. Uedaira, H. Uedaira, Activity coefficients of aqueous xylose and maltose solutions, Bull. Chem. Soc. Jpn. 42 (1969) 2137–2140.
[40] Acetic acid/Water–Vapor–Liquid Equilibrium, Activity Coefficient, VLE-15.1980 (DECHEMA), DETHERM – Thermophysical Properties of Pure Substances & Mixtures, 2011. <http://i-systems.dechema.de/detherm>.
[41] Acetic Acid/Water – Activity Coefficients at Infinite Dilution, PRP-18840d.1959 (DDB), DETHERM – Thermophysical Properties of Pure Substances & Mixtures, 2011. <http://i-systems.dechema.de/detherm>.
[42] Water/2-Furancarboxaldehyde – Isothermal VLE-Data (xyp), VLE-1113d.1970 (DDB), DETHERM – Thermophysical Properties of Pure Substances & Mixtures, 2011. <http://i-systems.dechema.de/detherm>.
[43] 2-Furancarboxaldehyde, NIST Chemistry webBook, 2011. <http://webbook.nist.gov/chemistry>.
[44] J.M. Prausnitz, R.N. Lichtenthaler, E.G. de Acevedo, Molecular Thermodynamics of Fluid-Phase Equilibria, PTR Prentice Hall Inc., Englewood Cliffs, United States of America, 1986.
[45] A.L. Horvath, Handbook of Aqueous Electrolyte Solutions, Ellis Horwood Ltd., Southampton, Great Britain, 1985.
[46] J.W. Mullins, Crystallization, third ed., Reed Educational and Professional Publishing Ltd., Cornwall, Great Britain, 1997.
[47] D.R. Lide (Ed.), CRC Handbook of Chemistry and Physics, 91st ed., Internet Version, 2011. <http://www.hbcpnetbase.com>.

Errata

In this paper, an erroneous form of Eq. (18) is provided due to a printing error. The correct form of Eq. (18) is:

$$\begin{aligned}\ln\gamma_{\mathrm{N}}^{(\mathrm{m})} = {} & 2m_{\mathrm{N}}\left\{\lambda_{\mathrm{NN}}^{(0)} + \frac{\lambda_{\mathrm{NN}}^{(1)}}{\left(\alpha_{\mathrm{NN}}\right)^2 m_{\mathrm{N}}}\left[1-\left(1+\alpha_{\mathrm{NN}}\sqrt{m_{\mathrm{N}}}-\frac{\left(\alpha_{\mathrm{NN}}\right)^2 m_{\mathrm{N}}}{2}\right)\exp\left(-\alpha_{\mathrm{NN}}\sqrt{m_{\mathrm{N}}}\right)\right]\right\} \\ & + 2m_{\mathrm{MX}}\left\{\chi^{(0)} + \frac{2\chi^{(1,0)}}{\left(\alpha_{\mathrm{NMX}}\right)^2 I_{\mathrm{m}}}\left[1-\left(1+\alpha_{\mathrm{NMX}}\sqrt{I_{\mathrm{m}}}\right)\exp\left(-\alpha_{\mathrm{NMX}}\sqrt{I_{\mathrm{m}}}\right)\right]\right. \\ & \left. + m_{\mathrm{N}}\frac{4\chi^{(1,1)}}{\left(\alpha_{\mathrm{NMX}}\right)^2 I_{\mathrm{m}}}\left[1-\left(1+\alpha_{\mathrm{NMX}}\sqrt{I_{\mathrm{m}}}\right)\exp\left(-\alpha_{\mathrm{NMX}}\sqrt{I_{\mathrm{m}}}\right)\right]\right\}\end{aligned} \quad . \quad \text{(A.1)}$$

PAPER V

Heinonen, J., Sainio, T., Electrolyte exclusion chromatography using a multi-column recycling process: Fractionation of concentrated acid lignocellulosic hydrolysate, submitted to *Separation and Purification Technology in 2013.*

Electrolyte exclusion chromatography using a multi-column recycling process: Fractionation of concentrated acid lignocellulosic hydrolysate

Jari Heinonen and Tuomo Sainio*

Lappeenranta University of Technology,
Laboratory of Separation Technology,
Skinnarilankatu 34, FIN-53850 Lappeenranta, Finland

*Corresponding author. Tel: +358-40-3578683, fax: +358-5-6212199, e-mail: tuomo.sainio@lut.fi

ABSTRACT

Use of a chromatographic multi-column process with an internal recycling for separation of electrolytes and non-electrolytes is investigated. The design of the process is simplified by utilizing the equilibrium theory of chromatography for developing a first sketch, which is then refined with numerical simulations. Fractionation of concentrated acid lignocellulosic hydrolysates was used as a model system. A four-column process scheme with four steps and closed loop recycling operation was developed. The process was validated experimentally using both synthetic solutions and authentic softwood hydrolysates. Good separation performance was achieved with both feed solutions. Recovery yield and purity were 98 % and 94 % for sulfuric acid, 85 % and 95 % for monosaccharides, and 88 % and 93 % for acetic acid. Due to implementation of internal recycling steps in the process, the eluent consumption was found to be 20 times lower than in a batch chromatographic process consisting of four parallel columns.

Keywords: simulated moving bed, multi-column chromatography, recycling, lignocellulose, hydrolysate, electrolyte exclusion

1. Introduction

Electrolyte exclusion chromatography (EEC) is an efficient method for the separation of strong electrolytes from weak electrolytes and nonelectrolytes [1,2]. Strong electrolytes are excluded from strong ion exchange resins completely or partially due to electrical repulsion caused by the fixed ionic groups in the resin [2]. In addition, the breakthrough volume of strong electrolytes equals the interstitial volume of the resin bed due to complete exclusion at infinite dilution [1,2]. Associated weak electrolytes and nonelectrolytes are unaffected by electrolyte exclusion and thus propagate through the column slower than strong electrolytes. No ion exchange occurs in the EEC unless the ions in the liquid phase are different to the exchangeable counterions in the resin phase.

Electrolyte exclusion chromatography is utilized for example in the chromatographic fractionation of sugar beet molasses into salt, sucrose, and betaine fractions [3-10]. For this purpose, Finnish Sugar Co. (now part of DuPont) has developed a multi-column process called Sequential Simulated Moving Bed process [3-9]. Despite its name, there is no similar counter-current movement of the liquid and stationary phases as in conventional simulated moving bed (SMB) processes as the inlet and outlet ports are not switched synchronously in the direction of the fluid flow during a cycle. In addition, in Sequential SMB, column outlet streams are not split at product collection nodes (extract and raffinate) as in conventional SMB processes. Instead, the whole stream is either taken out of the system or led to the next column. A common feature for both, conventional SMB and Sequential SMB, processes is their cyclic operation mode. Sequential SMB can be operated already with two columns, while typically three to eight columns are used [3-8,11].

Design methods of conventional SMB processes are well-known [12]. Since no such method is available for the Sequential SMB concept, the use of the equilibrium theory of chromatography [13] for the design is discussed here. From here on, we term the Sequential SMB as *Multi-Column Recycling Chromatography* (abbreviated as MCRC).

Recently, electrolyte exclusion chromatography has been successfully applied to the fractionation of concentrated acid lignocellulosic hydrolysates [14-19]. Such hydrolysates are intermediates in the production process of lignocellulose derived monosaccharides for chemical manufacturing. Polysaccharides (cellulose and hemicelluloses) in the lignocellulosic biomass are hydrolyzed to monosaccharides (e.g. glucose and xylose) with concentrated sulfuric acid as catalyst [14,20-22]. EEC has proven to be effective in fractionation of such hydrolysates into sulfuric acid, monosaccharide, and by-product fractions [14,15,18]. The sulfuric acid fraction is recycled back to the hydrolysis while the other fractions are taken to downstream processing. Sulfonated gel type strong acid PS–DVB cation exchange resins in acid form are typically used as stationary phase materials [15-17].

While batchwise EEC fractionation of concentrated acid hydrolysates has been investigated thoroughly [15-18,21-2632] studies regarding the use of multi-column chromatographic process schemes for this purpose are scarce [14,17,26,27]. Springfield and Hester [17,26] investigated the fractionation of a solution containing sulfuric acid (10 wt. %) and glucose (10 wt. %) using a four-zone SMB for binary separations. 98 % and 96 % yields were obtained for sulfuric acid and glucose, respectively [17]. Sun *et al.* [27] obtained 90.5 % pure sulfuric acid and 98.4 % pure monosaccharide streams in fractionation of concentrated acid (27 wt. % sulfuric acid) bamboo hydrolysate with Intermittent SMB [28]. Heinonen and Sainio [14] investigated the use of Japan Organo process [10,29,30] for ternary fractionation of concentrated acid hydrolysate by simulations. 97.3 % yield was obtained for sulfuric acid, 61.7 % for monosaccharides, and 93.5 % for acetic acid. Purities of the products were 89.0 %, 88.7 %, and 100 %, respectively [14]. So far, the use of the MCRC process for the fractionation of concentrated acid hydrolysates has not been investigated.

In this work, we first present the operating principle of MCRC process and discuss an equilibrium theory and numerical simulations based method to design it. This procedure is then demonstrated by designing an MCRC process scheme for the fractionation of concentrated acid lignocellulosic hydrolysates into three fractions: sulfuric acid, monosaccharides, and acetic acid. Further purification, e.g. removal of fermentation inhibitors, is best carried out by adsorption in a separate stage prior to the acid–monosaccharide separation [31] and is not considered here. Feasibility of the selected MCRC process scheme is investigated experimentally and evaluated using various performance indicators. In addition, the separation performance of the MCRC scheme is compared with a single-column batch process. Full optimization of the MCRC process for the fractionation of concentrated acid hydrolysates is beyond the scope of this study.

2. Multi-column recycling chromatography

2.1. Operating principle of MCRC process

A single cycle in MCRC consists of three types of operations: feeding, elution, and closed loop recycling (Fig. 1). Each operation is conducted at least once in a full cycle. They can be conducted in series or they can take place simultaneously. For example, recycling can be carried out in a closed loop of two columns while eluent is fed to and products are collected from other columns [3,4].

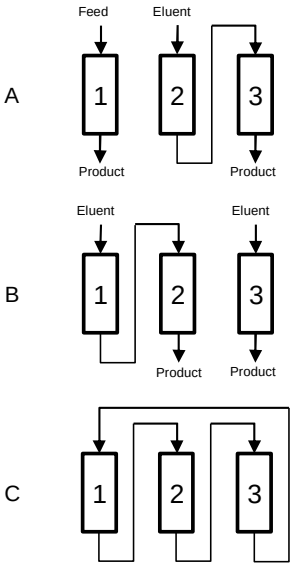

Figure 1. Operations carried out in a full cycle of Multi-Column Recycling Chromatography process. A = feeding; B = elution; C = closed loop recycling.

Typical operations of an MCRC cycle are illustrated in Fig 1. In feeding operation (Fig. 1A), the feed mixture is fed to at least one column. Simultaneously, eluent can be fed to at least one other column, and at least one product fraction is collected. If products are withdrawn from the same column where the feed is introduced into (Fig. 1A), the eluent consumption is typically reduced because the feed is used to elute the solutes in this column [3-8].

During the elution operation there is no feeding (Fig. 1B). The eluent is fed to at least one column and simultaneously product fractions are collected from at least one column [3,4]. The duration of this step depends on the purity constraints set.

In closed loop recycling operation, the solution in the system is circulated at least in one closed loop (Fig. 1C). No eluent or feed is introduced into the process and no products are withdrawn. Besides further separating the components, the purpose of such closed loop recycling is to adjust their positions relative to the outlets for product collection in the next step [3,4]. Eluent consumption can often be lowered considerably by the closed loop recycling.

If the separation of components is not sufficient at the outlet of the last column, the stream from the last column can be recycled to the first column to be processed during the following cycle. Such recycle fractions are termed as *prefeed fraction* (recycled before the next feeding) or *postfeed fraction* (recycled immediately after the next feeding). In ternary fractionation, the prefeed fraction typically contains the mixture of the first and the intermediate eluting components, whereas the postfeed fraction contains the mixture of the intermediate and the last eluting component.

Eluent consumption in MCRC process can be lowered also by reintroducing parts of the collected product fractions back to the process as eluent substitute. Position and time of such reintroduction must be so that the

components in these fractions do not end up as impurities in wrong product fractions. Such operation has positive effects on product yield and purity. [8]

2.2. Design of MCRC process

Since an MCRC process is a multi-column batch chromatographic process, it is natural to approach its design by using the ideal model and distance-time diagram [13] that are well known for single-column batch chromatographic separation. The theory of the design method is presented briefly in Appendix A. It is based on tracking the trajectories of constant concentration states as they travel through the column using the ideal model of chromatography and the sorption isotherm models. The trajectories are presented in so-called distance-time diagram. Durations of feed and elution steps are chosen such that the separation of the components is sufficient.

The use of the design method is demonstrated in Fig. 2A for the case of single-column batchwise fractionation of a binary mixture of a strong electrolyte and a nonelectrolyte. The elution behavior and separation of the component bands can be clearly seen from the distance-time diagram (Fig. 2A). The trajectories of the constant concentrations of component 1 (strong electrolyte) at the band front spread out while propagating through the column due the concave upward isotherm (see Eq. (A.5)). At the rear of component 1, a shock exists, as is typical for components with concave upward isotherms. The trajectory of this shock is linear until the point at which the feed plateau disappears (Fig. 2A). After this point, the trajectory of the rear shock becomes concave upward (Fig. 2A): as the peak shock concentration decreases, the propagation velocity of component 1 rear increases as a result from the shape of the isotherm. Due to the spreading of component 1 band, the difference between the front and rear of the band is larger at the column outlet than in the column inlet (Fig. 2A).

In the example shown in Fig. 2A, the sorption isotherm of component 2 (nonelectrolyte) is linear (see Eq. (A.6)). According to the ideal model, the band of this component does not spread out and each concentration state propagates through the column with equal velocity (Fig. 2A). As a result, the difference between the front and rear of the band is equal in the column inlet and outlet.

The fractionation cut-points (which fulfill the desired fractionation constraints) (Eqs. A.11 and A.12) and cycle time (Eq. A.13) can be determined on the basis of the distance-time diagram and ideal model from the points at which the trajectories of the constant concentrations exit the column. In addition, the maximum duration of feed to obtain complete separation (not the case in Fig. 2A) can be calculated using Eq. (A.9).

The design of an MCRC process with N columns is carried out similarly as that of single-column batch chromatography but the column is divided into N sections. Product fractions are collected from the section boundaries while simultaneously recycling or feeding eluent to upper sections. Collection time of components depends on the elution of the next eluting impurity to the section boundary, i.e. the time difference between the appearances of the band fronts of adjacent components to the outlet of same column.

A distance-time diagram representation of a three-column MCRC process for fractionation of a binary mixture of a strong electrolyte and a nonelectrolyte is shown in Fig. 2B. The total column length and the duration of the feed step are the same as in the case of the single-column batch process shown in Fig. 2A. The difference is collection of the separated parts of the component bands at the outlet of each section in the MCRC process (Fig. 2B). The distance-time diagrams of both processes would be equal if the components would be collected only at the outlet of the last section in the MCRC process.

The collection of the front of component 1 band at the outlet of each column in the MCRC process decreases the spreading of the band front considerably (Fig. 2B). Therefore, the lines describing the front of component 1 band emanate from a single point at the inlet of each section (Fig. 2B). The collection of component 1 between the sections does not affect the trajectory of the rear shock of this component: it is same as in the case of the single-column batch process (Fig. 2).

The collection of the separated parts of the rear of component 2 band is also done at the outlet of each section in the MCRC process (Fig. 2B). Because the isotherm is linear, fraction collection between the sections does not affect the shape of component 2 profile.

It is observed in Fig. 2 that the time between consecutive feed steps in MCRC process is considerably shorter than in the batch process for same loading factor. This is because collection of the separated components at the section boundaries narrows the component bands considerably. This allows more frequent injections. Alternatively, a much higher column loading can be applied with the MCRC process than with the single-column process during an equally long cycle.

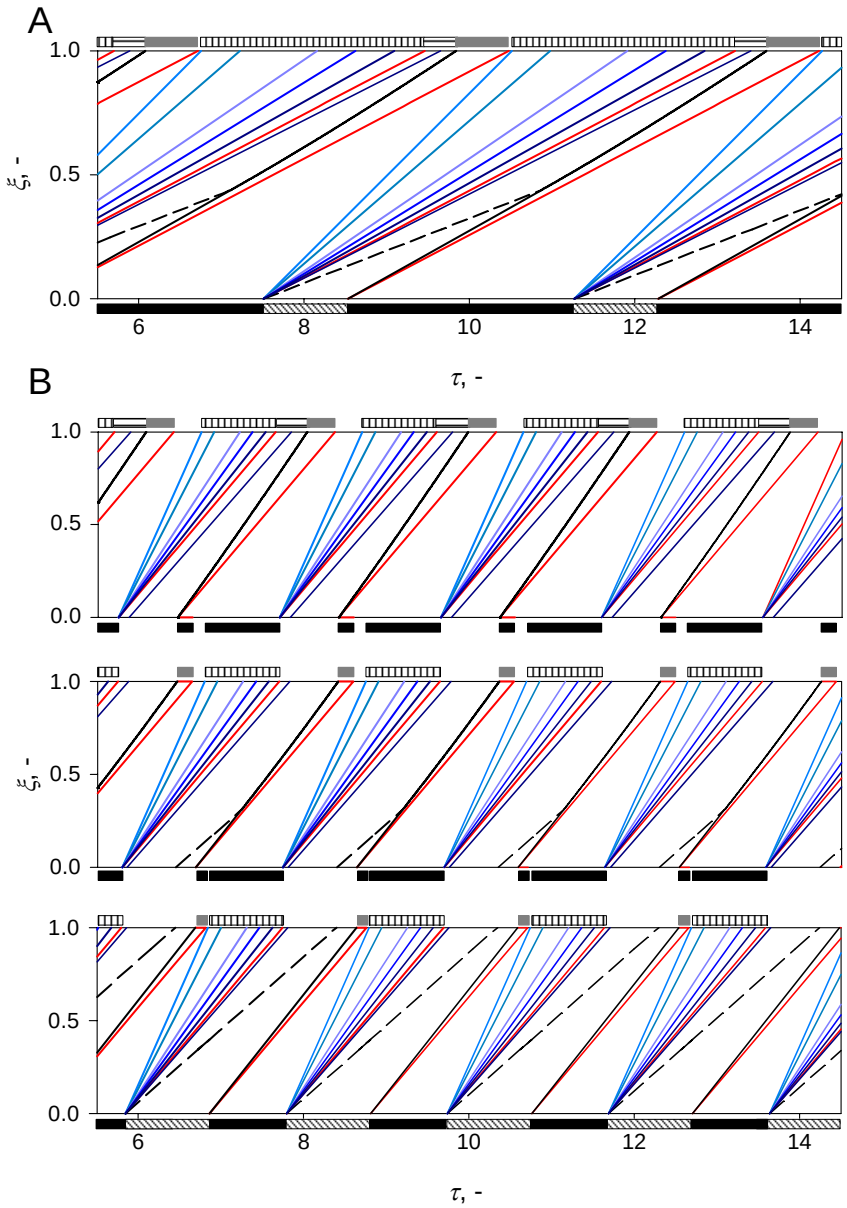

Figure 2. Distance-time diagrams of a single column batch chromatographic process (A; h_{bed} 3 m) and a three-column MCRC process (B; h_{bed} 1 m) for separation of a strong electrolyte (isotherm Eq. (A.5); $a_1 = 0.52$, $a_2 = 2$) and a nonelectrolyte (isotherm Eq. (A.6); $a_1 = 0.6$). Only a part of the τ axis is shown. Feed concentrations: 1 mol/L for each. Flow rates: 1 mL/min for all flows. Lines: blue = component 1 front; black = component 1 rear; red = component 2 front and rear; dashed line = trajectory of component 1 feed concentration. Bars: black bar = eluent introduction; bar with slashed lines = feed introduction; bar with vertical lines = collection of component one; grey bar = collection of component two; bar with horizontal lines = collection of mixed fraction.

A characteristic feature of electrolyte exclusion chromatography is that the strong electrolyte becomes increasingly diluted when the column length increases. The collection of the components at the outlet of each column in MCRC process minimizes the elution path (Fig. 2). Therefore, the MCRC also leads to more concentrated products when compared to the single column process.

The method outlined above gives a good starting point for detailed design of MCRC processes. The three-column MCRC process in Fig. 2B contains several steps in one cycle as the masses of four consecutive feed pulses are simultaneously inside the process. Numerical simulations should be used as a second step in the design procedure in order to reduce the number of steps in the process and to utilize closed loop recycling for lowering the eluent consumption. There are a few ways to accomplish this. Firstly, the inlet flow rates of each stream in each step can be adjusted so that component profiles are in suitable positions relative to the column outlets at the end of each step. Secondly, as very high product purity is often not needed, some process steps can be integrated. Thirdly, step durations can also be altered. In addition, due to the batchwise nature of the MCRC process, columns of different sizes can be used to obtain a simplified process [3-8].

3. Experimental

3.1. Materials and methods

Sulfonated gel type strong acid polystyrene–divinylbenzene cation exchange resin CS16GC (8 wt % DVB, Finex Oy, Finland) was used as a stationary phase. The resin was converted to acid form with 1 mol/L hydrochloric acid (37 %, pro analysi, Merck KGaA) using standard methods. The volumetric capacity of the resin was 1.93 mequiv (H^+)/mL, and average particle size 246 μm.

Pro analysis grade sulfuric acid (95–97 %, pro analysi, Merck KGaA), α-D-glucose (min. 99.5 %, Sigma–Aldrich Co.), D-(+)-xylose (min. 99 %, Sigma–Aldrich Co.), acetic acid (100 %, pro analysi, Merck KGaA), and purified and degassed water were used in the experiments. MCRC fractionation experiments were done at 50 °C temperature.

Two types of feed solutions were used: a synthetic solution presenting concentrated acid lignocellulosic hydrolysate and an authentic concentrated acid softwood hydrolysate (see Section 3.2). Synthetic feed solution contained 2.32 mol/L (20 wt. %) sulfuric acid, 0.35 mol/L glucose, 0.35 mol/L xylose, and 0.16 mol/L acetic acid.

The experimental setup used in this study consisted of six HPLC pumps (Intelligent pump AI-12, Flom Co.), eight 12-port motor valves (RV-750-116, IDEX Health & Science Group), two solenoid valves (MLV-3-1-1/4UKGH-3, Takasago Electric Inc.), four scales for flow rate monitoring (Talent TE-4101, Sartorius AG), a water circulation thermostat for column heating (Alpha A24, Lauda), three fraction collectors (one FRAC-100, Pharmacia; two FRAC-920, GE Healthcare), a liquid degasser unit (Degassex DG-4400, Phenomenex), and a datalogger (USB-6009, National Instruments). Labview program (version 12.0, National Instruments) was used in process control and scale data collection. The resin was packed into glass columns equipped with water heating jackets (ECO SR 25/200, Kronlab/YMC Europe). Resin bed diameter was 2.5 cm and bed length 20 cm.

The average bed porosity of the system was measured with Blue Dextran solution (C 1.5 g/L, BD 2000, Pharmacia). The void volume caused by the equipment was measured using 0.1 mol/L HCl. This void volume was taken into account in the total resin bed porosity.

3.1. Preparation of the concentrated acid lignocellulosic hydrolysate

Softwood hydrolysate was produced by hydrolyzing mixed spruce and pine cutter saw dust in two step concentrated acid hydrolysis using the procedure described in detail in Ref. [24]. In the first step, 200 g of saw dust was mixed with 428.6 g of 70 wt. % sulfuric acid. The first part of the hydrolysis was continued for two hours at 50 °C temperature. After the first step, the temperature was increased to 80 °C, and 1071.5 g of heated and purified water was added to the reactant mixture so that 20 wt. % sulfuric acid was obtained. The second step of the hydrolysis was continued for eight hours. Composition of the obtained hydrolysate is given in Table 1. The amounts of lignin and extractives are not listed in Table 1.

Table 1. Composition of concentrated acid lignocellulosic hydrolysate made from mixed spruce and pine cutter sawdust using two-step concentrated acid hydrolysis.

Component	*C*, mol/L	*Pu*, mol %
H_2SO_4	2.256	82.43
Glucose	0.228	8.33
Xylose	0.217	7.93
Acetic acid	0.034	1.25
HMF	$6.75 \cdot 10^{-4}$	0.02
Furfural	$1.10 \cdot 10^{-3}$	0.04

3.2. Chemical analyses

Monosaccharide and acetic acid concentrations were determined using HPLC (HP1100, Hewlett–Packard/Agilent) equipped with refractive index and variable wavelength UV detectors. Metacarb 87H column (Varian/Agilent) was used. Sulfuric acid concentrations were determined using potentiometric titration (automated titrator, Mettler Toledo DL25). For details, see [15,18,24].

4. Modelling and calculations

The sorption behavior of sulfuric acid, glucose, xylose, and acetic acid on CS16GC resin in acid (H^+) form, as well as different approaches for correlating the data, is well known on the basis of earlier studies [18,23,24]. The equations used in this work are those given in Ref. [18] and only a qualitative discussion with selected equations is included here.

Sulfuric acid sorption is affected by electrolyte exclusion. The sorbed amount of H_2SO_4 as well as the first derivative of the isotherm model must be zero at infinite dilution [2]. A simple power law isotherm model [18] was thus used to describe sulfuric acid sorption:

$$q_{\mathrm{H2SO4}} = \alpha_{\mathrm{H2SO4}} (C_{\mathrm{H2SO4}})^{\beta_{\mathrm{H2SO4}}}, \tag{1}$$

where C and q are liquid and adsorbed phase concentrations, and α and β are positive constants.

Sulfuric acid has a strong co-operative effect on the sorption of the other solutes in the system (glucose, xylose, and acetic acid) due to a salting out phenomenon [2,18]. In other words, the sorption of monosaccharides and weak acids increases with increasing concentration of the mineral acid. This effect is taken into account in the isotherm models of these solutes as a linear dependency of the Henry constant on the liquid phase concentration of sulfuric acid [18]. Thus, the sorption of the monosaccharides was modeled using an anti-Langmuir type isotherm model:

$$q_{\mathrm{k}} = \frac{(\alpha_{\mathrm{k}} + \beta_{\mathrm{k}} C_{\mathrm{H2SO4}}) C_{\mathrm{k}}}{1 - \sum_{\mathrm{j}=1}^{\mathrm{n}} \kappa_{\mathrm{j}} C_{\mathrm{j}}}, \tag{2}$$

where k stands for glucose and xylose, κ is a positive constant, and the sum in the nominator stands for the total monosaccharide concentration. Acetic acid sorption was modeled using a linear isotherm model:

$$q_{\mathrm{AcOH}} = (\alpha_{\mathrm{AcOH}} + \beta_{\mathrm{AcOH}} C_{\mathrm{H2SO4}}) C_{\mathrm{AcOH}}. \tag{3}$$

High sulfuric acid content in the concentrated acid lignocellulosic hydrolysates causes considerable shrinking of gel type resins. Here, a simple approach by Heinonen and Sainio [18] was used to describe resin shrinking: particle size was directly related to the adsorbed amount of sulfuric acid:

$$\theta = \frac{V_{\mathrm{bed,acid}}}{V_{\mathrm{bed,water}}} = 1 - \frac{\delta_1 q_{\mathrm{H2SO4}}}{\delta_2 + q_{\mathrm{H2SO4}}}, \tag{4}$$

where θ is the extent of resin shrinking i.e. the ratio of resin bed volume (V_{bed}) in acid to resin bed volume in water, q_{H2SO4} is the adsorbed amount of sulfuric acid, and δ_1 and δ_2 are positive parameters. Eq. (4) is scaled so that θ is unity in pure water.

Material balance equations that take into account the resin volume changes as a variable local bed porosity, as well as proper values for dispersion and mass transfer coefficients of the present system, are given in Ref. [18].

Pressure drop limits the maximum possible flow rates in chromatographic separation processes and has to be taken into account in the designing of these processes. Here, Ergun equation [32] was used to calculate the flow rates

$$\frac{\Delta p}{L} = \frac{150\mu v}{\Phi_S{}^2 d_p{}^2}\frac{\left(1-\varepsilon_{bed}\right)^2}{\varepsilon_{bed}{}^3} + \frac{1.75\rho v^2}{\Phi_S d_p}\frac{1-\varepsilon_{bed}}{\varepsilon_{bed}{}^3}, \tag{5}$$

where Δp is pressure drop, L is flow path length, μ is dynamic viscosity of the fluid, Φ_S is sphericity factor of solid particles (unity for spherical resin beads), ρ is density of the fluid, d_p is particle diameter, and v is superficial velocity.

Maximum allowed pressure drop from process inlet to outlet was set to 2 bar, which is typical for a large scale chromatographic process. Such a limit would allow very high flow rates in the small laboratory scale columns that were used in the experiments and simulations (d_{bed} = 2.5 cm, h_{bed} = 20 cm, d_p = 246 μm) and render the results irrelevant for large scale applications. The actual flow rates were thus chosen by considering an industrial scale column (d_{bed} = 1.5 m, h_{bed} = 3.0 m, d_p = 246 μm), applying a pressure limit of 2 bar, and scaling down while keeping the volumetric flow rate proportional to the bed volume constant.

Evaluation of process performance

Performance of the MCRC process was evaluated using various performance indicators. Productivity of the separation process with respect to the monosaccharides, Pr_{sugar}, was calculated with

$$Pr_{sugar} = \frac{n_{glucose}^{out} + n_{xylose}^{out}}{n_{col} V_{bed}\left(1-\varepsilon_{bed}\right) t_{cycle}}, \tag{6}$$

where n_i^{out} is the mole amount of i (= glucose, xylose) in their target fraction, n_{col} is number of columns, V_{bed} is bed volume, and t_{cycle} is cycle time.

Yield of component i at steady state, Y_i, is obtained from

$$Y_i = \frac{n_i^{out}}{C_i^{feed}\dot{V}_{step\,1}^{feed} t_{step\,1}}, \tag{7}$$

where C_i^{feed} is concentration of i in the feed, $\dot{V}_{step\,1}^{feed}$ is volumetric flow rate of the feed stream in feeding step, and $t_{step\,1}$ is duration of feeding step.

Purity of component i, Pu_i, in the target fraction:

$$Pu_i = \frac{n_i^{out}}{\sum_j n_j^{out}}, \tag{8}$$

where the summation term in the nominator stands for the total mole amount in the fraction. Eluent consumption, *EC*, i.e. the amount of eluent needed to purify one mole of product (monosaccharides) is obtained from

$$EC = \frac{\sum_{k=1}^{4}\sum_{m=1}^{n}\dot{V}_{k,m} t_k}{n_{glucose}^{out} + n_{xylose}^{out}}, \tag{9}$$

where $\dot{V}_{k,m}$ is volumetric flow rate of eluent stream m in step k and t_k is duration of step k. The double summation term in the numerator goes through all eluent streams in each step.

5. Results and discussion

In order to make the discussion of the results in the following sections more straightforward, characteristic features of the elution profiles obtained in single-column batchwise chromatographic fractionation of

concentrated acid hydrolysates are briefly discussed first. Typical elution profiles of the main components in the concentrated acid hydrolysates (sulfuric acid, glucose, xylose, acetic acid) obtained in the single-column case (see Ref. [18]) are shown in Fig. 3.

Sulfuric acid is the first eluting component due to the electrolyte exclusion (Fig. 3). As is typical for components affected by electrolyte exclusion, sulfuric acid profile has as diffuse front and a shock layer at the rear. In addition, the breakthrough of sulfuric acid occurs at the void volume of the resin bed due to complete exclusion at infinite dilution.

Monosaccharides elute after sulfuric acid (Fig. 3). The co-operative effect of sulfuric acid on the sorption of the monosaccharides due to salting out is obvious. The front parts of the monosaccharide profiles under the sulfuric acid profile are elongated due to this co-operation. In addition, focusing of the monosaccharides occurs at the rear of the sulfuric acid profile (Fig. 3). This is beneficial for the separation efficiency as it decreases the dilution of the product components. The co-operative effect of sulfuric acid on the sorption of acetic acid is not clearly seen in the single-column case (Fig. 3) due to rapid separation of these components.

As observed in Fig. 3, a good correlation between the experimental and calculated results can be obtained in the single-column case with the model described above. A detailed discussion of the single-column batchwise chromatographic fractionation of concentrated acid lignocellulosic hydrolysates can be found from Ref. [18].

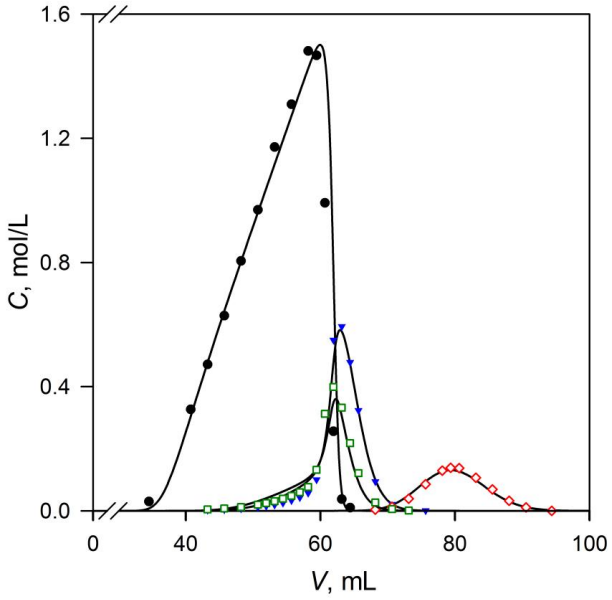

Figure 3. A typical elution profile obtained in single-column batchwise chromatographic fractionation of concentrated acid lignocellulosic hydrolysates with CS16GC resin in H^+ form. Feed composition: 2.22 mol/L sulfuric acid, 0.24 mol/L glucose, 0.38 mol/L xylose, and 0.16 mol/L acetic acid. Experimental details: T = 50 °C, u = 0.5 cm/min, ε_{bed} = 0.395, h_{bed} = 0.2 m, d_{bed} = 2.5 cm, top–down flow. Symbols: sulfuric acid (black ●), glucose (green □), xylose (blue ▼), and acetic acid (red ◇). Lines = calculated values.

5.1. MCRC process for the fractionation of concentrated acid hydrolysates

Following the procedure outlined in Section 2.2, an MCRC process was designed for the fractionation of concentrated acid lignocellulosic hydrolysate (containing mainly sulfuric acid, monosaccharides, and acetic acid). The number of columns was fixed to four, and bed length and diameter were set to 20 cm and 2.5 cm, respectively. For establishing an initial sketch of the process concept using ideal model and distance-time diagram, the co-operative effect of sulfuric acid on the sorption of the other solutes was neglected. Eq. (A.5) was used for sulfuric acid. The monosaccharides were treated as a single pseudo-component with a linear isotherm,

Eq. (A.6). Eq. (A.6) was used also for acetic acid. Isotherm parameters used with the ideal model are given in Table 2.

Table 2. Isotherm parameters used in the design of the four-column MCRC process with ideal model. Monosaccharide = pseudo-component of glucose and xylose.

	α	β
Sulfuric acid	0.072	2.03
Monosaccharide	0.199	-
Acetic acid	0.570	-

On the basis of the initial sketch, the final process scheme (Fig.4) was obtained by using numerical simulations and refining flow rates and step durations manually. Concentration profiles inside the columns at steady state are displayed in Fig. 5and the corresponding operating parameters are given in Table 3. As observed in the figures, the selected process scheme allows the introduction of a feed pulse to the process before the mass of the preceding feed pulse has been completely taken out (see also [3-8]). This reduces eluent consumption because part of the eluent is replaced with the fresh feed. In the final process scheme, monosaccharides and acetic acid are collected at one column outlet only to simplify the process. Sulfuric acid is collected at outlet of each column in order to minimize dilution and spreading of the profile.

Table 3. Operating parameters used in the simulated example run of the four-column MCRC process (Figs. 3 and 4). Numbers in parentheses mark the column into which the stream is introduced.

Step	t, s	$\dot{V}$, mL/min (col)			
		Hydrolysate	Water	Water	Recycle
1	317	8.57 (1)	4.29 (2)	5.25 (4)	0
2	472	0	0	0	4.12
3	371	0	1.75 (3)	7.99 (1)	0
4	444	0	1.72 (2)	4.12 (4)	4.12

In step I, feed is introduced to column 1 and sulfuric acid is collected from its outlet. At the same time, eluent is fed to columns 2 and 4, and sulfuric acid and monosaccharides are collected from columns 3 and 4, respectively (Fig. 4). It should be noted that column 1 is not empty in the beginning of step I because the unresolved parts of the sulfuric acid and monosaccharide profiles are recycled from column 4 as prefeed during step IV. The duration of step I depends on the flow rate of the feed stream and the amount of feed introduced. Eluent flow rates, on the other hand, depend on the set purity constraints.

After step I, closed loop recycling is conducted until sulfuric acid fronts from the feed pulses of the current and the previous cycle reach the outlets of columns 2 and 4, respectively. Duration and flow rates in step II must be adjusted so that the column train can be disconnected between columns 2 and 3 in step III (Fig. 4): i.e. the mass of the feed introduced in the current cycle resides in columns 1 and 2, and the mass of the feed introduced in the previous cycle resides in columns 3 and 4 (Fig. 5, step II).

In step III, eluent is fed to columns 1 and 3 while sulfuric acid is collected from columns 2 and 4 (Fig. 4). The operating parameters in this step must be adjusted so that acetic acid from the feed introduced in the previous cycle reaches the outlet of column 3 in the end of the step (Fig. 5) and purity constraints are fulfilled.

During step IV, acetic acid from the feed of the previous cycle is collected. In addition, the unresolved parts of sulfuric acid and monosaccharide profiles are recycled as prefeed from column 4 to column 1 to improve recovery yields. Duration and flow rates on this step depend on the purity constraints set for monosaccharide and acetic acid fractions.

Judging from Fig. 5, the selected MCRC scheme appears to be functioning inefficiently as in some steps one or more columns are empty. It should be noted, however, that the situation looks like that only because the spatial profiles in Fig. 5 are given at the end of each step. In addition, the example case shown in Fig. 5 is not fully optimized.

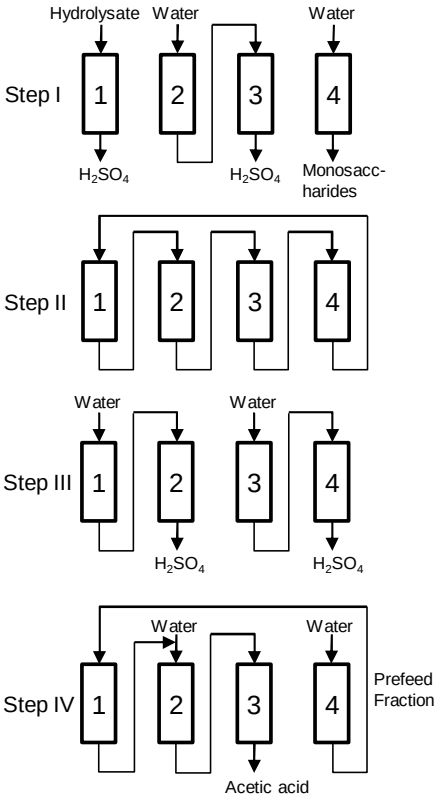

Figure 4. Four-column MCRC process for the chromatographic fractionation of concentrated acid lignocellulosic hydrolysates.

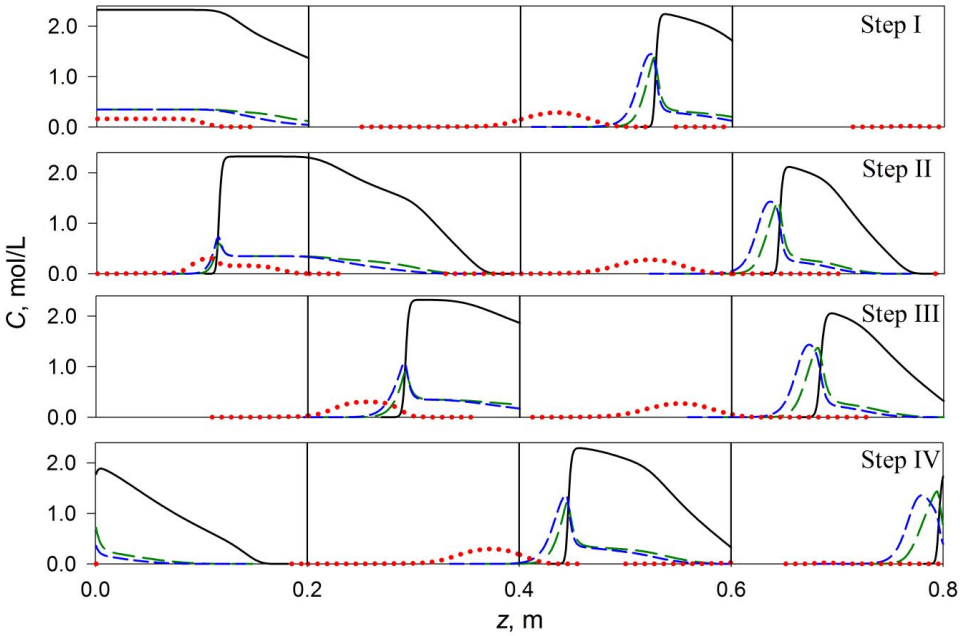

Figure 5. Spatial profiles at steady state of four-column MCRC process presented in Fig. 4. Simulated example. Feed composition: 2.32 mol/L sulfuric acid, 0.35 mol/L glucose, 0.35 mol/L xylose, and 0.16 mol/L acetic acid. Simulation details: n_{col} = 4, ε_{bed} = 0.42, h_{bed} = 0.2 m, d_{bed} = 2.5 cm, top–down flow; flow rates and step durations are listed in Table 3. Lines: black solid line = sulfuric acid; green dashed line = glucose; blue dashed line = xylose; red dotted line = acetic acid. Vertical lines mark the column boundaries.

5.2. Experimental validation of the four-column MCRC process

The four-column MCRC process in Fig. 4 was validated experimentally with four runs. Synthetic feed solution was used in three of these experimental runs (Section 5.2.1). The goal of these runs was to demonstrate how process performance parameters (see Section 4) could be adjusted by changing the operating parameters while keeping the amount of feed introduced to the process constant (same flow rate and feeding duration in each run). In addition to the three experimental runs with the synthetic feed solution, one run was done with an authentic concentrated acid lignocellulosic hydrolysate as the feed (Section 5.2.2). Operating parameters for each MCRC run are shown in Fig. 6.

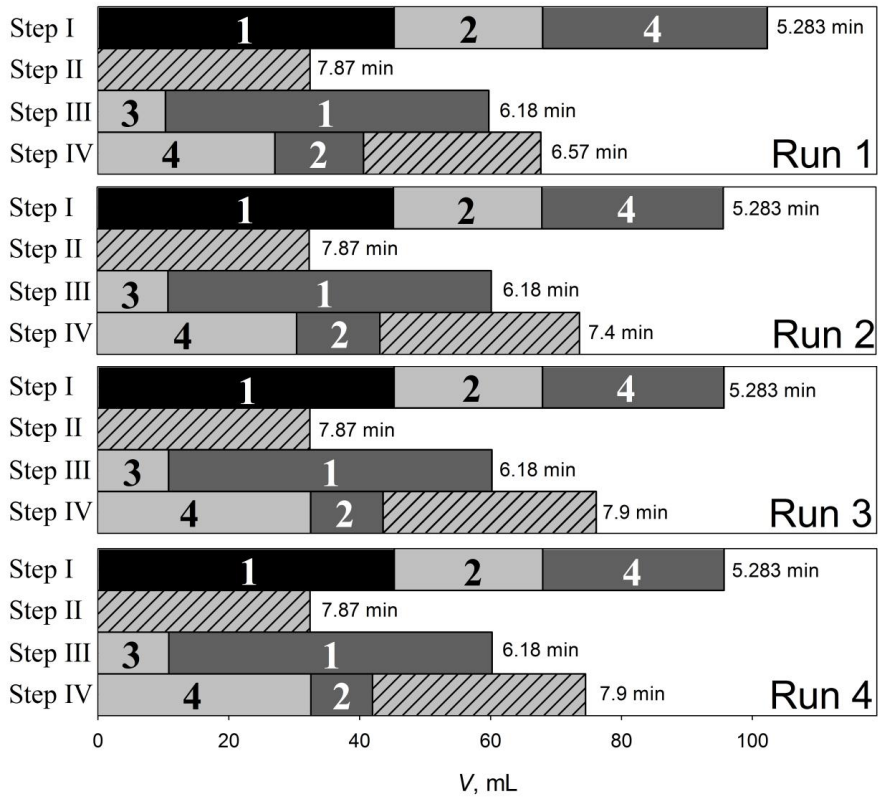

Figure 6. Flow rates of inlet streams in the MCRC process validation runs given as volume of solutions fed to a column. Durations of steps are given beside the bars. Runs 1-3: synthetic feed solution; run 4: authentic concentrated acid hydrolysate. Roman number = column into which the stream is led (see Fig. 4). Bars: black bar = feed; grey bar = eluent; dark grey bar = eluent; slashed grey bar = recycle.

5.2.1 Fractionation of synthetic feed solution

The synthetic feed solution contained sulfuric acid (72.5 mol %), glucose (10.0 mol %), xylose (12.5 mol %), and acetic acid (5.0 mol %). Furfural and hydroxymethyl furfural (HMF) that are typically present in lignocellulosic hydrolysates were not considered because they are easily removed using adsorption [31,33-34] in a separate process step prior to the acid–monosaccharide separation. The operation parameters (flow rates, step durations) were obtained by simulations using the model described above.

Four sulfuric acid fractions are collected in one cycle of the selected MCRC scheme (see Fig. 4). Overall purity of the fractions was approximately 94 mol % in run 1 (Table 4). Due to the co-operative effect of sulfuric acid on the monosaccharide sorption [18], the monosaccharides have elongated fronts eluting under the sulfuric acid profile which slightly decreases the overall purity of sulfuric acid.

All monosaccharides eluting behind sulfuric acid were collected to their target fraction in run 1 (Fig. 7). However, a large part of sulfuric acid ended up to this fraction as well and decreased the purity considerably (Table 4). This was due to too low flow rate inside column 4 in step IV. In run 1, however, the productivity of the monosaccharides was the highest (Table 4) as the largest part of the monosaccharides was collected to their target fraction. Collection of the rear of the sulfuric acid profile to the monosaccharide fraction also lowered the sulfuric acid yield (Table 4).

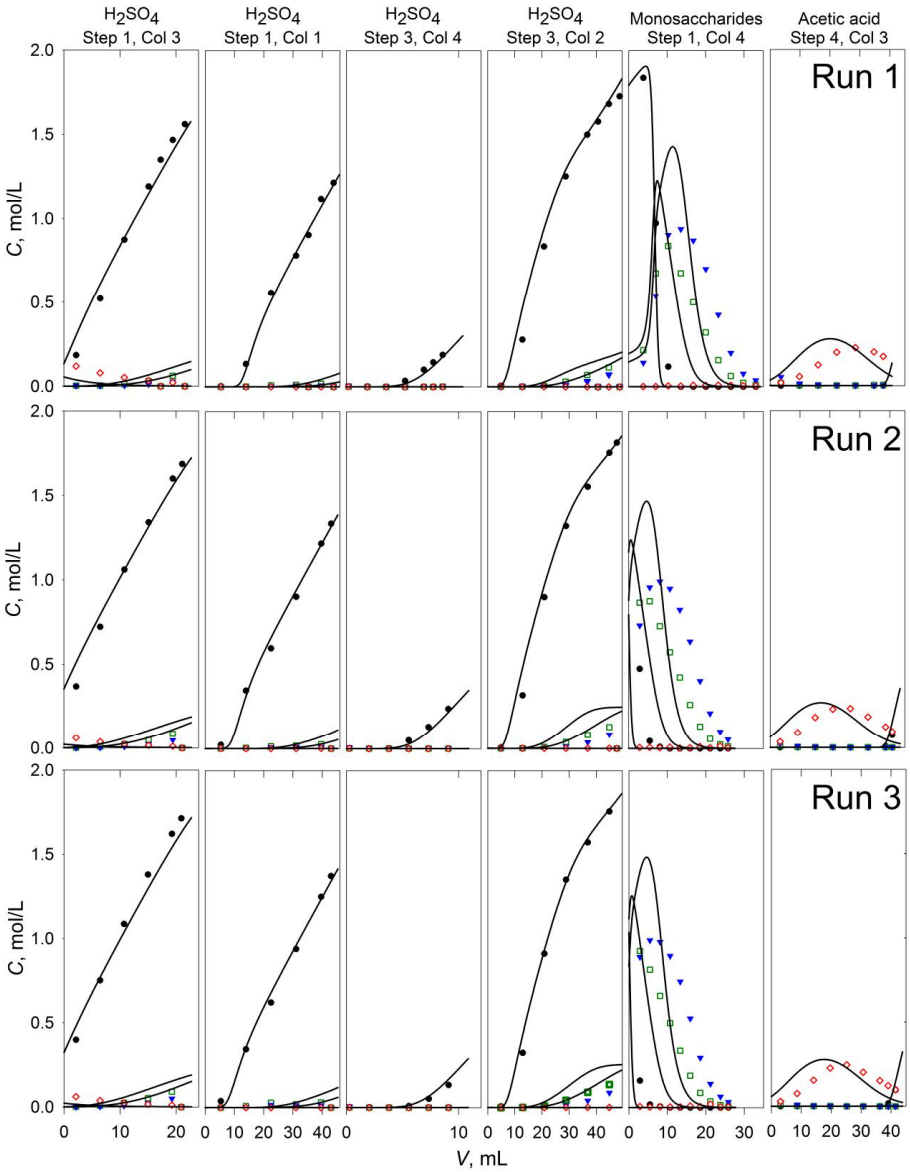

Figure 7. Outlet profiles at steady state in the fractionation of concentrated acid hydrolysate using the four-column MCRC process (Fig. 4). Feed composition: 2.33 mol/L sulfuric acid, 0.32 mol/L glucose, 0.40 mol/L xylose, and 0.16 mol/L acetic acid. Experimental details: T = 50 °C; for other details, see see Caption of Fig. 5. Operating parameters: see Fig. 6. Symbols: see Caption of Fig. 3. Lines = calculated values.

Table 4. Performance of the four-column MCRC process (Fig. 3) in the fractionation of concentrated acid lignocellulosic hydrolysates. Data from experiments. For details: see Fig. 5, caption of Fig. 6. Composition of the authentic hydrolysate is given in Table 1.

	Run 1	Run 2	Run 3	Run 4
Hydrolysate type	Synthetic	Synthetic	Synthetic	Authentic
Pr_{sugar}, mol/(m^3 h)	280.61	255.45	235.93	142.48
Y_{H2SO4}, %	84.64	92.47	97.95	95.78
Y_{sugar}, %	85.58	84.77	80.77	72.09
Y_{AcOH}, %	76.74	88.24	88.09	83.12
Pu_{H2SO4}, %	93.96	94.24	93.69	95.89
Pu_{sugar}, %	67.08	90.30	96.40	93.77
Pu_{AcOH}, %	90.28	93.43	91.46	41.04
EC_{Sugar}, L/mol	5.76	5.73	5.56	10.47

The focusing effect of the monosaccharides observed in the single-column case (see Fig. 3) is also seen in the MCRC process (Fig. 7). The maximum monosaccharide concentrations are significantly larger (0.84 mol/L glucose; 0.94 mol/L xylose) than in the feed solution (0.32 mol/L glucose; 0.4 mol/L xylose). Also the average monosaccharide concentrations in their product fraction (0.34 mol/L glucose; 0.46 mol/L xylose) are slightly higher than in the feed. Elimination of dilution, which is typical for chromatographic processes, is highly beneficial for economy of large scale processes.

Acetic acid is well separated from sulfuric acid with the resin used (see Fig. 6) and the purity of acetic acid fraction taken from column 3 during step IV in MCRC is very good (90 mol %) considering its purity in the feed (5 mol %). However, in run 1, acetic acid yield was relatively low because of too low flow rate inside column 3 in step IV.

On the contrary to the single-column case (see Fig. 3), the co-operative effect of sulfuric acid on acetic acid sorption can be clearly seen in the outlet profile of acetic acid as focusing of this component (Fig. 7). Maximum concentration of acetic acid is 0.23 mol/L, which is higher than the feed concentration (0.16 mol/L). However, in the case of acetic acid, the focusing effect is too weak to completely prevent dilution of the acetic acid: average outlet concentration was 0.13 mol/L whereas the feed concentration was 0.16 mol/L.

The four-column MCRC process reached steady state in approximately five cycles (Fig. 8). Operation of the experimental system was stable: in 20 cycles, no notable drifting of the component bands was observed.

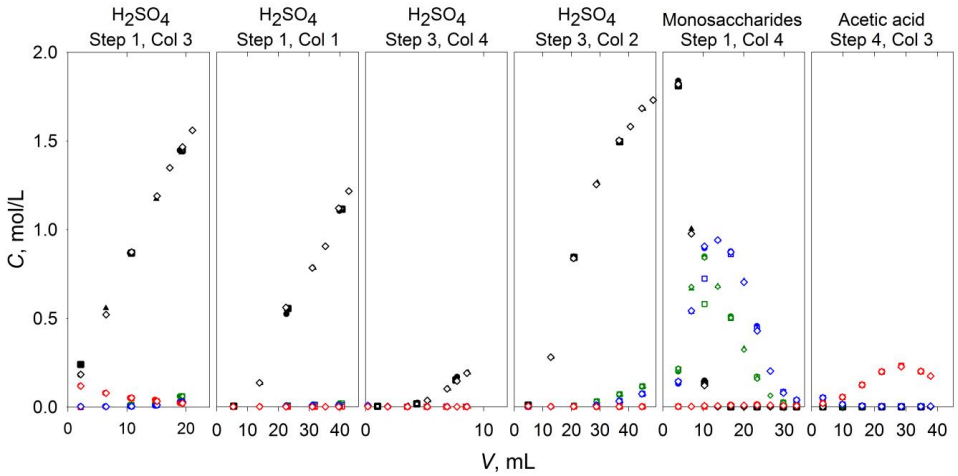

Figure 8. Comparison of outlet profiles obtained in experimental MCRC run 1 (Fig. 6) in cycles 5 (●), 10 (□), 15 (▲), and 20 (◇). Feed composition: see caption of Fig. 7. Experimental details and operating parameters: see Fig. 6 and caption of Fig. 7. Colors: sulfuric acid (black), glucose (green), xylose (blue), and acetic acid (red).

The goal of MCRC run 2 (Figs. 6 and 7) was to increase monosaccharide purity. This was done by increasing the duration of step IV (Fig. 4). To compensate the longer duration of step IV in run 2, eluent flow rate in step IV to column 2 (see Fig. 4) was lowered in order to prevent the contamination of acetic acid fraction with sulfuric acid (see Fig. 5: step 4). Also eluent flow rates to column 4 in step I and to column 3 in step III (see Fig. 4) were lowered in order to decrease eluent consumption, and to achieve higher product quality.

The longer duration of step IV in run 2 resulted in a larger prefeed fraction, and thus smaller part of the rear shock of the sulfuric acid profile ended to the monosaccharide fraction. This increased the purity of this fraction considerably from run 1 (Table 4). However, due to the larger prefeed fraction, smaller amount of monosaccharides could be collected to their target fraction and Pr_{sugar} decreased by 9.0 %. Also increase in cycle time lowered Pr_{sugar} in run 2. Yield of the monosaccharides also decreased due to the increase in the prefeed fraction volume (Table 4). Sulfuric acid and acetic acid yields and purities were increased in run 2 when compared to run 1 (Table 4).

In MCRC run 3 (Figs. 6 and 7), a further increase in the monosaccharide purity was desired. To reach this goal, duration of the step IV was increased and eluent flow rate to column 2 in step IV decreased from the values used in run 2 (Fig. 6). As a result, purity of the monosaccharides increased up to 96.4 mol %, while Pr_{sugar} decreased by 7.6 % from run 2 (Table 4). Yield of sulfuric acid increased, while the purity of H_2SO_4 was unchanged. Purity of acetic acid decreased slightly compared to run 2 as the flow rate inside column 3 in step IV was decreased. However, the acetic acid yield remained on the same level as in run 2.

It is worth noting that an increase in the product purity could be obtained also by fractionating the column outlet streams into smaller fractions that fulfill the set purity requirements. Those fractions that do not fulfill the purity requirements can then be fed back to the system as eluent substitute [8]. In this way, also an increase in product yield and decrease in eluent consumption could be obtained. On the other hand, the design of such an MCRC process would be challenging as timing should be such that the recycled masses would not end up as impurities in wrong product fractions.

The correlation between the experimental and calculated outlet profiles was found to be good (Fig. 7) although some differences are observed. The calculated sulfuric acid shock layer is steeper than the experimental one. This is because the simple resin shrinking model (see Ref. [18]) is unable to describe accurately enough the effect of sulfuric acid on the shrinking of particles and dispersion in the bed. The differences are more evident at low sulfuric acid concentrations.

The slightly incorrect prediction of the resin shrinking also affects the match between the experimental and calculated monosaccharide and acetic acid profiles (Fig. 7). According to the experimental results, the focusing of the monosaccharides is not as strong as the model predicts (Fig. 7). In addition, the calculated fronts of the monosaccharide profiles eluting under the sulfuric acid profile differ to some extent from the experimentally obtained ones. Despite these differences, the model used in this study is well suited for simulating and designing an MCRC process for the fractionation of the concentrated acid hydrolysates.

5.2.2 Comparison of MCRC and single-column batch chromatography

In order to obtain a better picture of the separation performance of the four-column MCRC process (see Fig. 4), it was compared with batchwise fractionation of concentrated acid lignocellulosic hydrolysates using four parallel columns (h_{bed} = 20 cm, d_{bed} = 2.5 cm). Same feed concentrations were used in the simulation of the batch process as in the MCRC experiments. It should be reminded that full optimization of the MCRC process was not attempted here.

The performance of the batch process with four parallel columns was evaluated using the same pressure drop limit as with the MCRC process (Δp_{max} = 2 bar). Since the MCRC reached 95 mol % purity of monosaccharide fraction, this level was used as target purity for the batch process. Highest productivity of the batch process was achieved with flow rate 14.8 mL/min and column loading 7.7 vol %. At this operation point, Pr_{sugar} of the batch process was 1930 mol/(m^3 h) which is approximately eight times larger than obtained in the experimental MCRC runs (235.93 mol/(m^3 h)). However, EC_{sugar} of the batch process was 111.5 L/mol which is approximately 20 times larger than obtained with the four-column MCRC scheme (Table 4). In addition, Y_{sugar} obtained in the batch process was considerably lower (42.2 %) than with the MCRC process.

Selection of process configuration depends on weighting of the performance parameters. In large scale fractionation of relatively cheap biomass based feedstocks, eluent consumption is often a critical factor due to evaporation costs. When yield and eluent consumption are considered more important than productivity, four-

column MCRC scheme becomes a better option than four parallel batch columns. Even if the batch process would be operated at its minimum eluent consumption (flow rate 3.9 mL/min, loading 14.1 %), EC_{sugar} would still be 10 times larger than in the four-column MCRC scheme. It should also borne in mind that with proper optimization the performance of the MCRC process could be increased considerably. This rough comparison demonstrates the efficiency of the MCRC concept in reducing eluent consumption, which in such biorefinery applications as investigated here is directly related to energy consumption and CO_2 emissions.

5.2.3 Fractionation of authentic concentrated acid lignocellulosic hydrolysate

Also fractionation of an authentic concentrated acid lignocellulosic hydrolysate (see Table 1) using the four-column MCRC scheme (see Fig. 4) was investigated. Same operating parameters were used as in MCRC run 3, except for the eluent flow rate to column two in step IV, which was decreased (see Fig. 6; run 4).

The monosaccharide concentrations in the authentic hydrolysate (see Table 1) were lower than in the synthetic feed solution (Section 5.2.1). Also the amount of acetic acid was lower due to the raw material used in the hydrolysis (see Table 1). The synthetic solution was made on the basis of a hardwood hydrolysate, whereas the authentic hydrolysate was prepared from softwood. It is known that softwoods (e.g. spruce and pine) contain less acetyl groups, from which acetic acid is derived in the hydrolysis, than hardwoods (e.g. birch, aspen) [15,35-36].

The authentic hydrolysate contained also small amounts of hydroxymethyl furfural (HMF) and furfural (see Table 1) formed from the monosaccharides during hydrolysis [20,37-38]. HMF and furfural were not included in the model (see Ref. [18]) due to their very low concentrations.

Good separation performance was achieved with the four-column MCRC scheme also using the authentic concentrated acid hydrolysate (see Table 4). The additional impurities (HMF, furfural, residual lignin and wood extractives) did not cause problems to the separation. HMF and furfural were distributed into every product fraction but their concentrations were very low, the highest values being 0.4 mmol/L for both. In steady state, the monosaccharide fraction contained in total 0.024 mol % of HMF and furfural (in total 0.065 mol % in the feed).

Direct comparison of the results obtained in run 4 with those obtained in the other runs is not possible due to different feed concentrations. Due to the lower amount of monosaccharides in the feed solution, Pr_{sugar}, Y_{sugar}, and EC_{sugar} differ considerably from the values obtained in the runs 1-3. However, for example the purity of the monosaccharides was on a similar level as in the third run using the synthetic feed solution (see Table 4). Acetic acid purity was on a reasonable level (41 mol %) in the run with the authentic hydrolysate, considering its extremely low purity in the feed solution (1.25 mol %).

6. Conclusions

Electrolyte exclusion chromatography using a Multi-Column Recycling Chromatography (MCRC) was investigated. A design procedure consisting of two parts was introduced for the MCRC process. First, the ideal model of chromatography and distance-time diagram are used to obtain an initial sketch of the process scheme. This scheme is then refined by trial-and-error method using numerical simulations. The procedure was validated by designing a four-column MCRC process with four steps for the fractionation of concentrated acid lignocellulosic hydrolysates.

Good product purities and yields were obtained in the fractionation experiments with the selected four-column MCRC scheme. It was demonstrated how purity and yield can be controlled by adjusting flow rates and step durations while keeping amount of feed introduced to the process constant.

When compared to a batch process with four parallel columns, the MCRC had approximately eight times lower productivity with respect to the monosaccharides. Eluent consumption, which is often the critical factor in processing of cheap raw materials, was 20 times smaller in the MCRC than in the batch process. In addition, two times higher monosaccharide yield was achieved with the MCRC scheme than with the batch process. Extensive comparison of these two processes necessitates full optimization of both processes, which was beyond the scope of this study.

Appendix. Equilibrium theory based design method

Let us consider a component that does not interact with other components during isocratic elution in a chromatographic column. Under ideal conditions, the mass balance is given in dimensionless units as

$$\frac{\partial C_i}{\partial \tau}\left(1+F\frac{\partial q_i}{\partial C_i}\right)+\frac{\partial C_i}{\partial \xi}=0, \tag{A.1A}$$

$$F=\frac{1-\varepsilon_{bed}}{\varepsilon_{bed}}, \tag{A.1B}$$

$$\xi=\frac{z}{h_{bed}}, \tag{A.1C}$$

$$\tau=\frac{tu}{h_{bed}}, \tag{A.1D}$$

where, C_i is liquid phase concentration of i, q_i is adsorbed phase concentration of i, F is phase ratio, ε_{bed} is resin bed porosity, τ is dimensionless time, ξ is dimensionless spatial coordinate, z is spatial coordinate, h_{bed} is column length, t is time, and u is interstitial velocity. An equation for the propagation direction of a constant concentration C_i is obtained as follows. The total derivative of dC_i is zero for a constant state, as shown in Eq. (A.2A).

$$dC_i=\frac{\partial C_i}{\partial \tau}d\tau+\frac{\partial C_i}{\partial \xi}d\xi=0 \tag{A.2A}$$

This can be rewritten as

$$\frac{\partial C_i}{\partial \tau}+\frac{\partial C_i}{\partial \xi}\frac{d\xi}{d\tau}=0 \tag{A.2B}$$

By comparing the left hand sides of Eqs. (A.1A) and (A.2B) it is apparent that the propagation direction of the constant state C_i is

$$\frac{d\xi}{d\tau}=\left(1+F\frac{\partial q_i}{\partial C_i}\right)^{-1}. \tag{A.3}$$

Since the slope of the isotherm at C_i is invariant in absence of interactions between eluting species, the trajectory of the constant state is a straight line in the distance time diagram as displayed in Fig. 2A. The dimensionless residence time of the constant state C_i in the column, τ' is obtained by integration of Eq. (A.3)

$$\tau'=1+F\frac{\partial q_i}{\partial C_i} \tag{A.4}$$

Eqs. (A.1) through (A.4) are valid for the continuous part of the profile (simple waves and constant states) but not for shocks. The propagation velocity of a shock is derived from the condition of no accumulation of mass in the shock, which yields an equation analogous to Eq. (A.3)

$$\frac{d\xi}{d\tau}=\left(1+F\frac{\Delta q_i}{\Delta C_i}\right)^{-1} \tag{A.5}$$

where Δ denotes a change in the state variable across the shock.

Let us consider binary mixture of a strong electrolyte and a nonelectrolyte in a column packed with a strong cation exchange resin. Typically, such components have concave upwards and linear isotherms, respectively

$$q_1=\alpha_1\left(C_1\right)^{\beta_1} \tag{A.6}$$

$$q_2=\alpha_2 C_2 \tag{A.7}$$

In Eqs. (A.6) and (A.7), α_i and β_i are positive parameters; for concave upward isotherm β_i is greater than unity. It is assumed here that the nonelectrolyte is more strongly retained than the strong electrolyte.

The residence times of concentration C_1 at the front and rear of the pulse are

$$\Delta\tau'^{\,\text{front}}_1 = 1 + F\alpha_1\beta_1 C_1^{(\beta_1 - 1)} \tag{A.8A}$$

$$\Delta\tau'^{\,\text{rear}}_1 = f\left(\Delta\tau^{\text{feed}}\right) = 1 + \left[\frac{\beta_1}{\beta_1 - 1}\left(F\alpha_1\beta_1\right)^{\frac{1}{\beta_1 - 1}} C_1^{\text{feed}}\Delta\tau^{\text{feed}}\right]\frac{\beta_1 - 1}{\beta_1}. \tag{A.8B}$$

Eq. (A.8B) gives the residence time of the rear concentration shock of component 1. For component 2 (linear isotherm) the residence times are independent of concentration and given by

$$\Delta\tau'^{\,\text{front}}_2 = 1 + F\alpha_2 \tag{A.9A}$$

$$\Delta\tau'^{\,\text{rear}}_2 = 1 + F\alpha_2 \tag{A.9B}$$

With the residence times given by Eqs. (A.8) and (A.9), a distance-time diagram for the design purposes of a batchwise chromatographic separation process of a strong electrolyte and a nonelectrolyte can be constructed.

When complete separation (100 % purity and yield for both components) between the components of a binary pair is desired, the maximum duration of feed is

$$\Delta\tau^{\text{feed}}_{\max} = \tau'^{\,\text{front}}_2 - \tau'^{\,\text{rear}}_1. \tag{A.10}$$

To obtain the yields and purities in the case of incomplete separation of a binary pair (for example in the case shown in Fig. 2A) the concentration profiles as a function of the dimensionless time at the column outlet must be presented. The yields and purities are obtained using this presentation from the areas under the concentration curves between given cutpoints. Yields of components 1 and 2 in the case of binary separation:

$$Y_1 = \frac{\int_{\tau'^{\,\text{front}}_1}^{\tau^F_1} C_1(\tau)\,d\tau}{C_1\Delta\tau^{\text{feed}}}\cdot 100\%, \tag{A.11A}$$

$$Y_2 = \frac{\int_{\tau^F_2}^{\tau'^{\,\text{rear}}_2} C_2(\tau)\,d\tau}{C_2\Delta\tau^{\text{feed}}}\cdot 100\%, \tag{A.11B}$$

where τ^F is the chosen fractionation cut point. Similarly, the purities of component 1 and 2 can be obtained from:

$$Pu_1 = \frac{\int_{\tau'^{\,\text{front}}_1}^{\tau^F_1} C_1(\tau)\,d\tau}{\int_{\tau'^{\,\text{front}}_1}^{\tau^F_1} C_1(\tau)\,d\tau + \int_{\tau'^{\,\text{front}}_1}^{\tau^F_1} C_2(\tau)\,d\tau}\cdot 100\%, \tag{A.12A}$$

$$Pu_2 = \frac{\int_{\tau^F_2}^{\tau'^{\,\text{rear}}_2} C_2(\tau)\,d\tau}{\int_{\tau'^{\,\text{rear}}_2}^{\tau^F_2} C_1(\tau)\,d\tau + \int_{\tau^F_2}^{\tau'^{\,\text{rear}}_2} C_2(\tau)\,d\tau}\cdot 100\%. \tag{A.12B}$$

Inversely, Eqs. (A.11) and (A.12) can be used to solve the cut points that give the desired yield or purity.

Cycle time $\Delta\tau^{\text{cycle}}$ for the binary separation is

$$\Delta\tau^{\text{cycle}} = \tau'^{\text{rear}}_{2} - \tau'^{\text{front}}_{1}. \quad \text{(A.13)}$$

Eluent feeding time $\Delta\tau^{\text{eluent}}$ required between two consecutive injections can be calculated from

$$\Delta\tau^{\text{eluent}} = \Delta\tau^{\text{cycle}} - \Delta\tau^{\text{feed}}. \quad \text{(A.14)}$$

Acknowledgements

The authors are grateful for M.Sc. Ilkka Suppula, Mr. Tuomas Sihvonen, and Ms. Jenni Skogström for their assistance in carrying out the experimental work.

Nomenclature

C_{i}	liquid phase concentration of i, mol/L
$C_{\text{i}}^{\text{feed}}$	feed concentration of I, mol/L
d_{bed}	resin bed diameter, cm or m
d_{p}	particle diameter, m
EC	eluent consumption, L/mol
F	phase ratio, -
h_{bed}	column length, cm or m
L	flow path length, m
n_{col}	number of columns, -
$n_{\text{i}}^{\text{out}}$	mole amount of i in target fraction, mol
Δp	pressure drop, Pa
Pr_{sugar}	monosaccharide productivity, mol/(m^3 h)
Pu_{i}	purity of component i, -
q_{i}	adsorbed phase concentration of i, mol/L
t	time, s
t_{cycle}	cycle time, h
$t_{\text{step 1}}$	duration of step one, min
u	interstitial velocity, m/s
V_{bed}	resin bed volume, m^3
$\dot{V}$	volumetric flow rate, mL/min
$\dot{V}_{\text{step 1}}^{\text{feed}}$	volumetric flow rate of the feed stream in step one, mL/min
v	superficial velocity, m/s
Y_{i}	yield of component I, -
z	spatial coordinate, m
Greek letters	
α	isotherm parameter
β	isotherm parameter
δ	resin shrinking model parameter
ε_{bed}	resin bed porosity, -
θ	extent of resin shrinking, -
κ	isotherm parameter
μ	dynamic viscosity of the fluid, mPas
ξ	dimensionless spatial coordinate, -
ρ	density of the fluid, kg/m^3
τ	dimensionless time, -
τ'	dimensionless residence time of a concentration wave in a column, -
$\Delta\tau^{\text{cycle}}$	cycle time (dimensionless), -
$\Delta\tau^{\text{eluent}}$	eluent feeding time (dimensionless), -
$\Delta\tau^{\text{feed}}$	feeding time (dimensionless), -
Φ_{S}	sphericity factor of solid particles, -

Subsripts and superscripts

bed	resin bed
col	column
cycle	cycle of a chromatographic process
eluent	eluent stream
F	fractionation cutpoint
feed	feed stream
i	component i
out	outlet stream
p	particle
S	sphericity
step	step of a chromatographic process
sugar	monosaccharide

References

1 R.M. Wheaton, W.C. Bauman, Ion exclusion – a unit operation utilizing ion exchange materials, Ind. Eng. Chem. 45 (1953) 228-233.

2 F. Helfferich, Ion exchange, Dower Publications, New York, 1995.

3 H. Heikkilä, G. Hyöky, J. Kuisma, Method for the recovery of betaine from molasses, European patent 0345511 A2, December 13, 1989.

4 H. Heikkilä, G. Hyöky, J. Kuisma, A method for the fractionation of molasses, International patent WO 94/17213, August 4, 1994.

5 H. Heikkilä, G. Hyöky, J Kuisma, Method for fractionation of a solution by a chromatographic simulated moving bed process, International patent WO 97/45185, December 4, 1997.

6 H. Heikkilä, G. Hyöky, J. Kuisma, Method for the fractionation of molasses, U.S. Patent 6093326, July 25, 2000.

7 H. Heikkilä, J. Lewandowski, J. Kuisma, Chromatographic seaparation method, U.S. Patent, 7229558 B2, June 12, 2007.

8 J. Airaksinen, H. Heikkilä, J. Lewandowski, K. Laiho, Separation process, U.S. Patent 2010/0212662 A1, August 26, 2010.

9 H. Paananen, F. Rousset, New generation of chromatographic separators using the FAST technology, Proceedings from the 31st Biennial Meeting Operations of the American Society of Sugar Beet Technologists, Vancouver, Canada, 2001, pp. 115-123.

10 T. Masuda, T. Sonobe, F. Matsuda, M. Horie, Process for fractional separation of multi-component fluid mixture, U.S. Patent 5198120, March 30, 1993.

11 Stefan Karlsson, Optimization of a sequential-simulated moving bed separation process with mathematical programming methods, dissertation, Åbo Akademi, Finland, 2001.

12 M. Mazzotti, Equilibrium theory based design of simulated moving bed processes for a generalized Langmuir isotherm, J. Chrom. A 1126 (2006) 311-322.

13 G. Guiochon, S.G. Shirazi, A.M. Katti, Fundamentals of preparative and non-linear chromatography, second ed., Academic Press, San Diego, United States, 2006.

14 J. Heinonen, T. Sainio, Chromatographic fractionation of lignocellulosic hydrolysates, in D.Y. Murzin (Ed.), Advances in chemical engineering, vol. 42: Chemical engineering for renewables conversion, Academic Press, San Diego, United States, 2013, pp. 261-350.

15 J. Heinonen, T. Sainio, Chromatographic recovery of monosaccharides for the production of bioethanol. Ind. Eng. Chem. Res. 49 (2010) 2907-2915.

16 R.P. Neuman, S.R. Rudge, M.R. Ladisch, Sulfuric acid–sugar separation by ion exclusion, React. Polym. 5 (1987) 55-61.

17 R.M. Springfield, R.D. Hester, Continuous ion-exclusion chromatography for acid/sugar separation, Sep. Sci. Technol. 34 (1999) 1217-1241.

18 J. Heinonen, T. Sainio, Modelling and performance evaluation of chromatographic monosaccharide recovery from concentrated acid lignocellulosic hydrolysates, J. Chem. Technol. Biotechnol. 87 (2012) 1676-1686.

19 S. Hellstén, T. Sainio, Steady state recycling chromatography in acid–sugar separation on an ion-exchange resin, Sep. Sci. Technol., 47 (2012) 2358-2365.

20 M.J. Taherzadeh, K. Karimi, Bioethanol: Market and production processes. In A. Nag (Ed.), Biofuels refining and performance, McGraw-Hill, Fairfield, United States, 2008, pp 69–106.

21 W.A. Farone, J.E. Cuzens, Method of producing sugars using strong acid hydrolysis of cellulosic and hemicellulosic materials, U.S. Patent No. 5562777, March 26, 1993.

22 W.A. Farone, J.E. Cuzens, Strong acid hydrolysis of cellulosic and hemicellulosic materials, U.S. Patent No. 5597714, June 7, 1995.

23 J. Heinonen, H.O. Rubiera Landa, T. Sainio, A. Seidel-Morgenstern, Use of Adsorbed Solution Theory to model competitive and co-operative sorption on elastic ion exchange resins, Sep. Purif. Technol. 95 (2012) 235-247.

24 J. Heinonen, A. Tamminen, J. Uusitalo, T. Sainio, Ethanol production from wood via concentrated acid hydrolysis, chromatographic separation, and fermentation, J. Chem. Technol. Biotechnol. 87 (2012) 689-696.

25 M. Laatikainen, J. Heinonen, T. Sainio, Modeling of chromatographic separation of concentrated-acid hydrolysates, Sep. Purif. Technol. 80 (2011) 610-619.

26 R.M. Springfield, R.D. Hester, Development and modelling of a continuous simulated moving bed ion exclusion process for the separation of acid and sugar, Sep. Sci. Technol. 36 (2001) 911-930.

27 Z.-Y. Sun, Y.Q. Tang, T. Iwanaga, T. Sho, K. Kida, Production of fuel ethanol from bamboo by concentrated sulfuric acid hydrolysis followed by continuous ethanol fermentation, Bioresour. Technol. 102 (2011) 10929-10935.

28 S. Katsuo, M. Mazzotti, M, Intermittent simulated moving bed chromatography: 1. Design criteria and cyclic steady-state, J. Chromatogr. A 1217 (2010) 1354-1361.

29 V.G. Mata, A.E. Rodrigues, Separation of ternary mixture by pseudo-simulated moving bed chromatography, J. Chromatogr. A 939 (2001) 23-40.

30 G. Agrawal, Y. Kawajiri, Comparison of various ternary simulated moving bed separation schemes by multi-objective optimization, J. Chromatogr. A 1238 (2012) 105-113.

31 T. Sainio, I. Turku, J. Heinonen, Adsorptive removal of fermentation inhibitors from concentrated acid hydrolysates of lignocellulosic biomass, Bioresour. Technol. 102 (2011) 6048-6057.

32 W.L. McCabe, J.C. Smith, P. Harriott, Unit operations of chemical engineering, seventh ed., McGraw-Hill, New York, 2005, pp. 163-167.

33 N.-O. Nilvebrant, A. Reimann, S. Larsson, L.J. Jönsson, Detoxification of lignocellulose hydrolysates with ion-exchange resins, Appl. Biochem. Biotechnol. 91-93 (2001) 35-49.

34 J.R. Weil, B. Dien, R. Bothast, R. Hendrickson, N.S Mosie, M.R. Ladisch, Removal of fermentation inhibitors formed during pretreatment of biomass by polymeric adsorbents, Ind. Eng. Chem. Res. 41 (2002) 6132-6138.

35 C.J. Biermann, Handbook of Pulping and Papermaking, second ed., Academic Press, San Diego, United States, 1996, p. 34.

36 M. Balaban, G. Uçar, Estimation of volatile acids in wood and bark, Holz als Roh- und Werkst, 61 (2003) 465-468.

37 E. Palmqvist, B. Hahn-Hägerdahl, Fermentation of lignocellulosic hydrolysates. I: inhibition and detoxification, Bioresour. Technol. 74 (2000) 17–24.

38 E. Palmqvist, B. Hahn-Hägerdahl, Fermentation of lignocellulosic hydrolysates. II: inhibitors and mechanisms of inhibition, Bioresour. Technol. 74 (2000) 25–33.

ACTA UNIVERSITATIS LAPPEENRANTAENSIS

514. PIRINEN, MARKKU. The effects of welding heat input usability of high strength steels in welded structures. 2013. Diss.

515. SARKKINEN, MINNA. Strategic innovation management based on three dimensions diagnosing innovation development needs in a peripheral region. 2013. Diss.

516. MAGLYAS, ANDREY. Overcoming the complexity of software product management. 2013. Diss.

517. MOISIO, SAMI. A soft contact collision method for real-time simulation of triangularized geometries in multibody dynamics. 2013. Diss.

518. IMMONEN, PAULA. Energy efficiency of a diesel-electric mobile working machine. 2013. Diss.

519. ELORANTA, LEENA. Innovation in a non-formal adult education organisation – multi-case study in four education centres. 2013. Diss.

520. ZAKHARCHUK, IVAN. Manifestation of the pairing symmetry in the vortex core structure in iron-based superconductors. 2013. Diss.

521. KÄÄRIÄINEN, MARJA-LEENA. Atomic layer deposited titanium and zinc oxides; structure and doping effects on their photoactivity, photocatalytic activity and bioactivity. 2013. Diss.

522. KURONEN, JUHANI. Jatkuvan äänitehojakautuman algoritmi pitkien käytävien äänikenttien mallintamiseen. 2013. Diss.

523. HÄMÄLÄINEN, HENRY. Identification of some additional loss components in high-power low-voltage permanent magnet generators. 2013. Diss.

524. SÄRKKÄ, HEIKKI. Electro-oxidation treatment of pulp and paper mill circulating waters and wastewaters. 2013. Diss.

525. HEIKKINEN, JANI. Virtual technology and haptic interface solutions for design and control of mobile working machines. 2013. Diss.

526. SOININEN, JUHA. Entrepreneurial orientation in small and medium-sized enterprises during economic crisis. 2013. Diss.

527. JÄPPINEN, EERO. The effects of location, feedstock availability, and supply-chain logistics on the greenhouse gas emissions of forest-biomass energy utilization in Finland. 2013. Diss.

528. SÖDERHOLM, KRISTIINA. Licensing model development for small modular reactors (SMRs) – focusing on the Finnish regulatory framework. 2013. Diss.

529. LAISI, MILLA. Deregulation's impact on the railway freight transport sector's future in the Baltic Sea region. 2013. Diss.

530. VORONIN, SERGEY. Price spike forecasting in a competitive day-ahead energy market. 2013. Diss.

531. PONOMAREV, PAVEL. Tooth-coil permanent magnet synchronous machine design for special applications. 2013. Diss.

532. HIETANEN, TOMI. Magnesium hydroxide-based peroxide bleaching of high-brightness mechanical pulps. 2013. Diss.

533. TYKKÄLÄ, TOMMI M. Real-time image-based RGB-D camera motion tracking and environment mapping. 2013. Diss.

534. PEKKOLA, SANNA. Performance measurement and management in a collaborative network. 2013. Diss.

535. PANOREL, IRIS CHERRY. Pulsed corona discharge as an advanced oxidation process for the degradation of organic compounds in water. 2013. Diss.

536. TORKKELI, LASSE. The influence of network competence of internationalization of SMEs. 2013. Diss.

537. MOLANDER, SOLE. Productivity and services – safety telephone services for the elderly. 2013. Diss.

538. SITARZ, ROBERT. Identification of research trends in the field of separation processes. Application of epidemiological model, citation analysis, text mining, and technical analysis of the financial markets. 2013. Diss.

539. KATTEDEN, KAMIEV. Design and testing of an armature-reaction-compensated permanent magnet synchronous generator for island operation. 2013. Diss.

540. HÄMÄLÄINEN, HARRI. Integration of learning supportive applications to development of e-portfolio construction process. 2013. Diss.

541. RATCHANANUSORN, WARIN. Development of a process for the direct synthesis of hydrogen peroxide in a novel microstructured reactor. 2013. Diss.

542. PERFILEV, DANIIL. Methodology for wind turbine blade geometry optimization. 2013. Diss.

543. STROKINA, NATALIYA. Machine vision methods for process measurements in pulping. 2013. Diss.

544. MARTTONEN, SALLA. Modelling flexible asset management in industrial maintenance companies and networks. 2013. Diss.

545. HAKKARAINEN, JANNE. On state and parameter estimation in chaotic systems. 2013. Diss.

546. HYYPIÄ, MIRVA. Roles of leadership in complex environments
Enhancing knowledge flows in organisational constellations through practice-based innovation processes. 2013. Diss.

547. HAAKANA, JUHA. Impact of reliability of supply on long-term development approaches to electricity distribution networks. 2013. Diss.

548. TUOMINEN, TERHI. Accumulation of financial and social capital as means to achieve a sustained competitive advantage of consumer co-operatives. 2013. Diss.

549. VOLCHEK, DARIA. Internationalization of small and medium-sized enterprises and impact of institutions on international entrepreneurship in emerging economies: the case of Russia. 2013. Diss.

550. PEKKARINEN, OLLI. Industrial solution business – transition from product to solution offering. 2013. Diss.

551. KINNUNEN, JYRI. Risk-return trade-off and autocorrelation. 2013. Diss.

552. YLÄTALO, JAAKKO. Model based analysis of the post-combustion calcium looping process for carbon dioxide capture. 2013. Diss.

553. LEHTOVAARA, MATTI. Commercialization of modern renewable energy. 2013. Diss.

554. VIROLAINEN, SAMI. Hydrometallurgical recovery of valuable metals from secondary raw materials. 2013. Diss.